A CONSISTENCY STUDY OF INTEGRAL AND DIFFERENTIAL NEUTRON CROSS-SECTION DATA

A thesis submitted for the award of the degree of Doctor of Philosophy of the University of London.

by

George Damalas

Physics graduate of the University of Athens,
M.Sc., D.Q.M.C., University of London.

University of London Reactor Centre,
Department of Mechanical Engineering,
Imperial College of Science & Technology

July, 1981

DEDICATED TO MY PARENTS

IOANNIS AND OURANIA

AND TO MY SISTER

EPHI

A B S T R A C T

The purpose of this work is a consistency study of integral and differential neutron cross-section data for iron and some other important reactor materials.

The integral quantity used is the transmission of fission-spectrum neutrons in spherical shells of varying thickness and composition for three different threshold reactions (^{27}Aℓ(n,p)^{27}Mg, ^{238}U(n,f)F.P. and ^{237}Np(n,f)F.P.).

The experimental Transmissions were taken from the Bethe, Beyster and Carter experiments undertaken at Los Alamos Scientific Laboratory in 1955.

The one-dimensional discrete ordinates code ANISN and the U K N D L and ENDF/B nuclear data libraries are used in the calculation of Transmissions. A detailed investigation of the effect on the calculated Transmission of various approximations in both the modelling of the experiments and the calculational method is undertaken and its importance in the comparison between experimental and calculated values is also demonstrated.

Detailed sensitivity studies reveal both which input data (fission spectrum, material and dosimetry cross-section data) and energy ranges the calculated Transmissions are sensitive.

These sensitivity profiles coupled with multigroup covariance matrices available for iron and some dosimetry reactions permit the determination of the uncertainty of calculated Transmissions. In the context of this analysis it is also demonstrated that the inelastic cross-section plays a predominant role and that observed discrepancies between experimental and calculated Transmissions are consistent with this uncertainty. This result, favoured by the fact that the uncertainty of the experimental Transmissions is much smaller than that of the calculated ones, allows the statistical combination of these two data sets (multigroup cross-sections, experimental Transmissions) and their re-estimation (both mean values and covariance matrices) based on the enlarged data ensemble.

The well-known least-squares method is employed in this analysis and the improvement of the adjusted data sets is shown. Both U K N D L and ENDF/B libraries are used and a tendency for a convergence towards a better final library is unequivocally shown.

A satisfactory comparison with other iron benchmark experiments is presented and a discussion upon both the advantages and shortcomings of adjusting nuclear data libraries based upon integral experiments concludes the present study.

ACKNOWLEDGEMENTS

The author wishes to thank the following people for their assistance with this work:

Dr. J.G. Williams of University of London Reactor Centre for offering and supervising this project.

Mr. P.W. Gray of ULRC for his invaluable help on the statistical aspect of this work, his interest and untiring disposition in answering questions at all times.

All members of the Winfrith Radiation Physics and Shielding Group for their generous and friendly assistance. In particular, Dr. J. Butler for allowing me to carry out the MCBEND calculations at A.E.E. Also Dr. C.J. Dean and, Mr. A. Packwood for their assistance in running the GALAXY, MCBEND and ANISN codes and Miss W. Wright for her help with computing problems.

Mr. J.A. Mason of ULRC for his help on technical and administrative matters of my work.

Dr. S. Walker for his advice on computing problems in running ANISN/SWANLAKE at University of London Computer Centre.

All members of staff of the University of London Reactor Centre for their help and friendship during my stay here. In particular, Mr. M. Kerridge, Director of ULRC, for his support and continual interest.

Bodossaki Foundation and Ministry of Coordination of Greece for awarding the scholarship to study in this country.

Last, but not least, Mrs. J. Vine, Miss C. Collins and Mrs. M. Robinson who jointly typed this thesis.

ASCOT 22nd July 1981.

LIST OF CONTENTS

		Page
ABSTRACT		1
ACKNOWLEDGEMENTS		3
LIST OF CONTENTS		4
LIST OF FIGURES		9
LIST OF TABLES		15
1.	INTRODUCTION	19
2.	EXPERIMENTAL TRANSMISSIONS	
	2.1 Introduction	24
	2.2 Historical review of spherical shell measurements.	26
	2.3 The sphere method	29
	2.4 B.B.C. Experiments	34
	2.4.1 Experimental arrangement	34
	2.4.2 Counting Conditions	38
	2.4.3 Results and Conclusions	41
	2.5 Uncertainty analysis of B.B.C. Experiments.	45
	2.5.1 Comparison of ideal and real conditions of B.B.C. experiments - Effect on Transmission.	46
	2.6 Experimental Transmissions and their final uncertainties	56
	2.7 Reasons for re-evaluating B.B.C. experiments	62
3.	CALCULATION OF TRANSMISSIONS	
	3.1 Introduction	64
	3.2 Schematization of the one-dimensional spherical geometry for the experimental arrangement.	66

Page

3.3 Main features of the discrete-ordinates method. 71

3.4 Optimization of the calculational procedure. 80

3.4.1 ANISN input data specification 81

3.4.2 Effect of the angular mesh and quadrature sets 85

3.4.3 Effect of the order of the Scattering kernel expansion. 87

3.4.4 Effect of the radial mesh 90

3.4.5 Optimum calculational scheme. 90

3.5 Supplementary ANISN calculations and tests. 92

3.5.1 Comparison of analytical and ANISN flux calculations. 92

3.5.2 Effect on Transmission of detector's size, shape and composition. 97

3.5.3 Equivalence of rectangular and shell sources. 102

3.6 MONTE - CARLO Calculations. 111

3.6.1 MONTE - CARLO Method. 111

3.6.2 MCBEND code. 112

3.6.3 MCBEND formulation of B.B.C. experiments. 114

3.6.4 Comparison of MCBEND and ANISN results. 118

3.7 Calculated Transmissions. 128

4. SENSITIVITY STUDIES

4.1 Introduction 145

4.2 Sensitivity of Transmission to material Cross-Sections. 147

4.2.1 SWANLAKE code. 150

Page

4.2.2 Input data specification 153

4.2.3 SWANLAKE analysis of calculated Transmissions. 159

4.2.4 SWANLAKE results and conclusions. 205

4.3 Sensitivity of Transmission to Legendre coefficients of the scattering kernel. 207

4.4 Sensitivity of Transmission to dosimetry cross-sections. 217

4.5 Sensitivity of Transmission to source spectrum. 223

4.6 Summary. 230

5. UNCERTAINTY ANALYSIS OF CALCULATED TRANSMISSIONS

5.1 Introduction 232

5.2 Basic multigroup formulation of uncertainty analysis 236

5.3 Sources of errors and correlations in nuclear cross-section data. 240

5.3.1 ENDF libraries 240

5.3.2 Point data errors 241

5.3.3 Correlations between Point data 242

5.3.4 Group processing errors 243

5.3.5 Evaluated data covariance files 245

5.4 Uncertainty analysis of calculated Transmissions 248

5.4.1 Status of the uncertainty information of input data. 248

5.4.2 Uncertainty analysis results. 256

Page

6. CROSS-SECTION ADJUSTMENTS

6.1 Introduction 272

6.2 A review of nuclear data adjustment methods. 277

6.3 Statistical formulation of the consistency problem. 284

6.4 Cross-section adjustments 292

6.5 Assessment of the adjusted cross-section data sets. 303

6.5.1 New estimates of Transmissions and their uncertainties. 304

6.5.2 Calculation of Transmissions and their uncertainties in terms of both unadjusted and adjusted data sets. 309

6.5.3 Comparison of the adjusted data sets. 312

6.6 Physical interpretation of the observed adjustments 315

6.7 Comparison with the WINFRITH iron benchmark experiment. 319

7. RECAPITULATION - CONCLUSIONS 323

REFERENCES 330

APPENDICES

Appendix A. Calculation of fluxes inside spherical shell sources. 334

Appendix B. Least-squares method. 342

100 Energy group structure (DLC-37/ENDF/B) 367

Page

55 Energy group structure. 368

37 Energy group structure 369

Angular quadrature sets. 370

LIST OF FIGURES

		Page
1.	The sphere method	30
2.	Schematic drawing of "Water Boiler" and the experimental arrangement.	35
3.	Source plate and a spiral counter in position at the centre of a hemisphere.	35
4.	External collimator with source and a typical 8-inch sphere on its supporting cone.	36
5.	Fission spectrum and detector responses	44
6.	Fission spectrum x detector response curves	44
7.	P_1 escape probability	53
8.	P_2 escape probability	53
9.	P_m escape probability	53
10.	A cross-sectional view of the experimental arrangement under ideal conditions.	67
11.	Equivalence of point and spherical shell sources.	68
12.	Transformation of the experimental arrangement into one-dimensional model.	69
13.	Geometry of a scattering event.	73
14.	Calculational flow in solution of finite difference equation by ANISN.	77
15.	Determination of the shell source boundaries.	84
16.	ANISN input data specification for preliminary calculations.	86
17.	ANISN and analytical scalar fluxes without the presence of the iron shell.	94
18.	Angular flux $\Phi(r,\mu)$ along the discrete directions for energy group 11, without the presence of a material shell.	96

		Page
19.	Diameter to height ratio for different detector shapes.	97
20.	A sectional view of the detector - material shell arrangement showing the equivalence between cylindrical and spherical detectors.	101
21.	Equivalence of rectangular and shell sources.	102
22.	$^{238}U(n,f)F.P$ Transmissions versus distance to source, shell thickness = 3.759cm.	107
23.	Effect on Transmission of "distance to source" variations.	108
24.	Variation of angle ϕ in terms of the distance to source.	109
25.	MCBEND formulation of B.B.C. experiments.	115
26.	Equivalence of MCBEND and ANISN formulations of B.B.C. experiments.	119
27.	ANISN and MCBEND scalar fluxes without the presence of the iron shell.	123
28.	Enlargement of Figure 27 in the energy range 0.1 MeV - 10.0 MeV.	124
29.	ANISN and MCBEND scalar fluxes inside the iron shell, thickness = 4.11cm.	125
30.	Enlargement of Figure 29 in the energy range 0.1 MeV - 10.0 MeV	126
31.	Neutron spectra at the centre of the iron shell, thickness = 1.90 cm.	133
32.	Neutron spectra at the centre of the iron shell, thickness = 4.11 cm.	134
33.	Neutron spectra at the centre of the iron shell, thickness = 9.16 cm.	135
34.	Neutron spectra at 4.15 cm from the centre of the iron shell, thickness = 4.11 cm.	137

		Page
35.	Neutron spectra at 8.36 cm from the centre of the iron shell, thickness = 4.11 cm.	138
36.	Neutron spectra at 16.35 cm from the centre of the iron shell, thickness = 4.11 cm.	139
37.	Neutron spectra at the centre of the copper shell, thickness = 4.12 cm.	140
38.	Neutron spectra at the centre of the lead shell, thickness = 6.24 cm.	141
39.	Neutron spectra at the centre of the tin shell, thickness = 7.01 cm.	142
40.	Neutron spectra at the centre of the zirconium shell, thickness = 3.30 cm.	143
41.	Sensitivity of Transmission to iron total cross-section, shell thickness = 9.16 cm.	156
42.	Dosimetry cross-sections.	157
43.	Iron cross-sections	158
44.	Sensitivity of $^{27}Al(n,p)^{27}Mg$ Transmission to iron total cross-section.	161
45.	Sensitivity of $^{238}U(n,f)$F.P Transmission to iron total cross-section.	162
46.	Sensitivity of $^{237}Np(n,f)$F.P Transmission to iron total cross-section.	163
47.	Sensitivity of $^{27}Al(n,p)^{27}Mg$ Transmission to iron cross-sections, thickness = 1.90 cm.	165
48.	Sensitivity of $^{238}U(n,f)$F.P Transmission to iron cross-sections, thickness = 1.90 cm.	166
49.	Sensitivity of $^{237}Np(n,f)$F.P Transmission to iron cross-sections, thickness = 1.90 cm.	167

Page

50. Sensitivity of $^{27}Al(n,p)^{27}Mg$ Transmission to iron cross-sections, thickness = 4.11 cm. 168

51. Sensitivity of $^{238}U(n,f)F.P$ Transmission to iron cross-sections, thickness = 4.11 cm. 169

52. Sensitivity of $^{237}Np(n,f)F.P$ Transmission to iron cross-sections, thickness = 4.11 cm. 170

53. Sensitivity of $^{27}Al(n,p)^{27}Mg$ Transmission to iron cross-sections, thickness = 9.16 cm. 171

54. Sensitivity of $^{238}U(n,f)F.P$ Transmission to iron cross-sections, thickness = 9.16 cm. 172

55. Sensitivity of $^{237}Np(n,f)F.P$ Transmission to iron cross-sections, thickness = 9.16 cm. 173

56. Sensitivity of $^{238}U(n,f)F.P$ Transmission to tin cross-sections, thickness = 7.01 cm. 175

57. Sensitivity of $^{238}U(n,f)F.P$ Transmission to lead cross-sections, thickness = 6.24 cm. 176

58. Sensitivity of $^{238}U(n,f)F.P$ Transmission to copper cross-sections, thickness = 4.12 cm. 177

59. Sensitivity of $^{238}U(n,f)F.P$ Transmission to zirconium cross-sections, thickness = 3.30 cm. 178

60. Total sensitivity to different excited levels, iron shell of thickness = 9.16 cm, $^{27}Al(n,p)^{27}Mg$ detector. 180

61. Total sensitivity to different excited levels, iron shell of thickness = 9.16 cm, $^{238}U(n,f)F.P$ detector. 181

62. Total sensitivity to different excited levels, iron shell of thickness = 9.16 cm, $^{237}Np(n,f)F.P$ detector. 182

63. Total sensitivity to different excited levels, lead shell of thickness = 6.24 cm. $^{238}U(n,f)F.P$ detector. 185

		Page
64.	Total sensitivity to different excited levels, copper shell of thickness = 4.12 cm. $^{238}U(n,f)F.P$ detector.	186
65.	Total sensitivity to different excited levels, zirconium shell of thickness = 3.30 cm $^{238}U(n,f)F.P$ detector.	187
66.	P_o and P_3 neutron spectra at the centre of the iron shell, thickness = 9.16 cm.	193
67.	P_o sensitivity of $^{27}Al(n,p)^{27}Mg$ Transmission to iron cross-sections, thickness = 9.16 cm.	195
68.	P_o sensitivity of $^{238}U(n,f)F.P$ Transmission to iron cross-sections, thickness = 9.16 cm.	196
69.	P_o sensitivity of $^{237}Np(n,f)F.P$ Transmission to iron cross-sections, thickness = 9.16 cm.	197
70.	Mean angle of elastic scatter versus energy for iron.	199
71.	Elastic scattering distribution functions for various forms of scattering.	202
72.	Transmission variation in terms of mean cosine of elastic scatter for iron shells	212
73.	Sensitivity of Transmission to $^{27}Al(n,p)^{27}Mg$ dosimetry data, thickness = 9.16 cm.	218
74.	Sensitivity of Transmission to $^{238}U(n,f)F.P$ dosimetry data, thickness = 9.16 cm.	219
75.	Sensitivity of Transmission to $^{237}Np(n,f)F.P$ dosimetry data, thickness 9.16 cm.	220
76.	Sensitivity of Transmission to various input data, iron shell of thickness = 4.11 cm.	227

		Page
77.	Sensitivity of Transmission to various input data iron shell of thickness = 4.11 cm.	228
78.	Sensitivity of Transmission to various input data, iron shell of thickness = 4.11 cm.	229
79.	Pictorial view of the uncertainty equation.	258
80.	Fine and broad-group structures in uncertainty calculations.	259
81.	Experimental and calculated Transmissions and their standard deviations for iron shells.	270
82.	Relation between experimental, calculated and re-estimated Transmission vectors.	307
83.	Normal distributions of measured Transmissions and cross-section evaluations before and after adjustment.	308

LIST OF TABLES

		Page
1.	Measured Transmissions and deduced inelastic cross-sections for different detectors and materials.	40
2.	Corrected Transmissions for the detector's angular anisotropy.	54
2A.	Corrected Transmissions and components of their final uncertainties.	57
3.	Mean values of experimental Transmissions and their standard deviations.	61
4.	Initial radial mesh for optimisation calculations.	85
5.	Effect of the angular mesh and quadrature sets on Transmission.	88
6.	Effect of the order of scattering kernel expansion on Transmission.	89
7.	Effect of radial mesh on Transmission	91
8.	Analytical and ANISN scalar fluxes.	93
9.	Effect on Transmission of changes in the detector radius.	99
10.	Effect on Transmission of the detector's material.	100
11.	Effect on Transmission of different shell source allocations.	104
12.	Calculated Transmissions for different distances to course ($^{238}U(n,f)$F.P reaction).	106
13.	MCBEND and ANISN reaction rates and Transmissions for the two thin iron shells.	121
14.	Experimental and calculated Transmissions for different materials, shell thicknesses, threshold detectors and data sets.	129

		Page
15.	Integrated forward and adjoint responses for some cases of Table 14.	155
16.	Inelastic scattering data representation for elements in DLC-37/EPR	160
17.	Total sensitivity of Transmission to total, elastic, absorption and inelastic cross-sections.	184
18.	Relative importances of the partial cross-section sensitivities for the iron shells.	189
19.	Percetage changes in Transmissions for P_3, P_o calculations.	192
20.	P_o, P_3 Transmissions and total sensitivities for the iron shell of thickness = 9.16 cm.	203
21.	Total sensitivity to the 1^{st}-order expansion coefficient of the scattering kernel for various iron cases.	211
22.	Percentage Transmission differences between P_1, P_o calculations for various iron cases.	214
23.	Sensitivities to total, elastic, and 1^{st} order expansion coefficient for iron shells.	216
24.	Sensitivity of Transmission to fission spectrum, iron shell of thickness = 4.11 cm.	224
25.	Relative multigroup covariance matrix of elastic cross-section for iron.	250
26.	Relative multigroup covariance matrix of non-elastic cross-section for iron.	251
27.	Relative multigroup covariance matrix of elastic to non-elastic cross-section for iron.	252
28.	Relative multigroup covariance matrix for $^{238}U(n,f)F.P$ reaction.	253

		Page
29.	Relative multigroup covariance matrix for $^{27}A\ell(n.p)^{27}Mg$ reaction.	254
30.	Percentage uncertainties of experimental and calculated Transmissions in iron shells.	263
31.	Broad-group sensitivity coefficients to iron elastic and non-elastic cross-sections.	264
32.	Broad-group sensitivity coefficients of Transmission to $^{27}A\ell(n,p)^{27}Mg$ dosimetry data.	265
33.	Broad-group sensitivity coefficients of Transmission to $^{238}U(n,f)F.P$ dosimetry data.	266
34.	Elastic and non-elastic partial uncertainties of the calculated Transmission in iron shells.	267
35.	A comparison between "calculational" and "data" uncertainties of Transmissions in iron shells.	269
36.	Relative covariance matrix of experimental Transmissions in iron shells.	294
37.	Broad-group sensitivity coefficients of Transmissions to iron elastic and non-elastic cross-sections (U K N D L (2))	295
38.	Fractional differences between experimental and calculated Transmissions in iron shells.	293
39.	Percentage adjustment factors and standard deviations for iron broad-group elastic and non-elastic cross-sections.	297
40.	Relative broad-group covariance matrix of iron elastic cross-section after adjustment.	298
41.	Relative broad-group covariance matrix of iron non-elastic cross-section after adjustment.	299
42.	Relative broad-group covariance matrix of iron elastic to iron non-elastic cross-section after adjustment.	300

		Page
43.	Iron Transmissions and their uncertainties before and after adjustment.	305
44.	Calculated values and standard deviations of a Transmission before and after adjustment.	310
45.	Adjusted and unadjusted broad-group elastic and non-elastic iron cross-sections.	313
46.	A comparison between WINFRITH and B.B.C. iron benchmark experiments.	320

CHAPTER ONE

INTRODUCTION

An understanding of neutron behaviour in matter is a necessary requirement for the successful design and operation of a nuclear reactor. Such an understanding requires as a starting point an adequate model of the reactor with an adequate solution for the neutron transport equation for the model, and an accurate knowledge of the microscopic cross-section data for various neutron interactions with nuclei as a function of incident neutron energies and angles. Additionally one needs procedures for processing these data for use in transport calculations which, because of their complexity, are carried out numerically. Particularly, the multigroup methods of solving the neutron transport equation require the generation of "effective" cross-section data meant to describe various aspects of neutron interaction with matter between well-defined energy limits. These average quantities are obtained by weighting the basic nuclear data with some function meant to represent the energy and angular distribution of the flux at the position of interest.

Because these stringent and inter-related requirements so far have rarely, if ever, been met, the important role of integral experiments for the successful design and operation of a nuclear reactor has long been recognised and a multiplicity of applications has already been in use. The so-called integral quantities are just certain functions, defined by the neutron transport equation, of the cross-sections of the isotopes of which the system under consideration is composed (resonance integrals, diffusion lengths, neutron age, effective multiplication factor, reactivity worth, neutron spectra etc.). These quantities can accurately be measured either in simulations of certain design environments or in simple geometry - single material experimental

arrangements. They can then be used either to judge the quality of cross-section data files and computational methods or, directly, as input data in practical design computations.

Furthermore, in cases where modelling and calculational errors are unimportant, cross-section data can be adjusted and optimised for neutronic calculations in similar environments by combining the two independent pieces of experimental information (microscopic neutron cross-section data/measured integral quantities) according to an appropriate statistical model.

To extract the useful information these adjustments may contain for the basic nuclear data is a much more difficult matter and requires the validity of some assumptions which are not easily met in practice.

More details and clarification of various uses of integral experiments and cross-section adjustment techniques are given in the following chapters.

The main purpose of this thesis is to examine if well-designed, precise integral experiments can significantly improve fine-multigroup or pointwise basic nuclear data files and to outline the requirements, conditions and assumptions under which this goal can be accomplished. The improvement of the basic nuclear data is perceived in terms of better values and higher accuracies, is justified on the basis of the enlarged data ensemble to which the new estimates correspond and is meant to be problem-independent, a real contribution to a better knowledge of these physical quantities. This estimation procedure if it proves workable, will constitute an alternative, to differential measurement, in the evaluation of nuclear data with very important practical implications.

Indeed, the development of multi-dimensional MONTE - CARLO and two-dimensional discrete-ordinates methods together with the increasing

availability of high speed big-storage computers has produced very powerful computer codes which have largely minimised modelling and computational uncertainties for many of design and experimental configurations. This fact in conjunction with the definition of target accuracies for some important fast reactor core and shield design quantities has resulted in the establishment of lists of requests for non-existent or improved nuclear data. The nuclear data measurers advise that these high accuracy requests will,in most cases,be costly and time-consuming to achieve. Taking into consideration the high priorities and short-time scales over which these data are needed, it is clear that properly designed and analysed integral experiments may have a very decisive role in fulfilling these requirements.

Chapter 2 deals with the experimental information concerning the integral quantities used in the present study which are Transmissions of fission-spectrum neutrons through spherical shells of varying thickness and composition for three different threshold reactions. In this chapter the real experimental arrangement and measurement conditions are transformed into a simple experimental model manageable by current transport codes. A comparison between ideal and real experimental conditions is undertaken and the effect on Transmission of various simplifications and approximations is fully studied. The chapter concludes with the experimental knowledge of Transmissions comprising both corrected values and error bounds, under the established ideal experimental conditions.

Chapter 3 undertakes the task of calculating the Transmissions in terms of existing nuclear data libraries using a well-established transport code. The ideal experimental model established in the previous chapter is transformed into a one-dimensional geometrical configuration required by the transport code used. The implications of this transformation together with the effect of the approximations due to the calculational algorithm itself are fully studied by differ-

ent and independent calculational methods and by additional transport calculations, tests and comparisons with experimental information or theoretical reasoning. Based on this investigation a quantitative assessment of modelling and calculational errors of Transmissions is attempted. Calculated Transmissions for various elements, shell thicknesses, threshold detectors and nuclear data sets conclude the chapter, while cases of large discrepancies between experimental and calculated values requiring further investigation are noted.

Chapter 4 treats the sensitivity problem of the present study which amounts to establishing the relationship between nuclear data-originated errors and calculated Transmission uncertainties. The sensitivity of Transmission to various input data is fully studied as a function of energy for those data categories for which sensitivity tools either exist or can easily be derived (material scalar cross-sections for various reactions, dosimetry cross-sections). For the remainder of the input data approximate or simple methods are followed in determining the energy-integrated sensitivity of Transmission to these quantities. (Fission spectrum, quantities describing angular and/or energy distributions of secondary neutrons).
The energy-dependence of the sensitivity, total (energy integrated) sensitivities and approximate sensitivity estimates give a full picture of the reactions, energy ranges and other nuclear data parameters to which the calculated Transmissions are more sensitive and which are more likely to be responsible for large discrepancies between experimental and calculated Transmissions.

Chapter 5 combines the sensitivity information derived in the previous chapter with relative error matrices available for some input data in a condensed form, to yield estimates of nuclear data-originated errors of calculated Transmissions. In representing the error information of nuclear data, the concept of the covariance matrix is used

throughout and the sources of errors and correlations (variance and covariance terms in the covariance matrix, respectively) of the multi-group and basic nuclear data are identified and discussed in some detail. The effect on the calculated uncertainty of omitting important input data in the uncertainty analysis, due to the lack of suitable covariance information, is also studied. In addition, the implications of the condensed form of the covariance information available are discussed and evaluated. Finally the data-related and calculational method-originated uncertainties of Transmissions are compared and the statistical consistency of experimental and calculated Transmissions is examined and assessed.

Chapter 6 attempts to improve the nuclear data used in the calculations on the basis of the experimental Transmissions and their relationship with the nuclear data. The statistical model employed in pursuing this course of analysis is derived in Appendix B.
The importance of the quality and structure of the covariance information in the feedback of experimental integral information to basic nuclear data is examined and the improved data sets derived from two nuclear data libraries are assessed both in predicting similar integral quantities and in general terms. The drawbacks of the adjusted data sets and their causes are also discussed and the conditions and requirements under which the deduced improvements could be real, permanent and problem-independent are outlined. Finally a comparison with a similar analysis based on another experiment is undertaken.

Chapter 7 summarises the most important findings of the present study and the conclusions reached.

CHAPTER TWO

EXPERIMENTAL TRANSMISSIONS

2.1 INTRODUCTION

The integral quantity being used in the present consistency analysis of integral and differential neutron cross-section data is the Transmission through spherical shells of varying thickness and composition of thermal-fission neutrons, for three different threshold reactions.

The experimental information concerning this quantity comes from the work of Bethe, Beyster and Carter, (hereinafter referred to as B.B.C) who in 1955 measured the Transmissions for 15 different elements of varying shell thickness using $^{238}U(n,f)F.P$ and $^{237}N_p(n.f)F.P$ fission counters, and $^{27}Al(n,p)^{27}Mg$ threshold detectors (Ref. 1-4).

Transmission experiments with spherical shells give useful information about the non-elastic (especially inelastic) component of neutron interactions with matter. A historical review of this kind of experiment is given in the following section.

A simplistic but quite comprehensive and instructive theoretical analysis of sphere transmission experiments established by B.B.C is outlined next and the assumptions under which this approach is valid are clearly stated.

A brief description of the B.B.C experiments together with their results and conclusions follows, where the points of interest to our method of analysis are presented and discussed in detail.

The calculation of Transmissions in the following chapter is undertaken under some ideal conditions which are cited next. Much of the remainder of this chapter is devoted to the study of the possible effect on Transmission of the differences between ideal and real experimental

conditions.

The chapter concludes with the experimental values of Transmissions accompanied by their final uncertainties originating from the statistical nature of the measurement techniques and the approximations and corrections involved.

2.2 HISTORICAL REVIEW OF SPHERICAL SHELL MEASUREMENTS

The measurement of non-elastic neutron cross-sections by observing the counting-rates of an energy-dependent detector with and without a spherical shell of scattering material around the detector has been used for several decades.

Early measurements were made by Gittings et al (5) in 1949 with a 14MeV D-T neutron source and threshold activation detectors.

Phillips et al (6) extended the 14-MeV measurements and made some valuable contributions to the understanding of some of the corrections involved in the sphere method.

The work of B.B.C in 1955 extended the reliable use of this method to a wide range of neutron energies and experimental conditions.

Kh R. Poze and N.P. Glazkov (7) in 1956 placed photo-neutron sources ($Na-\gamma-D_2O$, $La-\gamma-Be$ and $Na-\gamma-Be$ giving, respectively, 0.3, 0.77 and 1.0 MeV neutrons) inside spheres of various materials. The Transmissions of the spheres were measured with hydrogen or helium recoil ionization chambers. The cross-sections were computed with some multiple scattering corrections. Some information about inelastically scattered neutrons was also obtained.

Ball, MacGregor and Both (8) in 1956 used the sphere method to measure non-elastic cross-sections for 7,8,10,11,13,14,21,25 and 29 MeV neutrons. An organic sintillator was used as a neutron detector. The values obtained at several biases were extrapolated to give the total non-elastic cross-sections. B.B.C corrections were applied.

W.G. Davey & P.I. Amundson (9) in 1967 measured the change in some fission ratios near the centre of the zero-energy fast reactor assembly when a spherical shell was placed around the chambers. The change in the fission ratios was interpreted in terms of the scattering and absorption cross-sections of the shell. Using different data sets, fission ratios

and changes in ratios were calculated and compared with experimental values; from this comparison useful information about the correctness of the inelastic scattering cross-sections of the data sets used was acquired.

The measurement of neutron spectra in the energy range 10KeV-14MeV emitted from shells made of Fe,Ne and H_2O for a 14 MeV neutron source by L.F. Hansen and J.D. Anderson(10) in 1971-73, demonstrated that the use of simple integral experiments to evaluate the performance of a given set of cross-sections or the accuracy of calculational techniques was quite valuable.

Shell measurements with monoenergetic neutrons have largely been superseded by neutron time - of - flight and gamma - ray excitation techniques which are capable of providing detailed inelastic scattering data, but it is believed that the shell technique may be valuable as a reactor physics tool. Shell measurements are capable of providing accurate data which, although of an integral nature, can be used to check cross-section sets and computational techniques.

In addition, it should be noted that the use of several different threshold detectors provides broad-group downscattering cross-sections which are precisely those needed for multigroup fast reactor analysis. Further, it is worth noting that the shell technique examines non-elastic cross-sections over the entire high-energy portion of the fast reactor-spectrum so that they are, in a sense, complete. This is in contrast with the current microscopic data where detailed cross-sections for individual level excitation to lower energies are mated with statistical model high-energy data, and where the intermediate region may be filled in with informed guess work.

Clearly, shell measurements in reactor spectra will be completely superfluous when precise, consistent, microscopic inelastic cross-

sections are available for the entire energy range of interest in reactors, but currently they appear to have some value. Possibly their main use will be to show in what materials and energy regions better data are needed.

This work is a contribution to this end.

2.3 THE SPHERE METHOD

In principle, the sphere Transmission method works as follows:

If we place an isotropic threshold neutron detector at a large distance from an isotropic source and count with and without a sphere of material surrounding the source, the resulting Transmission:

$$T = \frac{\text{counts (sphere on)}}{\text{counts (sphere off)}} \tag{2.1}$$

is a measure of the amount of inelastic scattering.

We can think of this as follows: with only isotropic elastic scattering in the shell, a Transmission of unity will be obtained, because of spherical symmetry. Therefore, when both elastic and inelastic collisions occur in the shell one might tend to believe that the number of inelastic collisions is, more or less, independent of the elastic cross-sections. If this were true, the elastic scatterings would again give essentially no effect and, with the absorption being negligible, only the inelastic cross-section would be important in determining the sphere Transmission. On the basis of this argument it has often been assumed that the Transmission is given by an exponential:

$$T = e^{-\Sigma_{in} X} \tag{2.2}$$

where : $\Sigma_{in} = N\sigma_{in}$, N is the atom density of the material, σ_{in} is the microscopic inelastic cross-section in barns (for its definition see Equation (2.6)) and X is the shell thickness (see Figure 1).

It is clear, however, that if the elastic scattering properties of the nuclei of the sphere can produce much of an increase in path length through the shell, Equation (2.2) will be only an approximation to the correct description of the physical picture. However,

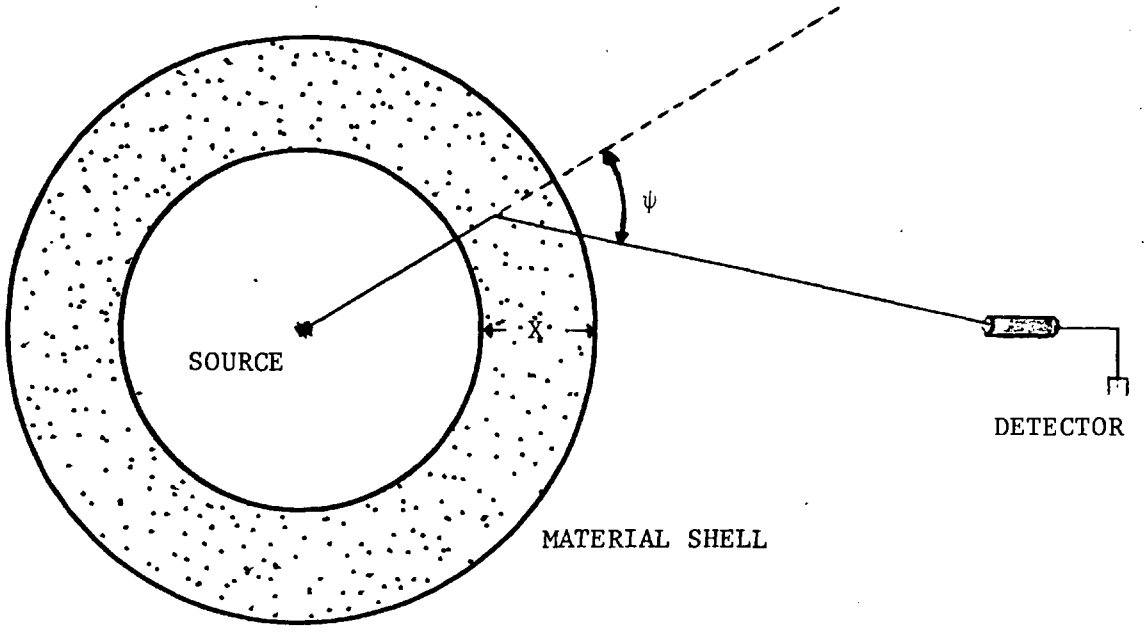


FIGURE 1 THE SPHERE METHOD

there are two general conditions in which Equation (2.2) will not be very much in error:

(a) if the thickness of the shell is so small that:

$$T = 1 - \Sigma_{in} X \tag{2.3}$$

is applicable, or

(b) if the elastic transport cross-section

$$\sigma_{et} = \int_{\Omega} \sigma_{el} \psi \, (1 - \cos\psi) d\Omega \tag{2.4}$$

(see Figure 1) is small compared with σ_{in}.

These conditions severly limit the use of Equation (2.2) because the Transmission of a shell thin enough to satisfy condition (a) is, in general, so large that it prohibits accurate cross-section measurements. Condition (b) restricts one to situations in which the inelastic cross-section is about one-half of the total cross-section, and in which the elastic scattering is peaked strongly in the forward direction. Then an elastic scattering acts like no scattering at all. Therefore,

condition (b) limits one to incident neutron energies of several MeV where inelastic cross-sections are no longer very dependent on neutron energy.

A tested theory to use in the evaluation of fairly thick spherical shells and for a wide range of neutron energies has been developed by Bethe , Beyster and Carter using a collision probability technique and taking into account multiple scattering in the shells. The B.B.C. analytical method is still considered as an adequate, well-established physical model for interpreting sphere transmission measurements.

Under the conditions that the shell thickness is of the order of one mean free path, rather than many and making the following assumptions:

1. the source is a point non-absorbing isotropic emitter.
2. the detector is small and isotropic.
3. the source-to-detector distance is large, relative to the sphere radius.
4. no energy losses occur on elastic collisions.
5. a neutron suffering an inelastic collision is rendered undetectable.
6. inelastic scattering is the only process which renders neutrons undetectable (i.e. that neutron absorption is negligibly small).

Bethe , Beyster and Carter showed that the Transmission is given by the formula: (Ref. 1, pages 214-221)

$$T = 1 - (1 - T_o)\frac{\sigma_{in}}{\sigma_{tr}}\left[1 + \frac{\sigma_{et}}{\sigma_{tr}}(1 - P_1) + \frac{(1 - P_1)(1 - P_2)\sigma_{et}^2}{\sigma_{tr}(\sigma_{in} + \sigma_{et} P_m)}\right] \quad (2.5)$$

where:

$T_o = e^{-\Sigma_{tr} X}$, the number of neutrons which emerge from the

sphere without any collision, supposing that one neutron is emitted by the source.

P_1, P_2, P_m = average escape probabilities for neutrons emerging from first, second and higher order collisions, correspondingly.

σ_{tr}, σ_{et} = total transport and elastic transport cross-sections being used instead of σ_t, σ_{el}.

The use of transport cross-sections instead of total and elastic ones greatly simplified the theory, since it permitted the scattering to be treated as isotropic while it was also shown that this was a good approximation.

Cross-sections included in Eqn. (2.5) must be understood as average, over the source spectrum and detector response, quantities of the general form:

$$\sigma = \frac{\int_0^\infty N(E)\ \sigma(E)\ \sigma^D(E)dE}{\int_0^\infty N(E)\ \sigma^D(E)dE} \qquad (2.6)$$

where

$N(E)$ = the energy-distribution function of the source neutrons.

$\sigma^D(E)$ = the detection cross-section for neutrons of energy E

$\sigma(E)$ = the cross-section of interest at energy E.

Eqn. (2.5) can be simplified if we assume that the escape probability is the same for the first, second and higher order collisions, i.e. $P_1 = P_2 = P_m$.

Then Eqn. (2.5) reduces to:

$$1 - T = (1 - T_o)\ \left(\frac{\sigma_{in}}{\sigma_{in} + \sigma_{et} P_m}\right) \qquad (2.7)$$

This formula allows a simple physical interpretation. The total number of neutrons which "are supplied" to the shell is $1 - T_o$. These can be removed from the shell by two processes, either by inelastic scattering or by escape. In a given collision, the probability of inelastic

scattering is σ_{in}, that of elastic scattering followed by escape is $\sigma_{et} P_m$.

This gives for the fraction scattered inelastically the expression of Eqn. (2.7).

2.4 B.B.C. EXPERIMENTS

In the B.B.C. experiments an intense, well-collimated beam of thermal neutrons from the thermal column of a "water boiler" reactor irradiated a plate of ^{235}U producing a fission spectrum source of about 2×10^{10} neutrons/sec.

Threshold detectors located at varying distance from the plate and surrounded by spherical shells of different thickness and composition allowed the determination of transmission ratios for a series of cases. The shell and detector were sited well away from the floor and the reactor so that the effect on T of neutrons scattered on surrounding objects to be minimised.

The source strength was monitored by two fission chambers located in the thermal column.

^{238}U, ^{237}Np fission threshold detectors and aluminium foils ($^{27}A\ell(n,p)^{27}Mg$ reaction) were used, thus giving data for three different energies.

By careful control of counting conditions the Transmissions were measured with 0.2 to 1.2% accuracy.

A more detailed description of the experimental arrangement and counting conditions is given next, necessary for the evaluation of the corrections, uncertainties and errors associated with the reported Transmissions.

2.4.1 Experimental Arrangement

A schematic diagram and typical photographs of the experimental set up at the "water boiler" reactor are given in Figs. 2, 3 and 4. The large cavity in the graphite thermal column provides an external thermal neutron flux of relatively high intensity and cadmium ratio. Both internal and external collimators are made of materials which either produce low-energy capture γ-rays, or have low thermal-neutron capture cross-sections. This measure was taken because the photo fission cross-sections of the detectors are not zero.

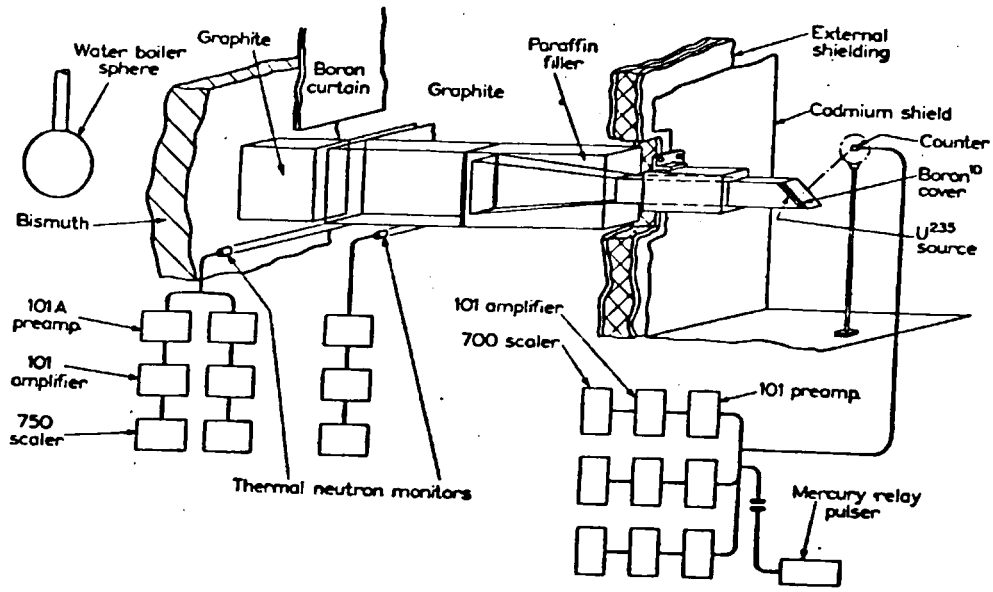


FIGURE 2 SCHEMATIC DRAWING OF "WATER BOILER" AND THE EXPERIMENTAL ARRANGEMENT

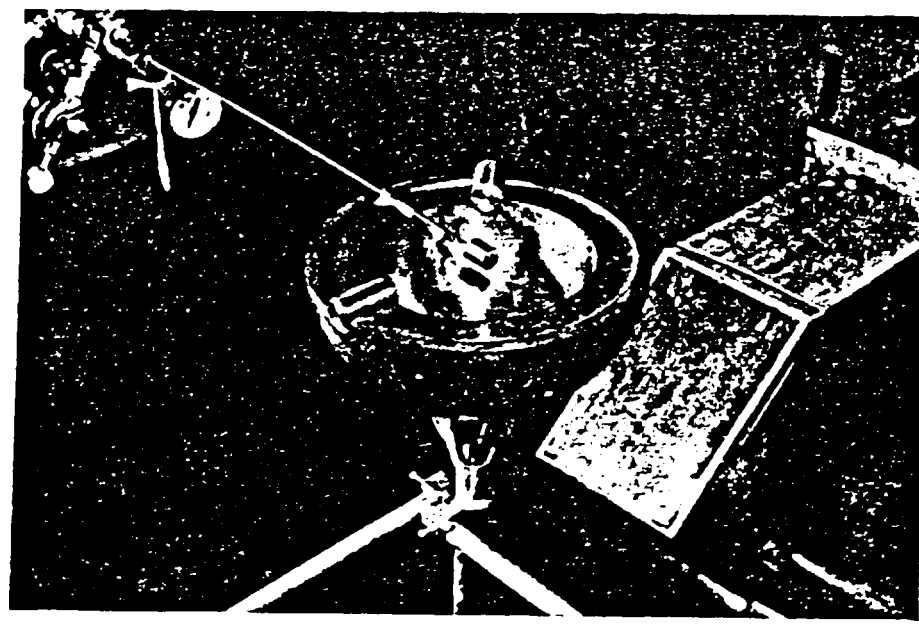


FIGURE 3 SOURCE PLATE AND A SPIRAL COUNTER IN POSITION AT THE CENTRE OF A HEMISPHERE

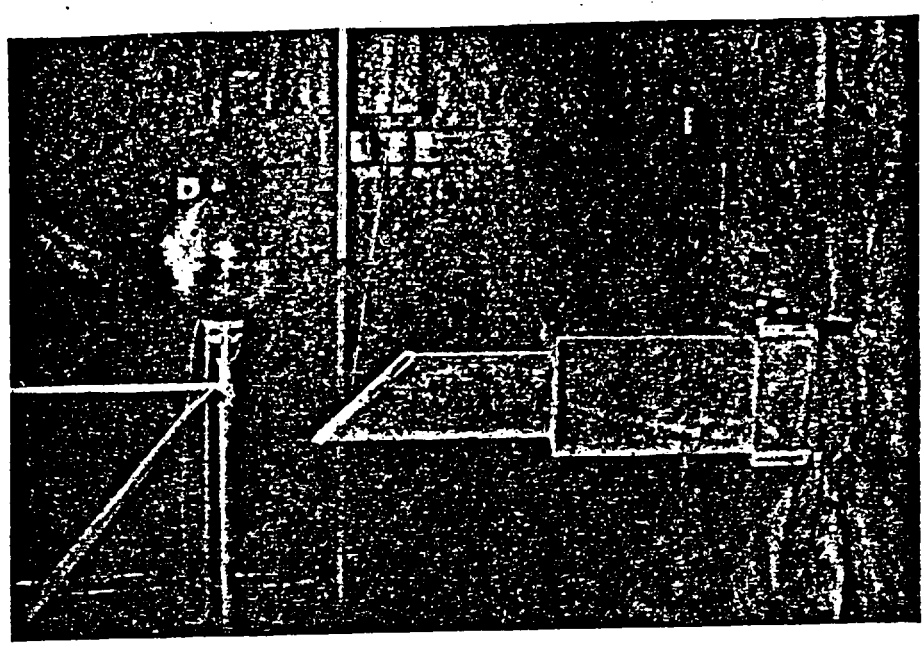


FIGURE 4 EXTERNAL COLLIMATOR WITH SOURCE AND A TYPICAL 8-INCH SPHERE ON ITS SUPPORTING CONE

The uranium plate, of dimensions 4½ by 6 inches, was covered on the outside by a thin sandwich of aluminium and boron-10. This had two functions : (1) to attenuate the scattered thermal neutrons which pass through the uranium plate, and (2) to prevent causing fission. It was calculated that less than 2% of the fast-source neutrons suffered collisions in the uranium and aluminium-boron cover plate before escaping. The last 10 inches of the collimator, onto which the source plate was fastened, was a thin aluminium box containing boron-10 (Fig. 3). Not more than about 1% of the neutrons reaching the detector resulted from single scattering in this collimator.

The fast neutron detectors were held in position by a system of clamps and stands which were completely independent of the sphere supports. The spheres were held by an aluminium cone, supported on a thin aluminium vertical tube and braced at right angles by aluminium tubes.

The source to detector distance was measured from the midpoint of the uranium plate to the centre of the detector and was accurate to about 1/16 inch.

The neutron monitors were inserted into the side of the thermal column (see Fig. 2). The positions in the column of these two monitors were arranged so that their counting rates were approximately equal, and about 10 to 100 times the counting rates of threshold detectors. The monitor counts were always used to normalize the data.

The spheres were machined as two hemispheres with an overlap in the equatorial plane. There was one hole, centred in this plane, through which the counter stem entered. The area of the hole was, in general, much less than 1% the sphere surface area, and faced normal to the line joining source and detector.

All sphere dimensions were measured with a micrometer to the nearest 0.001 inch and the spheres were weighed to an accuracy of better than

0.1%. Average densities were then computed to about 0.1% and usually agreed with the best handbook values.

The composition or uniformity of some spheres was questionable. Spectroscopic analyses or radiographic measurements were made, and where these indicated a necessity, corrections were made.

2.4.2 Counting Conditions

$^{238}U(n,f)F.P.$ and $^{237}Np(n,f)F.P.$ Counting Systems

In order to obtain sufficient sensitivity in the fission-threshold detectors, spiral counters were used.

Special measures and precautions were taken for the electronic-counting systems to obtain accuracies in Transmissions of the order of 0.1% and to promote reliability and convenience in the measurements.

Estimates of counting rate stability, based on the gain checks and bias curves of the counters, were as follows:

α	^{238}U counter	$\pm$	0.05%
β	^{237}Np counter	$\pm$	0.09%

During the counting procedure, with the reactor off, the source, counter and sometimes a sphere were set up. The amplifier gains were checked with the pulser, and the noise patterns were observed with the oscilloscope. The reactor was started. Personnel left the reactor room, the boron curtain was raised, and three to six 10-minute runs were taken. Three sets of counts from the threshold detector and three sets from monitors were recorded for each run. All counting rates were examined to ensure that all systems indicated the same changes, if any. The boron curtain was then lowered, the amplifier gains were checked with the pulser, and the sphere was changed, if appropriate. After more data were taken, Transmissions were computed for each of the six electronic channels. If there was not agreement to well within the statistics for at least two of the three systems on the threshold detector, the data were not used, but the counter and electronics were

suspected and investigated. When at least two of the systems did agree, which usually occurred, the average of these was computed, and this was divided by the average ratio of counts for the monitors. The resultant Transmissions are given in Table 1.

The statistical uncertainty reported in this Table is that computed from the numbers of counts recorded. The fractional statistical uncertainty in the monitor Transmissions has about one-sixth of that for the threshold detectors.

In many cases, Transmissions from Table 1 are the average of two or more independent measurements made on different days. Such repeat runs were seldom outside of the combined statistical accuracies.

^{27}Aℓ(n,p)^{27}Mg counting system

For sensitivity reasons, spirals of aluminium foil were used as detectors. Pure 2-S aluminium foils were cut uniformly to the following dimensions: 0.010 inch thick by 0.50 inch wide by 18 inches long. During irradiation, a foil was rolled into a tight spiral and inserted into a small brass holder which was similar in design to, and supported like, the fission detectors. The foil then was covered by a 1/64 inch thick cadmium cup.

During counting, the foil was wrapped around a 0.003 inch thick aluminium sleeve which fitted snugly over a cylindrical, aluminium-walled, proportional methane flow β-counter. The uniformity of sensitivity of the counter was checked by sliding a ^{137}Cs β-source over the surface of the aluminium sleeve. The counting rate over most of the surface was constant to within ± 1%.

For the aluminium foils used, the self-attenuation of neutrons during irradiation and of β's during counting are both small, and are about the same for both sphere-off and sphere-on runs. Errors of this sort tend to cancel out but a directional assymetry in sensitivity of the spiral is an indication that effects caused by attenuations will not

TABLE 1. MEASURED TRANSMISSIONS AND DEDUCED IN ELASTIC CROSS SECTIONS FOR DIFFERENT DETECTORS AND MATERIALS.

CASE	MATERIAL	SPHERE OUTSIDE RADIUS cm	SHELL THICKNESS cm	DISTANCE TO SOURCE cm	RESULTS								
					$^{27}Al(n, P)^{27}Mg$ 4.4 MeV			$^{238}U(n, f)$ F.P. 1.5 MeV			$^{237}Np(n, f)$ F.P. 0.6 MeV		
					TRANSMISSION	σ_{in} (Eqn. 2.2) barns	σ_{in} (with all corrections) barns	TRANSMISSION	σ_{in} (Eqn. 2.2) barns	σ_{in} (with all corrections) barns	TRANSMISSION	σ_{in} (Eqn. 2.2) barns	σ_{in} (with all corrections) barns
1.	Al	6.35	1.900	25.40	0.9009±0.007	0.909	0.760±0.062	0.9493±0.0020	0.453	0.319±0.046	-		
2.	Al	10.16	3.841	25.40	0.7901±0.0065	1.02		0.8953±0.0023	0.478		0.9665±0.0030	0.150	0.087±0.038
3.	Ti	5.715	2.546	25.40	-			0.8940±0.0022	0.776	0.563±0.051	0.9644±0.0040	0.251	0.187±0.037
4.	V	3.20	1.320	25.40	-			0.9298±0.0026	0.764	0.575±0.050	0.9727±0.0035	0.29	0.224±0.026
5.	Fe	6.35	1.900	25.40	0.7938±0.0071	1.43	1.20 ±0.084	0.868 ±0.0017	0.877	0.686±0.043	0.9450±0.0030	0.350	0.276±0.031
6.	Fe	10.16	4.111	25.40	-			0.7120±0.0018	0.974	>>	0.8616±0.0030	0.427	>>
7.	Fe	10.16	9.162	25.40	-			0.4678±0.0040	0.977	>>	0.7237±0.0042	0.416	>>
8.	Fe	6.35	3.795	50.80	-			0.7354±0.0030	0.927	>>	-		
9.	Fe	6.35	3.795	25.40	-			0.7414±0.0018	>>	>>	-		
10.	Fe	6.35	3.795	13.33				0.749 ±0.0018	>>	>>	-		
11.	Ni	6.655	2.070	25.40	0.7398±0.006	1.59	1.31 ±0.078	0.8370±0.0020	0.942	0.713±0.048	0.9284±0.0030	0.393	0.276±0.041
12.	Cu	10.16	4.115	25.40	-			0.6483±0.0016	1.24	0.900±0.053	0.8409±0.0031	0.496	0.304±0.046
13.	Cu	10.16	2.059	25.40	0.7460±0.010	1.68	1.41 ±0.097	-			-		
14.	Zr	5.715	3.304	25.40	0.7736±0.0080	1.81	1.57 ±0.094	0.8429±0.0028	1.205	0.960±0.059	0.9409±0.0035	0.430	0.302±0.050
15.	W	6.285	1.065	25.40	0.8288±0.0066	2.86	2.72 ±0.16	0.8503±0.0018	2.57	2.23 ±0.13	0.920 ±0.003	1.32	1.080±0.145
16.	Sn	10.16	3.503	25.40	0.7524±0.0060	2.20	2.01 ±0.11	0.8380±0.0022	1.362	1.12 ±0.061	0.9430±0.0030	0.450	0.369±0.050
17.	Sn	10.16	7.009	25.40	-			0.6938±0.0020	1.408	>>	-		
18.	Pb	10.16	3.124	25.40	0.7727±0.014	2.47	2.21 ±0.15	0.9106±0.0013	0.895	0.712±0.043	0.9783±0.0040	0.210	0.208±0.05
19.	Pb	10.16	6.243	25.40	-			0.8160±0.0018	0.972	>>	-		

cancel in a sphere transmission.

The foils which were used in these experiments have been checked in a well-collimated fast neutron beam and recut to decrease such asymmetry to not more than 1%..

With the reactor off, the foil was inserted into its holder. The reactor was brought up to operating power in about 1 minute, and a 30-minute irradiation was timed by a stop-watch and monitored with counters. Shutting off the reactor ended the irradiation. The aluminium foil was unwound, washed in clean acetone and wrapped around an aluminium sleeve, which was slid over the β-counter. Counts were taken every 30 seconds for about 10 minutes, and then every minute for about 20 minutes more. Two or three more counts were taken at intervals of a couple of hours to determine the effective background, of which about 60% was true counter background and about 40% was due to the foil. The half-life of this latter activity was about 14 hours and presumably was caused by the $^{27}Al(n,\alpha)^{29}Na$ reaction.

The background long-lived activity and short-lived $^{27}Al(n,\gamma)^{28}Al$ activity were subtracted graphically from the total counts in 30 minutes. This left only counts caused by the $^{27}Al(n,p)^{27}Mg$ reaction. Of approximately 10^5 counts recorded for each irradiation, about 90% were due to (n,p) reaction. A systematic method of making the subtractions had been established by studying foils whose activations were much higher than the foils irradiated in the Transmission experiments.

2.4.3 Results and Conclusions

The main aim of the B.B.C. experiments was the calculation of energy-averaged inelastic cross-sections appearing in Eqn. (2.5) using the measured Transmissions. However, before inserting the Transmissions reported in Table 1 into Eqn. (2.5) corrections had to be made due to extraneous effects and counting conditions (fast neutrons not produced by the source, room scattering of source neutrons, scattering

from supports, non-threshold neutron detection, γ-ray effect, counting rate stability, etc, and to the assumptions made in deriving Eqn. (2.5) (see page 31)). Simultaneously an estimation of the final total uncertainty accompanying the measured Transmissions had to be attempted. The fact that in the real experiment the material shells surrounded the detector rather than the source does not alter the assumptions of page 31 drastically, except that the internal detector is considered now as a point non-absorbing isotropic detector and the external source is a small isotropic emitter (assumptions 1 and 2). This is justified by virtue of the reciprocity theorem which can be summarised as follows: The number of neutrons coming from an isotropic source at the centre of a spherical shell of matter, and detected in an isotropic detector outside the sphere is equal to the number of neutrons detected, if the positions of source and detector are interchanged.

In interpreting the measured Transmissions in terms of inelastic cross-sections of the material shell, B.B.C. showed that no corrections due to extraneous effects and counting conditions were necessary, and that the reported statistical uncertainty was the predominant source of error associated with the experimental Transmissions. A closer and more detailed examination of this kind of error, imposed by the nature and aims of our work, is given in the following section. On the other hand, B.B.C. corrected the Transmissions in Table 1 for deviations from the ideal experimental conditions imposed by the above-mentioned assumptions in deriving Eqn. (2.5). These corrected values were then used in deducing the inelastic cross-sections given in the same Table. Also, uncertainties in these corrections contributed to the final error accompanying the inelastic cross-section.

Table 1 summarizes the results of B.B.C. experiments for the most important cases studied and for materials included in the ENDF/B-IV library. (Evaluated Nuclear Data File, see Chapter 2 for more details.)

It must be pointed out that the inelastic cross-sections, reported in column 3 for each reaction, are not the average total inelastic cross-sections for neutrons with energy above the effective threshold as defined in Eqn. (2.6), but average cross-sections for inelastic collisions leading to energies below the effective energy threshold of the detector. This happens because for many elements considered there is inelastic scattering without sufficient energy loss to place the resultant neutron below the energy threshold. Thus σ_{in} in column 3 gives only a lower limit to the total average inelastic cross-section. Figure 5 attributes the fission spectrum and response functions of the threshold detectors employed. Figure 6 depicts an apparent spectrum shape found as the product $N(E)\sigma^{D}(E)$ over which the cross-sections are averaged.

Comparing the inelastic cross-sections derived using Eqns. (2.2) and (2.5). (columns 2 and 3 for each reaction), it is apparent that the evaluation of the data with multiple scattering theory gives essentially one cross-section independent of shell thickness, while the exponential theory does not.

It is also evident from this comparison that one must make an effort to correct for multiple scattering of neutrons in shells even a few tenths of a mean free path thick, if accuracies of a few per cent are desired.

The most striking result of the measurements with ^{237}Np, ^{238}U and $^{27}A\ell$ counters is that the inelastic cross-section increases strongly as the threshold is raised. For instance, iron has inelastic cross-sections of 0.28, 0.69 and 1.2 barns, respectively, as measured by the three counters. This behaviour of σ_{in} with neutron energy is entirely reasonable; at low energies only a few levels are available for inelastic scattering, while for high energies there are many.

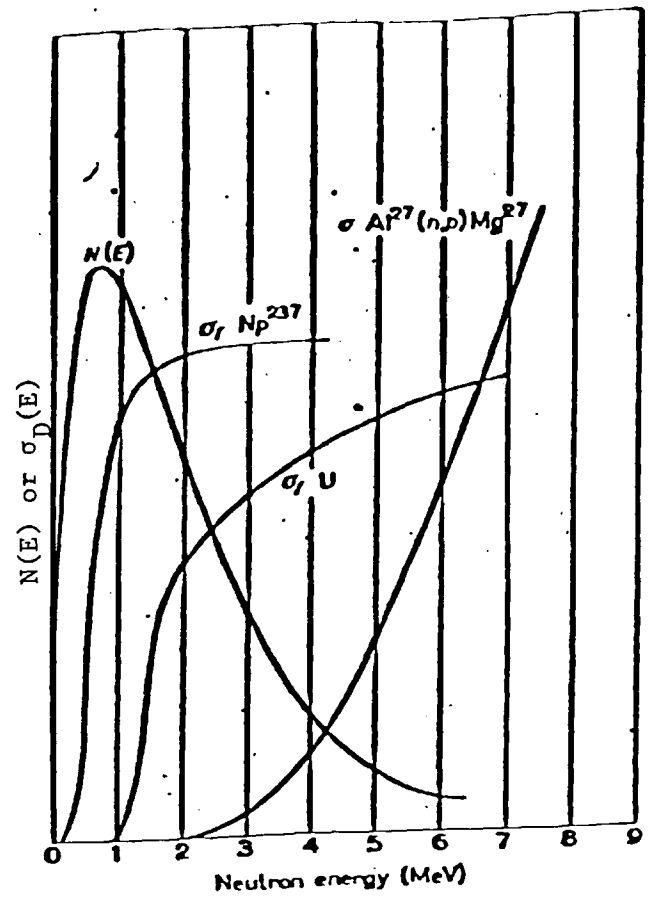


FIGURE 5 FISSION SPECTRUM AND DETECTOR RESPONSES

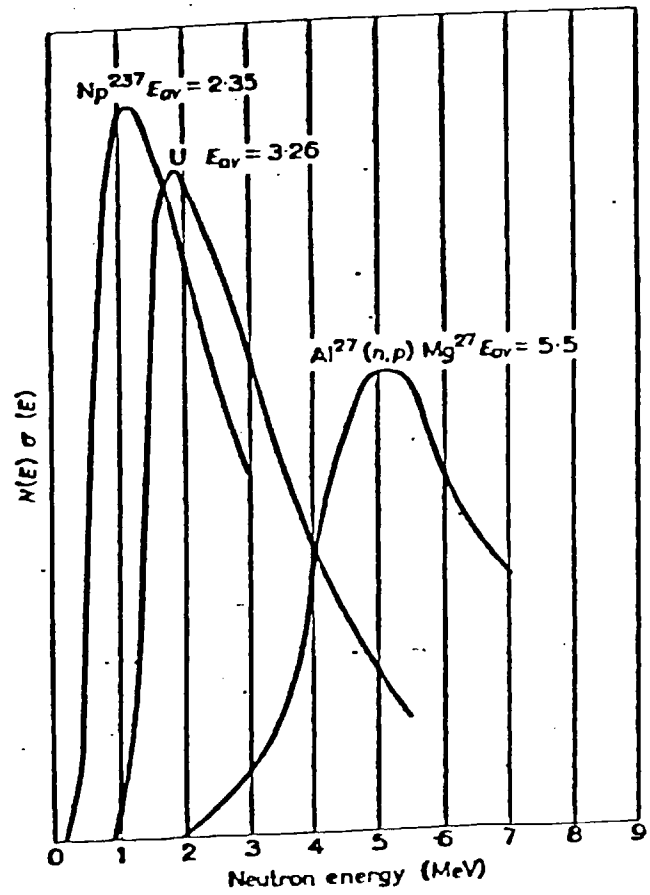


FIGURE 6 FISSION SPECTRUM X DETECTOR RESPONSE CURVES

2.5 UNCERTAINTY ANALYSIS OF B.B.C. EXPERIMENTS

In the present method of analysis the measured Transmissions are not treated as experimental data from which, by applying a proper theoretical model, energy-averaged inelastic cross sections will be explicitly deduced.

In this work the experimental Transmissions are considered as certain functionals depending on the source spectrum, material and dosimetry cross section data, viz:

$$T = T(\vec{\phi}, \vec{\sigma}_i, \vec{P}_i, \vec{\sigma}_D) \quad i = 1,2....NOR \tag{2.8}$$

where:

$\vec{\phi}$ = a vector representing the source spectrum

$\vec{\sigma}_i$ = a vector representing the material cross section for reaction i

$\vec{P}_i$ = a vector of parameters describing the angular and/or energy distribution of secondary neutrons for reaction i, if any

$\vec{\sigma}_D$ = a vector representing the response function of the detector.

Eqn. (2.8) shows that the measured Transmissions contain some information concerning the material and dosimetry cross section data of the isotopes and threshold detectors used.

It is this piece of information in which we are particularly interested, and which we shall try to evaluate in the following chapters. Something analogous can be said regarding the cross section data files being used in neutronic calculations:

In their multigroup structure, they contain some information about the cross-sections which are, in fact, unknown.

The purpose of this work is to examine the compatibility of these two pieces of information; in cases of large deviations an improvement of our knowledge about a certain cross-section may be attempted by combining these two sources of information.

The attainment of the above mentioned goals requires the calculation of the Transmissions using existing cross-section data files, and a transport code solving the Boltzmann Equation for the system under consideration. It is obvious that the ideal conditions and assumptions, under which the Boltzmann Equation is solved, must adequately represent the real experimental conditions, if a comparison between experimental and calculated Tranmissions is to be of any use.

As it will be seen in the following chapter, Transmissions can be calculated for fission-spectrum neutrons isotropically emitted from a rectangular surface. In its vicinity a small cylindrical isotropic detector is located which occasionally is sourrounded by spherical shells of varying thickness and composition.

From the detailed description of the B.B.C. experiments, given in this chapter, the real experimental conditions can easily be assessed and compared with the ideal conditions outlined above. Corrections and uncertainty adjustments must be applied to the Transmissions reported in Table 1 to match ideal and real conditions. This procedure should result in new values of Transmissions accompanied by their final uncertainties. These two sets of data will fully describe our experimental knowledge of the system being subjected to theoretical investigation in the following chapter.

2.5.1 Comparison of Ideal and Real Conditions of B.B.C. Experiments - Effect on Transmission

The assessment of the experimental arrangements, counting

techniques, special measures and precautions undertaken in B.B.C. work for an accurate measurement of Transmissions, will show that the reported Transmissions constitute reliable quantities with their statistical uncertainty comprising the major part of the final error associated with these values. We shall discuss in this section supplementary experimental work and additional calculations undertaken by B.B.C. in backing the above statement.

A primary comparison between ideal experimental conditions as outlined in the previous section and the real ones, as drawn from the detailed description of the experiments, reveals two major differences which may affect the Transmissions: (a) In the real experiment the neutron flux as incident on the material shells and/or the detector differs in geometry, energy and angular dependence from that of a fission plate source characterizing the ideal situation and (b) the threshold detectors used in the experiments are not isotropic as required by the ideal conditions. Simultaneously, sources of errors for the measured Transmissions are recognised due to the statistical nature of the counting techniques and the uncertainties accompanying counting rates stabilities and any kind of corrections applied to them for the aforementioned differences.

(a) Deviations from the Fission Plate Source

A thorough examination of the experimental conditions gives the following list of factors which are responsible for the discrepancies between ideal and real neutron spectrum, as detected by the material shells and/or the detectors, and which may affect the Transmissions:

1. Neutron collisions in uranium and aluminium-boron plate
2. Neutron collisions in the collimator (aluminium box, 10 inches long, containing boron-10)
3. Presence of fast neutrons not produced by the source.
4. Source neutrons scattered on the floor, reactor face and

cone support

5. γ-fission in threshold detectors

6. Photo-neutron production in the sphere.

The first four factors essentially constitute a "background" of uncertain spectrum and geometry and generally alter the source spectrum from that emitted isotropically from the fission plate. The effect of the energy composition of this background on the measured Transmissions can, in principle, be assessed from the impact of uncertainties in fission spectrum on the calculated Transmissions. Such a study is undertaken in Chapter 4 and shows that considerably large uncertainties in the fission spectrum do not affect the calculated Transmission. As far as the unknown geometry of this background is concerned, it is shown in Chapter 3 that for the same shell the calculated Transmission is a decreasing function of the detector-to-source distance, asymptotically reaching a constant value for distances greater than about 28 cm. Therefore, the geometry of the background becomes important for relatively short source-to-detector distances for which its effect on Transmission will be negligible since it constitutes, in these cases, only a tiny portion of the source neutrons.

In the light of the above arguments and taking into account that (a) less than 2% of the fast neutrons produced by the ^{235}U plate suffered collisions in the uranium and aluminium-boron cover before escaping (b) not more than about 1% of the neutrons reaching the detector resulted from single scattering in the collimator and (c) the amount of the fast neutrons not produced by the source was around 1% for all source-to-detector distances, we understand that the first three factors listed above have no considerable effect on the measured Transmissions.

Detailed studies of the background comprising the source neutrons scattered on the floor, reactor face and cone support and its effect on T were undertaken by B.B.C. (ref. 3, pages 21-23). They

measured and calculated a relative background of about 6% at 20 inches from the source for the ^{235}U detector and 8.5% for the ^{237}Np one. Since the neutron flux coming directly from the source will fall off approximately as the inverse of the square of the distance, it is understood that at 10 inches from the source, where almost all the measurements listed in Table 1 were taken, the relative background will be several times smaller and consequently, according to the argument mentioned above, its effect on the Transmissions is rather unimportant. B.B.C. measured directly the Transmission of the background at 20 inches from the source while the counter and the entire sphere were shielded from the ^{235}U source by bulk shadow shields. They found it within 2% of that obtained with no shadow shield.

This experimental information is enough to give us a quantitative relation between measured Transmission and that due only to source neutrons. If we denote by I the neutron flux at the centre of the detector with the sphere off, made up from the flux due to source neutrons I_s, and that due to background I_B, by I' the neutron flux with the sphere on, and with T_M representing the measured Transmission, T that due to source neutrons and T' the Transmission of the background, then the following relations hold for the ^{238}U detector:

$$\begin{aligned} I &= I_S + I_B \\ \frac{I_B}{I} &= 0.06 \\ \frac{I_S}{I} &= 0.94 \\ I' &= TI_S + T'I_B \\ T_M &= I'/I \\ T' &= T_M \pm 0.02\, T_M \end{aligned} \qquad (2.9)$$

from which, we easily get:

$$T = T_M \pm 0.0013\, T_M \qquad (2.10)$$

Eqn. (2.10) indicates that at 20 inches the effect of the background on

the measured Transmissions is not more than 0.13%. This effect is expected to be several times smaller at 10 inches from the source and, therefore, negligibly small compared to the statistical uncertainties in Table 1. The same justification can be followed for the ^{237}Np detector, while the background in the $^{27}Al(n,p)^{27}Mg$ detector is expected to be even lower than that of the ^{238}U counter because of the shape of the fission spectrum and the positions in energy of the thresholds.

High energy γ-rays can produce photo-fission in the detectors. The two principal γ-ray sources are capture of thermal neutrons in the collimator and γ-rays accompanying fission or radiative capture in the ^{235}U source. The first was minimized as has been pointed out in paragraph 2.3.1. The second could not be avoided.
In the experimental evaluation of these effects, a low atomic-weight shadow shield was inserted between source and detector and caused an attenuation in the neutron flux by a factor of about 20, whereas the high energy γ-rays were attenuated by a factor of 2. This increased the relative number of γ-rays by a factor of about 10. Sphere Transmissions behind the shadow shield thus gave an upper limit of the relative numbers of photo-fissions in the detector. The relative number of photo-fissions in the detector with no shadow shield and no sphere was 0.000 ± 0.005 (ref. 3, p 24). With no sphere around the detector the number of photo-fissions in the ^{238}U detector was computed to be around 0.1% of the number of neutron fissions (ref. 3, p 24). Both values suggest that the effect of the photo-fissions in the detector on the measured Transmissions can be considered as negligible since, additionally, there is a tendency to cancel out.

The γ-n cross-section of many of the sphere materials is not zero at the γ-ray energies involved. Some of the neutrons produced are above the counter thresholds. However, the contribution is less than 0.01% in Transmission (ref. 3, p 24). Consequently neither

correction is required, nor is subsequent error generated assuming uncertainty in the correction of not more than 100%.

Finally, spurious counter effects, such as dead-time counting losses, γ-ray pile-up pulses, α-pulses, and temperature effects have been looked for and no observable effect was shown in the measured Transmission, at least for the cases reported in Table 1 and used in the testing of existing cross-section data files.

(b) Effect of the Asymmetry of the Detectors

The fission spiral detectors and aluminium foils used in the experiments were not isotropic as required by both B.B.C. analysis (Eqn. (2.5)) and our ideal conditions, set up in section 2.4.1, for which calculated Transmissions are given in the next chapter.
Let us assume that our detector has a reduced efficiency Δ over a solid angle Ω and an efficiency of unity over a solid angle (1 - Ω). If we denote by $T_{(away)}$ the Transmission with the reduced efficiency region of the neutron detector directed away from the source (no neutrons enter through this region with the sphere removed) then the following relation between $T_{(away)}$ and T, as given by Eqn. (2.5), holds: (Ref 2, page 296).

$$T_{(away)} = T-(1-e^{-\Sigma_{tr}X})\left[\frac{\sigma_{et}}{\sigma_{tr}} P_1+(1-P_1) \frac{\sigma_{et}}{\sigma_{tr}} P_2 + \frac{(1-P_1)(1-P_2)\sigma_{et}^2 P_m}{\sigma_{tr}(\sigma_{in} + \sigma_{et} P_m)}\right](1-\Delta)\Omega \qquad (2.11)$$

If we accept that the Transmissions Tm, given in Table 1 coincide with $T_{(away)}$ (it is not clear from the B.B.C. work) and since T corresponds to an isotropic detector, we can then establish a correction factor C_T, applicable to T_m and accounting for the detector asymmetry, by the following relations:

$$C_T = (1-e^{-\Sigma_{tr}X}) \frac{\sigma_{et}}{\sigma_{tr}} \left[P_1 + (1-P_1) \frac{\sigma_{et}}{\sigma_{tr}} P_2 + \frac{(1-P_1)(1-P_2)\sigma_{et}^2 P_m}{\sigma_{tr}(\sigma_{in}+\sigma_{et}P_m)} \right] (1-\Delta)\Omega \tag{2.12}$$

$$T_E = T_m + C_T \tag{2.13}$$

Where T_E is the corrected experimental Transmission. Values of Δ and Ω were measured for all the detectors used, both directly by placing the detector in a beam of fast neutrons and counting with the detector oriented at several angles with respect to the direction of the fast beam, and by using Eqn (2.11) and an analogous one giving $T_{(forward)}$ (Ref 2, page 296). Both methods agreed with the following values: (Ref 3, page 25).

^{238}U detector: $\Omega = 0.1$ $\Delta = 0.95 \pm 0.004$

^{237}Np " $\Omega = 0.1$ $\Delta = 0.976 \pm 0.010$

aluminium foils (properly cut) - $\Delta = 1.00 \pm 0.01$

We calculated correction factors, C_T, for both ^{238}U and ^{237}Np detectors for almost all the cases listed in Table 1, using Eqn. (2.12) with σ_{tr}, σ_{et} and σ_{in} taken from B.B.C. work (Ref 4, pages 149, 153 and 155), and P_1, P_2, P_m from graphs included in B.B.C. work (Ref 2, pages 283, 286) and given in Figures 7, 8 and 9. Because of uncertainties in Δ and Ω, a 50% error will accompany these corrections.

Table 2 summarizes the results of our calculations together with the corrected values of Transmissions T_E, and their uncertainties δT_1 due only to the detector asymmetry correction. In this Table and the graphs mentioned above, r_1 represents the sphere inside radius while r_2 the sphere outside radius. We note that in some cases (thick shells of Fe, Pb for ^{238}U detector) the calculated correction is quite high reaching the statistical uncertainties of Table 1.

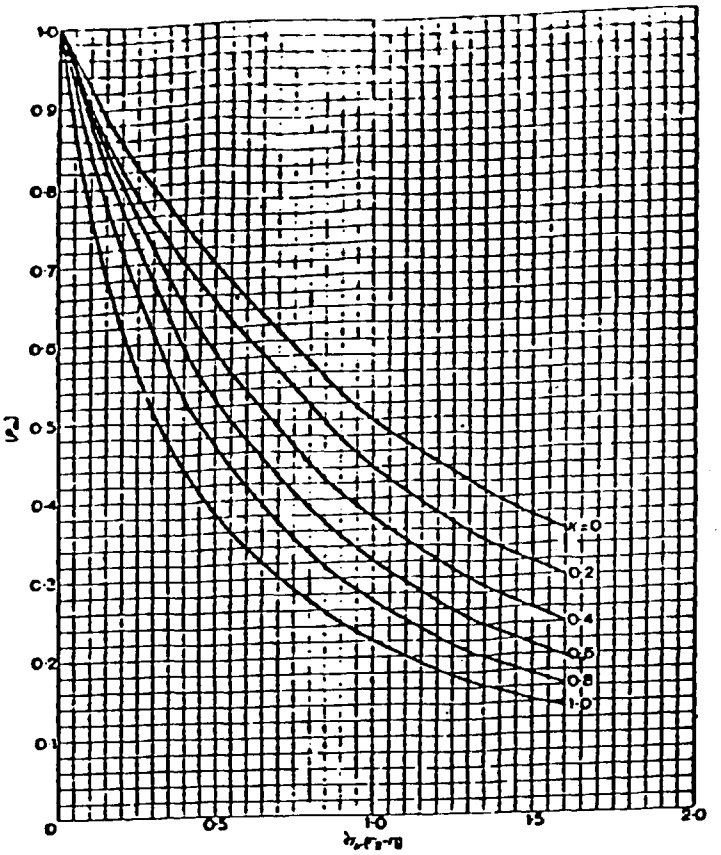


FIGURE 7 P_1 ESCAPE PROBABILITY

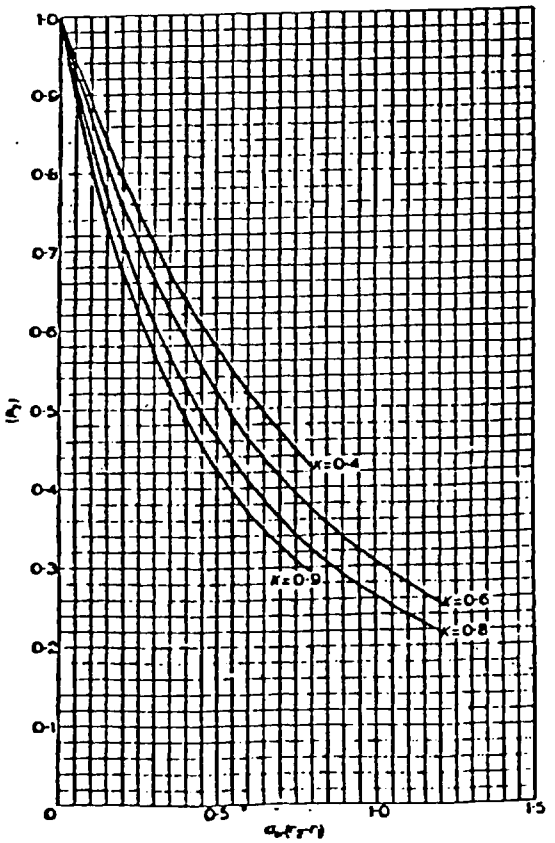


FIGURE 8 P_2 ESCAPE PROBABILITY

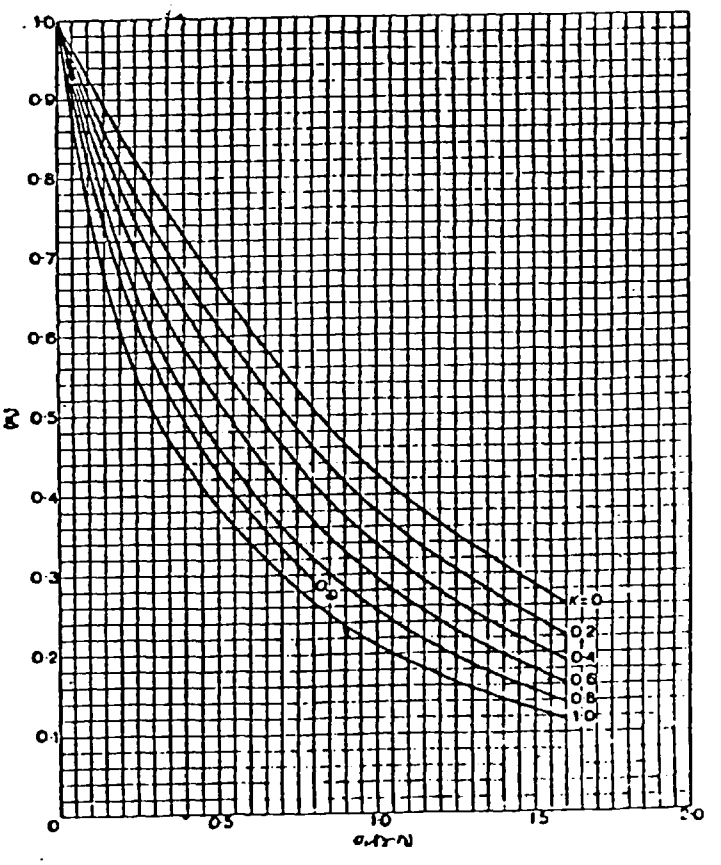


FIGURE 9 P_m ESCAPE PROBABILITY

TABLE 2. CORRECTED TRANSMISSIONS FOR THE DETECTOR'S ANGULAR ANISOTROPY.

	MATERIAL	DETECTOR	T_M	DATA									C_T	T_E	δT_1
				$X = r_2 - r_1$ cm	$K = r_1/r_2$	$\Sigma_{tr} X$	σ_{tr} barns	σ_{et} barns	σ_{in} barns	P_1	P_2	P_m			
1.	Al	^{238}U	0.8953	3.841	0.62	0.39	1.68	1.36	0.319	0.590	0.580	0.580	0.0012	0.8965	0.0006
2.	Al	^{237}Np	0.9665	3.841	0.62	0.48	2.07	1.98	0.087	0.540	0.530	0.530	0.0008	0.9673	0.0004
3.	Ti	^{238}U	0.8940	2.546	0.55	0.35	2.47	1.90	0.563	0.640	0.630	0.630	0.0010	0.8950	0.0005
4.	Ti	^{237}Np	0.9644	2.546	0.55	0.32	2.24	2.05	0.187	0.650	0.640	0.640	0.0006	0.9650	0.0003
5.	V	^{238}U	0.9298	1.320	0.58	0.22	2.34	1.76	0.575	0.760	0.750	0.740	0.0007	0.9305	0.0004
6.	V	^{237}Np	0.9727	1.320	0.58	0.22	2.35	2.12	0.224	0.760	0.750	0.740	0.0004	0.9731	0.0002
7.	Fe	^{238}U	0.8680	1.900	0.70	0.35	2.13	1.44	0.686	0.660	0.590	0.590	0.0008	0.8688	0.0004
8.	Fe	^{238}U	0.7120	4.111	0.60	0.74	2.13	1.44	0.686	0.410	0.390	0.390	0.0012	0.7132	0.0006
9.	Fe	^{238}U	0.4678	9.162	0.09	1.65	2.13	1.44	0.686	0.350	0.270	0.250	0.0016	0.4694	0.0008
10.	Fe	^{237}Np	0.9450	1.900	0.70	0.32	2.01	1.73	0.276	0.600	0.600	0.600	0.0005	0.9455	0.0003
11.	Fe	^{237}Np	0.8616	4.111	0.60	0.70	2.01	1.73	0.276	0.420	0.400	0.400	0.0009	0.8625	0.0005
12.	Fe	^{237}Np	0.7237	9.162	0.09	1.56	2.01	1.73	0.276	0.370	0.230	0.270	0.0013	0.7250	0.0007
13.	Ni	^{238}U	0.8370	2.070	0.69	0.42	2.26	1.54	0.713	0.560	0.550	0.550	0.0009	0.8379	0.0005
14.	Ni	^{237}Np	0.9284	2.070	0.69	0.44	2.38	2.10	0.276	0.550	0.540	0.540	0.0007	0.9291	0.0004
15.	Cu	^{238}U	0.6483	4.115	0.59	0.82	2.35	1.45	0.900	0.390	0.380	0.370	0.0011	0.6494	0.0006
16.	Cu	^{237}Np	0.8409	4.115	0.59	0.92	2.64	2.34	0.304	0.350	0.340	0.330	0.0010	0.8419	0.0005
17.	Zr	^{238}U	0.8429	3.304	0.42	0.43	3.06	2.09	0.960	0.630	0.630	0.620	0.0010	0.8439	0.0005
18.	Zr	^{237}Np	0.9409	3.304	0.42	0.56	3.99	3.68	0.302	0.550	0.540	0.530	0.0009	0.9418	0.0005
19.	W	^{238}U	0.8503	1.065	0.83	0.25	3.82	1.58	2.230	0.650	0.650	0.620	0.0003	0.8506	0.0002
20.	W	^{237}Np	0.9200	1.065	0.83	0.25	3.69	2.61	1.080	0.650	0.650	0.620	0.0003	0.9203	0.0002
21.	Sn	^{238}U	0.8380	3.503	0.65	0.38	3.00	1.87	1.120	0.580	0.580	0.570	0.0008	0.8388	0.0004
22.	Sn	^{238}U	0.6938	7.009	0.31	0.77	3.00	1.87	1.120	0.480	0.470	0.460	0.0012	0.6950	0.0006
23.	Sn	^{237}Np	0.9430	3.503	0.65	0.45	3.51	3.14	0.369	0.540	0.540	0.530	0.0007	0.9437	0.0004
24.	Pb	^{238}U	0.9106	3.124	0.69	0.40	3.84	3.12	0.712	0.560	0.560	0.560	0.0012	0.9118	0.0006
25.	Pb	^{238}U	0.8160	6.243	0.38	0.80	3.84	3.12	0.712	0.440	0.420	0.420	0.0018	0.8178	0.0009
26.	Pb	^{237}Np	0.9783	3.124	0.69	0.43	4.16	3.94	0.208	0.550	0.550	0.550	0.0008	0.9791	0.0004

Another possible source of error in the Transmissions is the uncertainty associated with the counting-rate stabilities of the ^{237}Np and ^{238}U detectors. These uncertainties were, as has already been reported, 0.05% for the ^{238}U detector and 0.09% for the ^{237}Np. These are responsible for 0.07% and 0.12% errors in Transmissions.

2.5 EXPERIMENTAL TRANSMISSIONS AND THEIR FINAL UNCERTAINTIES

The measured values of Transmissions being corrected for the detectors' angular anisotropy (column 14 in Table 2) will constitute, hereinafter, the experimental Transmissions we shall make use of in later chapters.

As far as the final uncertainty accompanying these values and its distribution is concerned, we realize that from all the possible sources of error encountered so far, the following uncertainties are worth considering:

I. The statistical uncertainty, given as standard deviation $\Delta T'$ in Table 1, which constitutes the predominant source of error in the Transmissions.

II. The uncertainty δT_1 (see Table 2) due to the correction for the detectors' angular anisotropy.

III. Uncertainty δT_2 due to the counting rate instabilities of the ^{237}Np and ^{238}U detectors. This uncertainty, as has already been seen, amounts to 0.07% of Transmission for the ^{238}U detector and 0.12% for the ^{237}Np.

IV. An uncertainty δT_3 is established to account for any background effects on Transmissions. According to the analysis of paragraph 2.4.2, uncertainties in Transmissions of 0.04% for the ^{238}U detector and 0.06% for the ^{237}Np must be considered quite conservative for "distance to source" equal to 25.40 cm. No uncertainty due to background effects was established for $^{27}A\ell(n,p)^{27}Mg$ reaction both for reasons mentioned earlier and because the statistical uncertainty of these Transmissions is very high. The second reason is responsible for overlooking any other source of uncertainty which may affect the $^{27}A\ell$ Transmissions. The corrected experimental Transmissions together with the uncertainties $\Delta T'$, δT_1, δT_2, δT_3 are given in Table 2A.

TABLE 2A. CORRECTED TRANSMISSIONS AND COMPONENTS OF THEIR FINAL UNCERTAINTIES.

	MATERIAL	DETECTOR	T_E	$\Delta T'$	δT_1	δT_2	δT_3	ΔT
1.	Al	^{238}U	0.8965	0.0023	0.0006	0.0006	0.0003	0.0025
2.	Al	^{237}Np	0.9673	0.0030	0.0004	0.0011	0.0005	0.0033
3.	Ti	^{238}U	0.8950	0.0022	0.0005	0.0006	0.0003	0.0024
4.	Ti	^{237}Np	0.9650	0.0040	0.0003	0.0011	0.0005	0.0042
5.	V	^{238}U	0.9305	0.0026	0.0004	0.0006	0.0004	0.0027
6.	V	^{237}Np	0.9731	0.0035	0.0002	0.0011	0.0005	0.0037
7.	Fe	^{238}U	0.8688	0.0017	0.0004	0.0006	0.0003	0.0019
8.	Fe	^{238}U	0.7132	0.0018	0.0006	0.0005	0.0003	0.0020
9.	Fe	^{238}U	0.4694	0.0040	0.0008	0.0003	0.0002	0.0041
10.	Fe	^{237}Np	0.9455	0.0030	0.0003	0.0011	0.0006	0.0033
11.	Fe	^{237}Np	0.8625	0.0030	0.0005	0.0010	0.0005	0.0033
12.	Fe	^{237}Np	0.7250	0.0042	0.0007	0.0008	0.0004	0.0044
13.	Ni	^{238}U	0.8379	0.0020	0.0005	0.0006	0.0003	0.0022
14.	Ni	^{237}Np	0.9291	0.0030	0.0004	0.0011	0.0005	0.0033
15.	Cu	^{238}U	0.6494	0.0016	0.0006	0.0005	0.0002	0.0018
16.	Cu	^{237}Np	0.8419	0.0031	0.0005	0.0010	0.0005	0.0033
17.	Zr	^{238}U	0.8439	0.0028	0.0005	0.0006	0.0003	0.0030
18.	Zr	^{237}Np	0.9418	0.0035	0.0005	0.0011	0.0005	0.0037
19.	W	^{238}U	0.8506	0.0018	0.0002	0.0006	0.0003	0.0020
20.	W	^{237}Np	0.9203	0.0030	0.0002	0.0011	0.0005	0.0033
21.	Sn	^{238}U	0.8388	0.0022	0.0004	0.0006	0.0003	0.0024
22.	Sn	^{238}U	0.6950	0.0020	0.0006	0.0005	0.0003	0.0022
23.	Sn	^{237}Np	0.9437	0.0030	0.0004	0.0011	0.0005	0.0033
24.	Pb	^{238}U	0.9118	0.0013	0.0006	0.0006	0.0003	0.0015
25.	Pb	^{238}U	0.8178	0.0018	0.0009	0.0006	0.0003	0.0020
26.	Pb	^{237}Np	0.9791	0.0040	0.0004	0.0011	0.0006	0.0042

In order to calculate the final uncertainty of Transmissions in terms of the partial uncertainties we proceed as follows:
The effect of the background neutrons, at least for distances to source equal to 25.40 cm, can be interpreted as additional uncertainties to the fission spectrum, $\vec{\phi} = (\phi_1, \phi_2 .. \phi_K)$. On the other hand uncertainties due to the angular anisotropy of detectors and to the instability of counting-rates can be expressed in terms of uncertainties in quantities $\vec{x} = (x_1, x_2, x_M)$ which describe this angular anisotropy (e.g. Δ,Ω) and in quantities $\vec{y} = (y_1, y_2 ... y_L)$ which determine the counting-rate stability (Ref. 3, page 18).
Hence as far as the determination of the final uncertainty is concerned, the experimental Transmission can be considered as a function of C_1, C_2, $\vec{\phi}$, $\vec{x}$, $\vec{y}$, that is:

$$T = T(C_1, C_2, \vec{\phi}, \vec{x}, \vec{y}) \qquad (2.14)$$

where C_1, C_2 are the counting rates for "sphere on" and "sphere off" cases, correspondingly. (They are included as independent variables in the above function because of their statistical nature). For clarity and convenience, we represent all the variables in Eqn. (2.14) as components of a vector $\vec{\theta}$, that is:

$$T = T(\vec{\theta}) \qquad (2.15)$$

where $\vec{\theta} = (\theta_1, \theta_2 ..... \theta_N)$

and $N = K + M + L + 2$

Now if the true values (in practice estimates of these quantities are usually used) of θ_i are θ_i^* and the quantities $(\theta_i - \theta_i^*)$ are small, then it can be proved that: (Ref 11 , pages 53-54).

$$\text{var}T = \sum_{i=1}^{N} \sum_{j=1}^{N} \left[\left. \frac{\partial T(\vec{\theta})}{\partial \theta_i} \right|_{\vec{\theta}=\vec{\theta}^*} V_{ij} \left. \frac{\partial T(\vec{\theta})}{\partial \theta_j} \right|_{\vec{\theta}=\vec{\theta}^*} \right] \qquad (2.16)$$

where: $V_{ij} = E\left[(\theta_i - \theta_i^*)(\theta_j - \theta_j^*)\right]$

and the notation $E[\quad]$ denotes the expectation value (mean) of the quantity enclosed in the square brackets.

Furthermore, if we recognise the variance of a quantity as the square of its standard error ($VarX = (\Delta X)^2$) and if the various errors are uncorrelated (i.e. $Vij = 0$, for any i,j with $i \neq j$, as is valid for the problem under discussion, see page 292) then Eqn. (2.16) reduces to:

$$(\Delta T)^2 = \sum_{i=1}^{N} \left[\frac{\partial T(\vec{\theta})}{\partial \theta_i}\Big|_{\theta_i=\theta_i^*} \Delta\theta_i\right]^2$$

or, in an explicit form:

$$(\Delta T)^2 = \sum_{i=1}^{2} \left(\frac{\partial T}{\partial C_i}\right)^2 (\Delta C_i)^2 + \sum_{i=1}^{K} \left(\frac{\partial T}{\partial \phi_i}\right)^2 (\Delta \phi_i)^2 + \sum_{i=1}^{M} \left(\frac{\partial T}{\partial x_i}\right)^2 (\Delta x_i)^2 + \sum_{i=1}^{L} \left(\frac{\partial T}{\partial y_i}\right)^2 (\Delta y_i)^2$$

(2.17)

In the above expression ΔC_1, ΔC_2 are the statistical uncertainties (standard deviations) of the counting-rates. However, we are not going to apply Eqn. (2.17) in estimating the final uncertainty ΔT mainly because most of the derivatives in this formula cannot be calculated, since the function $T = T(C_1, C_2, \vec{\phi}, \vec{x}, \vec{y})$ is unknown, and because most of the partial errors are also unknown. Instead we shall make use of the collective uncertainties in T attributable to the four main causes and given in Table 2A, viz:

$$\sum_{i=1}^{2} \left(\frac{\partial T}{\partial C_i}\right)(\Delta C_i)^2 = (\Delta T')^2$$

$$\sum_{i=1}^{K} \left(\frac{\partial T}{\partial \phi_i}\right)^2(\Delta \phi_i)^2 \simeq (\delta T_3)^2$$

$$\sum_{i=1}^{M} \left(\frac{\partial T}{\partial x_i}\right)^2(\Delta x_i)^2 \simeq (\delta T_1)^2$$

$$\sum_{i=1}^{L} \left(\frac{\partial T}{\partial y_i}\right)^2(\Delta y_i)^2 \simeq (\delta T_2)^2$$

Eqn. (2.17) takes then the final approximate form:

$$(\Delta T)^2 \simeq (\Delta T')^2 + (\delta T_1)^2 + (\delta T_2)^2 + (\delta T_3)^2 \qquad (2.18)$$

Values of ΔT have been calculated according to Eqn (2.18) for all the cases included in Table 2A and are tabulated in the last column of the same Table. We notice that the final uncertainties slightly differ from the corresponding statistical ones. Therefore we can consider that the measured Transmissions follow a normal distribution whose mean value is the corrected experimental value T_E and standard deviation the quantity ΔT calculated via Eqn. (2.18).

Table 3 summarizes our experimental knowledge about the Transmissions in spherical shells of different materials and thicknesses, for a thermal-fission source and three different threshold isotropic detectors.

These experimental Transmissions are meant to follow normal distributions whose means and standard deviations are given in the same Table. The "distance to source" for all these cases is 25.40 cm.

TABLE 3. MEAN VALUES OF EXPERIMENTAL TRANSMISSIONS AND THEIR STANDARD DEVIATIONS.

CASE	MATERIAL	SPHERE OUTSIDE RADIUS cm	SHELL THICKNESS cm	TRANSMISSIONS		
				$^{27}Al(n, P)^{27}Mg$ 4.4 MeV	$^{238}U(n, f)$ F.P. 1.5 MeV	$^{237}Np(n, f)$ F.P. 0.6 MeV
1.	Al	10.16	3.84	0.7901 ± 0.0065	0.8965 ± 0.0025	0.9673 ± 0.0033
2.	Ti	5.71	2.54	-	0.8950 ± 0.0024	0.9650 ± 0.0042
3.	V	3.20	1.32	-	0.9305 ± 0.0027	0.9731 ± 0.0037
4.	Fe	6.35	1.90	0.7938 ± 0.0071	0.8688 ± 0.0019	0.9455 ± 0.0033
5.	Fe	10.16	4.11	-	0.7132 ± 0.0020	0.8625 ± 0.0033
6.	Fe	10.16	9.16	-	0.4694 ± 0.0041	0.7250 ± 0.0044
7.	Ni	6.65	2.07	0.7398 ± 0.0060	0.8379 ± 0.0022	0.9291 ± 0.0033
8.	Cu	10.16	2.06	0.7460 ± 0.010	-	-
9.	Cu	10.16	4.12	-	0.6494 ± 0.0018	0.8419 ± 0.0033
10.	Zr	5.71	3.30	0.7736 ± 0.0080	0.8439 ± 0.0030	0.9418 ± 0.0037
11.	W	6.28	1.06	0.8288 ± 0.0066	0.8506 ± 0.0020	0.9203 ± 0.0033
12.	Sn	10.16	3.50	0.7524 ± 0.0060	0.8388 ± 0.0024	0.9437 ± 0.0033
13.	Sn	10.16	7.01	-	0.6950 ± 0.0022	-
14.	Pb	10.16	3.12	0.7727 ± 0.014	0.9118 ± 0.0015	0.9791 ± 0.0042
15.	Pb	10.16	6.24	-	0.8178 ± 0.0020	-

2.7 REASONS FOR RE-EVALUATING B.B.C. EXPERIMENTS

Results of experiments undertaken 25 years ago are going to be re-analysed in the following chapters and employed in testing of existing modern nuclear data files. This apparent contradiction indicates that these experiments contain reliable information not being used so far, which is both appropriate and valuable in checking and even improving nuclear data files.

We shall reason on the points made above and hence we shall justify the choice of B.B.C. experiments for our work. Despite their "age" these experiments are characterized, as we have seen, by some very important advantages which make them exceptionally appropriate and rather unique amongst similar experiments for such a kind of analysis. We summarize these points:

(1) They are of single-material and simple-geometry, that is, clean "benchmark" experiments with the important consequence of very small modelling and calculational errors in their theoretical formulation. This, as will be seen, is of great significance in interpreting discrepancies between experimental and calculated values.

(2) The measured quantity, that is the Transmission, is accompanied by an uncertainty which is small and follows a normal distribution. Both these characteristics, attained through special precautions and measures in both setting up and counting conditions, fulfil the requirements and enhance the standards of a consistency analysis between experimental and calculated Transmissions. The experiments are also documented in sufficient detail to make a re-analysis possible.

(3) Radioactivation and fission detectors were exclusively used in entire contrast with other spherical shell measurements, where proportional counters and organic scintillators were mainly employed. (The most important of these experiments have been reviewed in section

2.2). This makes possible the formulation of the response function of these detectors in terms of the reaction cross-sections used as monitors, (dosimetry cross-sections) and consequently, the calculation of Transmissions. Also the source used was the ^{235}U fission spectrum whose characteristics are now well known. These facts reveal the uniqueness of B.B.C. experiments as far as a computational formulation and theoretical investigation can be achieved.

(4) The measured quantities happened to be sensitive to those reactions and energy ranges for which either lack of data and/or need for better accuracy still exist.

At this point the following question seems plausible: Should these experiments be so well-defined and accurate and the information they can provide so valuable, why then the deduced inelastic cross-sections have not be included in the derivation of existing data files we are intending to test? The answer to this question simply lies on the fact that the uncertainties of the derived inelastic cross-sections due to method of analysis, to different kinds of corrections (especially that for loss of energy on elastic collisions, see page **31** , assumption 4) and to the additional data entering Eqn. (2.5) are very high indeed (varying from 6% to 45%!). Therefore these very large uncertainties in conjunction with the fact that the deduced inelastic cross-sections are not the real total inelastic cross-sections averaged over a certain energy region (see page 43) inhibited their inclusion in any recent nuclear data evaluation procedure.

The practicability and usefulness of a re-evaluation of B.B.C. experiments,we are attempting in this thesis, emerge from our intentions to fully exploit the useful information incorporated in the well defined and precisely-measured Transmissions by employing a completely different method of analysis.

CHAPTER THREE

CALCULATION OF TRANSMISSIONS

3.1 INTRODUCTION

Neutronic calculations play an important role in analysing and interpreting reactor experiments, and are the vital tools of the core and shield designer in predicting their performance and in establishing the appropriate geometrical and material requirements for proper functioning.

Modelling the experimental arrangement according to specific requirements of the particular transport code used, very often involves approximations and simplifications which may cause systematic errors on the calculated quantity of unknown magnitude and distribution. A quantitative assessment of this sort of error together with those due to the calculational method itself (approximations in solving the neutron transport equation) is always necessary and of great importance, if the calculated quantity is to be of any use. Since a statistical analysis of this category of uncertainties can hardly be achieved, current practice in their evaluation is the use of different codes and/or different but equivalent formulations of the problem under investigation, and the study of their effect on the calculated quantity. In cases where these modifications have no considerable effect on the result, the calculated quantity can be considered immune to systematic errors originated in the modelling and calculational algorithm and its error will due then only to uncertainties accompanying the input data. Provided that the errors of the input data are known both in magnitute and distribution (these input data are mainly cross-sections and for most of them the "error files" are still unknown or, at least, unavailable) then an estimation of the uncertainty of the calculated quantity is, in principle, possible.

The purpose of this chapter is the calculation of the B.B.C. Transmissions using an appropriate, well-established transport code and the source and cross-section data needed for this calculation. Furthermore, a quantitative assessment of the modelling and calculational method errors is attempted. This will be proved, in following chapters, to be of crucial importance in interpreting large discrepancies between experimental and calculated Transmissions in terms of inadequacies in the nuclear data used.

In the following section the implementation of the B.B.C. experimental arrangement into the one-dimensional geometry system is given together with the main features of the discrete-ordinates method of solving the neutron transport equation. The optimization of the calculational procedure follows and some additional calculations are presented next which examine the reliability and efficiency of both the calculational scheme and geometrical configuration employed. As an independent overall test on the whole calculational process (one-dimensional geometry, discrete-ordinates approximations, group averaging etc.) MONTE-CARLO calculations follow, and DISCRETE-ORDINATES/MONTE-CARLO results are compared. The chapter concludes with the calculated Transmissions using different nuclear data files.

3.2 SCHEMATIZATION OF ONE-DIMENSIONAL SPHERICAL GEOMETRY FOR THE EXPERIMENTAL ARRANGEMENT.

Figure 10 gives a cross-sectional view of the experimental arrangement (Figures 2-4) as reformed by the ideal conditions described in the previous chapter.

In calculating the Transmissions, we shall make use of the Transport code ANISN (12) solving the neutron transport equation for one-dimensional geometries only. Hence, in order to be able to employ this code for the system of Figure 10, the isotropic cylindrical detectors must be replaced by isotropic spherical ones of the same volume and composition, and the source plate by a sort of spherical source, compatible with the specific requirements of the aforementioned code.

We shall deal with the latter modification first. The ANISN code can treat either spherical surface (= zero thickness shell) both isotropic and anisotropic sources (neutrons/cm^2/sec), or shell (= finite thickness shell) isotropic sources (neutrons/cm^3/sec). To find out which of these two ANISN options is both suitable and adequate in representing the fission plate source we proceed as follows:

Suppose that instead of the plate source we had, in Figure 10, a point source and a spherical isotropic detector (see Figure 11). Then the reaction-rates would be the same as those obtained by uniformly spreading the point source strength over a spherical surface located at the same distance from the detector. This is valid for both "sphere on" and "sphere off" cases. This simply happens because of the spherical symmetry of the system, that is, both the detection of a neutron for the "sphere off" case, and its luck after striking the material shell for the "sphere on" case, do not depend on which particular position the point source occupies on the spherical surface (A), but only on the angle Ψ (see Figure 11) by which the neutron leaves the point source.

Needless to say the above arguments are valid only if the composition and

uniformity of the material shells and the isotropy of the detectors are not questionable.

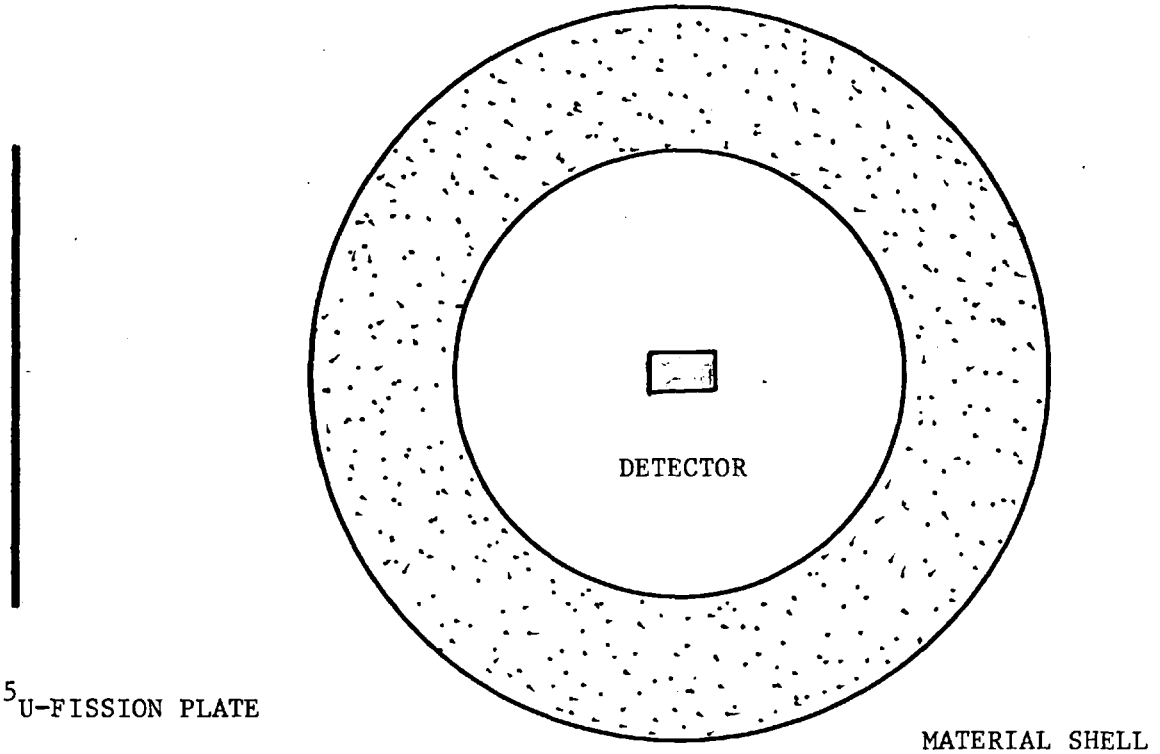


FIGURE 10. A CROSS-SECTIONAL VIEW OF THE EXPERIMENTAL ARRANGEMENT UNDER IDEAL CONDITIONS.

We can now consider the fission plate as consisting of a distribution of point sources and as shown in paragraph 3.5.3, it is equivalent to a shell source of the same strength and of thickness $S = R_5 - R_4$ (see Figure 12). In Figure 12, R_4 denotes the minimum distance between the centre of the detector and any point on the plate, (this coincides with the distance between the centre of the detector and the centre of mass of the plate), while R_5 stands for the maximum (equal to the

distance between the centre of the detector and one of the corners).

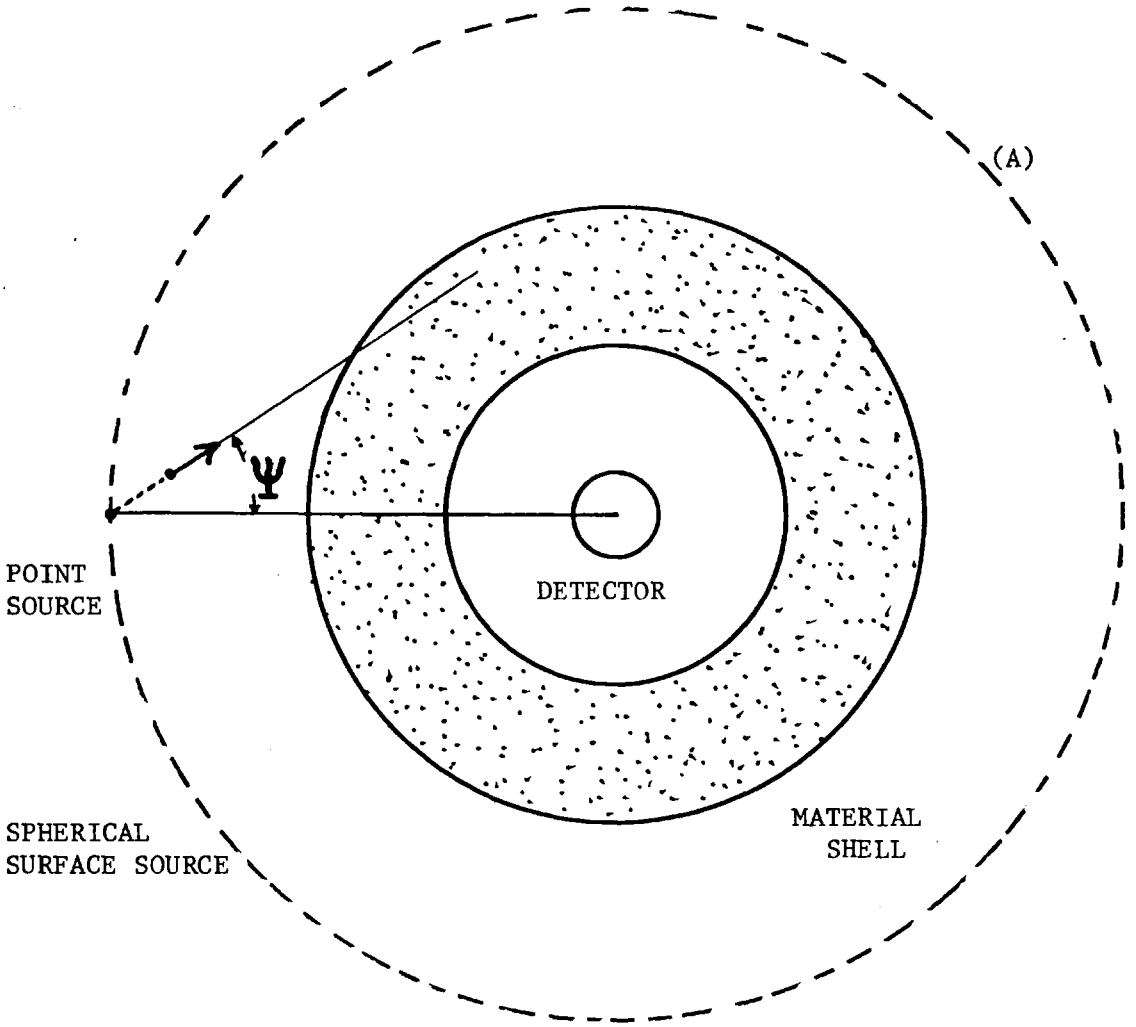


FIGURE 11 EQUIVALENCE OF POINT AND SPHERICAL SURFACE SOURCES.

The equivalence of rectangular and shell sources necessary for the validity of the above approach, together with experimental and calculated information reinforcing the aforementioned arguments are given in Section 3.5.3.

As far as the replacement of the cylindrical detector by an equivalent spherical one is concerned (see Figure 12), it will be

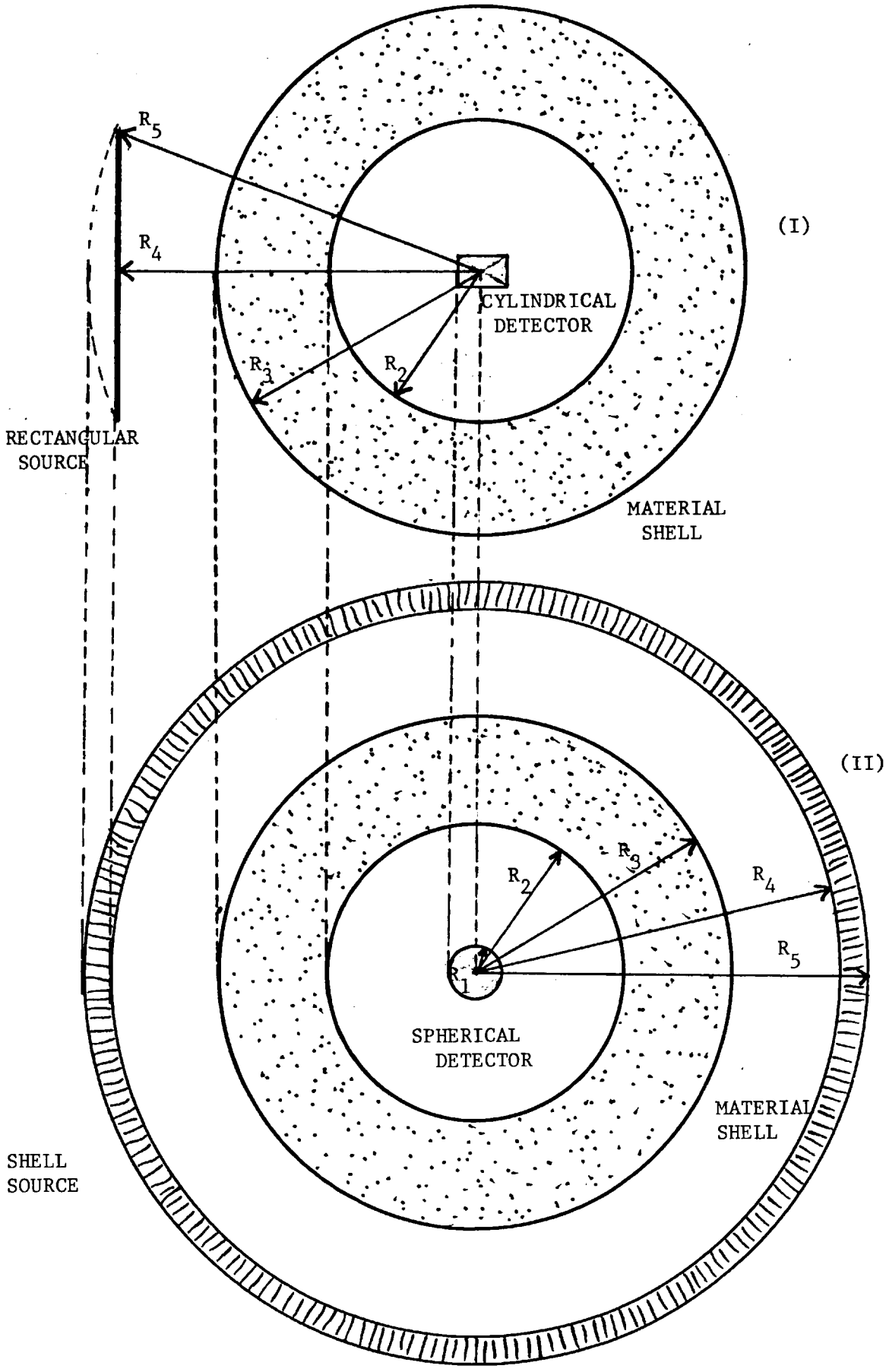


FIGURE 12. TRANSFORMATION OF THE EXPERIMENTAL ARRANGEMENT INTO ONE-DIMENSIONAL MODEL.

demonstrated in Section 3.5.2 that its relatively small size together with a diameter to height ratio approaching unity make not only the change in the shape but also its material composition unimportant. The radius R_1 in Figure 12 is that which makes the volumes of the cylindrical and spherical detectors equal.

Concluding we note that the "ideal" experimental arrangement, Figure 12(I), is equivalent to that of Figure 12(II) which possesses spherical symmetry and can be treated by one-dimensional transport codes such as ANISN.

3.3 MAIN FEATURES OF THE DISCRETE-ORDINATES METHOD

ANISN solves the neutron transport equation approximately by employing the discrete-ordinates technique. An outline of this method is given in this section.

The stationary space, angle and energy distribution of neutrons in any macroscopic medium is governed by the analytical linear integro-differential Boltzmann Equation which expresses the conservation of angular flux.

This Equation can be written as follows:

$$\vec{\Omega}.\vec{\nabla}\,\Phi(\vec{r},E,\vec{\Omega}) + \Sigma_T(\vec{r},E)\,\Phi(\vec{r},E,\vec{\Omega}) =$$

$$= S(\vec{r},E,\vec{\Omega}) + \int dE' \int d\vec{\Omega}'\; \Sigma(\vec{r},E'\rightarrow E,\vec{\Omega}'\rightarrow\vec{\Omega})\,\Phi(\vec{r},E',\vec{\Omega}') \qquad (3.1)$$

where:

$\Phi(\vec{r},E,\vec{\Omega})$ = angular flux (neutrons cm^{-2} MeV^{-1} $ster^{-1}$ sec^{-1})

$S(\vec{r},E,\vec{\Omega})$ = neutron source : external + fission (neutrons cm^{-3} MeV^{1} $ster^{-1}$ sec^{-1})

$\Sigma(\vec{r},E'\rightarrow E,\vec{\Omega}'\rightarrow\vec{\Omega})$ = differential scattering cross-section (cm^{-1} MeV^{-1} $ster^{-1}$)

$\Sigma_T(\vec{r},E)$ = position and energy-dependent macroscopic total cross-section ($cm^{-1}MeV^{-1}$)

The three space variables, plus the two angular and the energy define a six-dimensional phase space.

If we multiply Eqn (3.1) throughout by an infinitesimal volume of this phase space, then, this Equation shows that the mechanisms which decrease the number of neutrons in that cell (leakage, absorption and out-scattering - L.H.S. of Eqn. (1)) are compensated by the mechanisms causing an increase of the neutrons in the same cell (external source, fission, in-scattering-R.H.S. of Eqn. (1)).

The Boltzmann Equation, written in spherical geometry, takes the form:

$$\frac{\mu}{r^2}\frac{\partial}{\partial r}\left[r^2\Phi(r,\mu,E)\right] + \frac{1}{r}\frac{\partial}{\partial \mu}\left[(1-\mu^2)\,\Phi(r,\mu,E)\right]$$

$$+ \Sigma_T(r,E)\ \Phi\ (r,\mu,E) = S\ (r,\mu,E)$$
$$+ \int_{-1}^{+1} \int_{o}^{\infty} \Sigma(r;E'\rightarrow E,\mu_o)\ \Phi\ (r,E',\mu')d\ E'd\mu' \qquad (3.2)$$

where:

r: is the distance from the centre of the sphere (system of reference)

μ, μ': are the cosines of the angles θ,θ' determining the directions of neutron motion before and after the collision with respect to position vector $\vec{r}$

μ_o is the cosine of the scattering angle θo, which can be expressed in terms of, μ,μ',ϕ,ϕ' (see Figure 13).

The neutron transport equation even in its simplified form of Eqn (3.2) is difficult to solve analytically and only approximate methods can give satisfactory solutions with acceptable or desirable accuracy. Such an approximate method is the discrete-orginates method. The main idea behind this method is the discretization of all the phase space-variables of Eqn (3.2) and the subsequent derivation of a set of coupled finite difference Equations solved by an especially constructed computer code.

More precisely, the three-dimensional phase space of Eqn (3.2) is divided into an adequate number of properly chosen finite cells:

$$\Delta V\Delta\mu\Delta E = V_I DG = \frac{4\pi}{3}\ (r_{i+1}^3 - r_i^3)(\mu_{d+1}-\mu_d)(E_{g+1}-E_g)$$

By applying the integral operator:

$$\int_{reV_I} \int_{\mu\varepsilon D} \int_{E\varepsilon G} 4\pi r^2 dr d\mu dE$$

over a mesh cell to both sides of Eqn (3.2) and by making the necessary approximations in evaluating the integrals and in handling the differential scattering cross-section, we end in the following form of the discrete-ordinates finite difference Equation:

$$\mu_D[A_{i+1}\,\Phi_{G,i+1,D} - A_i\,\Phi_{G,i,D}] + \frac{1}{W_D}\,[B_{d+1}\,\Phi_{G,I,d+1} - B_d\,\Phi_{G,I,d}]$$

$$+V_I\,\Sigma^T_{G,I}\,\Phi_{G,I,D} = V_I\,S_{G,I,D}$$

$$+V_I \sum_{\ell=o}^{L} P_\ell(\mu_D) \sum_{G'=1}^{NOG} \Sigma^{\ell,I,mod}_{G'\to G} \sum_{D'=1}^{NOA} \Phi_{I,G',D'} P_\ell(\mu_{D'})\,W_{D'} \qquad (3.3)$$

with i = 1, NOS (number of space intervals)

G = 1, NOG (number of energy intervals)

d = 1, NOA (number of angle intervals)

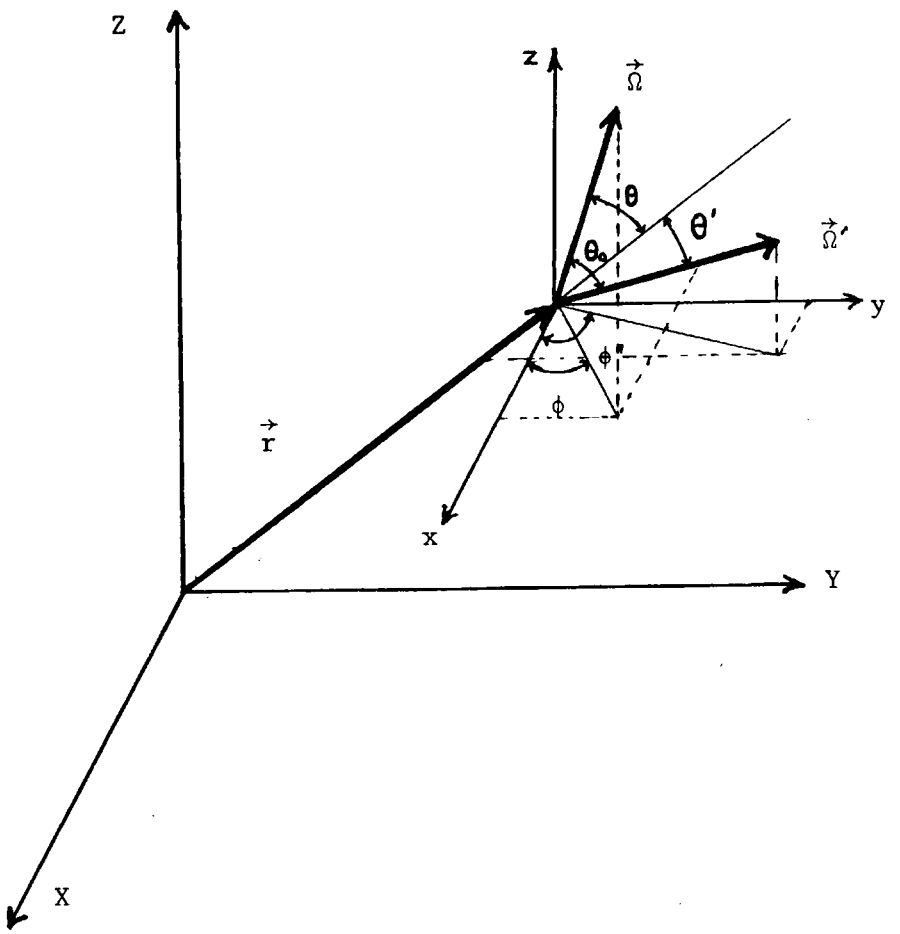


FIGURE 13 GEOMETRY OF A SCATTERING EVENT.

In Eqn. (3.3) upper-case indices denote mean values over the interval (e.g. D,I), except for the flux and external source in which the upper-case G refers to an integral over the energy interval. Lower case-indices denote values of the function at the limits of the interval (e.g. d+1,i).

μ_D, W_D are the cosines and their associated weights (fraction of solid angle associated with direction μ_D) for which Eqn. (3.3) is solved and are chosen by the user of the code in such a way so that the integrals on the cosine D interval can be best approximated by the mean value theorem, viz:

$$\int_{\mu_d}^{\mu_{d+1}} \mu f(\mu)d\mu \simeq \mu_D f(\mu_D) \Delta\mu_D, \qquad \mu_d<\mu_D<\mu_{d+1}$$

For the scalar flux we have, then, the approximation:

$$\Phi(r,E) \equiv 2\pi\int_{-1}^{+1} \Phi(r,E,\mu)d\mu \simeq 2\pi\Sigma_{D=1}^{NOA} W_D \Phi(r,E,\mu_D) \qquad (3.4)$$

which is the main feature of the discrete-ordinates method.

$\Sigma^T_{G,I}$ and $\Sigma^{\ell,I,mod}_{G',G}$, commonly called group constants, are the multigroup total cross-section and the ℓ-coefficient of the expansion of the transfer cross-section $\Sigma^I_{G'\to G}(\mu_D)$ into Legendre Polynomials, respectively. Although the expansion of the scattering kernel $\sigma(r,E'\to E,\mu_o)$ into Legendre Polynomials, viz:

$$\sigma(r,E'\to E,\mu_o) \simeq \sum_{\ell=o}^{L} \frac{2\ell+1}{4\pi}\sigma_\ell(r,E'\to E)P_\ell(\mu_o) \qquad (3.5)$$

is not a necessary feature of the discrete-ordinates method, it is preferred to other techniques (other polynomials, polynomials plus delta functions,etc) because it appears to be the natural approach, since spherical harmonics are a representation of the three-dimensional rotation group.

The group constants appearing in Eqn (3.3) are defined as follows:

$$\Sigma^T_{G,I} = \Sigma^{T,o}_{G,I} = \frac{\int_{r\in V_I}^{4\pi r^2}\int_{E\in G} \Sigma^T(r,E)\ \Phi^o(r,E)dEdr}{\int_{r\in V_I}^{4\pi r^2}\int_{E\in G} \Phi^o(r,E)dEdr}$$

$$= \frac{\int_{r\epsilon V_I} 4\pi r^2 \int_{E\epsilon G} \Sigma^T(r,E) \int_{-1}^{+1} \Phi(r,\mu,E)\, d\mu dE dr}{\int_{r\epsilon V_I} 4\pi r^2 \int_{E\epsilon G} \int_{-1}^{+1} \Phi(r,\mu,E)\, d\mu dE dr} \qquad (3.6)$$

$$\Sigma^{\ell,I,mod}_{G'\to G} = \frac{\int_{r\epsilon V_I} 4\pi r^2 \int_{E\epsilon G} \int_{E'\epsilon G'} \Sigma^{\ell}(r,E'\to E) \int_{-1}^{+1} \Phi(r,E',\mu') P_\ell(\mu')\, d\mu dE' dE dr}{\int_{r\epsilon V_I} 4\pi r^2 \int_{E'\epsilon G'} \int_{-1}^{+1} \Phi(r,E',\mu') P_\ell(\mu')\, d\mu' dE' dr}$$

$$+ (2\ell+1)(\Sigma^T_{G,I} - \Sigma^{T,\ell}_{G,I})\delta_{G,G'} \qquad (3.7)$$

$$\text{with} \qquad \Sigma^{T,\ell}_{G,I} = \frac{\int_{r\epsilon V_I} 4\pi r^2 \int_{E\epsilon G} \Sigma^T(r,E)\Phi^{\ell}(r,E)\, dE dr}{\int_{r\epsilon V_I} 4\pi r^2 \int_{E\epsilon G} \Phi^{\ell}(r,E)\, dE dr}$$

and $\delta_{G,G'}$ = delta of Kronecker.

It is recognised, as well, that in Eqn (3.7) the integral:

$$\int_{-1}^{+1} \Phi(r,E,\mu')\, P_\ell(\mu')\, d\mu' = \Phi^{\ell}(r,E')$$

is the ℓ^{th}- Legendre coefficient of the angular flux.

The modification of the ℓ- coefficient of the transfer cross-section expansion accounts for the fact that the dependence of the multi-group total cross-section, $\Sigma^T_{G,I}$, on the cosine μ caused by the integration of the third term of Eqn (3.2) over $E\epsilon G$, has been avoided.

It must be pointed out here that the estimation of the within-group fluxes needed in expressions (3.6) and (3.7) and generally the evaluation of the group constants constitute a major aspect of the whole problem and they have a decisive impact on the accuracy of the numerical solution.

A_{i+1}, A_i are the surface areas of the volume mesh given by:

$$A_{i+1} = 4\pi r_{i+1}^2$$

$$A_i = 4\pi r_i^2$$

while B_{d+1}, B_d are the curvature coefficients, given by the recursion relation:

$$B_{d+1} = B_d - \mu_D W_D (A_{i+1} - A_i)$$

with $B_1 = 0$.

Having identified all the quantities involved in Eqn (3.3), it is easily perceived that this Equation expresses the neutron balance in the finite phase space cell. In fact the first term in the L.H.S. of this Equation represents the leakages through the spherical boundaries of the mesh of the phase space while the second term represents the "leakages" through the faces corresponding to coordinate μ of the mesh due to the variation of the angular coordinate system with the position. The third term attributes the neutron losses in the finite mesh due to any kind of interaction (absorption, scattering) while the fourth and fifth terms, in the R.H.S. of Eqn. (3.5), represent the neutron gains due to external sources (fixed source, fission) and to scattering mechanism.

For a given mesh in the three-dimensional phase space and by postulating a value for the scattering source term and, possibly, for the fission source in Eqn. (3.3), we are left with five unknowns, namely, the five angular fluxes on and inside the edges of a finite cell in the r,μ phase space (shown in Figure 13),keeping of course the calculation within the same energy group. Normally, a particular direction of cosine -1.0 and weight equal to 0.0 is added to NOA set for initializing the angular redistribution calculations (see the recursion relation for the curvature coefficients, from which $B_{NOA+1} = B_1 = 0$), since a particle for which the direction has a cosine equal to -1.0 moves through every running surface according to the same angle.

Two of the fluxes at the interfaces are known either from boundary conditions or from calculations of adjacent cells. Consequently two additional equations:

$$\Phi_{G,I,D} = A\,(\Phi_{G,i+1,D};\ \Phi_{G,i,D})$$

$$\Phi_{G,I,D} = B\,(\Phi_{G,I,d+1};\ \Phi_{G,I,d})$$

are required for solving Eqn (3.3). The simplest forms these equations can take are either the diamond difference scheme wherein Φ is assumed

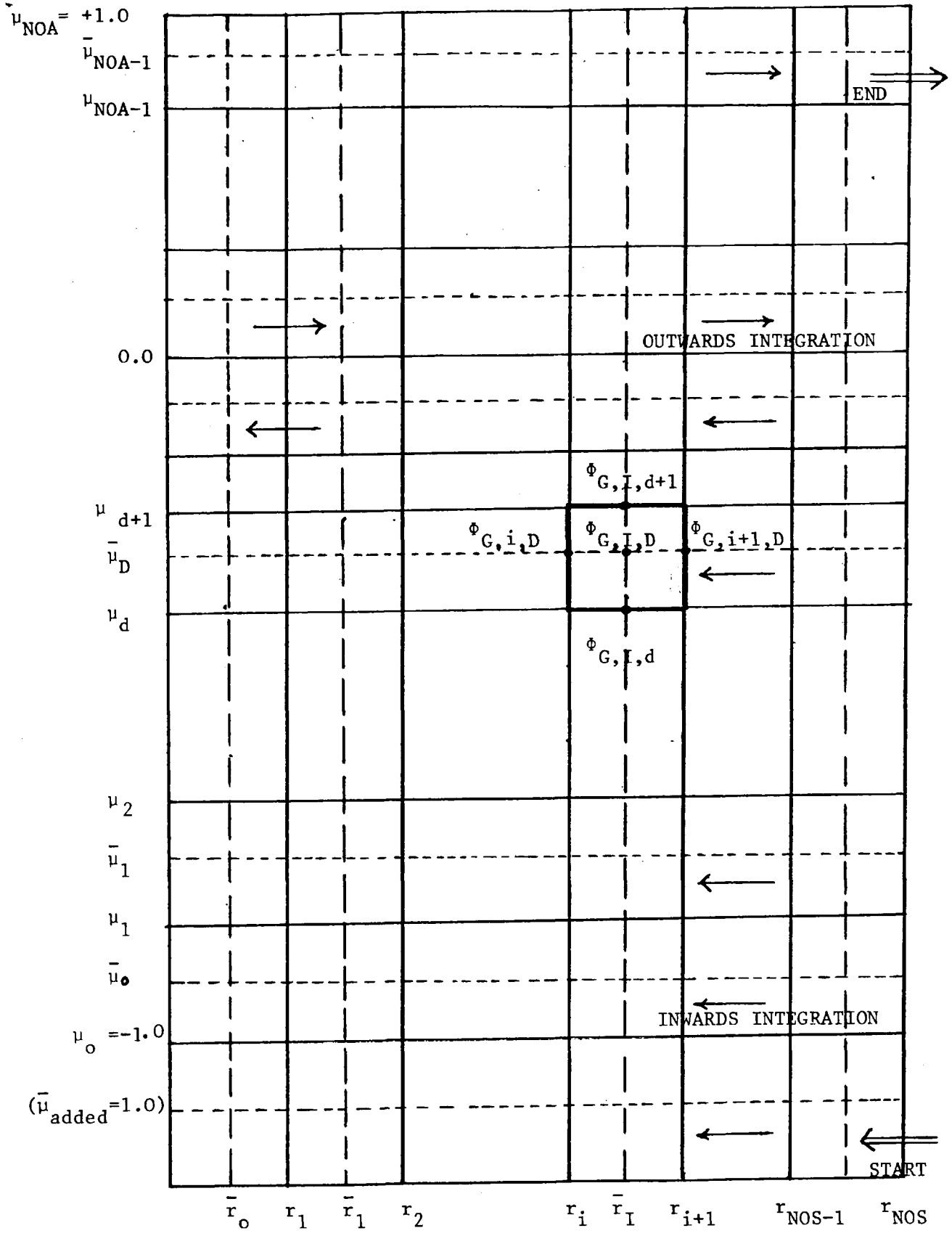


FIGURE 13. CALCULATIONAL FLOW IN SOLUTION OF FINITE DIFFERENCE EQUATION BY ANISN

to be linear between adjacent r ,μ mesh points, viz:

$$\Phi_{G,I,D} = 1/2(\Phi_{G,i+1,D} + \Phi_{G,i,D})$$

$$\Phi_{G,I,D} = 1/2(\Phi_{G,I,d+1} + \Phi_{G,I,d})$$

or, when this scheme gives zero or negative fluxes at the interfaces, a step model is employed, namely:

$$\Phi_{G,i+1,D} = \Phi_{G,I,D} \quad \text{for } \mu>0$$

or

$$\Phi_{G,i,D} = \Phi_{G,I,D} \quad \text{for } \mu<0$$

and

$$\Phi_{G,I,d+1} = \Phi_{G,I,D}$$

ANISN contains both schemes as options.

A typical numerical solution of Eqn (3.3) is basically one of iterating the solution to some prescribed degree of convergence. Since all the scattered neutrons undergo, in their first collisions, an energy loss (in most problems solved by ANISN up-scattering is not taken into account at all) the calculation begins with the highest energy group (G = 1) and progresses sequentially through the lower energy groups. Solving Eqn. (3.3) for G = 1, we start with some postulated values for the $\Phi_{1,I,D}$ fluxes required in the estimation of scattering term ($\Sigma^{\ell,I,mod}_{G'\to 1} = 0$ for G'>1); in the case of an eigenvalue problem with fission source included in the fourth term ($V_I S_{G,I,D}$), guesses are also made for the rest descrete $\Phi_{G,I,D}$ fluxes. Using the appropriate boundary conditions, the diamond difference and/or the step model equations and following the calculational flow of Figure 13, all the $\Phi_{1,I,D}$ fluxes can be calculated. These estimated values of $\Phi_{1,I,D}$ fluxes are used for a re-computation of the scattering and, possibly, fission source terms and this process is repeated until convergence is attained. By employing convergence criteria and proper scaling techniques for accelerating the inner-iteration process, any desirable degree of accuracy for the within group fluxes, $\Phi_{1,I,D}$, can in principle be achieved. Next we proceed to

following lower energy groups where we apply the same procedure with the fluxes required in the calculations of source terms obtained either from preceding calculations for G'>G or for the group G'=G from the preceding inner iteration.

Once the finite cell-averaged descrete fluxes $\Phi_{G,I,D}$ have been calculated for all the energy groups, angles and space midpoints, a new estimation of the fission source is attempted and the whole procedure is iterated until new convergence criteria for the eigenvalue (e.g. effective multiplication factor) or for the scalar fluxes over a selected set of space points and energy groups are met. The second sequence of iterations are called outer (or source or power) iterations to distinguish them from the inner iterations for the within-group fluxes.

Having precise numerical estimates of the $\Phi_{G,I,D}$ fluxes and the dosimetry cross-sections of different detectors in the same energy group structure, reaction rates and, consequently, transmission ratios can easily be estimated.

3.4 OPTIMIZATION OF THE CALCULATIONAL PROCEDURE

The geometrical model of Figure 12(II) is implemented into ANISN code by specifying the geometrical, material and calculational parameters required by this code.

In optimising the calculational procedure, we are concerned with the effect on Transmission of the approximations involved in the derivation of the finite difference equation.

The definition of a finite mesh of the phase space and the approximations used to perform the integrations over the mesh constitute the major approximations. It is presently impossible to determine the precision corresponding to a given mesh for non-analytical problems. Since the mesh is adjustable, the current practice is to first select a reasonable mesh based on experience and then make some variations to evaluate the effect of finer splitting on the desired result.

For a given mesh of the phase space the choice of the discrete directions and associated weights can largely affect calculated quantities. It does not appear that a most accurate (or best) quadrature scheme for a specific problem can be selected a priori. The efficiency of a given set of discrete directions depends on problem parameters such as geometry, optical thickness, energy group structure, spatial mesh, and a generalization of these dependencies is not possible.

The remaining major approximation is the truncated polynomial expansion of the differential scattering cross-sections. The effect of this approximation is evaluated by the influence of an increasing order expansion of the scattering cross-section on the calculated quantity. Experience to date has shown that low order approximations such as P_2 and P_3 are adequate for most practical problems.

It must be pointed out here that numerical estimates of Transmissions will be considered as precise and immune to errors due to aforementioned

approximations only if changes in T acquired by improving these approximations are small compared to its inherent error originated in the input data. Since this inherent error is expected to be more than 2% for most of the cases of Table 3,it is understood that a tolerance factor in the optimization procedure averaged around 0.1% and not exceeding 0.2% of the corresponding Transmission can be considered adequate and, consequently, a yardstick for avoiding better approximations.

It will also be assumed that the difference between the precise numerical and exact solution of the problem is not larger than the established tolerance factor.

3.4.1 ANISN Input Data Specification

One of the iron cases (case 6 in Table 1) is picked up and used in the preliminary calculations. We consider the iron shell of thinkness d = 4.11 cm as a representive case of all those included in Table 1, because the variation of iron cross-sections with energy is quite complicated and the shell thickness corresponds to an average of all the thicknesses used.

Source Spectrum

The ^{235}U thermal neutron fission spectrum was calculated according to the Grundl's recent formula (13):

$$\Phi(E) = \mu(E)\ (0.7501)\ \sqrt{E}\ \exp(-1.5/1.97E) \qquad (3.8)$$

where:

$$\mu(E) = 0.847 + 0.8E \quad \text{for } E<0.25 \text{ MeV}$$

$$= 1.087 - 0.14E \quad \text{for } 0.25\text{MeV}<E<0.8\text{MeV}$$

$$= 0.938 + 0.04E \quad \text{for } 0.8\text{MeV}<E<1.5\text{MeV}$$

$$= 9.983 + 0.01E \quad \text{for } 1.5\text{MeV}<E<6.0\text{MeV}$$

$$= 1.043.\exp(-0.06/1.043(E-6.0)) \text{ for } E > 6.0\text{MeV}$$

A specially constructed programme was used for transforming this spectrum

into desired energy group structure. This code employed the Simpson's method for obtaining the integral value of $\Phi(E)$ between two energy boundaries. The representation of fission spectrum given by Eqn (3.8) was used for both preliminary and final calculations.

It must be mentioned here that the present situation for the ^{235}U spectrum is unsatisfactory since the measurement errors exceed 2.5% (see Ref 13 and page 255)

Dosimetry cross - sections

The ENDF/B-IV dosimetry data file were used throughout the calculations. The collapsing from the original 620-energy group structure into the desired few group scheme was accomplished using the code SIGMA (14); the above mentioned fission spectrum was used as weighting function.

Material cross sections

An old version of the United Kingdom Nuclear Data Library (U K N D L) (Data File Number for iron = 906) was used in the optimisation procedure while the final calculations were accomplished using the ENDF/B-IV library. Calculations were also carried out using the ENDF/B-III for those materials included in this library.

The preliminary calculations were done in a 37-energy group scheme while those using ENDF/B data were undertaken in the DLC-37 100-group structure. More information and comments on the aforementioned data files remain to be given in Chapter 5. Both 100 and 37 energy group structures are tabulated in the end of the thesis.

Boundary conditions

Reflection ($d\Phi/dx = 0$) was specified for the centreline of the sphere (see Figure 16) in accordance with the spherical symmetry of the system. A vacuum was specified as the right (outer) boundary condition since every neutron leaving the material shell and moving outwards is lost.

Zone structure and initial spatial mesh determination

The number and material composition of the zones required by ANISN were made according to the geometrical model of Fig. 12 (II), representing the experimental arrangement under the ideal conditions.

Based on this model four zones were established as follows:

ZONE 1, the detector region, with radius $0<R\leq R_1$, made of aluminium for the preliminary calculations. The boundary radius R_1 was calculated by equalizing the volumes of the cylindrical aluminium detector used in the experiments with a hypothetical spherical one. Since the spirals of aluminium foils used had dimensions 0.010 inch thick by 0.50 inch wide by 18 inches long the volume of the cylindrical detector formed was 1.474 cm^3 and, therefore, the radius of an equivalent spherical detector was $R_1 = 0.706$ cm.

ZONE 2, a void region, with radius $R_1<R\leq R_2$ representing the empty space between detector and material shell. The radius R_2 was always equal to "sphere inside radius" determined from Table 1 as the difference between sphere outside radius and shell thickness.

ZONE 3, the material region, with radius $R_2<R\leq R_3$ made of iron for the preliminary calculations. The radius R_3 was the "sphere outside radius" given in Table 1.

ZONE 4, a void region, with radius $R_3<R\leq R_5$, representing the space between material shell and fission plate. The last spatial interval of this zone had always fixed boundaries, determined by the radii R_4, R_5 and contained a uniformly distributed isotropic fission source. R_4 and R_5 were calculated from Figure 15.

According to this Figure the following relation holds for R_4 and R_5.

$$R_5^2 = R_4^2 + \frac{d^2}{4} + \frac{\ell^2}{4} \qquad (3.9)$$

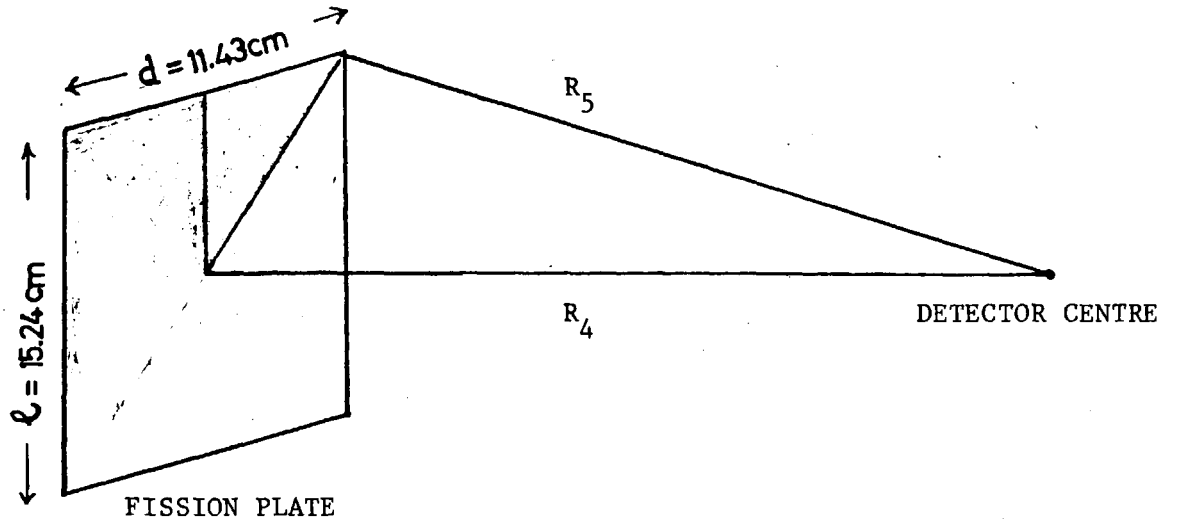


FIGURE 15 DETERMINATION OF THE SHELL SOURCE BOUNDARIES

If we recognise R_4 as the "distance to the source" given in Table 1 (it is not quite obvious since this distance is described in B.B.C. work as "the average distance between the counter and the effective centre of the neutron source") then R_5 is easily calculated from Eqn. (3.7). However, calculations have shown that (see Page 103) considering the "distance to source" as that to outer, inner or simply to an intermediate point of the last interval does not affect the Transmissions. According to Eqn (3.9) the width, S, of the last interval for all "25.40 cm - distance to source" cases has been estimated to be

$S = R_5 - R_4 = 1.79$ cm.

In all the calculations for which the "distance to source" was 25.40 cm, R_4, R_5 were taken equal to

$$R_4 = 24.63 \text{ cm.}$$

$$R_5 = 26.42 \text{ cm.}$$

(For more explanation see Table 11, and pages 118-121 .)

The initial spatial mesh was established according to ANISN manual instructions and is given in Table 4. However the effect on T of a

finer and wider radial mesh is to be examined.

Figure 16 summarizes the input data to ANISN which are common to all optimization calculations.

TABLE 4 INITIAL RADIAL MESH FOR OPTIMIZATION CALCULATIONS

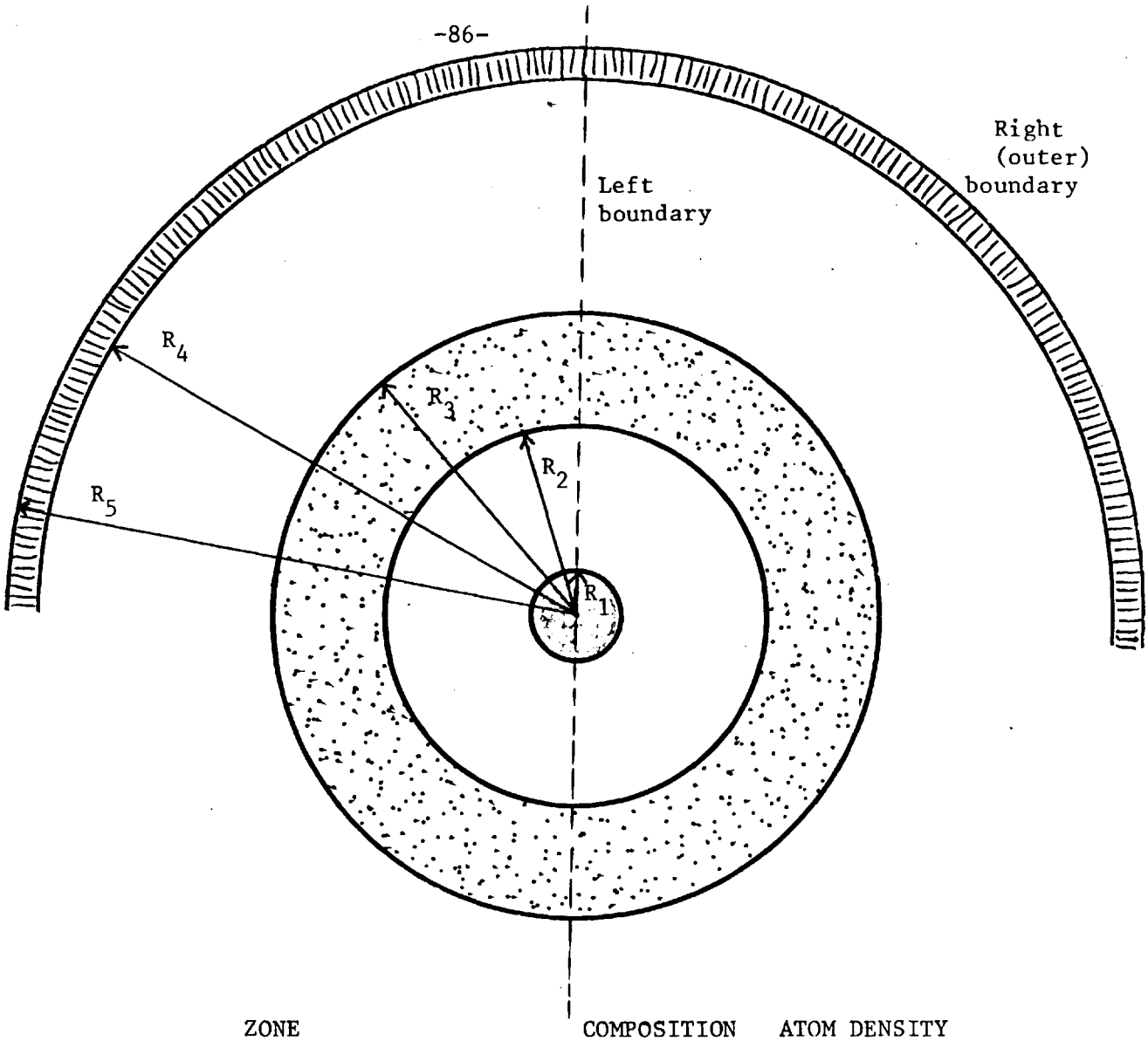
ZONE	NUMBER OF INTERVALS
1	1
2	6
3	21
4	8

3.4.2 Effect of the Angular Mesh and Quadrature Sets

As mentioned in section 3.3, the number of disrete directions and the quadrature sets used in the calculations can largely affect the calculated quantity.

Table 5 summarizes the results of the effect on T of varying angular mesh and different quadrature sets. The activities in this and following Tables are given in reactions/cm^3/sec/ unit fission source. Also, every calculated value of Transmission is accompanied by a percentage change attained by employing a better approximation than the preceding one. Percentage changes falling below 0.2% will terminate, as we have explained, the process of achieving better approximations. A gradual increase of the Transmission is noted in Table 5 as we move towards finer angular mesh. This table also reveals that a S_{16} calculation with even moments' quadrature sets can hardly be considered as adequate.

Comparing even moments with Gauss-Legendre calculations we note that the second quadrature sets are more advantageous than the first in two respects: (a) for the same order of angular quadrature they give



ZONE			COMPOSITION	ATOM DENSITY
$0<R\leq R_1$ = 0.706 cm	ZONE 1	DETECTOR	Aluminium	0.06023
$R_1<R\leq R_2$ = 6.049 cm	ZONE 2	VOID	-	-
$R_2<R\leq R_3$ = 10.16 cm	ZONE 3	MATERIAL	Iron	0.08487
$R_3<R\leq R_5$ = 26.42 cm	ZONE 4	VOID	-	-

$R_4(=24.63)\leq R\leq R_5$ = SOURCE INTERVAL

DOSIMETRY CROSS-SECTIONS:	ENDF/B-IV Dosimetry Data Library
IRON CROSS-SECTIONS:	UKNDL data (DFN = 906)
ENERGY GROUP STRUCTURE:	37
SOURCE SPECTRUM:	GRUNDL'S recent formula
BOUNDARY CONDITIONS:	Left : Reflection
	Right: Vacuum.

FIGURE 16 ANISN INPUT DATA SPECIFICATION FOR PRELIMINARY CALCULATIONS.

better (nearer the experimental) results and (b) the effect on T of a finer angular mesh is either zero or well below the pre-established tolerance factor.

The even moments' quadrature sets were developed in such a way so as to be completely symmetric about $\mu = 0.0$ and satisfy certain even moments' and rotational invariance conditions.

The Gauss-Legendre quadrature sets are also symmetric about $\mu = 0$, that is,

$$\mu_i = -\mu_{NOA+1-i} \qquad W_i = W_{NOA+1-i}$$

The cosines μ_i, are chosen so as to satisfy the relation:

$$P_{NOA}(\mu_i) = 0$$

where $P_{NOA}(\mu)$ are the Legendre polynomials of order NOA

Both quadrature sets satisfy the relations:

$$\sum_{i=1}^{NOA} W_i = 1.0$$

$$\sum_{i=1}^{NOA} W_i \mu_i = 0.0$$

$$\mu_i \neq 0.0 \text{ for all } i$$

as required by ANISN, and are tabulated in the last pages of this work.

Table 5 suggests that, as far as the approximation of the angular dependence of the flux is concerned, a S_8 calculation with Gauss-Legendre quadrature sets will be adequate.

3.4.3 Effect of the Order of the Scattering Kernel Expansion

Table 6 attributes the effect on T of the order of the transfer cross-section expansion (see Eqn. 3.5).

It must be mentioned here that anisotropic effects of scattering are generally important whenever the neutron energy is high and/or the scatterer has a large mass.

From this Table it is clear that a P_3 approximation is sufficient

TABLE 5. EFFECT OF THE ANGULAR MESH AND QUADRATURE SETS ON TRANSMISSION.

INPUT DATA

RADIAL MESH = as in Table 4

QUADRATURE ORDER AND SETS = being studied

ORDER OF SCATTERING KERNEL EXPANSION = P_0

REACTION	$E_{THRESHOLD}$ MeV	STATUS	EVEN MOMENTS' QUADRATURE SETS								GAUSS-LEGENDRE QUADRATURE SETS			
			S_4		S_8		S_{12}		S_{16}		S_8		S_{16}	
			ACTIVITIES	TRANSMISSION CHANGE	ACTIVITIES	TRANSMISSION CHANGE	ACTIVITIES	TRANSMISSION CHANGE	ACTIVITIES	TRANSMISSION CHANGE	ACTIVITIES	TRANSMISSION CHANGE	ACTIVITIES	TRANSMISSION CHANGE
$^{27}Al(n, P)^{27}Mg$	4.4	ON	1.462 E-08	0.4710	1.433 E-08	0.4810	1.428 E-08	0.4842	1.426 E-08	0.4856	1.425 E-08	0.4901	1.425 E-08	0.4901
		OFF	3.102 >>	-	2.979 >>	+2.12%	2.949 >>	+0.66%	2.936 >>	+0.29%	2.907 >>	+1.8%*	2.907 >>	0.0%
$^{238}U(n, f)F.P.$	1.5	ON	1.467 E-06	0.6508	1.423 E-06	0.6575	1.414 E-06	0.6601	1.411 E-06	0.6618	1.408 E-06	0.6666	1.408 E-06	0.6666
		OFF	2.254 >>	-	2.164 >>	+1.02%	2.142 10^{-6}	+0.40%	2.132 >>	+0.25%	2.112 >>	+1.38%	2.112 >>	0.0%
$^{237}Np(n, f)F.P.$	0.6	ON	8.736 E-06	0.8456	8.410 E-06	0.8480	8.342 E-06	0.8498	8.321 E-06	0.8515	8.293 E-06	0.8568	8.297 E-06	0.8573
		OFF	1.033 10^{-5}	-	9.917 >>	+0.28%	9.816 >>	+0.21%	9.773 >>	+0.18%	9.678 >>	+1.03%*	9.678 >>	+0.06%

* This change refers to the S_8 calculation with even moments' quadrature sets.

1.462 E-08 is read as 1.462×10^{-8}

TABLE 6. EFFECT OF THE ORDER OF SCATTERING KERNEL EXPANSION ON TRANSMISSION.

INPUT DATA

RADIAL MESH = as in Table 4

QUADRATURE ORDER AND SETS = S_8 with Gauss-Legendre data

ORDER OF SCATTERING KERNEL EXPANSION = being studied

REACTION	$E_{THRESHOLD}$ MeV	P_0			P_1		P_2		P_3	
		STATUS	ACTIVITIES	TRANSMISSION CHANGE	ACTIVITIES	TRANSMISSION CHANGE	ACTIVITIES	TRANSMISSION CHANGE	ACTIVITIES	TRANSMISSION CHANGE
$^{27}Al(n, P)^{27}Mg$	4.4	ON	1.425 E-08	0.4901	1.510 E-08	0.5194	1.522 E-08	0.5235	1.521 E-08	0.5232
		OFF	2.907 >>	-	2.907 >>	+5.97%	2.907 >>	+0.78%	2.907 >>	-0.06%
$^{238}U(n, f)$ F.P.	1.5	ON	1.408 E-06	0.6666	1.446 E-06	0.6846	1.451 E-06	0.6870	1.448 E-06	0.6856
		OFF	2.112 >>	-	2.112 >>	+2.70%	2.112 >>	+0.35%	2.112 >>	-0.20%
$^{237}Np(n, f)$F.P.	0.6	ON	8.293 E-06	0.8568	8.404 E-06	0.8683	8.413 E-06	0.8692	8.409 E-06	0.8688
		OFF	9.678 >>	-	9.678 >>	+1.34%	9.678 >>	+0.10%	9.678 >>	-0.04%

in describing the anisotropic scattering of neutrons by iron shells of reasonably large thickness.

3.4.4 Effect of the Radial Mesh

Table 7 describes the effect on T of a varying radial mesh. The number of spatial intervals in the material region (ZONE 3) was both doubled and reduced by a factor 2. The intervals in the void regions (ZONE 2 and 4) were only doubled resulting in no observeable change in T.
All the final calculated values of Transmissions in Table 14 were checked for possible changes caused by reducing the number of intervals in ZONE 3 by a factor 2 from that initially established for that particular case. Such changes were never observed in the final calculations. The percentage changes of Transmission in Table 7 are relative to the initial radial mesh (column 1).

3.4.5 Optimum Calculational Scheme

Concluding this section we note that a S_8P_3 approximation employing the Gauss-Legendre quadrature sets and a properly chosen radial mesh constitutes an optimum scheme for our calculations ensuring an uncertainty on T, due to the discrete ordinates approximation, no more than about 0.2% for most of the cases studied.
However, the uncertainty due to approximations in the discrete ordinates method of solving the neutron transport equation is only part of the final error attributable to the whole calculational procedure. The one-dimensional modelling of both the fission plate and cylindrical detectors may cause systematic errors which in turn, will complicate the interpretation of differences between measured and calculated Transmissions in terms of nuclear data shortcomings.
A quantitative assessment of this uncertainty and of the final error accompanying the Transmissions and due to the whole calculational procedure is attempted in the following sections.

TABLE 7. EFFECT OF RADIAL MESH ON TRANSMISSION.

INPUT DATA

RADIAL MESH = being studied

QUADRATURE ORDER AND SETS = S_8 with Gauss-Legendre data

ORDER OF SCATTERING KERNEL EXPANSION = P_3

REACTION	$E_{THRESHOLD}$ MeV	INTERVALS PER ZONE								
		1 - 6 - 21 - 8			1 - 6 - 41 - 8		1 - 6 - 11 - 9		1 - 12 - 21 - 17	
		STATUS	ACTIVITIES	TRANSMISSION CHANGE	ACTIVITIES	TRANSMISSION CHANGE	ACTIVITIES	TRANSMISSION CHANGE	ACTIVITIES	TRANSMISSION CHANGE
$^{27}Al(n, P)^{27}Mg$	4.4	ON	1.521 E-08	0.5232	1.521 E-08	0.5232	1.521 E-08	0.5232	1.521 E-08	0.5232
		OFF	2.907 >>	-	2.907 >>	0.0%	2.907 >>	0.0%	2.907 >>	0.0%
$^{238}U(n, f)F.P.$	1.5	ON	1.448 E-06	0.6856	1.448 E-06	0.6856	1.449 E-06	0.6860	1.448 E-06	0.6856
		OFF	2.112 >>	-	2.112 >>	0.0%	2.112 >>	+0.06%	2.112 >>	0.0%
$^{237}Np(n, f)F.P.$	0.6	ON	8.409 E-06	0.8688	8.409 E-06	0.8688	8.411 E-06	0.8690	8.409 E-06	0.8688
		OFF	9.678 >>	-	9.678 >>	0.0%	9.678 >>	+0.02%	9.678 >>	0.0%

3.5 SUPPLEMENTARY ANISN CALCULATIONS AND TESTS

Additional calculations and tests are undertaken in this section aiming at both demonstrating the validity of the assumption and quotations we have made so far and checking the reliability and overall efficiency of the one-dimensional modelling of B.B.C. experiments in predicting the measured Transmissions.

3.5.1 Comparison of Analytical and ANISN Flux Calculations.

A valuable indication of how well ANISN calculations predict exact analytical solutions can be acquired for the simple case of flux calculations in the space inside the shell source and without the material shell. This case is depicted and formulated in Appendix A.

In accordance with Appendix A, the scalar neutron flux in the space inside a uniformly distributed shell source of strength S_v (neutrons/cm^3/sec) is given by the formula:

$$\Phi(r) = \frac{S_v}{4r}\left[(R_5^2-r^2)\ln\left(\frac{R_5+r}{R_5-r}\right) - (R_4^2-r^2)\ln\left(\frac{R_4+r}{R_4-r}\right)+2r(R_5-R_4)\right]$$

for $0 < r < R_4 < R_5$ (3.10)

We make Eqn. (3.10) compatible with ANISN calculations by applying the same source normalization, viz:

$$\frac{4\pi}{3}(R_5^3 - R_4^3)\, S_v = 1 \qquad (3.11)$$

and end with the following final formula for the flux:

$$\Phi(r) = \frac{3}{16\pi r(R_5^3-R_4^3)}\left[(R_5^2-r^2)\ln\left(\frac{R_5^2+r}{R_5-r}\right) - (R_4^2-r^2)\ln\left(\frac{R_4+r}{R_4-r}\right)+2r(R_5-R_4)\right] \qquad (3.12)$$

Equation (3.12) has been employed in calculating the scalar neutron flux.

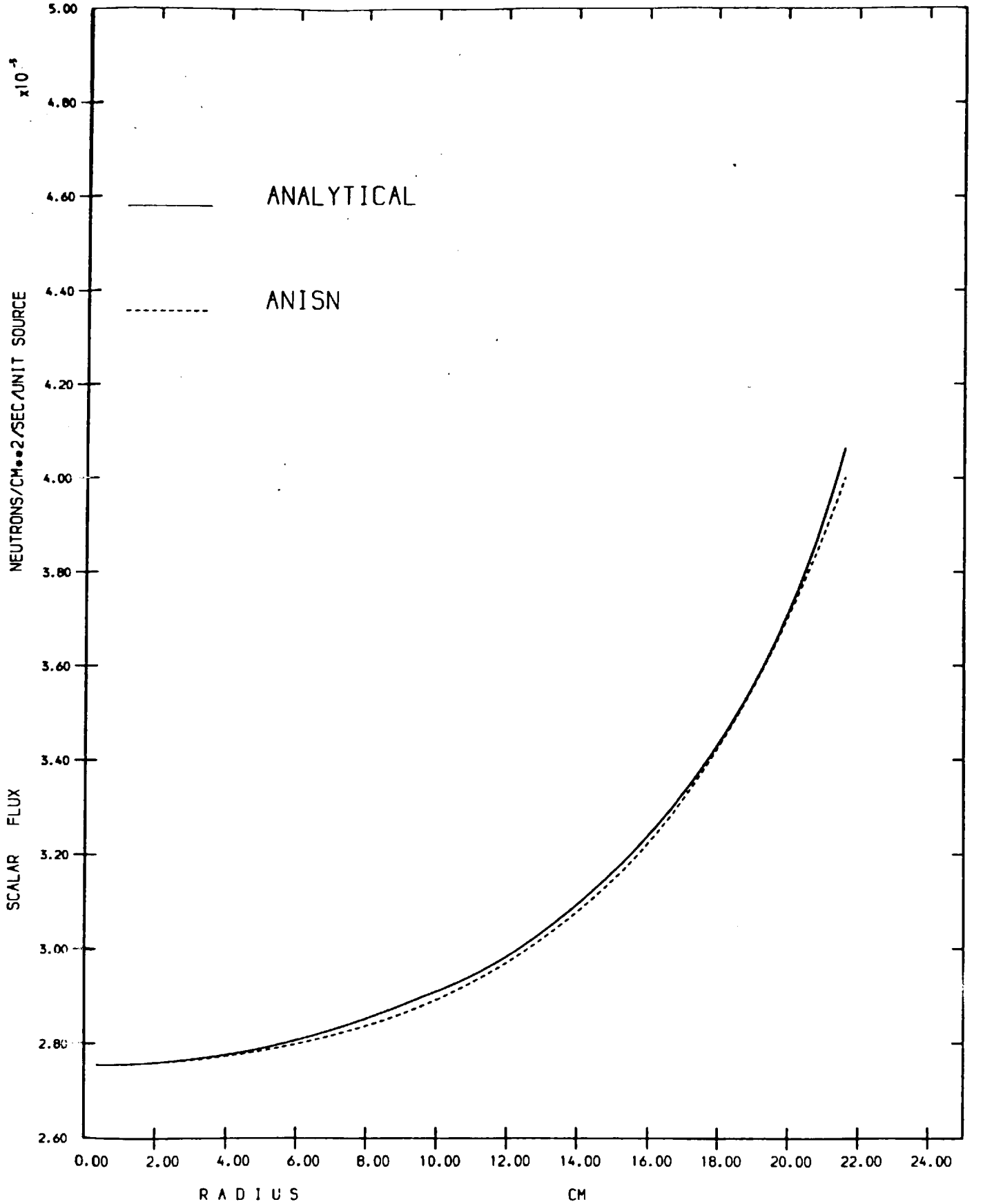
Table 8 summarizes the results of this calculation for different radii together with ANISN results for a certain energy group (energy

TABLE 8. ANALYTICAL AND ANISN SCALAR FLUXES

INPUT DATA

R_4 = 24.62 R_5 = 26.43 χ_i = fission spectrum for group i $\sum_{i=1}^{37} \chi_i = 1$ χ_{11} = 2.257 E-01

No	RADIUS cm	SCALAR FLUX (Eqn 3.10) (neutrons/cm^2/sec/unit source)	SCALAR FLUX FOR GROUP 11 $\Phi(r)\chi_{11}$	ANISN SCALAR FLUXES FOR GROUP 11
1	0.353	1.2203 E-04	2.7544 E-05	2.7542 E-05
2	0.8775	1.2206 >>	2.7550 >>	2.7548 >>
3	3.549	1.2281 >>	2.7720 >>	2.7693 >>
4	7.460	1.2574 >>	2.8382 >>	2.8251 >>
5	9.660	1.2848 >>	2.9001 >>	2.8813 >>
6	13.630	1.3602 >>	3.0703 >>	3.0552 >>
7	15.630	1.4217 >>	3.2091 >>	3.1924 >>
8	17.630	1.5019 >>	3.3901 >>	3.3812 >>
9	21.630	1.8006 >>	4.0641 >>	4.0012 >>



ANISN AND ANALYTICAL SCALAR FLUXES WITHOUT THE PRESENCE OF THE IRON SHELL

FIGURE 17

group 11 was arbitrarily chosen). Both analytical and ANISN - calculated scalar fluxes are plotted in Figure 17. It is seen that there is an absolute coincidence between the two fluxes (0.0007% difference) around the centre of the shell while small deviations are observed as we approach the shell source (1.5% the largest difference between the two fluxes at r = 21.63 cm).

The rather increasing difference between the two fluxes as we move away from the centre can easily be explained in terms of the corresponding increasing anisotropy of the angular flux. More precisely, the scalar flux in transport calculations is defined as the integral of the angular flux over all directions. For spherical geometry:

$$\Phi(r) = 2\pi \int_{-1}^{+1} \Phi(r,\mu)\,d\mu$$

and for the discrete-ordinates approximation: (see Eqn. (3.4))

$$\Phi(r) \simeq 2\pi \sum_{i=1}^{NOA} \Phi(r,\mu_i)W_i$$

The above expression indicates that the smaller the anisotropy of the angular flux $\Phi(r,\mu)$ the better the approximation attained by Eqn. (3.4). Since the anisotropy of the angular flux increases with the radius (see Figure 18) it is understood why ANISN fluxes are identical with those analytically obtained for short distances from the centre and differ significantly, in relative terms, as we approach the source.

If we accept that the same arguments are approximately valid for the "sphere on" (the angular flux is still found to be isotropic around the centre of the detector, though is strongly affected by the multiple scattering of neutrons in the material shell), and since our detectors are both small and located at the centre of the shell, we realize that a precise numerical calculation of Transmissions is really attained by ANISN. This fact supports the assumption made in a previous paragraph

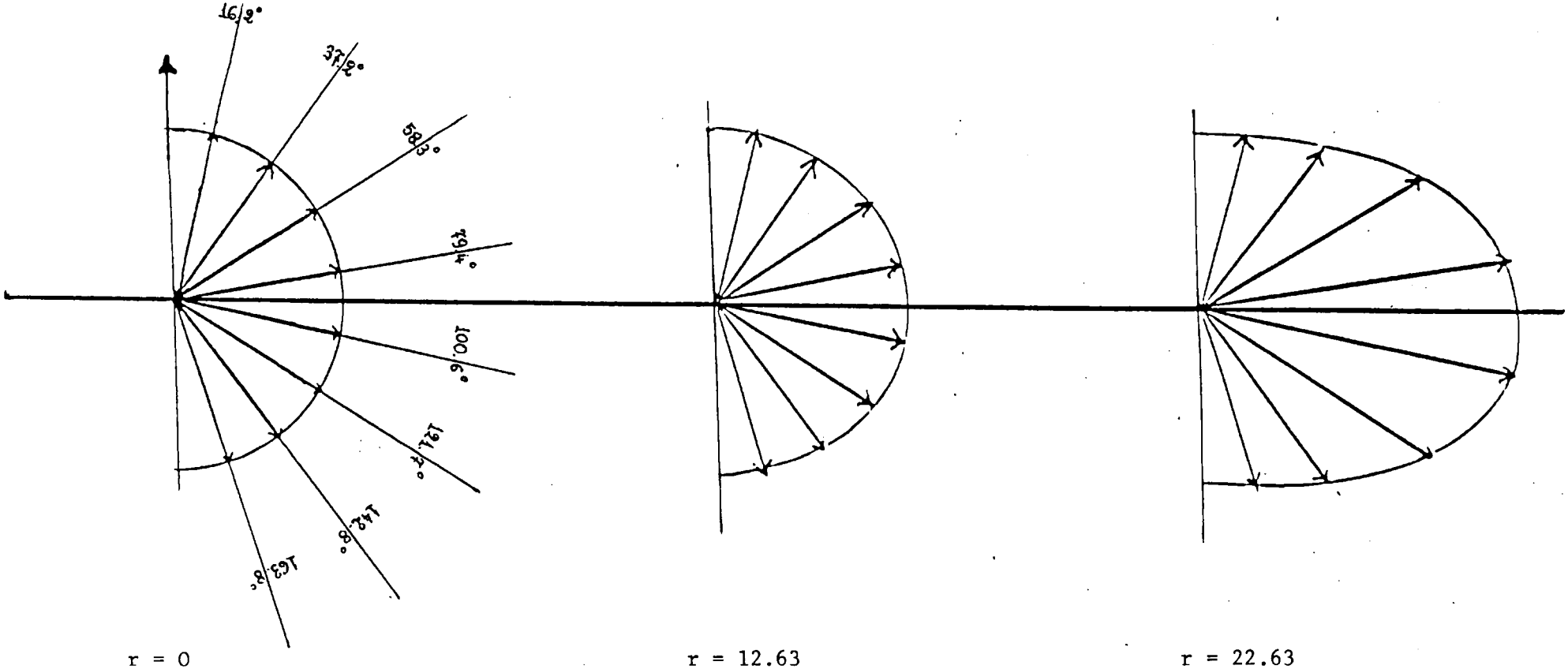
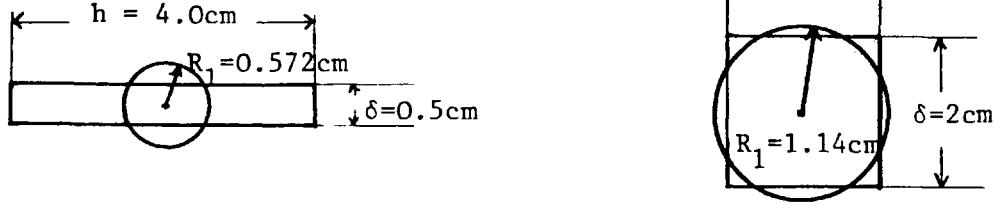


FIGURE 18 ANGULAR FLUX $\Phi(r,\mu)$ ALONG THE DISCRETE DIRECTIONS (GAUSS-LEGENDRE SET) FOR ENERGY GROUP 11 (1.74MeV<E<2.87MeV) AS CALCULATED BY ANISN WITHOUT THE PRESENCE OF A MATERIAL SHELL

SCALE: 1cm ~ 10^{-5} neutrons cm^{-2} sec^{-1} unit fission $source^{-1}$ unit $weight^{-1}$



(I) (II)

$K = \frac{\delta}{h} = 0.125$ $K = \frac{\delta}{h} = 1.0$

FIGURE 19. DIAMETER TO HEIGHT RATIO FOR DIFFERENT DETECTOR SHAPES.

that the deviation between discrete-ordinates and exact calculations of Transmissions does not exceed the pre-established tolerance factor.

3.5.2 Effect on Transmission of Detector's Size, Shape, and Composition.

In our final calculations the cylindrical fission counters and rolled aluminium foils are replaced by spherical ones of the same volume but with no material composition. The effect on Transmission of this approximation is studied in this section.

Firstly, it is easily realized that, regardless of the size and composition of a detector, the replacement of a cylindrical counter, characterized by a very small diameter to height ratio, by an equivalent spherical one will introduce errors in the reaction-rates due to different flux conditions under which the two detectors will be found. This uncertainty decreases as the above ratio approaches unity where

the uncertainty should acquire its minimum value.

The above arguments are depicted in Figure 19 where two ficticious cases are presented for which the ratio $K = \delta/h$ is quite small and unity, correspondingly. Figure 21 shows a sectional view of the real detector-material shell arrangement for which the ratio $K = \delta/h = 0.957$. Since this value is very close to 1.0 we do not expect the calculated Transmission to be largely affected by changes in the detector shape.

In order to study the sensitivity of Transmission to changes in the size of the spherical detectors which may reflect uncertainties either originating from the above approximation or due to errors accompanying the detector dimensions (note that the dimensions of the spiral fission counters are not given in B.B.C. work, but we expect them to be approximately equal to that of aluminium foils), we calculated the effect on Transmission in changing the detector radius by $\pm$ 30%. This corresponds to more than doubling the volume of the detector. The results are given in Table 9.

From Table 9 we realize that even 100% error in the size of a spherical detector has a negligible effect on the calculated Transmission.

In studying the effect of the material composition of a detector on Transmission we re-calculated the Transmissions with the detector region (ZONE 1) being essentially void. (density reduced by 10^{-7}). Table 10 suggests that the absorption and scattering properties of the detector material do not affect the Transmissions, provided that its radius does not exceed ~ 1.0cm.

Strictly speaking,the above conclusion concerns detectors consisting of pure aluminium. Although the exact composition of the spiral fission counters is not given in B.B.C. work, we do not have any indication suggesting that the absorption and scattering properties of the fission counters differ significantly from that of aluminium. Consequently it is believed that the same will be valid for these detectors.

TABLE 9. EFFECT ON TRANSMISSION OF CHANGES IN THE DETECTOR RADIUS.

INPUT DATA

RADIAL MESH = As in Table 4

QUADRATURE ORDER AND SETS = S_8 with Gauss-Legendre data

ORDER OF SCATTERING KERNEL EXPANSION = P_3

REACTION	$E_{THRESHOLD}$ MeV	R_1 = 0.706			R_1 = 0.906		R_1 = 0.506	
		STATUS	ACTIVITIES	TRANSMISSION CHANGE	ACTIVITIES	TRANSMISSION CHANGE	ACTIVITIES	TRANSMISSION CHANGE
$^{27}Al(n, P)^{27}Mg$	4.4	ON	1.521 E-08	0.5232	1.508 E-08	0.5228	1.534 E-08	0.5231
		OFF	2.907 >>	-	2.884 >>	-0.07%	2.932 >>	-0.02%
$^{238}U(n, f)$ F.P.	1.5	ON	1.448 E-06	0.6856	1.442 E-06	0.6856	1.454 E-06	0.6858
		OFF	2.112 >>	-	2.103 >>	0.0%	2.120 >>	+0.03%
$^{237}Np(n, f)$F.P.	0.6	ON	8.409 E-06	0.8688	8.393 E-06	0.8684	8.425 E-06	0.8691
		OFF	9.678 >>	-	9.664 >>	-0.05%	9.693 >>	+0.03%

TABLE 10. EFFECT ON TRANSMISSION OF THE DETECTOR MATERIAL.

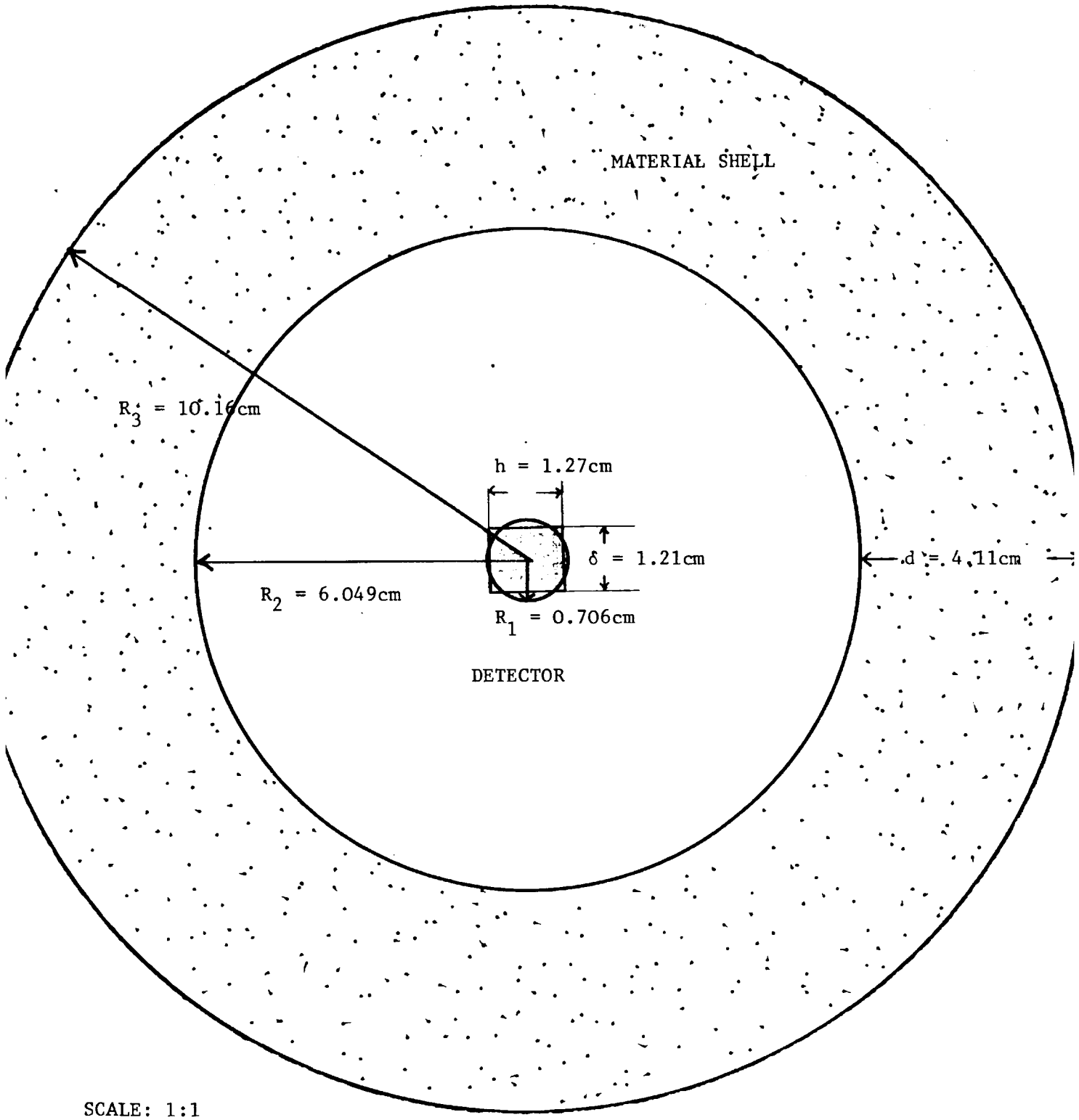
INPUT DATA

RADIAL MESH = As in Table 4 R_1 = 0.706 cm

QUADRATURE ORDER AND SETS = S_8 with Gauss-Legendre data

ORDER OF SCATTERING KERNEL EXPANSION = P_3

REACTION	$E_{THRESHOLD}$ MeV	DETECTOR = ALUMINIUM			DETECTOR = VOID	
		STATUS	ACTIVITIES	TRANSMISSION CHANGE	ACTIVITIES	TRANSMISSION CHANGE
$^{27}Al(n, P)^{27}Mg$	4.4	ON	1.521 E-08	0.5232	1.566 E-15	0.5230
		OFF	2.907 >>	-	2.994 >>	-0.03%
$^{238}U(n, f)$ F.P.	1.5	ON	1.448 E-06	0.6856	1.469 E-13	0.6861
		OFF	2.112 >>	-	2.141 >>	+0.07%
$^{237}Np(n, f)$F.P.	0.6	ON	8.409 E-06	0.8688	8.462 E-13	0.8695
		OFF	9.678 >>	-	9.731 >>	+0.08%



$$K = \frac{\delta}{h} = 0.957$$

FIGURE 20 A SECTIONAL VIEW OF THE DETECTOR-MATERIAL SHELL ARRANGEMENT SHOWING THE EQUIVALENCE BETWEEN CYLINDRICAL AND SPHERICAL DETECTORS.

In conclusion we note that:

(1) the fact that the diameter and height of the cylindrical detector are almost the same makes unimportant the transition to an equivalent spherical one, and

(2) the relatively small size of the detectors makes it possible to neglect their material properties.

3.5.3 Equivalence of Rectangular and Shell Sources.

In the schematization of the geometry of the experimental arrangement we replaced the fission plate by a spherical shell source with the same strength and appropriate thickness.

As seen in Figure 12, the inner boundary of the shell source has only one common point with the plate source, point O in Figure 21, while the outer boundary touches the plate on its four corners, points A, B, C, D in Figure 21. Any spherical surface with radius $R_4<R<R_5$ has an infinite number of common points with the plate lying on a circumference centred at O, as shown in the same Figure.

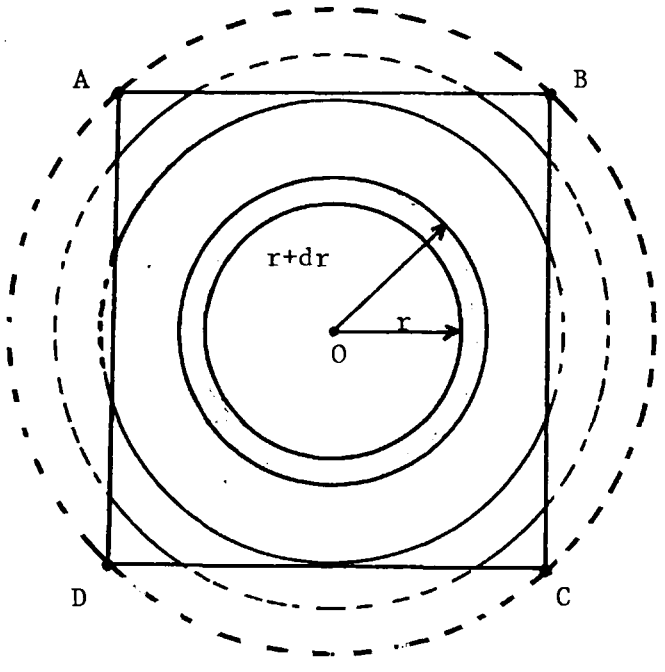


FIGURE 21 EQUIVALENCE OF RECTANGULAR AND SHELL SOURCES

Consider an infinitesimal part of the plate source enclosed between two circles of radii r to r+dr. According to the analysis of paragraph 3.2 this is equivalent to an infinitesimal shell source around the centre of the detector and enclosed within the spherical surfaces of radii R, R+dR, where R and dR are estimated from formulae similar to that of Eqn. (3.7). Consequently the whole fission plate must be equivalent to a shell source with boundaries R_4 and R_5 as calculated according to Figure 15.

We did not proceed to make the above integration and to study the uniformity of the resultant shell source because of the mathematical complexities involved and mainly because we considered it unnecessary. Instead we accepted that a uniformly distributed shell source with boundaries defined by R_4, R_5 and with the same strength as the fission plate constitutes an equivalent representation of the real fission source.

The effect on Transmission of a possible non-uniformity of the shell source is studied together with the effect on Transmission of considering the "distance to source" as the outer, inner or an intermediate radius of the shell source. The results of this investigation are given in Table 11. The changes in this Table are relative to the first colomn results.

We observe in Table 11 relatively high changes in Transmission due to different shell source allocations for a given "distance to the source", but they are still within the pre-established tolerance factor. Hence it is shown that both the way we interpret the "distance to the source" given in Table 3,and a possible non-uniformity of the equivalent, to the fission plate, shell source are responsible for uncertainties in Transmission much smaller than their inherent error due to the input data.

The compatibility of both zero and finite thickness shell sources can

TABLE 11. EFFECT ON TRANSMISSION OF DIFFERENT SHELL SOURCE ALLOCATIONS.

INPUT DATA

RADIAL MESH = As in Table 4

QUADRATURE ORDER AND SETS = S_8 with Gauss-Legendre data

ORDER OF SCATTERING KERNEL EXPANSION = P_3

DISTANCE TO SOURCE = 25.40 cm DETECTOR = void

REACTION	$E_{THRESHOLD}$ MeV	INDERMIDIATE RADIUS R_4 = 24.63, R_5 = 26.42			OUTER BOUNDARY R_4 = 23.61, R_5 = 25.40		INNER BOUNDARY R_4 = 25.40, R_5 = 27.19	
		STATUS	ACTIVITIES	TRANSMISSION CHANGE	ACTIVITIES	TRANSMISSION CHANGE	ACTIVITIES	TRANSMISSION CHANGE
$^{27}Al(n,P)^{27}Mg$	4.4	ON	1.566 E-15	0.5230	1.701 E-15	0.5237	1.475 E-15	0.5228
		OFF	2.994 >>	-	3.248 >>	+0.13%	2.821 >>	-0.02%
$^{237}U(n,f)$ F.P.	1.5	ON	1.469 E-13	0.6861	1.596 E-13	0.6870	1.383 E-13	0.6853
		OFF	2.141 >>	-	2.323 >>	+0.13%	2.018 >>	-0.11%
$^{237}Np(n, f)$F.P.	0.6	ON	8.462 E-13	0.8695	9.197 E-13	0.8709	7.966 E-13	0.8687
		OFF	9.731 >>	-	1.056 E-12	+0.16%	9.170 >>	-0.09%

be demonstrated by showing that the neutron scalar flux inside a spherical surface source is the limit-case of a shell source as its thickness tends to zero. This is done in Appendix A. It is also shown that, as far as the neutron flux at the centre of a shell is concerned, a uniformly distributed shell source with boundaries R_4, R_5 ($R_4<R_5$) is equivalent to a spherical surface source (zero thickness shell) with radius, R, calculated from the Equation:

$$R^2 = \frac{R_5^2 + R_4 R_5 + R_4^2}{3} \qquad (3.13)$$

In most cases Eqn. (3.13) can be approximated by:

$$R \simeq \frac{R_4 + R_5}{2} \qquad (3.14)$$

Since the detectors used are both small and located at the centre of the shell, we can consider the above approximation as suitable in Transmission calculations and therefore the shell source is equivalent to a spherical surface located at the midpoint of the shell. The distance between the centre of the detector and the midpoint of the shell will be called, hereinafter, "distance to source".

An indication of how well the shell source represents the fission plate for different detector - source positions can be acquired by plotting calculated and experimental Transmissions versus "distance to source". We calculated the Transmissions for the $^{238}U(n,f)F.P$ reaction in iron spheres of outside radius 6.35 cm and thickness d = 3.795 cm for varying distance to source. For this case we have experimental information concerning three different distances to source, cases 8, 9 and 10 in Table 1. The results of the calculations together with the experimental values available are given in Table 12.

Table 12 indicates that both "sphere off" and "sphere on" activities approximately follow the $1/R^2$ law, something which verifies the equivalence

TABLE 12. CALCULATED TRANSMISSIONS FOR DIFFERENT DISTANCES TO SOURCE

(^{238}U (n, f) F.P. reaction)

INPUT DATA

RADIAL MESH = varying

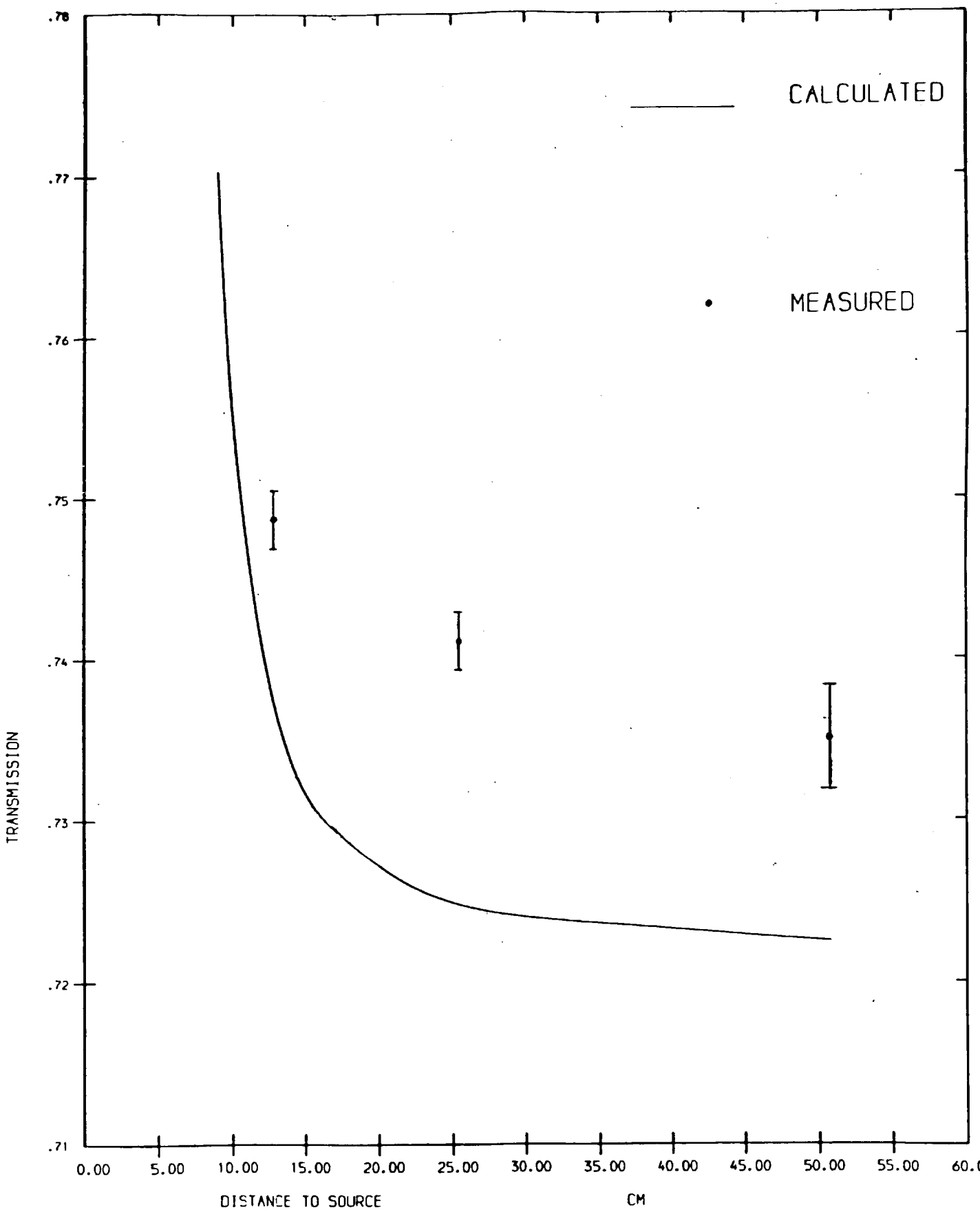
QUADRATURE ORDER AND SETS = S_8 with Gauss-Legendre data

ORDER OR SCATTERING KERNEL EXPANSION = P_3

DETECTOR = void R_1 = 0.706 cm

R_2 = 2.555 cm R_3 = 6.35 cm

CASE	R_{cm}	$R_{4\,cm}$	$R_{5\,cm}$	ACTIVITY ON	ACTIVITY OFF	CALCULATED TRANSMISSION	EXPERIMENTAL TRANSMISSION
1	9.00	7.00	11.10	1.251 E-12	1.624 E-12	0.7703	-
2	10.00	8.10	11.90	1.019 >>	1.249 >>	0.7553	-
3	10.50	8.665	12.335	9.236 E-13	1.230 >>	0.7508	-
4	13.33	11.830	14.920	5.671 >>	7.709 E-13	0.7356	0.749 ± 0.0018
5	18.00	16.820	19.180	3.130 >>	4.294 >>	0.7289	-
6	25.40	24.630	26.420	1.552 >>	2.141 >>	0.7248	0.7414 ± 0.0018
7	35.00	34.40	35.60	8.250 E-14	1.140 >>	0.7236	-
8	42.00	41.50	42.56	5.718 >>	7.907 >>	0.7231	-
9	50.80	50.40	51.20	3.911 >>	5.413 >>	0.7225	0.7354 ± 0.0030



238U(N,F)F.P TRANSMISSIONS VERSUS DISTANCE TO SOURCE, SHELL THICKNESS=3.795CM

FIGURE 22

of point and spherical surface sources. Both calcualted and experimental Transmissions are plotted in Figure 22. Three important conclusions can be drawn from this Figure:

(1) The calculated Transmission is a rapidly decreasing function of the distance to source up to about 20 cm, approaching a constant value for R > 35 cm.

(2) An "eye-guided" curve drawn through the experimental point shows, more or less, the same slope with the calculated curve, something which reinforces the validity of our formulation of B.B.C. experiment. It must be mentioned here that the first experimental point (R = 13.33cm) does not carry as much weight as the others, because, at this position, the way we interpret the "distance to source" given in B.B.C. work strongly influences the allocation of this experimental point, as explained below.

(3) It is rather unimportant how we interpret the "distance to source", given in Table 1 if it exceeds the value of about 30 cm but it is of crucial importance for the Transmission in cases where it falls below 15 cm. Since all the cases included in Table 3 correspond to a distance to source equal to 25.40 cm and taking into account the results of Table 11, we realize that this problem does not affect our work.

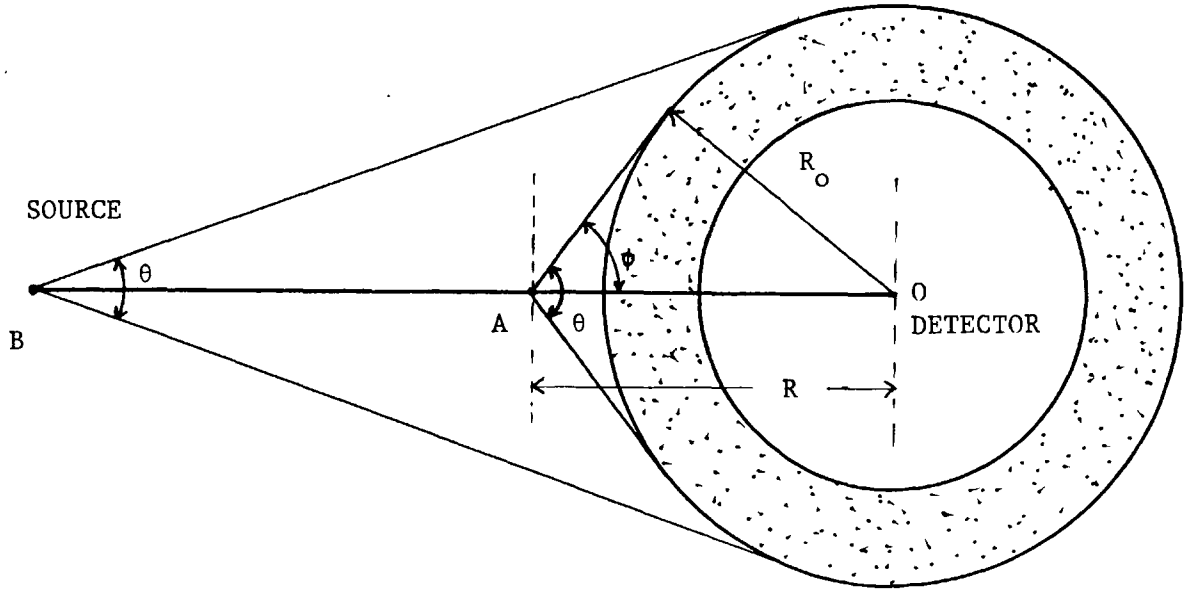
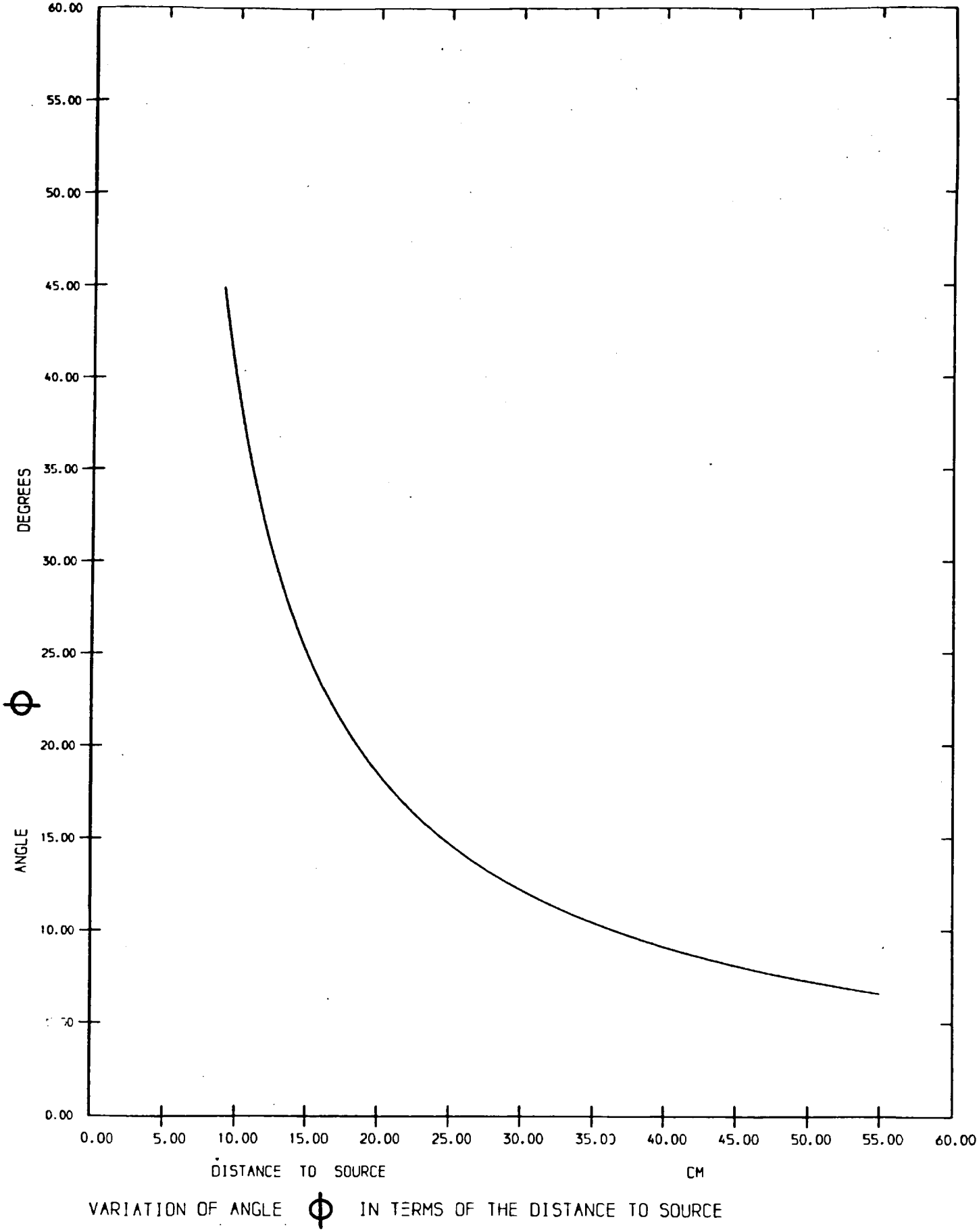


FIGURE 23. EFFECT ON TRANSMISSION OF "DISTANCE TO SOURCE" VARIATIONS.



VARIATION OF ANGLE Φ IN TERMS OF THE DISTANCE TO SOURCE

FIGURE 24

The behaviour of the calculated Transmission in terms of the "distance to source", shown in Figure 22, can easily be explained. Consider for convenience, and clarity, an isotropic point neutron source and a point isotropic detector surrounded by a material shell, as shown in Figure 23. (It is realized that these conditions do not essentially differ from that of the ideal experimental arrangement for reasons we have discussed so far). According to this Figure it is easily understood that as the point source approaches the material shell neutrons emitted within the increasing solid ange Θ and previously lost acquire a certain probability of being detected at O through the multiple scattering process in the shell, while the fraction of source neutrons moving along the path BO and being removed remains constant, as it depends on the material properties and thickness of the shell. Hence,it is expected the function $T = f(R)$ to have a similar structure to that of $\Theta = f'(R)$ or, equivalently, $\phi = f'(R)$, since $\phi = \Theta/_2$. It is easily found from Figure 23 that the function $\phi = f(R)$ has the form:

$$\phi = \arcsin \left(\frac{Ro}{R}\right) \tag{3.15}$$

Formula (3.15) is plotted in Figure 24. From this graph it becomes evident that both $T = f(R)$ and $\phi = f'(R)$ curves have a similar structure, as expected.

The fact that as the point source approaches the detector more and more source neutrons are scattered in the material shell,with an increasing effect on the Transmission,can be explained in terms of the percentage changes in the activities. So,while the "sphere off" activity increases by 278% in going from the R = 18.0 cm to R = 9.0 cm position the corr-esponding "sphere on" activity increases by 299%. The additional increase of 21% due to the aforementioned effect is small compared to that caused by the $1/R^2$ law, but still noticable and responsible for a 5.67% increase in Transmission.

3.6 MONTE - CARLO CALCULATIONS

The main reason for embarking on a MONTE - CARLO analysis of B.B.C. experiments is the acquisition of an independent, self-sufficient yardstick against which we can measure the credibility and adequacy of the calculational scheme we have been constructing so far, before putting it into action.

Since MONTE - CARLO methods can accurately treat three-dimensional complicated geometrical configurations and their algorithm constitutes a statistical simulation of the natural interactions of moving particles with matter, we realize that the approximations of both one-dimensional modelling and discrete ordinates method can unequivocally be tested. Furthermore, the fact that the MONTE - CARLO code used can treat both "pointwise" and "multigroup" cross section data allows an evaluation of the effect of the group-averaging process on the calculated Transmissions.

3.6.1 MONTE - CARLO Method

The MONTE - CARLO method is a numerical procedure based on statistical (or probability) theory. In neutron transport calculations, the applicability of MONTE - CARLO techniques arises from the fact that the (macroscopic) cross-section may be interpreted as a probability of interaction per unit distance travelled by a neutron. Thus, in the MONTE - CARLO method, a set of neutron histories is generated by following individual neutrons through successive collisions. The locations of actual collisions and the results of such collisions, e.g. direction and energy of the emerging neutron, are determined from the range of possibilities by sets of random numbers.

In solving the neutron transport equation by MONTE - CARLO methods, there are uncertainties which are not due to explicit approximations to the flux, such as arise in multigroup methods, but to the limitation in the (finite) number of neutrons examined. Such errors are more or

less random and procedures have been developed for reducing the uncertainty associated with a given amount of numerical work. These are variance reducing techniques; they modify the random walk problem so as to leave the desired expectation value unchanged but reduce the variance.

Most of what can be said about MONTE - CARLO methods is concerned with a detailed discussion of techniques that lies outside the scope of this thesis (15).

There is no doubt that MONTE - CARLO methods are capable of solving a variety of problems for which multigroup methods are inaccurate. Unfortunately this method has also a number of serious drawbacks (in particular, computation times often are very long) and is not as widely used in reactor computations as the multigroup methods which, in these environments, are simpler to apply and sufficiently accurate. MONTE - CARLO methods have been utilized extensively in reactor shielding computations, however, to determine the leakage of neutrons (and photons) through a shield.

3.6.2 MCBEND Code

MCBEND is a MONTE - CARLO deep penetration shielding code for neutrons and gammas. MCBEND has RZ, XYZ and CG (combinational geometry) geometry options; it uses either point energy or group-averaged cross-sections; it can score time-dependent quantities from pulsed sources. There is a complex source shape option, and albedo methods may be used to improve estimation in very difficult attenuation problems.

For XYZ geometry, material regions are formed by the intersection of sets of planes perpendicular to the three axes.

CG geometry is a very general specification in which bodies of different simple shapes may be combined. Sub-zones are defined first as the intersection of the simple bodies and zones are defined as the union

of sub-zones. Zones are regions containing homogeneous material. The problem space must be encased in zones containing a special material called external void.

As the program is designed specifically for problems involving deep penetration special methods of variance reduction are incorporated; however they are optional and the code may be used satisfactorily without them for cases where little or no attenuation occurs. The most significant variance reduction method will be called the SR method; it combines splitting and Russian roulette (16).

The program estimates mean values of scalar fluxes of particles in a number of specified flux energy groups and over the material regions. The flux may be scored in a given volume either by total weighted tract length or by total weighted collisions.
In addition, the activation of up to seven cross-sections may be estimated and these are averaged over the flux scoring regions; each such activation is called the response of a detector. The values of the activation cross-sections are provided in the input data as a set of group-averaged values with respect to energy which will also be called a response function.

The MCBEND source must be a point source, a volume source, or a surface source. In the latter two cases two options, called simple and complex are available for describing the geometrical configuration of the source. A point source may be positioned quite generally in all three geometries. A simple volume source takes the geometry of the material regions when this is RZ or XYZ. When the material regions have CG geometry however the simple source may be either RZ or XYZ in the cartesian co-ordinates framework of the CG geometry. The boundaries of the source regions are always chosen independently from the material region boundaries. The source intensities are taken to be uniform inside each source region. A

complex source option is available in all geometries. The volume or surface source may occupy or take the shape of a collection of simple bodies which may be orientated freely with respect to the material geometry and may even overlap.

The energy spectrum of the simple source option may be continuous or discrete. The continuous spectrum is represented as a histogram over a set of source energy groups and the discrete spectrum is given as a series of monoenergetic values. However, two special spectra are available as built-in functions, these are a representative fission spectrum and an inverse energy spectrum.

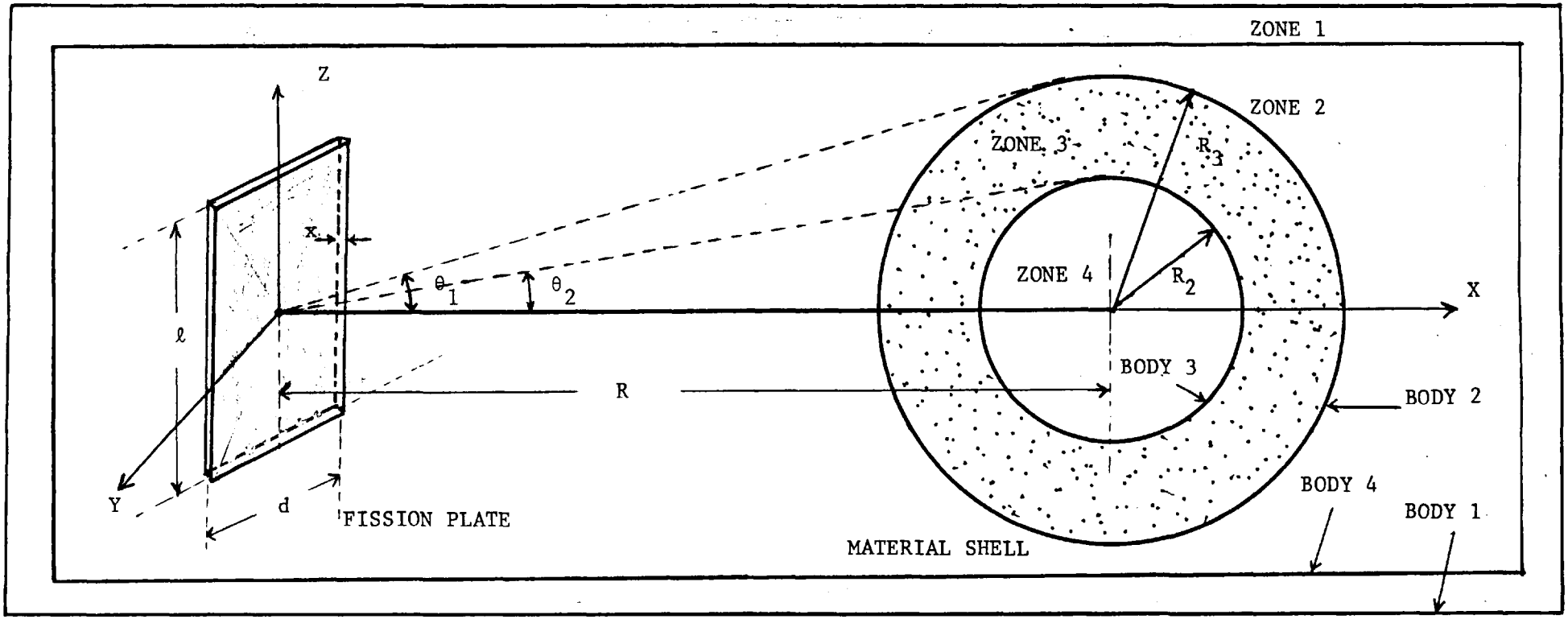
For a simple volume source or a point source the angular distribution can be either isotropic or uni-directional.

For neutron problems the cross-section either are given at point energies down to a pre-assigned cut-off energy which may be followed by a single thermal group or are given a group representation throughout. For the point energy case above the thermal cut-off energy the nuclear interactions are dealt with by the DICE collision package (17). The point cross-sections are obtained from the UKNDL files (18) using a pre-processing code MOULD (17). For the group case the neutron interactions are dealt with by the MORSE package (19). The group cross-sections are presented in the ANISN format for each case. More details about the code itself and a full description of the input/output data can be found in Reference (20).

3.6.3 MCBEND Formulation of B.B.C. Experiments

Despite the generality and power of MCBEND code an exact simulation of the real experimental arrangement can not be practically attained because of the small size of the detectors.

If we were to simulate the real experimental arrangement in a MONTE-CARLO calculation of scalar fluxes and responses and require the



BODIES DEFINITION

BODY 1	RPP	- 1.0	37.0	-12.0	12.0	-12.0	12.0
BODY 2	SPH	R	0.0	0.0	R_2		
BODY 3	SPH	R	0.0	0.0	R_3		
BODY 4	RPP	-0.5	36.0	-11.0	11.0	-11.0	11.0

ZONES DEFINITION

ZONE 1	+1 - 4 EXTERNAL VOID (Black Absorber)
ZONE 2	+4 - 2 ORDINARY VOID
ZONE 3	+2 - 3 MATERIAL (iron)
ZONE 4	+3 ORDINARY VOID (Detection Region)

DATA SPECIFICATION

R = 25.40cm, ℓ = 15.24 cm

d = 11.43cm, x = 0.01 cm

1) IRON SHELL OF THICKNESS = 1.20cm

R_2 = 4.45cm, R_3 = 6.35cm.

2) IRON SHELL OF THICKNESS = 4.11cm

R_2 = 6.05cm, R_3 = 10.16cm

FIGURE 25 MCBEND FORMULATION OF B.B.C. EXPERIMENTS.

statistical uncertainty of the responses to be much smaller than that due to nuclear data used, the runs would be prohibitively expensive and most of the target accuracies unattainable within pre-established large but reasonable time limits.

To this end we decided to score fluxes and responses in the space inside the material shell instead of the tiny sphere of radius R_1 = 0.706 cm representing the actual detectors. Since, in general, the variance on any of the scored quantities in MCBEND decreases with increasing region size, it is perceived that a desirably small statistical uncertainty on volume-averaged reaction rates can be achieved.

It is self-evident that in comparing ANISN - MCBEND results the ANISN runs will be undertaken using exactly the same fission spectrum representation, nuclear data and detection region as in MCBEND calculations. The fact that the perturbed scalar flux varies, though slowly, along the radius of the shell following a variety of patterns for different energy groups while the unperturbed one presents the structure of Figure 17 throughout the whole energy range, does not permit a direct comparison between experimental and MCBEND - calculated Transmissions.

Figure 25 shows the experimental arrangement of B.B.C. experiments as studied with MCBEND.

CG geometry was obviously used in establishing the material regions, while a simple volume source in XYZ geometry represented the fission plate. In this Figure bodies 1 and 4 are rectangular parallelepipeds (RPP) and the six numbers given define the six faces in the X,Y,Z axes, correspondingly (2 consecutive numbers for each direction). Bodies 2 and 3 are spheres (SPH). The first three quantities define the centre of the sphere (X,Y,Z) while the fourth is the radius.

The zones are defined by the intersection of the simple bodies listed. + before a body number implies space within the body while - means space

outside the body. Zone 1 is specified as black absorber to guarantee that any neutron crossing the zone is lost from the system and consequently its history is terminated.

In order to decrease the variance for a given running time, we eliminated the unnecessary tracking of source neutrons leaving the plate and not moving towards the shell, by employing the angular weighting option of MCBEND and specifying zero weight for the source neutrons emitted within the angle $180^{o} - \Theta_1$ and 1.0 for those emitted within Θ_1. The fluxes and responses without the presence of the material shell were obtained by simply considering the material composition of zone 3 as ordinary void. In these cases the source neutrons leaving the plate within the angle Θ_2 were taken with weight 1.0.

The simple volume source representing the fission plate was considered uniform and was normalized to 1.0.

Only the two thin iron shells were studied with MCBEND. The third one of thickness 9.16 cm could not be investigated because of the small size of zone 4 (R_1 = 1.0 cm) and the poor statistics implied.

The U K N D L (2) was used in creating both "pointwise" and "multigroup" neutron cross-section data for iron in a form compatible with MCBEND requirements. The cross-section data in multigroup form were obtained by running the code GALAXY (21) on the U K N D L/DFN = 908 using a 55 energy group structure and 1/E weighting. The 55-energy group scheme used is a subset of DLC-37 100-group structure where the first 35 groups are exactly the same in both structures. This collapsing was undertaken in fulfilling core memory requirements of U L C C computer and has no effect on the calculated Transmissions. This happens because the Transmissions are not sensitive to cross-section data below the 35^{th} group. The 1/E weighting was also used in the creation of the DLC/37 ANISN - formatted multigroup libraries from ENDF/B pointwise library by

employing the processing code AMPX (22). Consequently the fact that in our calculations with the U K N D L data energy group structure and weighting function are the same with that used in creating the DLC-37 multigroup libraries implies that any comments or conclusions concerning the differences between pointwise and multigroup calculations will be approximately valid for the ENDF/B Library.

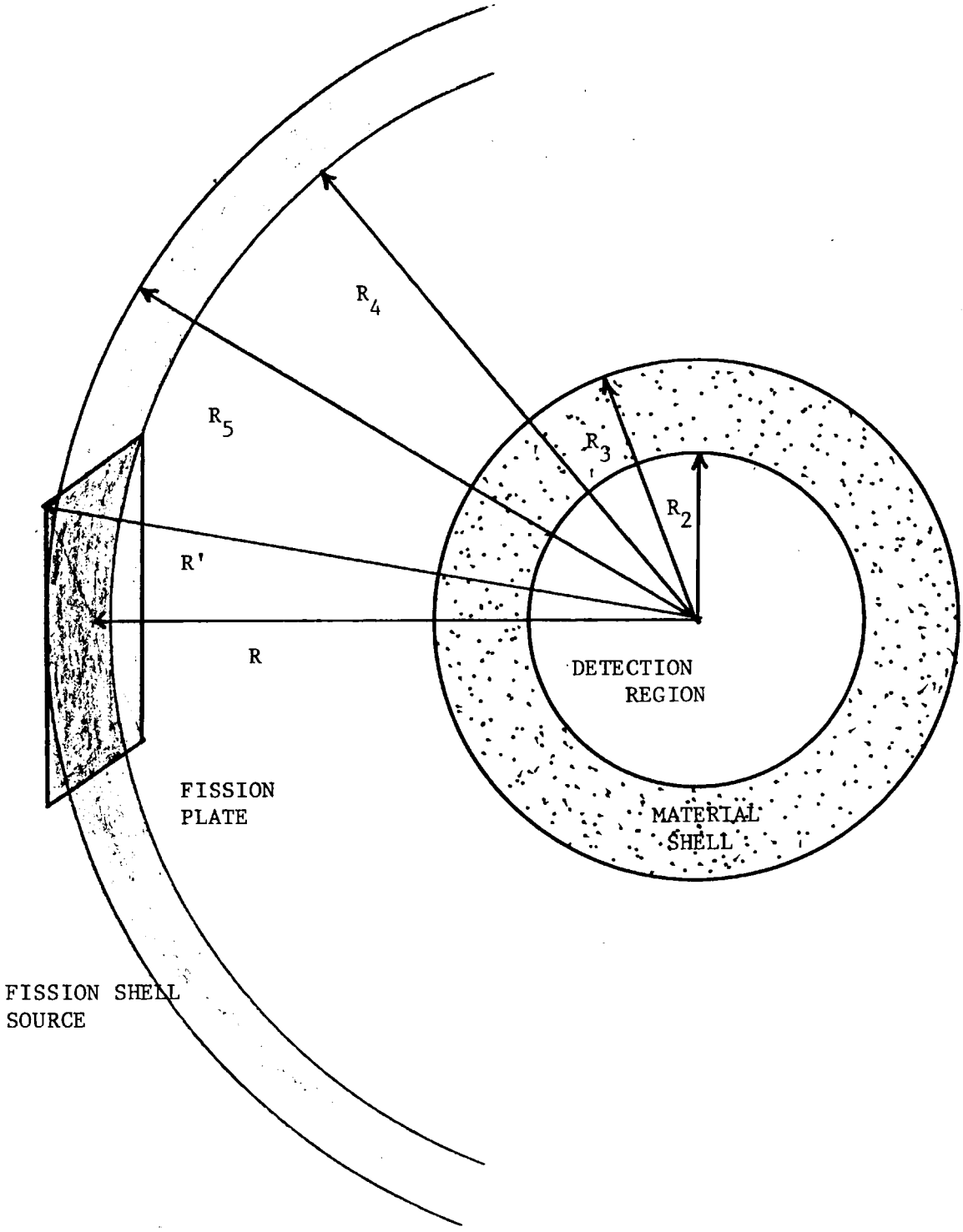
The format conversion code CALCON (23) was finally used in converting the GALAXY - processed multigroup cross-section data into ANISN-formatted matrices compatible with both ANISN and MCBEND codes.

Both DLC-37 100-energy group structure and its subset of 55 groups are tabulated in the end of this thesis.

3.6.4 Comparison of MCBEND and ANISN Results

The MONTE-CARLO analysis of B.B.C. experiments was undertaken at Atomic Energy Establishment (A.E.E), Winfrith where the MCBEND code has been developed and satisfactorily functioning for several years. Table 13 presents the reaction-rates and Transmissions for the two thin iron shells (d = 1.90 cm and d = 4.11 cm) as calculated by MCBEND pointwise, MCBEND - multigroup and ANISN. The units of the reaction-rates in this Table are: Reactions/sec/ nuclide/cm^3/unit fission source. The error accompanying the MCBEND results is the statistical uncertainty mentioned in section 3.6.1 and due to the finite number of neutron histories examined.

In running ANISN for these two cases studied with MCBEND, it was ensured that apart from the different geometrical representation of the fission source all the remaining input data, namely, fission spectrum, material and dosimetry cross-section data, were exactly the same. Consequently what is being assessed in comparing ANISN and MCBEND-multigroup results is the consistency of the two calculational methods (discrete-ordinates / MONTE - CARLO) and the adequacy of the one-dimensional source representation. The optimum shell source boundaries,



R = 25.40 cm

R' = 27.12 cm

R_4 = 25.14 cm

R_5 = 26.86 cm

I) For the iron shell of thickness = 1.90cm

R_2 = 4.45 cm

R_3 = 6.35 cm

II) For the iron shell of thickness = 4.11 cm

R_2 = 6.05 cm

R_3 = 10.15 cm

FIGURE 26 EQUIVALENCE OF MCBEND AND ANISN FORMULATIONS OF B.B.C. EXPERIMENTS.

for which ANISN-calculated fluxes and reaction-rates were as close as possible to corresponding MCBEND - multigroup ones for both thicknesses and "sphere on", "sphere off" cases, were found to be:

$$R_4 = 25.14$$

$$R_5 = 26.86$$

Figure 26 compares the geometrical modellings of the experimental arrangement as studied by MCBEND and ANISN and according to which the quantities in Table 13 were evaluated.

The point source option of the MCBEND code challenged us to investigate the equivalence of the fission plate to a point source of the same strength and spectrum, independently of the analysis followed in section 3.5.3. In pursuing this study the fission plate was replaced by a point source located at varying distance from the centre of the detection region. With the iron shell of thickness d = 1.90 cm it was then found that the fission plate was equivalent to a point source located at about 25.9 cm from the centre of the detection region for the "sphere on" case and at 26.1 cm for the "sphere off". Note that these differences were statistically significant. (e.g. this implies that a point source located at 25.9 cm and representing the fission plate for the "sphere off" case gave inconsistent (higher) reaction-rates with that actually obtained). These important results are of significant importance in our analysis because they show that:

I. The analysis pursued in section 3.5.3 in justifying the equivalence of the fission plate to a shell source of certain thickness is valid and satisfactorily accurate. Indeed, the shell source, with the established boundaries of R_4 = 25.14 and R_5 = 26.86, is equivalent, according to that analysis, to a spherical surface source located at $R = (R_4 + R_5)/2$ = 26.0 cm from the centre of the detection region; this, in turn, is equivalent to a point source located at the same

TABLE 13. MCBEND AND ANISN REACTION RATES AND TRANSMISSIONS FOR THE TWO THIN IRON SHELLS.

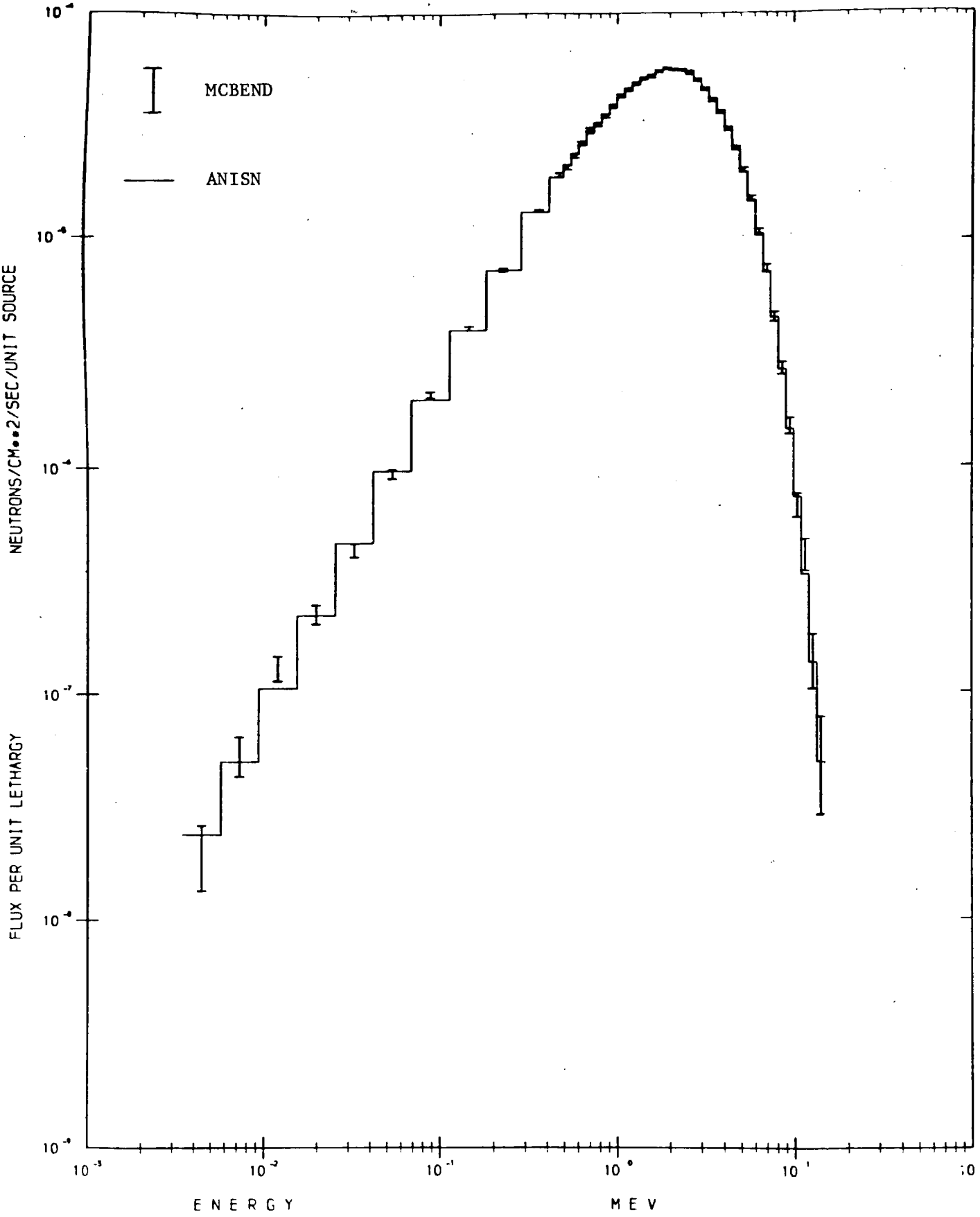
DETECTOR	MCBEND POINTWISE		MCBEND MULTIGROUP		ANISN	
	REACTION RATES	TRANSMISSION	REACTION RATES	TRANSMISSION	REACTION RATES	TRANSMISSION
SHELL THICKNESS = 1.90 cm						
$^{27}Al(n, P)^{27}Mg$	3.501 ± 0.028 E-31 4.629 ± 0.023 >>	0.7563 ± 0.0071	3.429 ± 0.024 E-31 4.629 ± 0.023 >>	0.7407 ± 0.0063	3.430 E-31 4.605 >>	0.7448
$^{238}U(n, f)$ F.P.	3.034 ± 0.009 E-29 3.494 ± 0.007 >>	0.8683 ± 0.0031	3.000 ± 0.009 E-29 3.494 ± 0.007 >>	0.8586 ± 0.0030	2.993 E-29 3.511 >>	0.8524
$^{237}Np(n, f)$F.P.	1.472 ± 0.004 E-28 1.547 ± 0.002 >>	0.9515 ± 0.0029	1.467 ± 0.003 E-28 1.547 ± 0.002 >>	0.9482 ± 0.0021	1.467 E-28 1.565 >>	0.9378
SHELL THICKNESS = 4.11 cm						
$^{27}Al(n, P)^{27}Mg$	2.432 ± 0.041 E-31 4.689 ± 0.042 >>	0.5186 ± 0.0100	2.483 ± 0.029 E-31 4.689 ± 0.042 >>	0.5295 ± 0.0080	2.467 E-31 4.661 >>	0.5292
$^{238}U(n, f)$ F.P.	2.478 ± 0.014 E-29 3.541 ± 0.010 >>	0.6998 ± 0.0046	2.417 ± 0.009 E-29 3.541 ± 0.010 >>	0.6825 ± 0.0034	2.445 E-29 3.553 >>	0.6881
$^{237}Np(n, f)$F.P.	1.367 ± 0.005 E-28 1.574 ± 0.003 >>	0.8684 ± 0.0038	1.354 ± 0.004 E-28 1.574 ± 0.003 >>	0.8602 ± 0.0031	1.352 E-28 1.584 >>	0.8535

distance. This value is very close to true values of 25.9 cm and 26.1 cm for the "sphere on" and "sphere off" cases, correspondingly. On the other hand, we do expect according to analysis of section 3.5.3 the non-uniform shell source defined by the centre of the rectangular plate and one of its corners to be equivalent to a point source which lies nearer the centre than the corner, both taken along the same radius (see Fig. 12I), as has actually been found.

II. It is reasonable to expect that the agreement between MCBEND-multigroup and ANISN calculations is better than that shown in Table 13 where the same shell sources boundaries were used for both "sphere on" and "sphere off" cases which amounts to accepting the same point source for both cases.

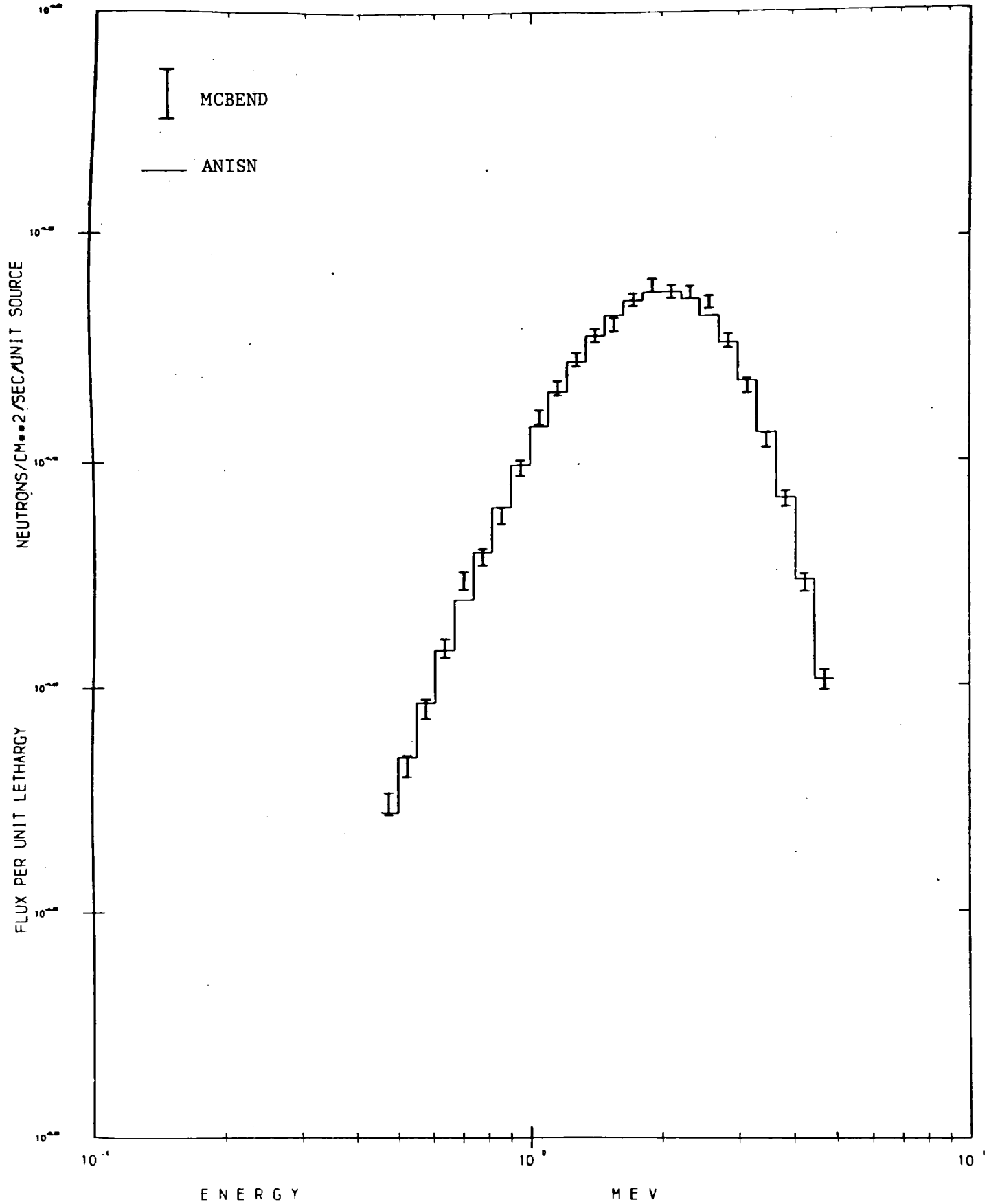
If it is postulated that the ANISN - calculated Transmissions are accompanied by the same uncertainty due to calculational method as the corresponding MCBEND - multigroup ones (this is a quite conservative assumption since the difference between converging ANISN approximations P_o, P_1, P_3 or S_8, S_{16} etc, in the last stage is smaller compared to this value) then it is realised that MCBEND and ANISN Transmissions are statistically consistent in almost all the cases presented in Table 13. What remains to be seen in the following chapters is how this "calculational uncertainty" is compared to that originating from the nuclear data used in the calculations. It is evident that this comparison is of crucial importance in interpreting discrepancies between measured and calculated Transmissions in terms of inadequacies of the nuclear data used.

Comparing MCBEND - pointwise and MCBEND - multigroup Transmissions in Table 13 it is noticed that the multigroup calculations tend to underestimate the Transmissions. The only exception is the $^{27}A\ell(n,p)^{27}$ Mg, d = 4.11 Transmission; the fact that the two (multigroup-pointwise) results agree to well within their standard deviations



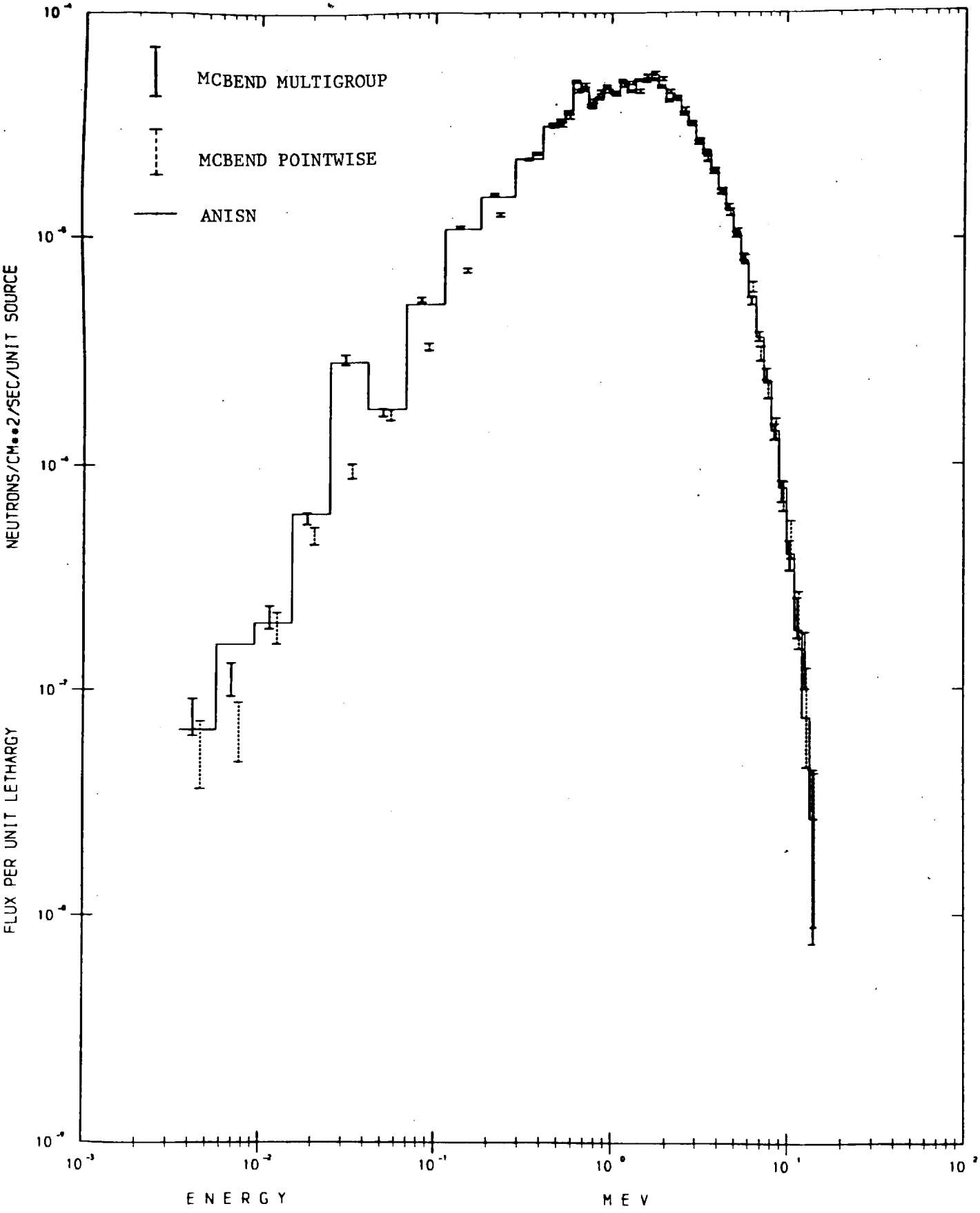
ANISN AND MCBEND SCALAR FLUXES WITHOUT THE PRESENCE OF THE IRON SHELL

FIGURE 27



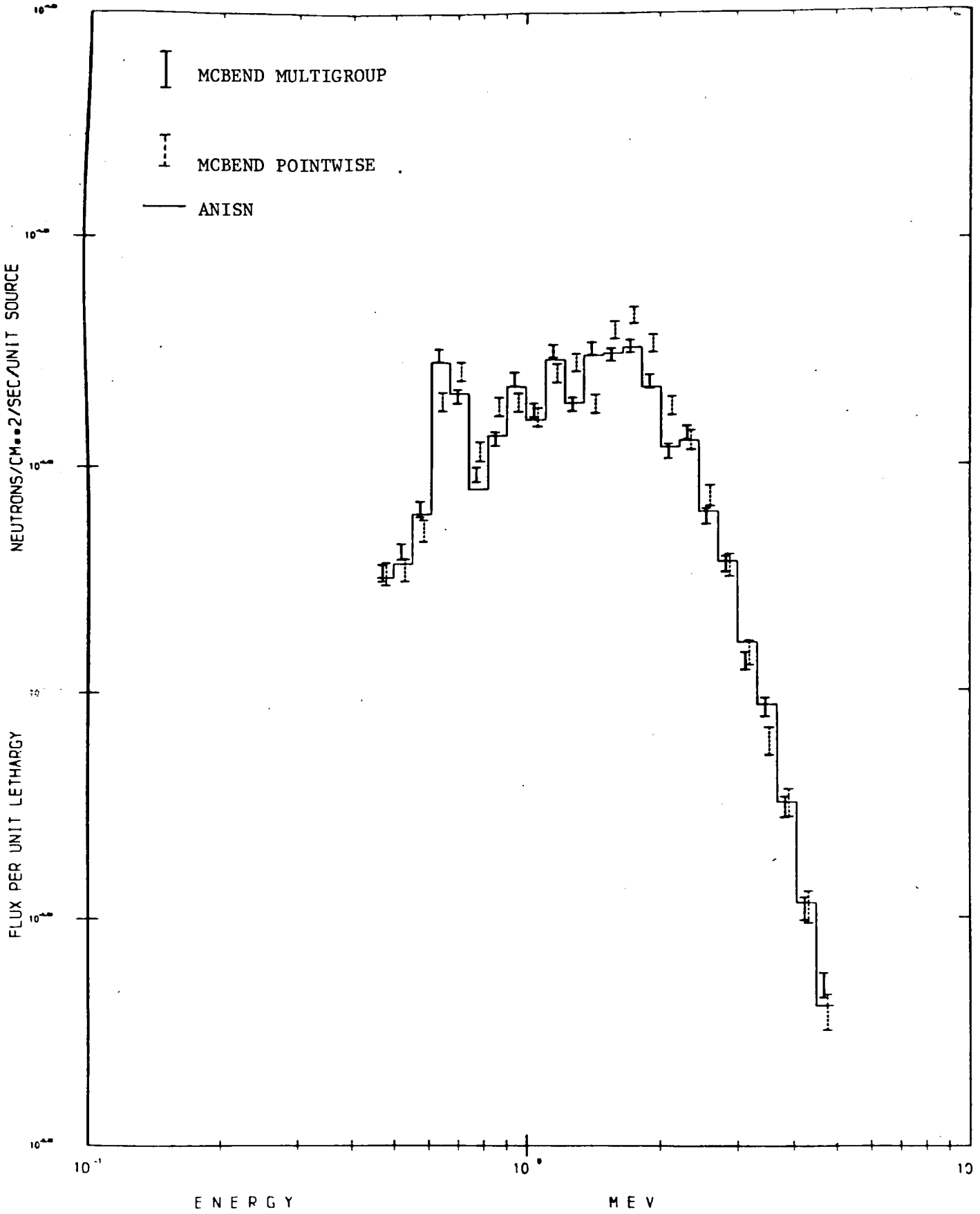
ENLARGEMENT OF FIGURE 27 IN THE ENERGY RANGE 0.1MEV - 10.0MEV

FIGURE 28



ANISN AND MCBEND SCALAR FLUXES INSIDE THE IRON SHELL . THICKNESS = 4.11 CM

FIGURE 29



ENLARGEMENT OF FIGURE 29 IN THE ENERGY RANGE 0.1MEV - 10.0MEV

FIGURE 30

makes this exception unimportant.

Figures 27, 28 and Figures 29, 30 present the MCBEND and ANISN volume-averaged scalar fluxes in the detection region without and with the presence of the iron shell of thickness d = 4.11 cm, correspondingly. In all the figures the agreement between MCBEND - multigroup and ANISN results is noticeably good. The MCBEND-pointwise fluxes scatter up and down along the ANISN histogram but still follow the broad structure of the ANISN - flux profile.

A salient and rather unexpected discrepancy between ANISN/MCBEND - multigroup and MCBEND - pointwise fluxes is a local peak observed in the 41st energy group (24.7KeV - 40.3KeV) which does not seem to exist in reality (pointwise fluxes). Most probably this discrepancy arises from a complete failure of the group constant to describe the neutron interactions in this energy range stemming from an inappropriate group-averaging procedure (complicated fine structure of the cross-section in this energy range, inadequate weighting function etc.).

Finally the fact that the agreement between ANISN/MCBEND - multigroup and MCBEND - pointwise fluxes appears to be poorer below the 35th group (450 KeV) should be closely related to the broader energy groups and to complicated fine structure of the cross-section (especially elastic) variation in terms of energy. However, this inconsistency is hardly responsible for the observed differences between multigroup and pointwise MCBEND Transmissions, simply because they are insensitive to cross-section data in this energy region.

3.7 CALCULATED TRANSMISSIONS

The optimum calculational scheme emerging from the optimisation procedure, additional ANISN and MCBEND calculations, tests and comparisons undertaken so far can be summarised as follows:

A S_8 P_3 discrete ordinates approximation with Gauss-Legendre quadrature sets and an adequate radial mesh.

Spherical detectors of radious R_1 = 0.706 cm without any material composition.

A uniformly distributed shell source of thickness 1.72 cm isotropically emitting thermal fission neutrons with boundaries located at R_4 = 25.14 cm and R_5 = 26.86 cm from the centre of the detector.

Grundl's recent formula was used in representing the thermal - fission spectrum while the ENDF/B-IV dosimetry data for the three threshold detectors were employed in both preliminary and final calculations.

Table 14 gives the calculated Transmissions for different isotopes, nuclear data files and shell thicknesses together with the corresponding experimental values taken from Table 3.

In this Table U K N D L (1) indicates a very old version of the U K N D L (DFN for iron = 906) in terms of which the optimisation procedure was undertaken in a 37 - group structure, while U K N D L (2) stands for the most recent version of the same library (DFN for iron = 908). All the calculations were carried out in the 55 - group scheme which essentially corresponds to DLC-37 100 - group structure. The only exception is the Fe and Al Transmissions using the U K N D L (1) data set which were accomplished in the 37 - group structure.

Since the choice of proper quadrature sets depends on the energy group structure employed, further optimisation tests were undertaken with the ENDF/B-1V data file to ensure that both a S_8 approximation is sufficient for our purposes and that the Gauss-Legendre quadrature

TABLE 14. EXPERIMENTAL AND CALCULATED TRANSMISSIONS FOR DIFFERENT ISOTOPES, SHELL THICKNESSES, THRESHOLD DETECTORS AND DATA SETS.

	MATERIAL	THICKNESS cm	SPHERE OUTSIDE RADIUS cm	TRANSMISSIONS						DATA SETS
				$^{27}Al(n, P)^{27}Mg$ 1.4 MeV		$^{238}U(n, f)$ F.P. 1.5 MeV		$^{237}Np(n, f)$ F.P. 0.6 MeV		
				EXPERIMENTAL	CALCULATED	EXPERIMENTAL	CALCULATED	EXPERIMENTAL	CALCULATED	
1.	Fe	1.90	6.35	0.7938 ± 0.0071	0.7625 0.7833 0.7831 0.7729 0.7735	0.8688 ± 0.0019	0.8610 0.8754 0.8745 0.8658 0.8669	0.9455 ± 0.0033	0.9480 0.9483 0.9479 0.9491 0.9493	U.K.N.D.L. (1) U.K.N.D.L. (2) DLC-2 D ENDF/B-III DLC-37D ENDF/B-IV DLC-37F >>
2.	Fe	4.11	10.16	-	0.5232 0.5784 0.5777 0.5620 0.5632	0.7132 ± 0.0020	0.6861 0.7226 0.7205 0.7045 0.7055	0.8625 ± 0.0033	0.8696 0.8732 0.8726 0.8754 0.8761	U.K.N.D.L. (1) U.K.N.D.L. (2) DLC-2 D ENDF/B-III DLC-37D ENDF/B-IV DLC-37F >>
3.	Fe	9.16	10.16	-	0.2312 0.2944 0.2937 0.2764 0.2778	0.4694 ± 0.0041	0.4254 0.4731 0.4700 0.4478 0.4495	0.7250 ± 0.0044	0.7169 0.7191 0.7187 0.7257 0.7272	U.K.N.D.L. (1) U.K.N.D.L. (2) DLC-2 D ENDF/B-III DLC-37D ENDF/B-IV DLC-37F >>
4.	Al	3.84	10.16	0.7901 ± 0.0065	0.7782 0.8002 0.8011 0.8012	0.8965 ± 0.0025	0.8780 0.8894 0.8954 0.8954	0.9673 ± 0.0033	0.9570 0.9621 0.9690 0.9691	U.K.N.D.L. (1) DLC-2 D ENDF/B-III DLC-37D ENDF/B-IV DLC-37F >>
5.	Cu	2.06	10.16	0.7460 ± 0.010	0.7343 0.7381	-	0.8102 0.8087	-	0.9302 0.9270	U.K.N.D.L. DLC-2 D ENDF/B-III DLC-37D ENDF/B-IV DLC-37F >>
6.	Cu	4.12	10.16	-	0.5276 0.5347 0.5349	0.6494 ± 0.0018	0.6334 0.6320 0.6323	0.8419 ± 0.0033	0.8440 0.8388 0.8394	U.K.N.D.L. DLC-2 D ENDF/B-III DLC-37D ENDF/B-IV DLC-37F >>
7.	Ni	2.07	6.65	0.7398 ± 0.0060	0.7327 0.7347	0.8379 ± 0.0022	0.8346 0.8290	0.9291 ± 0.0033	0.9397 0.9347	U.K.N.D.L. DLC-2 D ENDF/B-III DLC-37D ENDF/B-IV DLC-37F >>

TABLE 14. Continued.

	MATERIAL	THICKNESS cm	SPHERE OUTSIDE RADIUS cm	TRANSMISSIONS						DATA SETS
				$^{27}Al(n, P)^{27}Mg$ 1.4 MeV		$^{238}U(n, f)$ F.P. 1.5 MeV		$^{237}Np(n, f)$ F.P. 0.6 MeV		
				EXPERIMENTAL	CALCULATED	EXPERIMENTAL	CALCULATED	EXPERIMENTAL	CALCULATED	
8.	Pb	3.12	10.16	0.7727 ± 0.014	0.7649	0.9118 ± 0.0015	0.9032	0.9791 ± 0.0042	0.9782	U.K.N.D.L. DLC-2 D ENDF/B-III DLC-37D ENDF/B-IV DLC-37F >>
9.	Pb	6.24	10.16	-	0.5778 0.5751	0.8178 ± 0.0020	0.8021 0.8009	-	0.9445 0.9437	U.K.N.D.L. DLC-2 D ENDF/B-III DLC-37D ENDF/B-IV DLC-37F >>
10.	V	1.32	3.20	-	0.8782 0.8606	0.9305 ± 0.0027	0.9283 0.9158	0.9731 ± 0.0037	0.9750 0.9696	U.K.N.D.L. DLC-2 D ENDF/B-III DLC-37D ENDF/B-IV DLC-37F >>
11.	Sn	3.50	10.16	0.7524 ± 0.0060	0.7612	0.8388 ± 0.0024	0.8551	0.9437 ± 0.0033	0.9596	U.K.N.D.L. DLC-2 D ENDF/B-III DLC-37D ENDF/B-IV DLC-37F >>
12.	Sn	7.01	10.16	-	0.5750 0.5734	0.6950 ± 0.0022	0.7216 0.7198	-	0.9103 0.9078	U.K.N.D.L. DLC-2 D ENDF/B-III DLC-37D ENDF/B-IV DLC-37F >>
13.	Zr	3.30	5.71	0.7736 ± 0.0080	0.7760 0.7760	0.8439 ± 0.0030	0.8606 0.8606	0.9418 ± 0.0037	0.9488 0.9489	U.K.N.D.L. DLC-2 D ENDF/B-III DLC-37D ENDF/B-IV DLC-37F >>
14.	W	1.06	6.28	0.8288 ± 0.0066	0.8409	0.8506 ± 0.0020	0.8494	0.9203 ± 0.0033	0.9257	U.K.N.D.L. DLC-2 D ENDF/B-III DLC-37D ENDF/B-IV DLC-37F >>
15.	Ti	2.87	5.71	-	0.8140	0.8950 ± 0.0024	0.8954	0.9650 ± 0.0042	0.9624	U.K.N.D.L. DLC-2 D ENDF/B-III DLC-37D ENDF/B-IV DLC-37F >>

sets are more advantageous compared to that of even moments'.
For all the cases presented in Table 14 an adequate radial mesh was warranted by repeating the calculations with half the number of radial intervals in the material shell from that initially established and observing no effect on the Transmission.

Commenting on the results of Table 14 it is first noticed that the U K N D L (1) - calculated iron and aluminium Transmissions are in poorer agreement with the measured values than any other calculated values. This is mainly due to poor quality of the U K N D L (1) data and possibly to the broad energy group structure employed. Comparing ENDF/B - III and ENDF/B - IV results for the iron shells it is noticed that the ENDF/B-III Transmissions are over-estimates of the ENDF/B -IV ones for the $^{27}A\ell$ and ^{238}U detectors and under-estimates for the ^{237}Np. It seems as well that the overall agreement of ENDF/B-III iron Transmissions with the measured ones is better than that of the ENDF/B-IV. However, if we accept that multigroup calculations

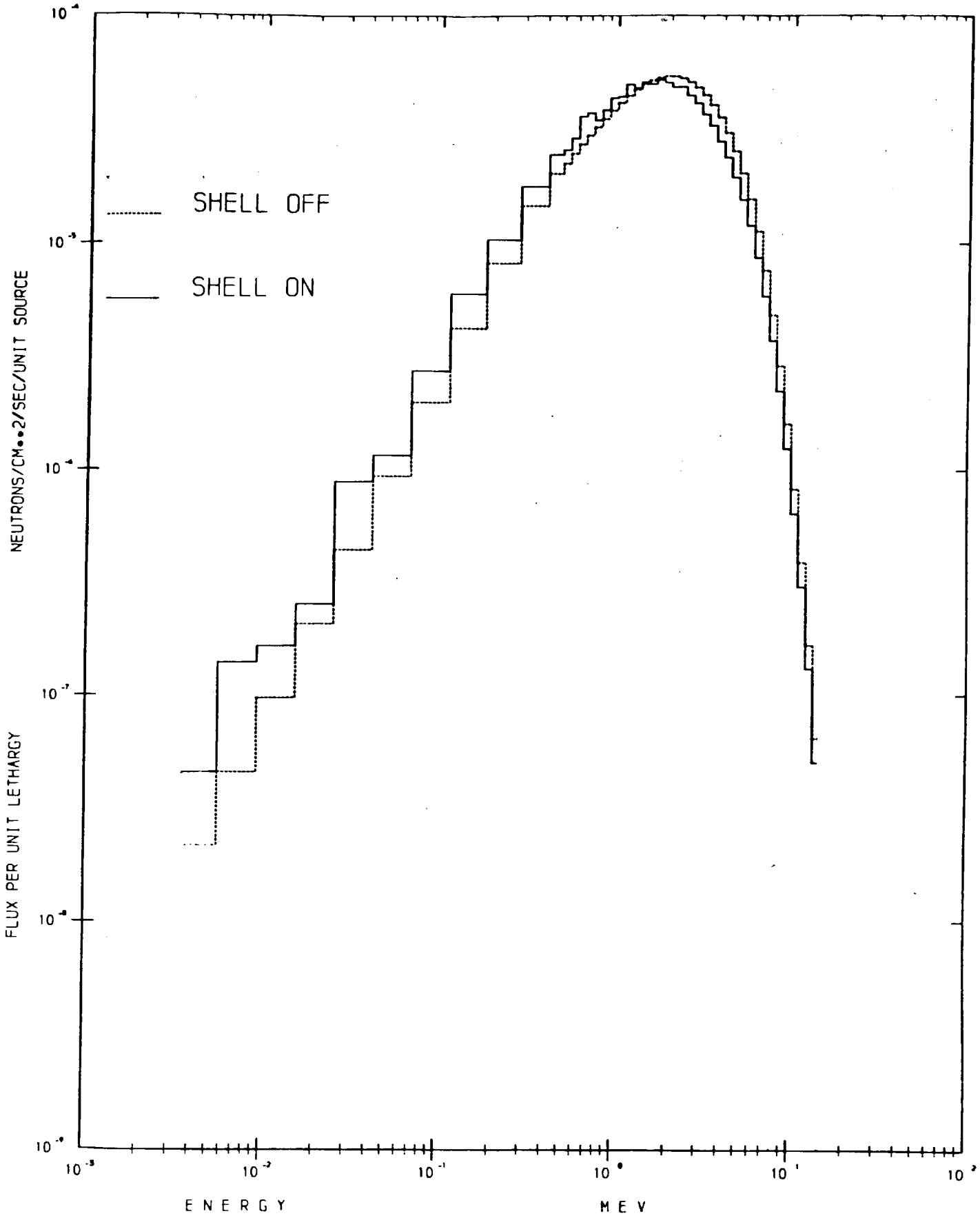
tend to underestimate the iron Transmissions, as found in section 3.6 with the U K N D L (2) data set then, since the ENDF/B-IV $^{27}A\ell$ and ^{238}U Transmissions are underestimates of the measured ones, it is perceived that the ENDF/B-IV iron data predict better the measured Transmissions than the ENDF/B-III library, at least for these two detectors.
We differentiate here between $^{27}A\ell/^{238}U$ and $^{237}N_p$ Transmissions because, as will be demonstrated in a later chapter, the quality of the dosimetry data is expected to play a much more important role in interpreting differences between calculated and measured values for the $^{237}N_p$ Transmissions than for the other two detectors.
The inter-comparison of ENDF/B-III, ENDF/B-IV and measured Transmissions for those isotopes for which ENDF/B-III data exist does not clearly demonstrate the superiority of the ENDF/B-IV file in predicting the

experimental values, as might be expected.

U K N D L (2) and ENDF/B-III iron Transmissions appear to be, more or less, the same for all the thicknesses and threshold detectors. The fact that U K N D L (2) is based on the ENDF/B-III pointwise data indicates that the AMPX and GALAXY multigroup processing codes produce compatible multigroup cross-section data libraries.

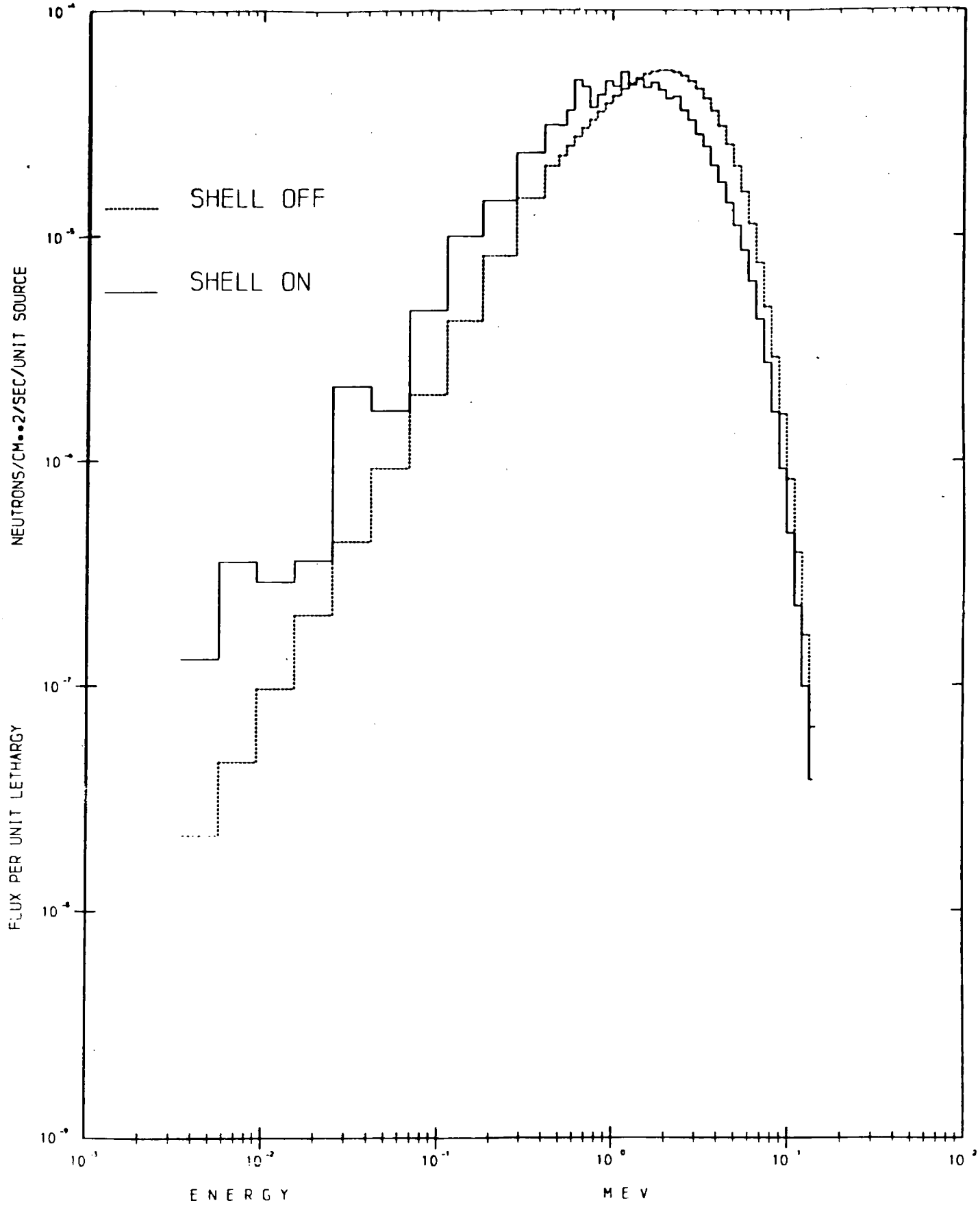
Comparing the U K N D L (2) iron Transmissions with the ANISN-calculated ones of Table 13 it is noticed that the Transmissions scored in the space inside the iron shells are smaller compared to those corresponding to the actual size of the detectors. The reason for this is that the unperturbed flux is an increasing function of the radius across the whole energy range (see Figure 17), while the perturbed one presents the opposite behaviour in the space inside the iron shells and up to 25th energy group. These flux patterns are responsible for higher volume - averaged "sphere off" reaction rates and lower "sphere on" ones as compared with those corresponding to the actual size of the detectors.

The characterization of the relation between measured and calculated values of a certain Transmission as being of satisfactory agreement or that of a large discrepancy can be based on the standard deviations of the measured values, the error of the calculated value attributable to calculational method and on our somewhat subjective judgement. Consequently the distinction between these two classifications is meant to be loose and not well defined in the following. According to this general criterion for aluminium, nickel, vanadium, tungsten and titanium the relation between measured and ENDF/B (III or IV)-calculated values is judged to be of satisfactory agreement and, consequently, these cases will not be subjected to further investigation.



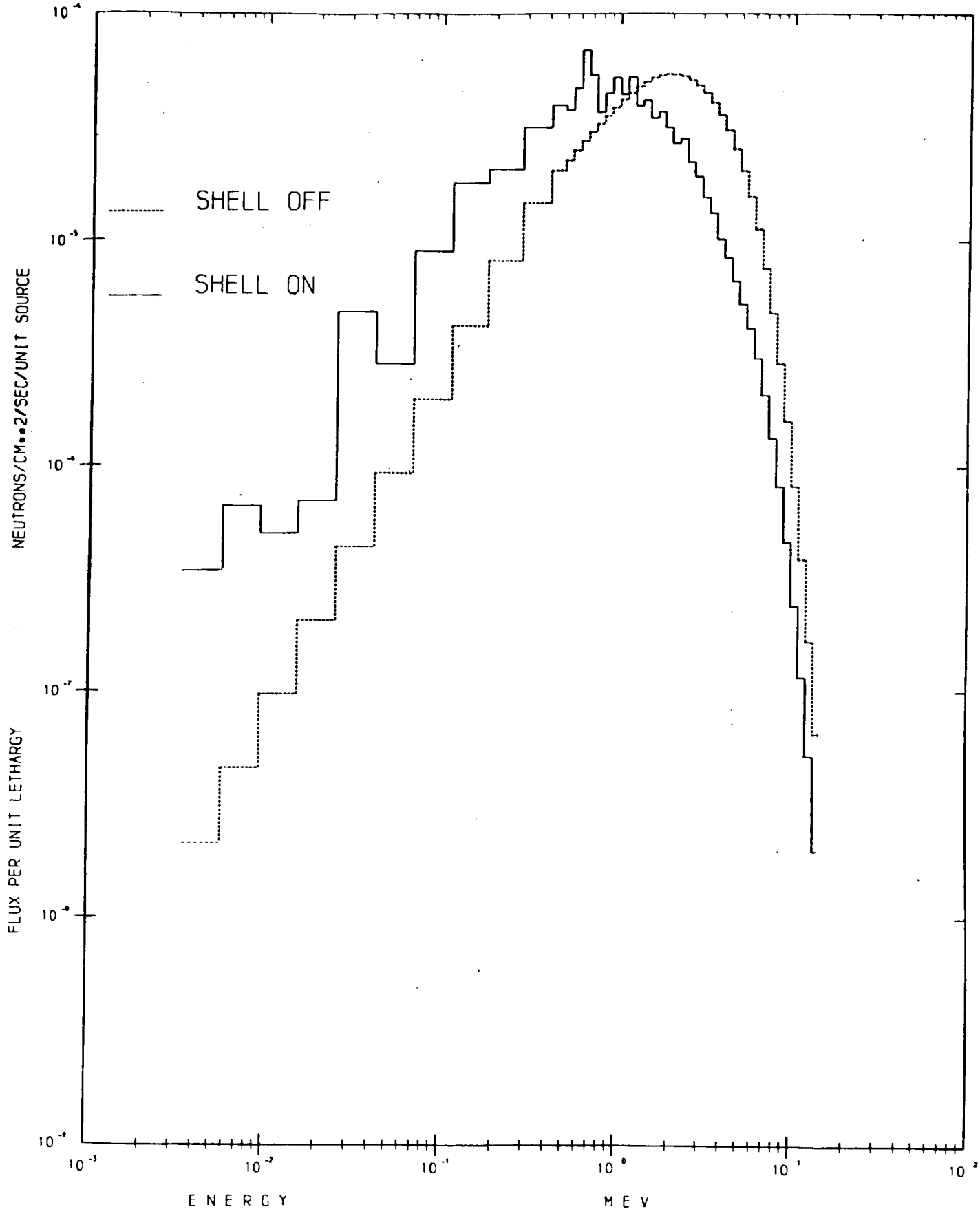
NEUTRON SPECTRA AT THE CENTRE OF THE IRON SHELL , THICKNESS = 1.90 CM

FIGURE 31



NEUTRON SPECTRA AT THE CENTRE OF THE IRON SHELL , THICKNESS = 4.11 CM

FIGURE 32



NEUTRON SPECTRA AT THE CENTRE OF THE IRON SHELL . THICKNESS = 9.16 CM

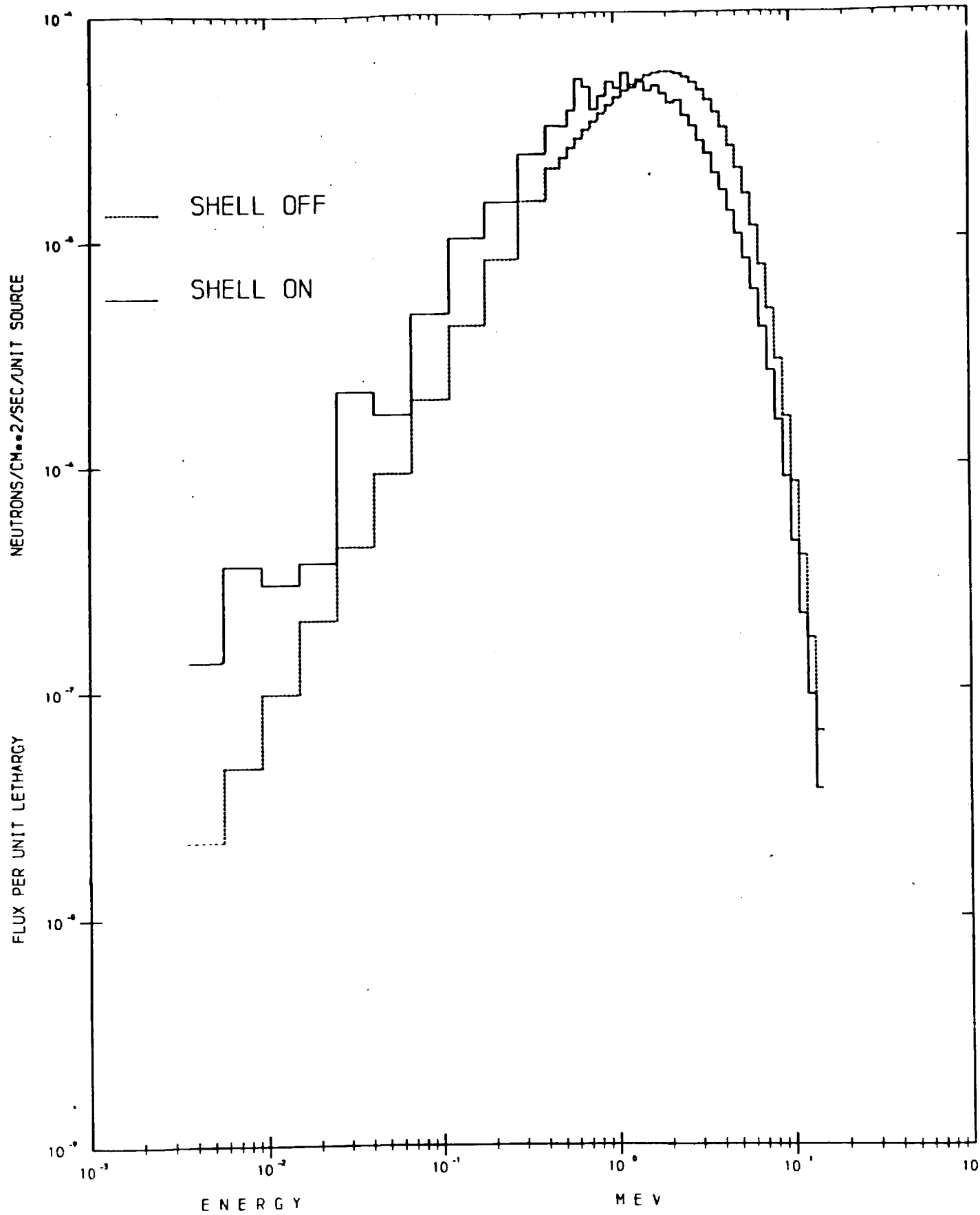
FIGURE 33

However, it must be pointed out here that this does not necessarily imply that the status of the corresponding ENDF/B data sets is equally satisfactory or that they do not need further improvement. What the observed agreement simply indicates is that the data set under investigation is collectively sufficient and satisfactory in those reactions and energy ranges for which the measured integral quantities are found to be sensitive. This, of course, does not exclude the possibility for the data set to be inadequate and unsatisfactory in general terms and for some individual items, with the apparent agreement being the net effect of competing inadequacies and shortcomings of various elements of the data set.

Large discrepancies between measured and calculated Transmissions which imply deficiences and/or a need for a better knowledge of the nuclear data used are experienced in the following cases: Some of the iron cases especially those referring to high threshold detectors and large thicknesses, ^{238}U Transmissions for copper, lead, tin and zirconium.

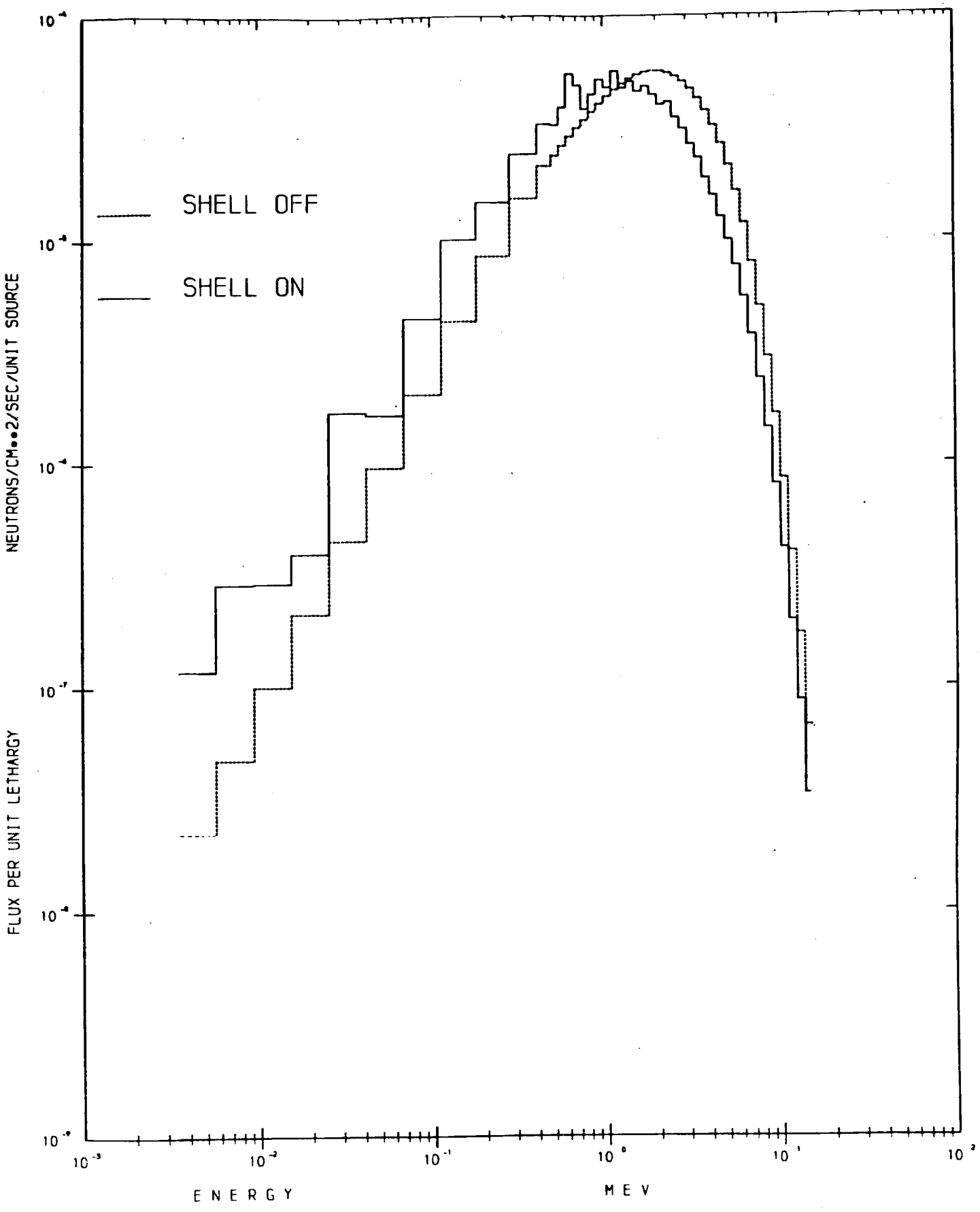
Figures 31, 32 and 33 present the unperturbed and perturbed neutron spectra at the centre of the three iron shells. We notice that the presence of the material shell causes a shift of high energy neutrons to low energy groups due mainly to inelastic and secondly to elastic scattering processes in the shell. This shift is stronger for the thickest shell, as expected.

Figures 34, 35 and 36 present the neutron spectra at a certain point in the space inside the iron shell (R = 4.15 cm), within the iron shell itself (R = 8.36 cm), and at a certain point between the iron shell and the shell source (R = 16.53 cm), correspondingly. It is observed that the neutron spectrum at R = 4.15 cm presents exactly the same structure with that at the centre. The spectrum within the iron shell



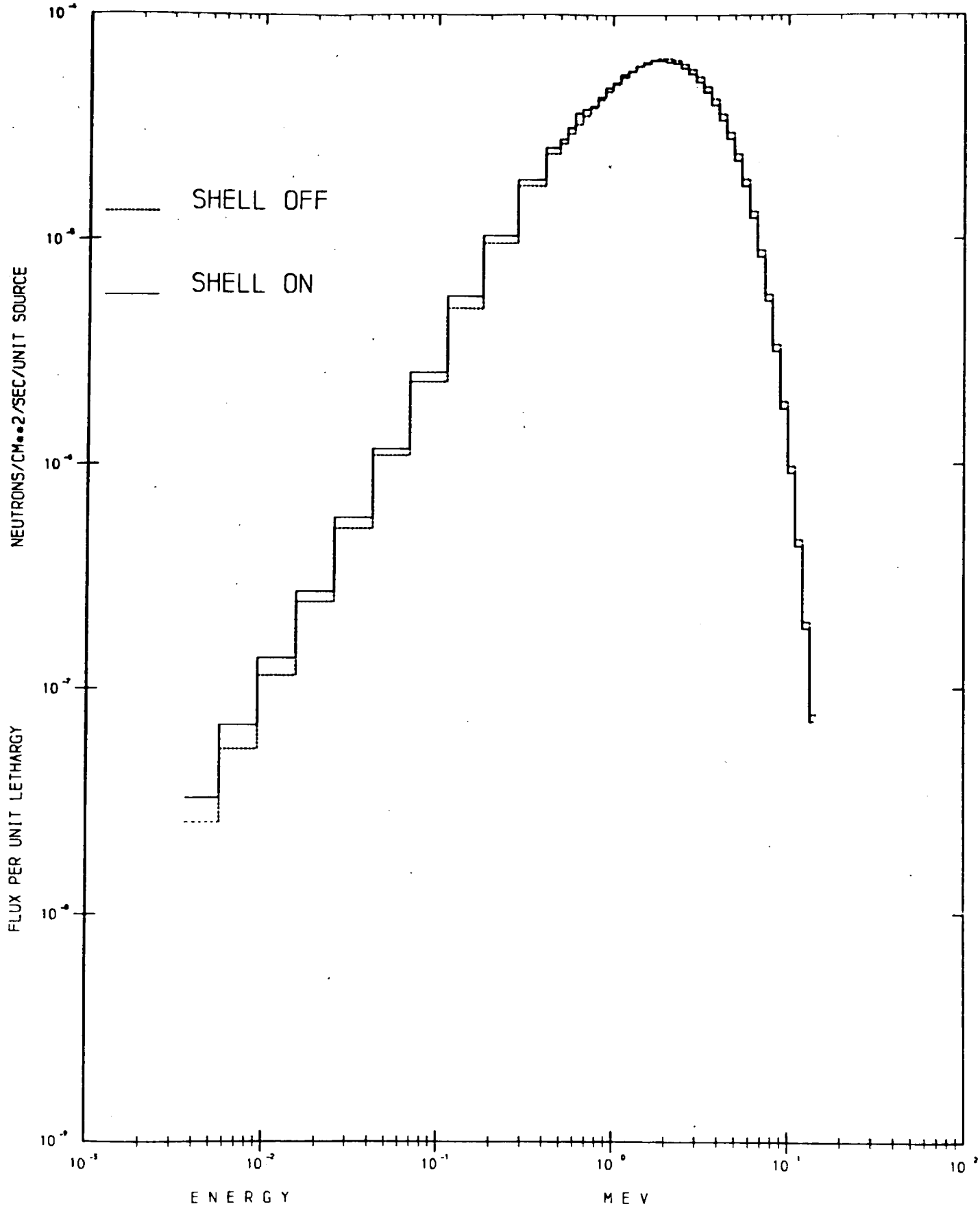
NEUTRON SPECTRA AT 4.15CM FROM THE CENTRE OF THE IRON SHELL, THICKNESS=4.11CM

FIGURE 34



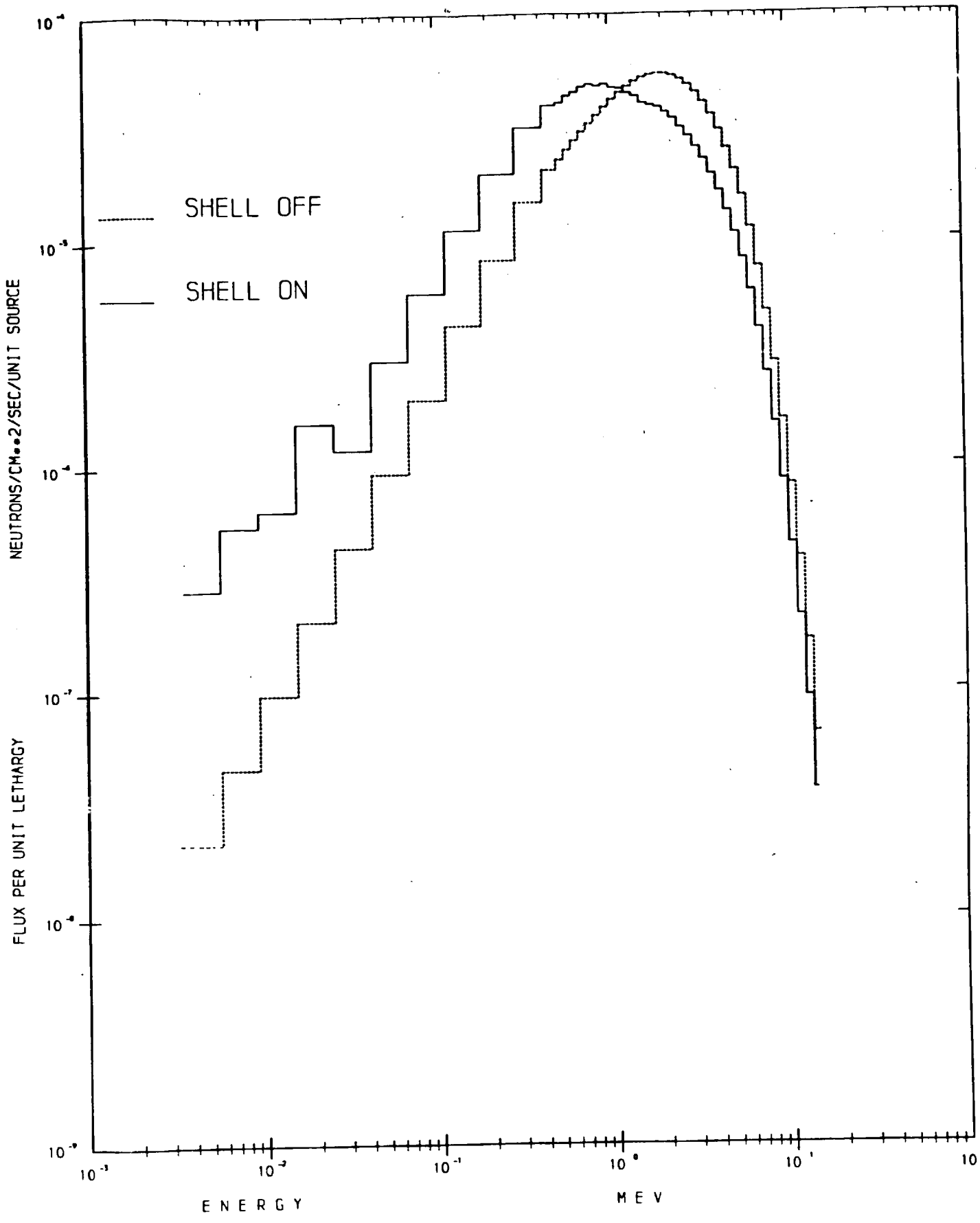
NEUTRON SPECTRA AT 8.36CM FROM THE CENTRE OF THE IRON SHELL. THICKNESS=4.11CM

FIGURE 35



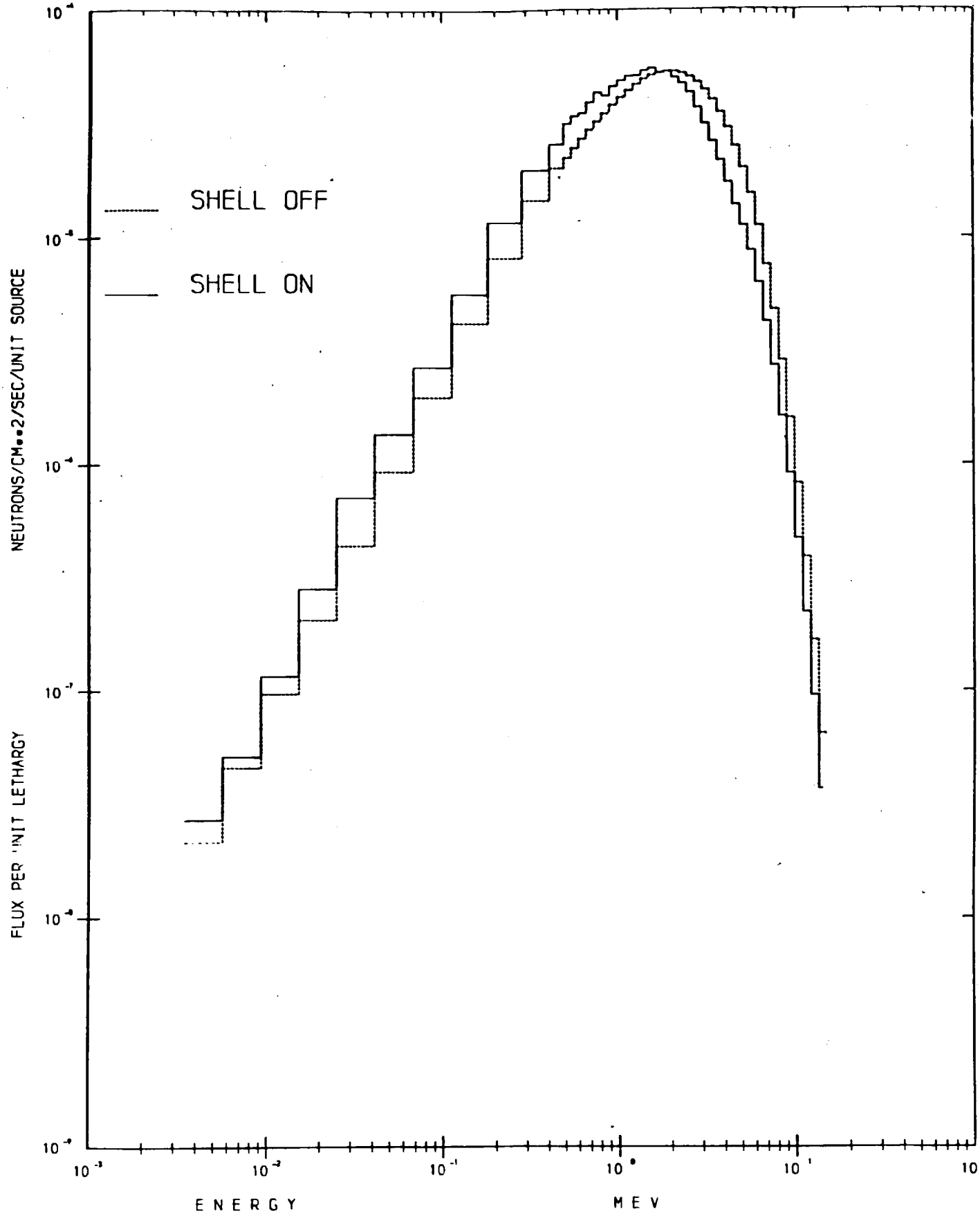
NEUTRON SPECTRA AT 16.53CM FROM THE CENTRE OF THE IRON SHELL, THICKNESS=4.11CM

FIGURE 36



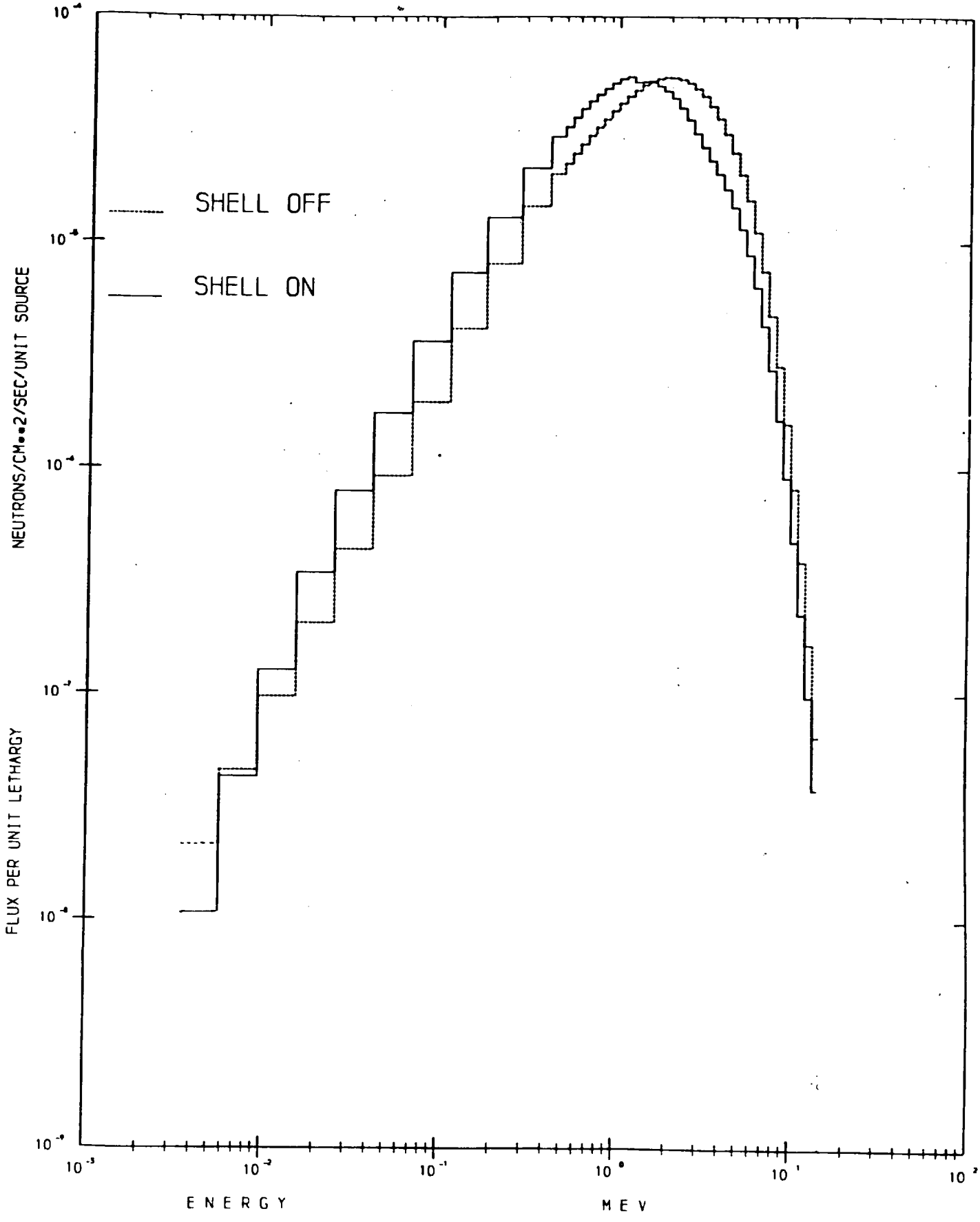
NEUTRON SPECTRA AT THE CENTRE OF THE COPPER SHELL. THICKNESS = 4.12CM

FIGURE 37



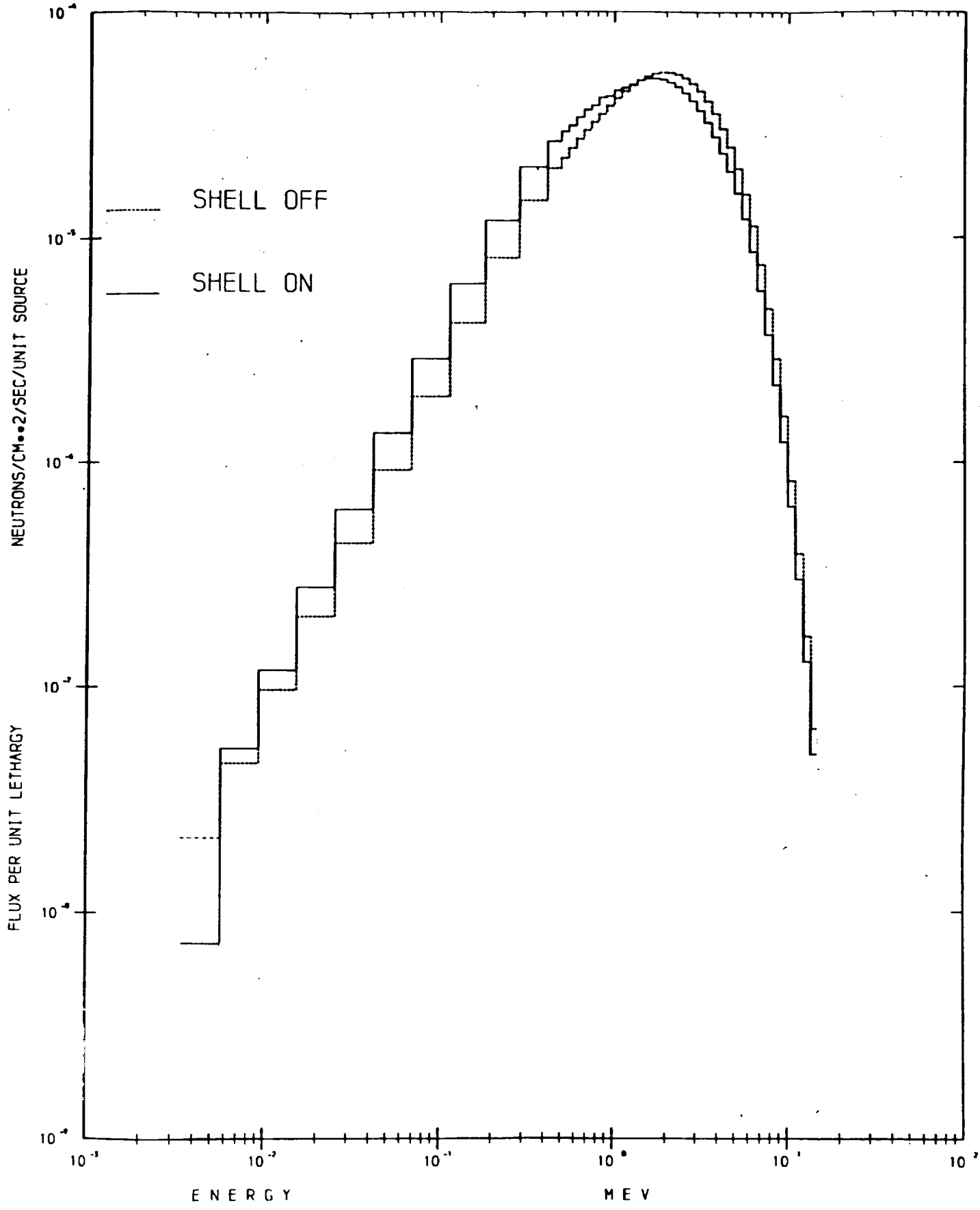
NEUTRON SPECTRA AT THE CENTRE OF THE LEAD SHELL, THICKNESS = 6.24CM

FIGURE 38



NEUTRON SPECTRA AT THE CENTRE OF THE TIN SHELL. THICKNESS = 7.01CM

FIGURE 39



NEUTRON SPECTRA AT THE CENTRE OF THE ZIRCONIUM SHELL, THICKNESS = 3.30CM

FIGURE 40

does not differ a lot compared to previous ones especially at high energies. In contrast, the spectrum in the space between material shell and shell source has a structure quite similar to the unperturbed fission spectrum where the mentioned shift of high-energy neutrons to low-energy ranges is hardly noticeable.

Finally, Figures 37, 38, 39 and 40 show the neutron spectra at the centre of the thickest copper, lead, tin and zirconium shells, correspondingly. It is seen in these graphs that the perturbed neutron spectra follow various patterns for different material shells which, to a large extent, depict the different scattering properties of these materials. What is worth mentioning from these graphs is that despite the relatively small thickness of the copper shell the shift of high energy neutrons to low energies seem to be quite high as compared with other isotopes.

In relating the large discrepancies between measured and calculated Transmissions to inadequacies of the input, to calculational procedure, data, the sensitivity of the estimated values to each and every item of the input data is required. A sensitivity analysis will reveal which input data (fission spectrum, material and dosimetry cross-section data) and which energy ranges are more likely to be responsible for the observed discrepancies and consequently need to be adjusted or to improve the accuracy with which they are required to be known.

In the following chapter this sensitivity problem is addressed and treated in detail.

CHAPTER FOUR

SENSITIVITY STUDIES

4.1 INTRODUCTION

Although in its infancy, sensitivity analysis is now established as the primary technique for the examination of nuclear data related effects in neutron transport. Its applications cover problems relating to uncertainty analysis, group scheme optimisation and consistency analysis. The growth in the use of sensitivity analysis has been prompted by recognition of the fact that recent improvements in the techniques for solving the transport equation have reduced method errors to the level where they are comparable with uncertainties arising from nuclear data. More precisely, the aim of sensitivity theory is to formalise the relationship between the solution of the transport equation and the quality of the nuclear interaction constants dictating the transport process.

The sensitivity function commonly used in reactor physics can be derived either by the use of the variational principle (24) or by the application of generalised perturbation theory to the linear Boltzmann equation (25). The perturbation treatment is usually limited to the first order variation of the multi-group averaged neutron interaction parameters (26) (cross-sections, secondary angular and energy distributions etc) of the one-dimensional time independent equation, although higher order approximations (27) and extensions to 2 - D (28) and 3 - D (29) have been investigated.

The sensitivity profile $U^{p,R}(E)$, obtained for an integral parameter R where:

$$R = R\,(x^{p}(E),\ldots\ ) \tag{4.1}$$

is defined as the fractional change in the predicted response, R, per unit fractional change in some dependent parameter $x^{p}(E)$:

$$U^{p,R}(E) = \frac{\delta \ell n R}{\delta \ell n x^{p}(E)} \qquad (4.2)$$

or, in discrete form:

$$U_k^{p,R} = \frac{\delta R/R}{\delta x_k^p / x_k^p} \qquad (4.3)$$

where x_k^p is some group averaged neutron transport parameter. The limitation of first order theory can be a particularly serious one. In radiation shielding, for instance, resonances, thresholds and interference minima tend to dominate the sensitivity profiles in design situations and it is in these regions that non-linear behaviour can become apparent after only small cross-section perturbations.

In this chapter the sensitivity profiles of Transmission to material cross-section data, dosimetry cross-sections and fission spectrum are derived and studied. As will be explained in the next chapter, the material cross-section data can, for this analysis, be adequately represented by the group cross-sections for various interactions. From all the other neutron transport parameters describing the angular and energy distributions of secondary neutrons the 1st order expansion coefficient of the elastic scattering kernel, $\sigma^1_{e\ell}$, has a considerable impact on the calculated Transmission. This can be seen from the differences between P_o, P_1 calculations (see Table 6). Though "error files" for this quantity are not yet available, a quantitative assessment of the sensitivity of Transmission to $\sigma^1_{e\ell}$ is attempted.

4.2 SENSITIVITY OF TRANSMISSION TO MATERIAL CROSS - SECTIONS

The sensitivity function for the material cross-sections can be derived by applying first-order perturbation theory to time-independent Boltzmann equation for a non-multiplying medium. This is nicely done in Reference 30 . According to that approach, the sensitivity of the result (e.g. reaction rate), R, to a particular cross section, x, at energy E may be expressed as:

$$\frac{\delta R/R}{\delta\Sigma_x(E)/\Sigma_x(E)} \simeq P_x(E) \equiv \frac{\partial R}{\partial\Sigma_x(E)}\frac{\Sigma_x(E)}{R} = \left[\int_{\vec{r}} d\vec{r} \int_{\vec{\Omega}} d\vec{\Omega}\rho_x(\vec{r})\{-\Phi^*(\vec{r},\vec{\Omega},E)\sigma_{x_T}(E)\Phi(\vec{r},\vec{\Omega},E)\right.$$

$$\left. + \int_{\vec{\Omega}'} d\vec{\Omega}' \int_{E'} dE'\Phi^*(\vec{r},\vec{\Omega},E')\sigma_x(\vec{\Omega}.\vec{\Omega}',E\to E')\Phi(\vec{r},\vec{\Omega},E)\}\right] \Big/ R \qquad (4.4)$$

where:

$\Phi^*(\vec{r},\vec{\Omega},E)$ is the unperturbed adjoint flux,

$\Phi(\vec{r},\vec{\Omega},E)$ is the unperturbed forward flux,

$\sigma_{x_T}(E)$ is the total cross-section for reaction type x,

$\sigma_x(\vec{\Omega}.\vec{\Omega}',E\to E')$ is the scattering cross-section from angle $\vec{\Omega}$ to $\vec{\Omega}'$ and energy E to E' for reaction type x,

$\rho_x(\vec{r})$ is the atomic number density,

R is the integrated response, given by:

$$R = \int_{\vec{r}} d\vec{r} \int_{\vec{\Omega}} d\vec{\Omega} \int_E dE\ D(\vec{r},\vec{\Omega},E)\Phi(\vec{r},\vec{\Omega},E) \qquad (4.5)$$

with $D(\vec{r},\vec{\Omega},E)$ the response function, which in our case coincides with the macroscopic dosimetry cross-section, $\Sigma_D(E)$.

All the above quantities are defined for the specific problem under consideration and x may refer to partial cross-sections such as elastic or inelastic as well as total collision cross-sections. (For an absorption reaction, there would be no scattering term).

It should be recalled here that the physical interpretation of the

adjoint flux $\Phi^*(\vec{r},\vec{\Omega},E)$ is that of neutron source importance, that is, the expected detector activity (e.g, expected number of counts that will be produced at all subsequent times by the neutron itself or by the secondary neutrons generated as a result of scattering, etc., by the neutron in question). The adjoint neutron flux is found by solving the adjoint Boltzmann equation (identical with the normal one, apart from the term $\vec{\Omega}.\nabla\Phi(\vec{r},\vec{\Omega},E)$ which is accompanied by a -) with the source term replaced by the response function $D(\vec{r},\vec{\Omega},E)$ (see Eqn (3.1) page 71).

It must be pointed out here that the derivation of Eqn (4.4) was undertaken under the important assumption that:

$$C \equiv \frac{\sigma^{\bar{p}}_{x_T}(\vec{r},E)}{\sigma_{x_T}(\vec{r},E)} = \frac{\sigma^{p}_{x}(\vec{r},\vec{\Omega}\to\vec{\Omega}',E\to E')}{\sigma_{x}(\vec{r},\vec{\Omega}\to\vec{\Omega}',E\to E')} \qquad (4.6)$$

for all E, $\vec{r}$, E', $\vec{\Omega}'$ and $\vec{\Omega}$. and where the upper index p denotes the perturbed value of the cross-section.

Eqn. (4.6) indicates that the sensitivity profile defined by Eqn. (4.2) and given by Eqn (4.4) for the material cross-sections requires the same fractional perturbation to be applied to all components of the cross-section for reaction type x. For example if x in Eqn. (4.4) refers to inelastic cross-section then the derived sensitivity profile implies the same fractional perturbation applied to cross-sections for different excited levels as well as to scattering kernels describing the angular and energy distributions of inelastically scattered neutrons. If x refers to total cross-section, the same fractional perturbation is implied for the absorption, elastic and inelastic components of the total. Note that in Eqn. (4.4) the perturbed values of the cross-sections and fluxes do not appear at all. This happens because this formula is obtained as the limit-case as the C ratio tends to unity. Consequently Eqn. (4.4) can be used analytically to

determine the relative sensitivity of the response, R, to the cross-sections used in the calculation. However, Eqn. (4.4) can be used for small changes in the cross-sections where the predicted change in R is expected to lie in the range of linear perturbations.

Eqn. (4.4) can be transformed to its discrete-ordinates equivalent by making use of the result and ideas of section 3.3 We consider it unnecessary to go through the mathematical details which are also outlined in Reference 30 . The result is:

$$\frac{\delta R/R}{\delta\sigma_x(I)/\sigma_x(I)} = P_x(I) = \left[\sum_{IZ=1}^{NZONE}\rho_x(IZ)\sum_{J=IZI}^{IZF}VOL(J)\{-\sum_{K=1}^{NOA}\Phi^*(J,K,I)\sigma_{x_T}(I)\Phi(J,K,I)WT(K)+\sum_{\ell=0}^{\ell max}\sum_{I'=I}^{IGM}\Phi^{*\ell}(J,I')\sigma_x^{\ell}(I\rightarrow I')\Phi^{\ell}(J,I)\}\right] \Big/ \left[\sum_{J=1}^{INT}\sum_{\ell=0}^{max}\sum_{I=1}^{IGM}D^{\ell}(J,I)\Phi^{\ell}(J,I)\right] \qquad (4.7)$$

where

$\rho_x(IZ)$ is the number density for cross-section x in spatial zone IZ,

IZI is the initial spatial interval in spatial zone IZ,

IZF is the final spatial interval in spatial zone IZ,

VOL(J) is the volume of interval J,

IGM, NOA, NZONE, INT are the numbers of energy groups, discrete angles, zones and intervals, respectively,

WT(K) is the weight given to flux at angle $\vec{\Omega}_K$ in the Gaussian quadrature.

Eqn. (4.7) gives the percentage change in the result due to a 1% increase in the group-cross-section for reaction x and group I. This quantity, also called the sensitivity coefficient, has been found to be convenient for identification of the most important cross-sections for a given problem in terms of element, isotope and specific reaction

cross-section.

Eqn. (4.7) can be integrated over the incident energy E to give the total sensitivity of the problem to the cross-sections for specific reaction types.

Also the effect of Legendre series truncation for a multigroup σ^{ℓ} cross-section set may be evaluated by examining sensitivity as a function of the number of expansion terms.

4.2.1 SWANLAKE Code

SWANLAKE is a sensitivity analysis code which basically calculates the sensitivity profiles according to Eqn. (4.7). This code was designed for the IBM 360/91 computer, and has been modified to be operable on the University of London CDC/6600 computer. The quantities $\Phi(J,K,I)$ and $\Phi^*(J,K,I)$ are read from angular flux tapes generated in forward and adjoint ANISN calculations respectively, of the problem of interest.

General requirements

The primary requirement for the proper functioning of SWANLAKE is that the transport problem be properly stated in that the forward and adjoint calculations give the same result.

For the forward calculation the response is given by:

$$R = \int_{\vec{r}} d\vec{r} \int_{\vec{\Omega}} d\vec{\Omega} \int_{E} dE \; D(\vec{r},\vec{\Omega},E)\,\Phi(\vec{r},\vec{\Omega},E)$$

while for the adjoint calculation:

$$R = \int_{\vec{r}} d\vec{r} \int_{\vec{\Omega}} d\vec{\Omega} \int_{E} dE \; S(\vec{r},\vec{\Omega},E)\,\Phi^{*}(\vec{r},\vec{\Omega},E)$$

where $D(\vec{r},\vec{\Omega},E)$ is the response function for the forward calculation and the source for the adjoint calculation

and $S(\vec{r},\vec{\Omega},E)$ is the source for the forward calculation and the response function for the adjoint calculation.

However we are interested in the discrete-ordinates form of the two responses because as such they will be compared. If some criteria concerning the input source and response data to ANISN forward and adjoint runs are met; (Ref 30 , pages 80-82) then the response calculated for interval J will be:

$$R_J^{for}\left(\frac{\text{response}}{\text{cm}^3\text{xsec}}\right) = \sum_{I=1}^{IGM} \Phi_{I,J}\left(\frac{\text{neutrons}}{\text{cm}^2\text{x sec}}\right) D_{I,J}\left(\frac{\text{response}}{\text{neutronxcm}}\right) \qquad (4.8)$$

in the forward case, and

$$R^{adj}\left(\frac{\text{response}}{\text{cm}^3\text{xsec}}\right) = \sum_{I=1}^{IGM} \Phi^{*}\left(\frac{\text{response}}{\text{neutron}}\right) S_{I,J}\left(\frac{\text{neutrons}}{\text{cm}^3\text{xsec}}\right) \qquad (4.9)$$

for the adjoint case.

To compare the total responses calculated by the forward and adjoint ANISN cases, the forward response by interval must be integrated over the domain of interest for the forward response function, and the adjoint response must be integrated over the domain of the forward source. Therefore, the total forward and adjoint responses to be compared may be expressed as:

$$R^{for}\left(\frac{\text{response}}{\text{sec}}\right) = \sum_{J}^{\text{Domain of interest for D}} R_J^{for}\, VOL(J) \qquad (4.10)$$

$$R^{adj}\left(\frac{\text{response}}{\text{sec}}\right) = \sum_{J}^{\text{Domain of S}} R^{adj} VOL(J) \qquad (4.11)$$

Partial Sensitivities

Apart from the sensitivity profiles, total sensitivities and effects by group of the order of the scattering kernel expansion on the response, SWANLAKE calculates sensitivities for each position

in the cross-section matrix as a function of P_ℓ and the sum of all expansion terms. In the case where the cross-section set input to SWANLAKE is that used in the ANISN calculations (a (IGM + 3) x IGM matrix containing the absorption, fission and total group cross-sections in the first three rows followed by the group transfers $\sigma_{I\to I'}$ which describe inseparably the elastic and inelastic processes) then the sensitivity $P_{S,I} = \sum_{I'\geq I} P_{II'}$ is the fractional change in the response per unit fractional change in $\sigma_{S,I}$ (scattering cross-section for group I) with the total cross section held constant, i.e. a reduction in $\sigma_{A,I}$ is implied. Similarly, $P_{T,I}$ is the effect on a response of increasing $\sigma_{T,I}$ without altering $\sigma_{S,I}$ an implied increase in $\sigma_{A,I}$. Thus we can choose to work in "true" partial sensitivities Q, in which any increase in a partial cross-section leads to the same increase in the total cross-section, by means of the following relations (31):

$$Q_{A,I} = P_{T,I} \frac{\sigma_{A,I}}{\sigma_{T,I}} \tag{4.12}$$

(This manipulation is performed by SWANLAKE and printed as $P_{A,I}$).

$$Q_{II'} = P_{T,I} \frac{\sigma_{I\to I'}}{\sigma_{T,I}} + P_{II'} \tag{4.13}$$

and hence:

$$Q_{S,I} = P_{T,I} \frac{\sigma_{S,I}}{\sigma_{T,I}} + P_{S,I} \tag{4.14}$$

Eqns. (4.12) and (4.14) give:

$$Q_{T,I} = Q_{A,I} + Q_{S,I} = P_{T,I} + P_{S,I} = P_{T,I} + \sum_{I'\geq I} P_{II'} \tag{4.15}$$

In Eqn. (4.15) $Q_{T,I}$ is the sensitivity profile for the total while the R.H.S. is calculated in terms of elements of the sensitivity matrix only. Eqn. (4.15) is verified by the SWANLAKE output. However, SWANLAKE was modified to give, according to Eqns. (4.12), (4.13) and

(4.15), the real partial sensitivity matrix.

Code limitations

Although the present version of SWANLAKE is applicable to a wide range of problems, some limitations should be noted. Problems must be time-independent and one-dimensional. The present sensitivity function only allows for energy downscatter, does not include the effect of fission cross-sections and cannot evaluate the sensitivity of the calculated response to the response function. In addition SWANLAKE must be provided with multigroup partial cross-sections which are often not considered an essential part of a multigroup cross-section library. It is anticipated that most, if not all of the above restrictions will be removed in future versions.

A MONTE - CARLO sensitivity code, DUCKPOND, is being developed at A.E.E. Winfrith which eliminates most of the restrictions mentioned above.

4.2.2 Input Data Specification

Most of the SWANLAKE input data are exactly the same with that required by ANISN (interval boundaries, zone definition, number densities, quadrature sets, cross-sections etc). However SWANLAKE can simultaneously calculate the sensitivity profiles to different ANISN - formulated data sets used in the ANISN calculation of forward and adjoint fluxes (total, elastic, inelastic for different excited levels etc.).

According to Eqn. (4.7) SWANLAKE requires the integrated response, R, given by either of Eqns. (4.10), (4.11). It is evident that in these two equations, "the domain of interest for D" is, for our case, the detector region while the domain of S is the last (27^{th}) spatial interval where the isotropic, uniformly distributed source was initially located. Furthermore, in Eqn. (4.8) $D_{I,J}$ stands for the macroscopic dosimetry cross-section of a certain detector, while in

Eqn. (4.9), $S_{I,J}$ is the normalized thermal fission source as appears in the ANISN output of the forward case.

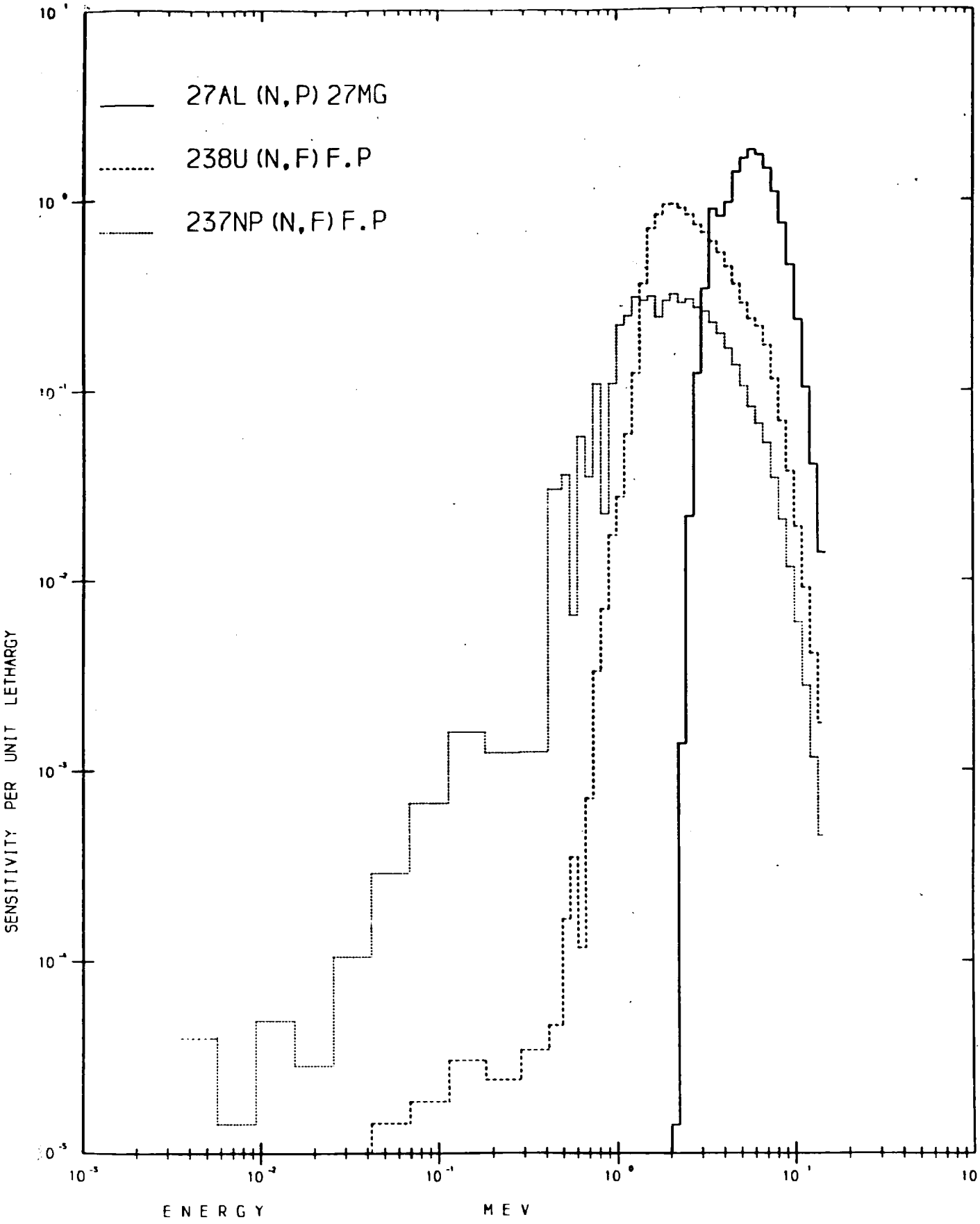
Table 15 presents the integrated forward and adjoint reaction rates, as given by Eqns (4.10) and (4.11), for all the iron cases and those from the other isotopes for which large discrepancies between experimental and calculated Transmissions occur (see Table 14). The percentage differences between forward and adjoint responses are also shown in this Table. Although it is obviously desirable to attain the best agreement possible, experience has shown that agreement within 10% is adequate for most analytical purposes. In general, agreement is easier to attain for slab and cylindrical geometries, and for spatially distributed source and response functions (30). In the light of the above comments it is realized that the agreement between forward and adjoint responses is satisfactory for all the cases of Table 15.

The 55-group structure is also supplied to SWANLAKE for the calculation of the sensitivity profile per unit lethargy which, obviously, is independent of the energy group structure used and provides a measure of the relative importance of the cross-section set investigated as a function of energy. In general the sensitivity profiles per unit lethargy, hereinafter simply called sensitivity profiles, tend to mirror the total cross-section for a certain reaction in the energy ranges which are important for a transmission problem such as the one calculated. An important minimum in the total cross-section then appears as a peak in the sensitivity profile, and a resonance in the total cross-section appears as a valley. The important energy ranges for a given problem are also determined by the energy distribution of the source and response functions and by the thickness of the material regions present.

A thorough and detailed sensitivity investigation of the

TABLE 15. INTEGRATED FORWARD AND ADJOINT RESPONSES FOR SOME CASES OF TABLE 14.

CASE	MATERIAL	THICKNESS cm	INTEGRATED REACTION RATES IN THE DETECTOR REGION (Reactions/nuclide/sec/unit fission source)								
			$^{27}Al(n, P)^{27}Mg$			$^{238}U(n, f)F.P.$			$^{237}Np(n, f)F.P.$		
			Forward	Adjoint	% Difference	Forward	Adjoint	% Difference	Forward	Adjoint	% Difference
1	Fe	1.90	5.5227 E-31	5.5909 E-31	1.23	4.4395 E-29	4.5539 E-29	2.57	2.1720 E-28	2.2449 E-28	3.35
2	Fe	4.11	4.0217 E-31	3.9388 E-31	2.06	3.6164 E-29	3.6404 E-29	0.66	2.0046 E-28	2.0620 E-28	2.86
3	Fe	9.16	1.9831 E-31	1.8726 E-31	5.57	2.3039 E-29	2.2720 E-29	1.38	1.6638 E-28	1.6981 E-28	2.05
4	Sn	7.01	-	-	-	3.6894 E-29	3.7371 E-29	1.29	-	-	-
5	Pb	6.24	-	-	-	4.1054 E-29	4.1749 E-29	1.69	-	-	-
6	Cu	4.12	-	-	-	3.239e E-29	3.2942 E-29	1.69	-	-	-
7	Zr	3.30	-	-	-	4.4109 E-29	4.5710 E-29	3.63	-	-	-



SENSITIVITY OF TRANSMISSION TO IRON TOTAL CROSS-SECTION, SHELL THICKNESS= 9.16CM

FIGURE 41

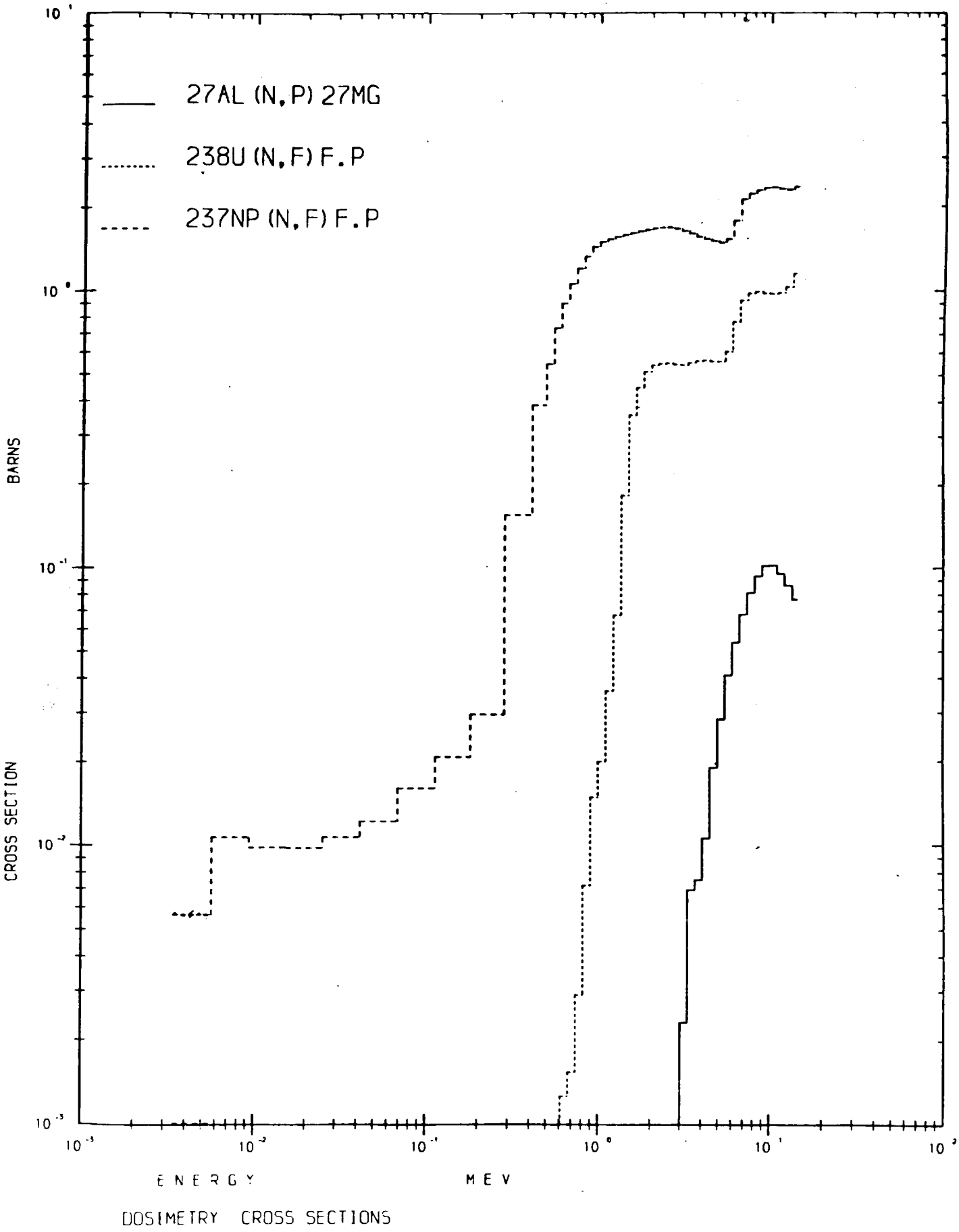

27AL (N,P) 27MG
238U (N,F) F.P
237NP (N,F) F.P
CROSS SECTION
BARNS
ENERGY
MEV
DOSIMETRY CROSS SECTIONS

FIGURE 42

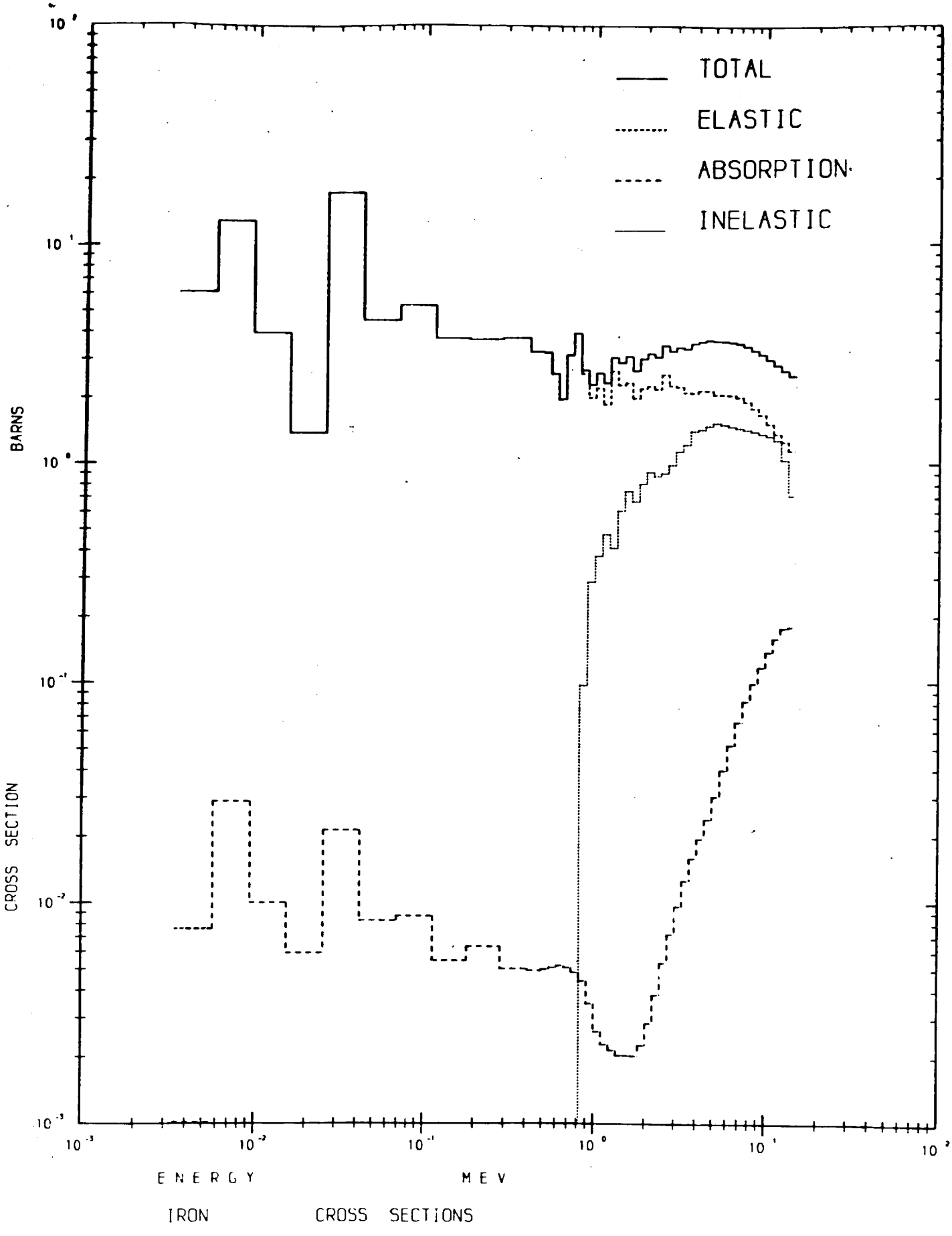

TOTAL
ELASTIC
ABSORPTION
INELASTIC
BARNS
CROSS SECTION
ENERGY
MEV
IRON
CROSS SECTIONS

FIGURE 43

cases presented in Table 15 is accomplished by employing ANISN-formatted cross-section data sets for all the isotopes included in this Table and for the following reactions: absorption, elastic, inelastic to different excited levels and to the continuum. These "sensitivity" cross-section matrices were prepared at the Radiation Shielding Information Centre of Oak Ridge National Laboratory (ORNL) by means of the modules NITAWL/AMPX-II working on DLC-52/EPRMASTER library (32).

Table 16 gives the number of excited levels and level energies for the isotopes of Table 15.

4.2.3 SWANLAKE Analysis of Calculated Transmissions.

Sensitivity profiles

Before proceeding to discuss SWANLAKE results it is worth making clear that the sensitivity profiles of the reaction rates to material group cross-sections defined by Eqn. (4.7) and calculated by SWANLAKE coincide with those of Transmissions since they are given in a fractional form and the reaction rates, with the material shell removed, do not depend on these cross-sections. Consequently any results and conclusions concerning the reaction rates for the "sphere on", cases and drawn from this section are equally valid for the Transmissions.

Figure 41 presents the sensitivity of Transmission per unit lethargy to iron total cross-section (that is, $P_T(I) = \frac{\delta T}{T} \frac{\Sigma_T(I)}{\delta \Sigma_T(I)} \frac{1}{\Delta U_I}$, with $\Delta U_I = \ell n \frac{E_{I+1}}{E_I}$, I = 1, IGM) versus neutron energy, for the three threshold detectors and for the thickest iron shell.

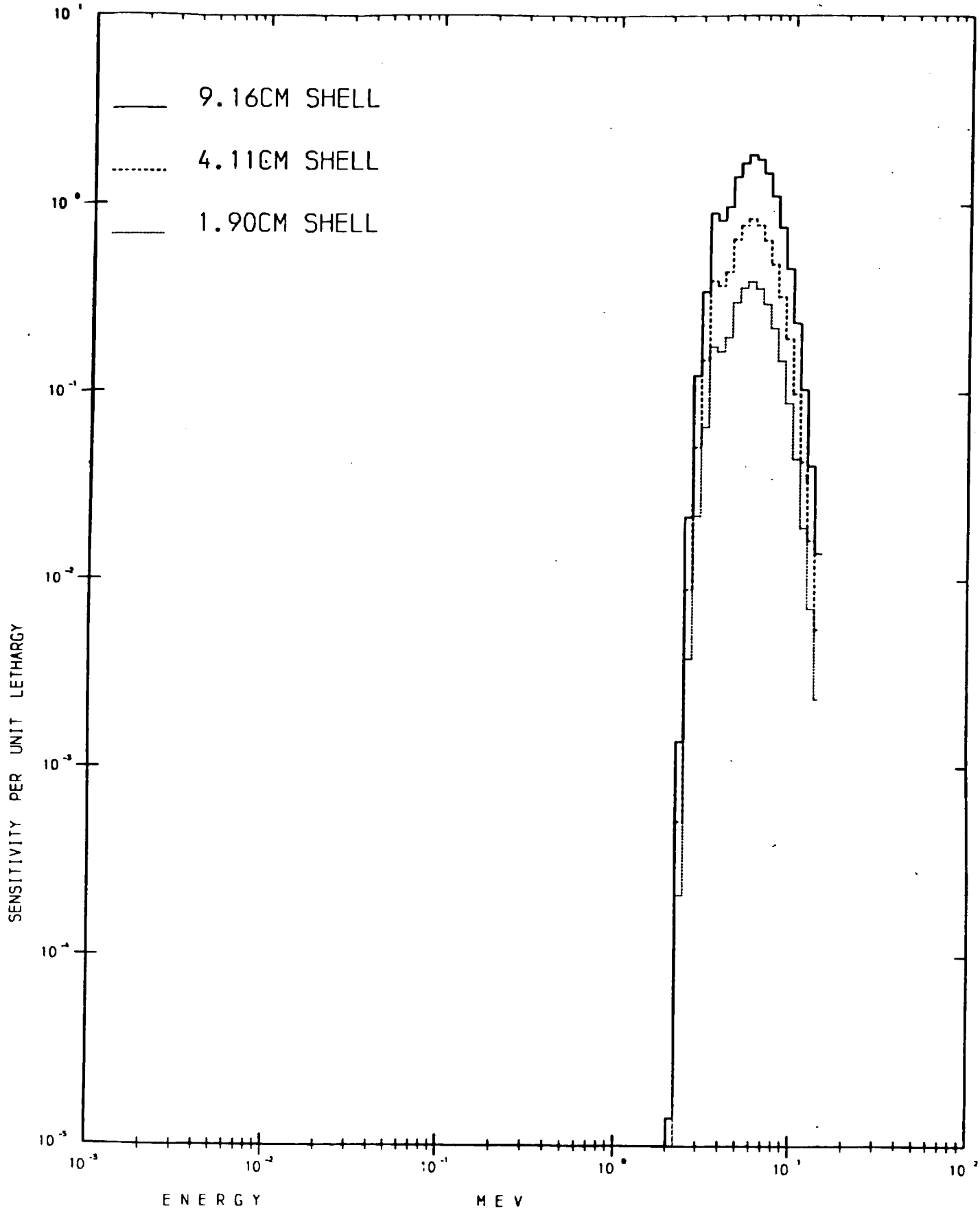
The broad structure of those sensitivity profiles corresponds to that of Fission Spectrum x detector response as can be deduced from Figure 33 and Figure 42 which gives the dosimetry cross-sections for the three detectors versus energy.

The fine structure of the sensitivity profiles, especially the fluc-

TABLE 16

INELASTIC SCATTERING DATA REPRESENTATION FOR ELEMENTS IN DLC-37/LPR

LEVEL No.	Pb (1288) Level Energy (MeV)	Upper Energy (MeV)	Fe (1192) Level Energy (MeV)	Upper Energy (MeV)	Cu (1295) Level Energy (MeV)	Upper Energy (MeV)	Zr (7141) Level Ener. (MeV)	Upper Energy (MeV)
1	0.570	9.0	0.846	20.0	0.670	20.0	0.9198	2.0001
2	0.803	20.0	1.408		0.770	20.0	1.210	2.0001
3	0.898	9.0	2.084		0.962	20.0	1.300	2.0001
4	1.175	9.0	2.654		1.115	20.0	1.380	
5	1.341	10.0	2.939		1.326	20.0	1.480	
6	1.462	9.0	2.957		1.412	16.0	1.660	
7	1.663	9.0	3.119		1.482	20.0	1.750	
8	1.682	20.0	3.122		1.547	16.0	1.8594	2.0001
9	1.762	9.0	3.368		1.623	16.0		
10	1.998	10.0	3.388		1.725	14.0		
11	2.160	11.0	3.445		1.865	16.0		
12	3.340	9.0	3.450					
13	2.385	10.0	3.600					
14	2.615	20.0	3.605					
15	2.624	20.0	3.747					
16	2.634	20.0	3.829					
17	2.783	11.0	3.856					
18	3.017	11.0	4.046					
19	3.057	10.0	4.099					
20	3.198	20.0	4.116					
21	3.25	11.0	4.298					
22	3.382	9.0	4.300					
23	3.453	10.0	4.389					
24	3.475	11.0	4.395					
25	3.560	11.0	4.453					
26	3.708	20.0	4.505					
27	3.750	20.0						
28	3.854	11.0						
29	3.920	12.0						
30	3.989	12.0						
31	4.076	20.0						
32	4.125	11.0						
33	4.200	12.0						
34	4.288	20.0						
35	4.339	20.0						
Cont.	4.4** (4.4214)	20.0	4.531 (4.6128)	20.0	1.900 (2.000)	20.0	--- (2.000)	20.00



SENSITIVITY OF 27AL (N,P) 27MG TRANSMISSION TO IRON TOTAL CROSS-SECTION

FIGURE 44

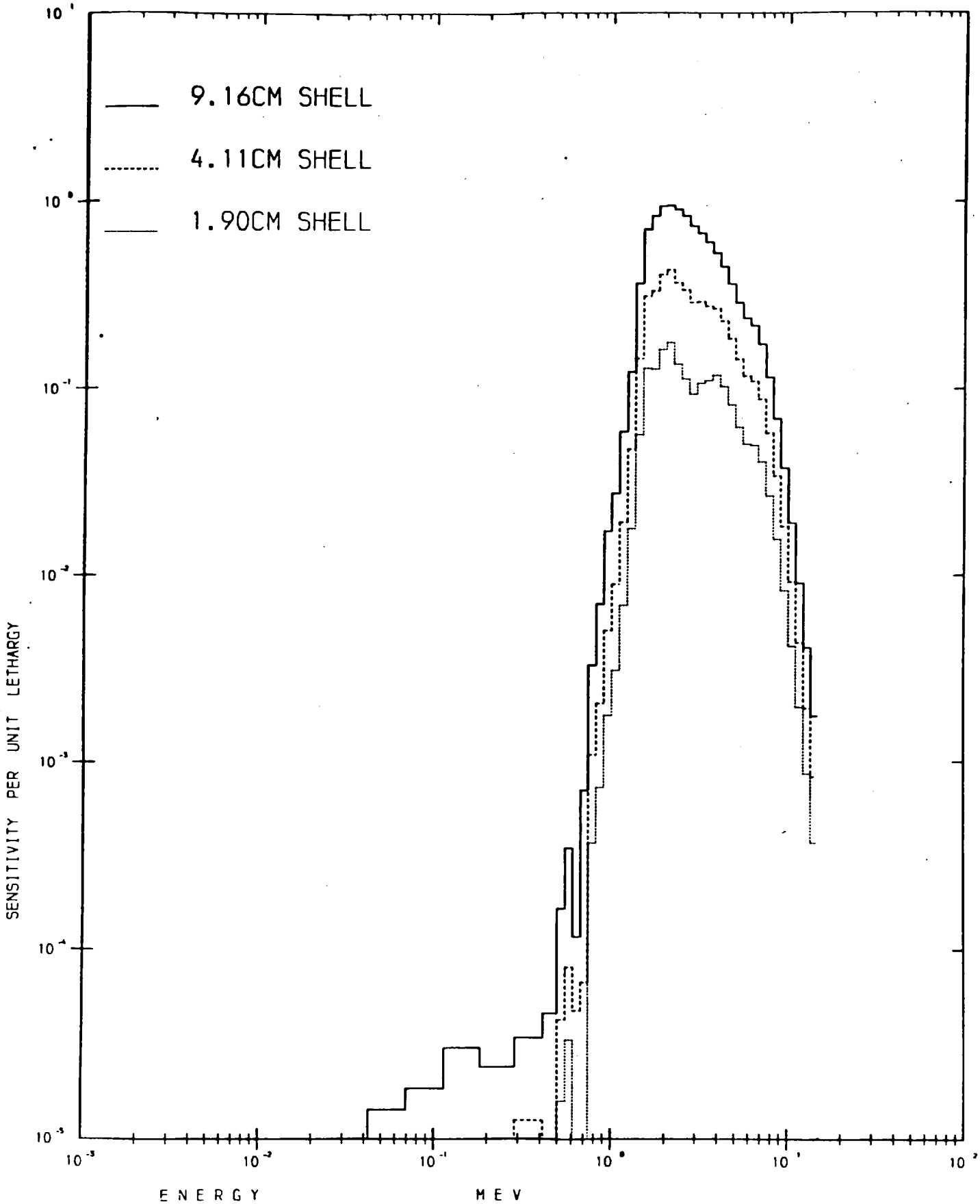

9.16CM SHELL
4.11CM SHELL
1.90CM SHELL
SENSITIVITY PER UNIT LETHARGY
ENERGY
MEV
SENSITIVITY OF 238U(N,F)F.P TRANSMISSION TO IRON TOTAL CROSS-SECTION

FIGURE 45

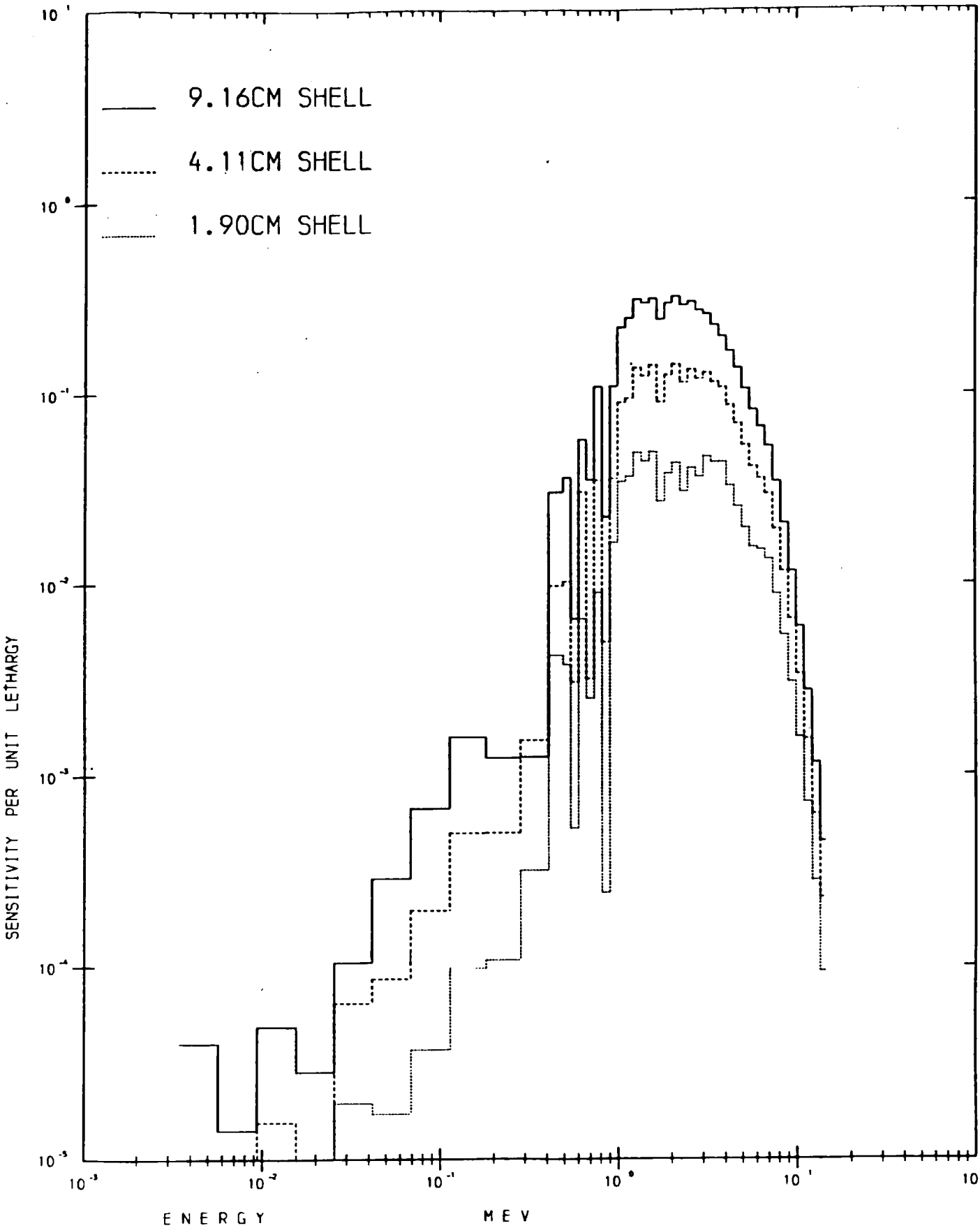

9.16CM SHELL
4.11CM SHELL
1.90CM SHELL
SENSITIVITY PER UNIT LETHARGY
ENERGY
MEV
SENSITIVITY OF 237NP(N,F)F.P TRANSMISSION TO IRON TOTAL CROSS-SECTION

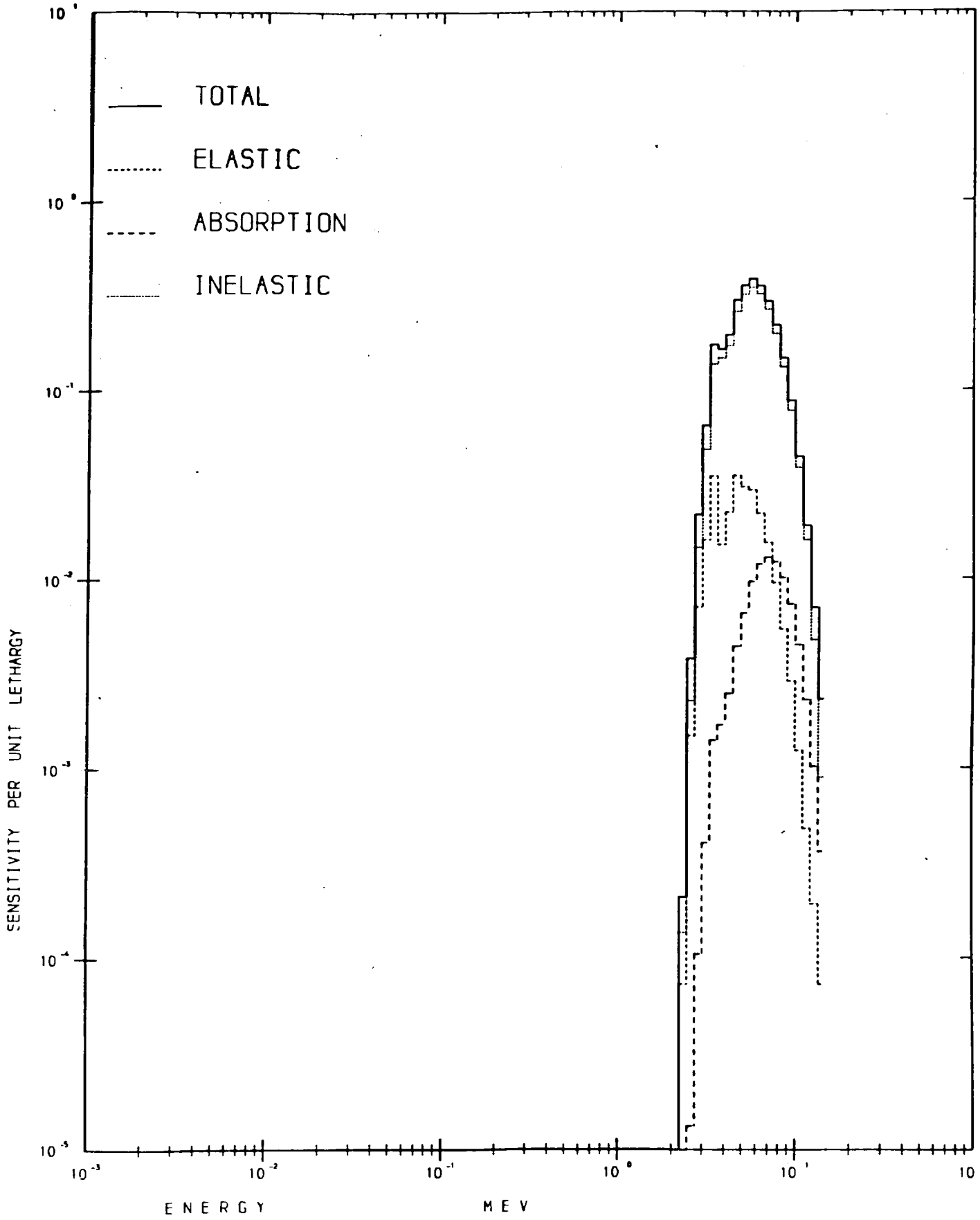
FIGURE 46

tuations of the $^{237}Np(n,f)F.P$ profile in the energy range of 0.5MeV 2MeV, generally correspond to similar cross-section variations in the same energy range, as seen in Figure 43 which presents the total, elastic, absorption and inelastic iron cross-sections in the energy range of 1keV - 15MeV. It is noticed in Figure 41 that as the detector threshold increases the region of high sensitivities shifts towards higher energies and higher values. The shift of the "sensitivity peak" towards higher energies as the detector threshold increases is self-evident, while the higher sensitivities attained is due to the fact that a certain change of a total group constant above the highest detector threshold available will affect a high threshold Transmission much more than a low threshold one for obvious reasons. This explains why, although the $^{27}Al(n,p)^{27}Mg$ dosimetry cross-sections are much lower compared to the other two reactions, the $^{27}Al(n,p)^{27}Mg$ sensitivity profile dominates the other two.

We do not expect the shell thickness to have any noticeable effect on the sensitivity profile structure, mainly because of the small thicknesses employed. So although the distortion caused to the fission spectrum by the iron shell strongly depends on its thickness (see Figures 31, 32 and 33), the effect on the sensitivity profile is a "vertical shift" towards higher sensitivity values as the shell thickness increases for all the detectors, shown in Figures 44, 45 and 46. Hence the broad structure of the sensitivity profiles for all the thicknesses and threshold detectors employed is entirely determined by the source spectrum and detector response.

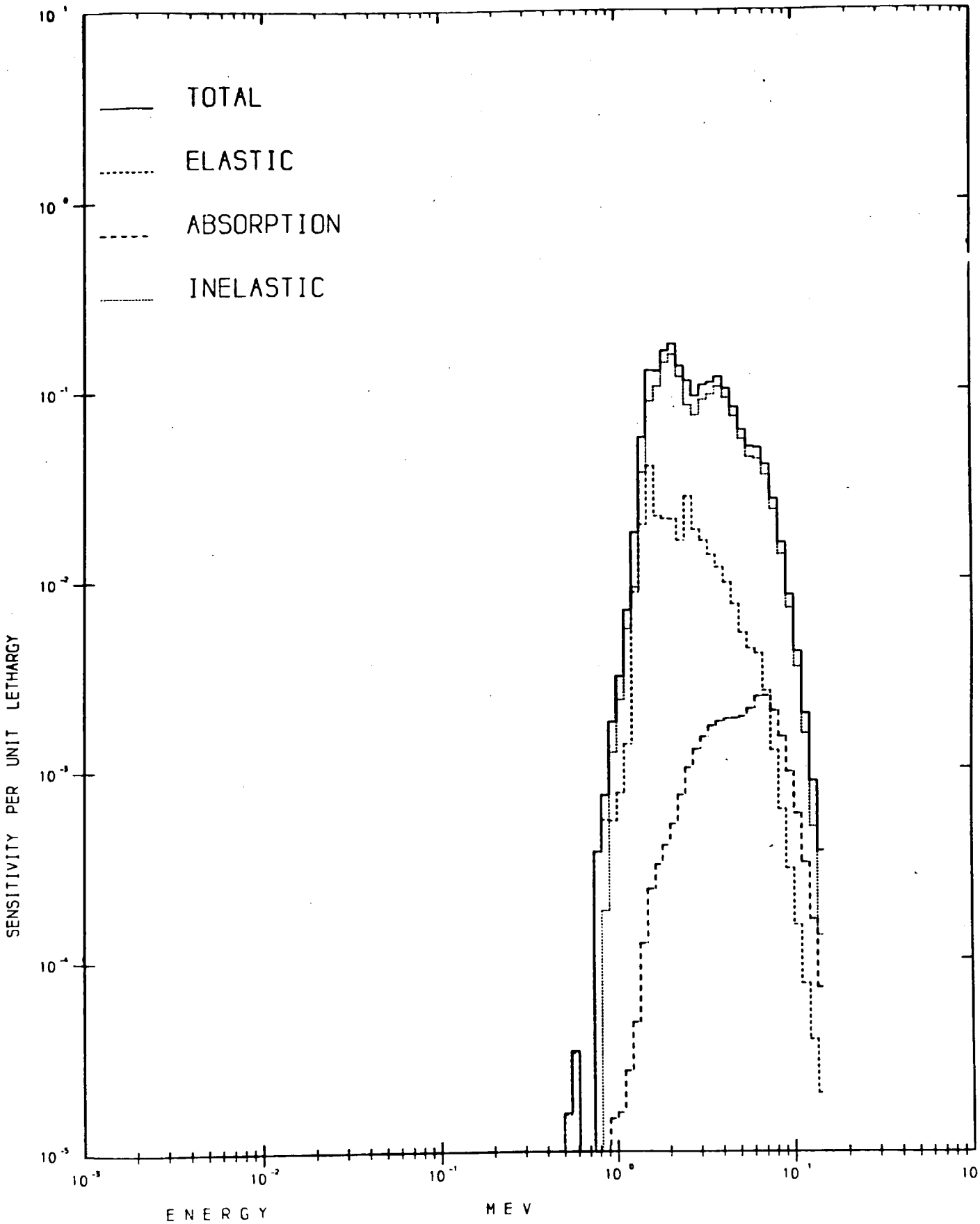
Figures 47 - 55 present the sensitivity profiles of Transmission to total, elastic, absorption and inelastic cross-sections for all the detectors and iron shells.

It must be mentioned here that these sensitivities are in general



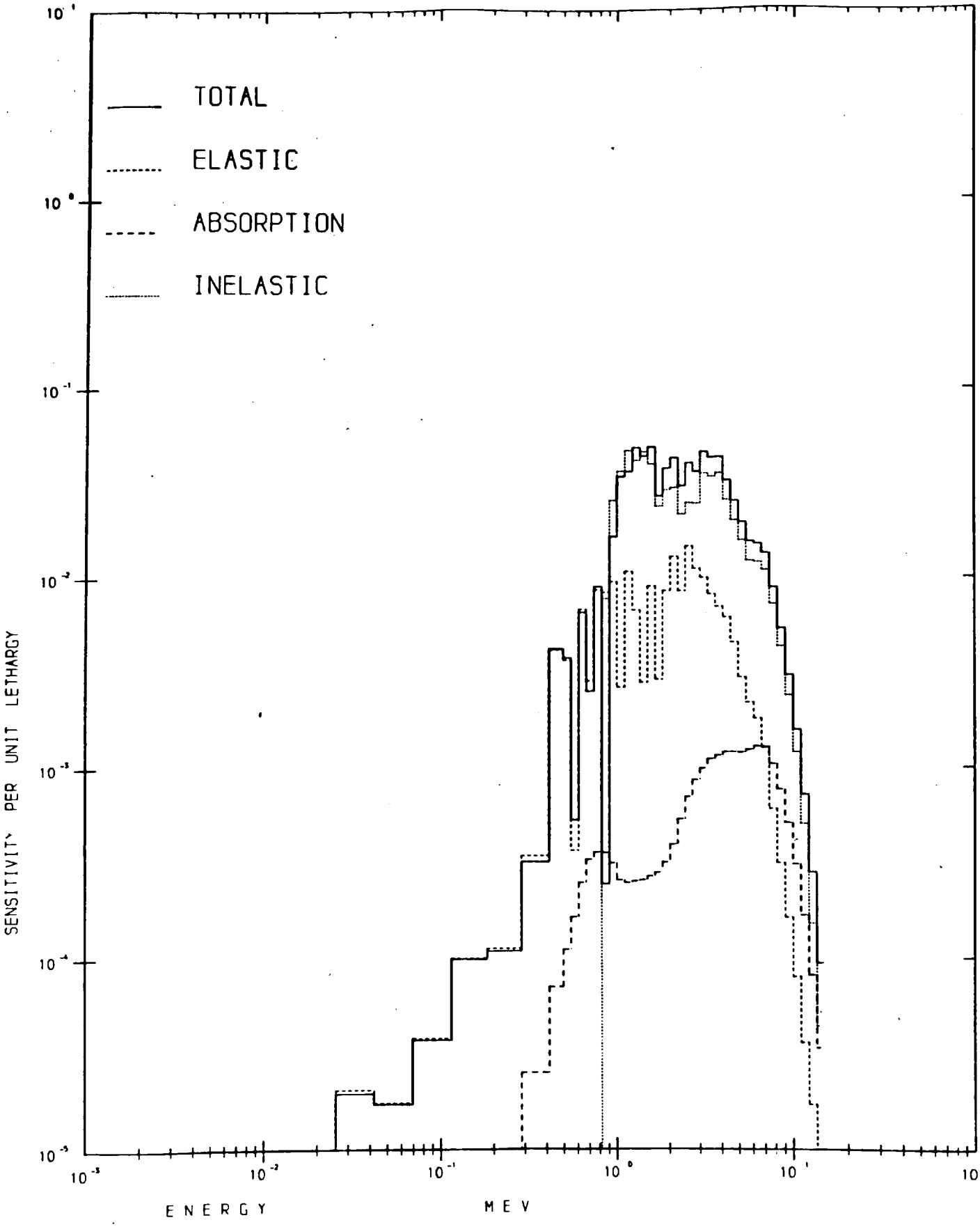
SENSITIVITY OF 27AL (N,P) 27MG TRANSMISSION TO IRON CROSS-SECTIONS, THICKNESS=1.90CM

FIGURE 47



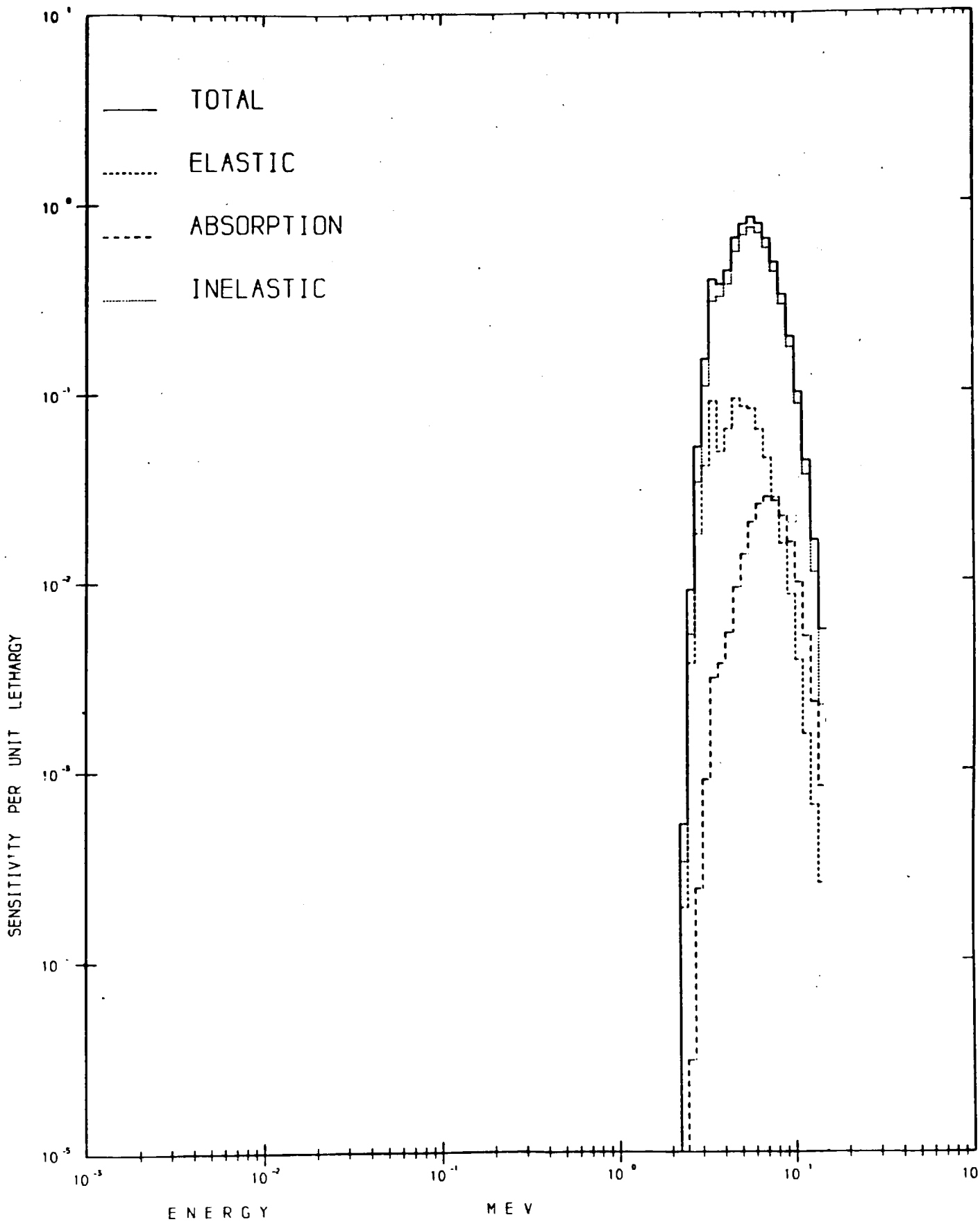
SENSITIVITY OF 238U(N,F)F.P TRANSMISSION TO IRON CROSS-SECTIONS, THICKNESS=1.90CM

FIGURE 48



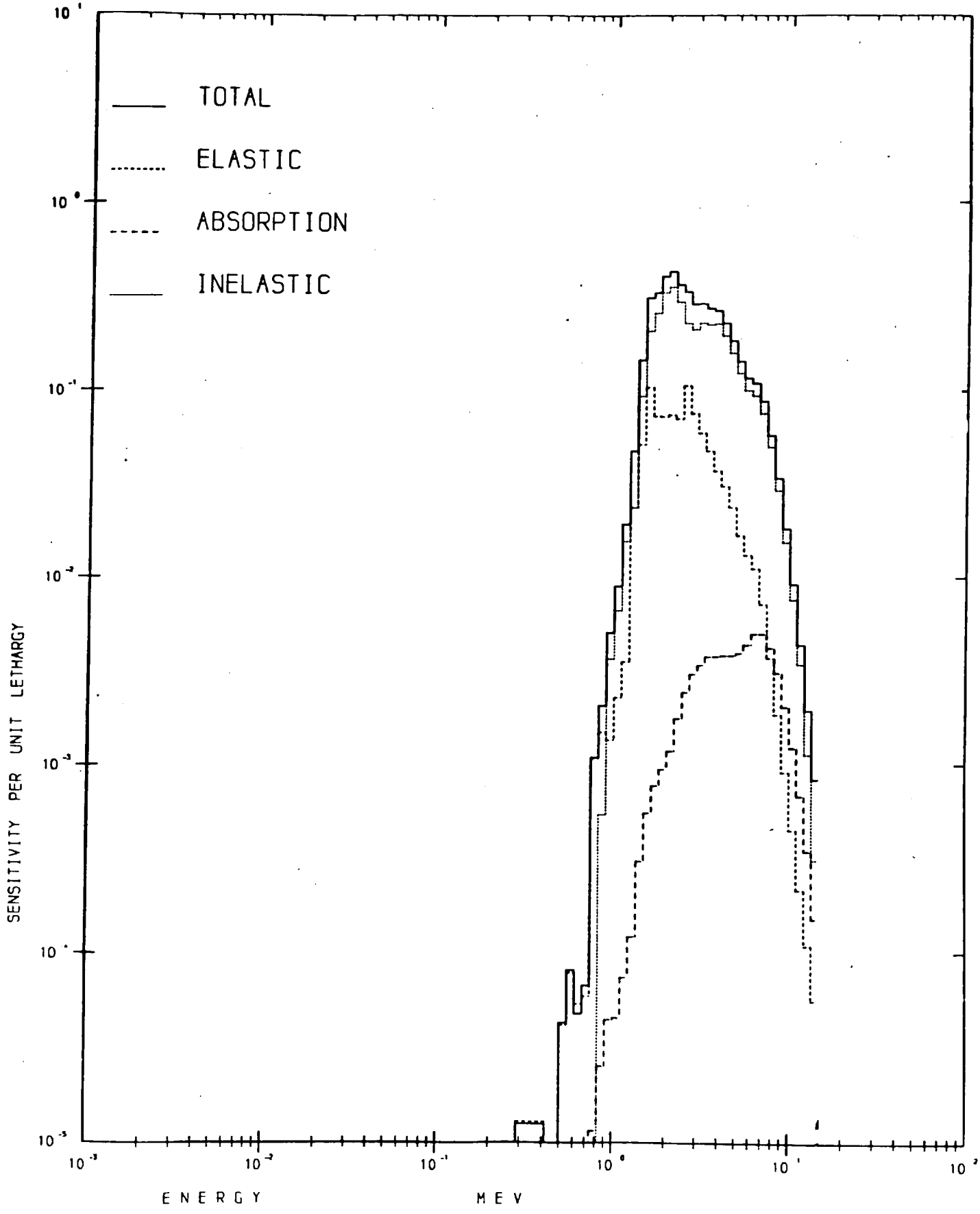
SENSITIVITY OF 237NP(N,F)F.P TRANSMISSION TO IRON CROSS-SECTIONS, THICKNESS=1.90CM

FIGURE 49



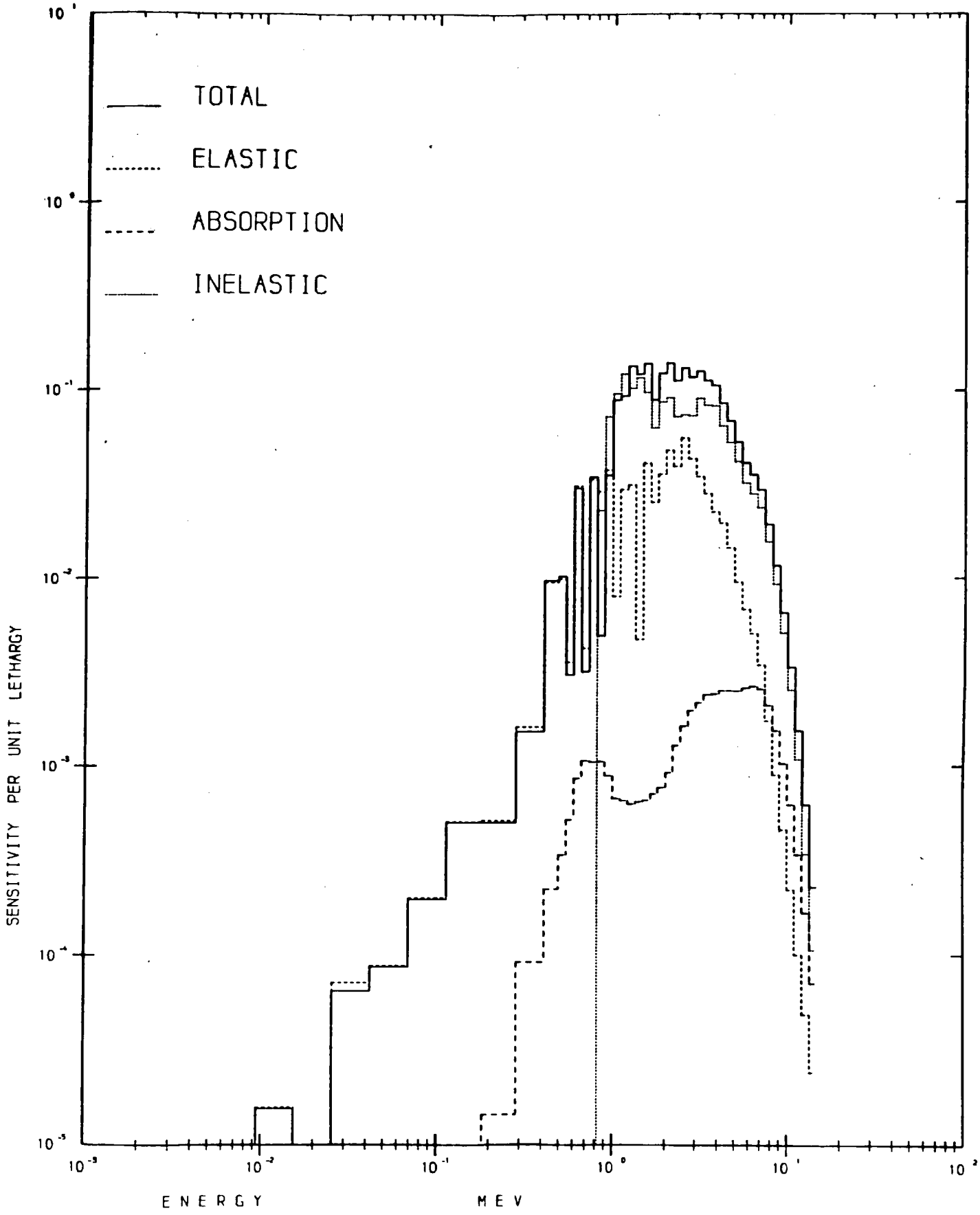
SENSITIVITY OF 27AL (N,P) 27MG TRANSMISSION TO IRON CROSS-SECTIONS, THICKNESS=4.11CM

FIGURE 50



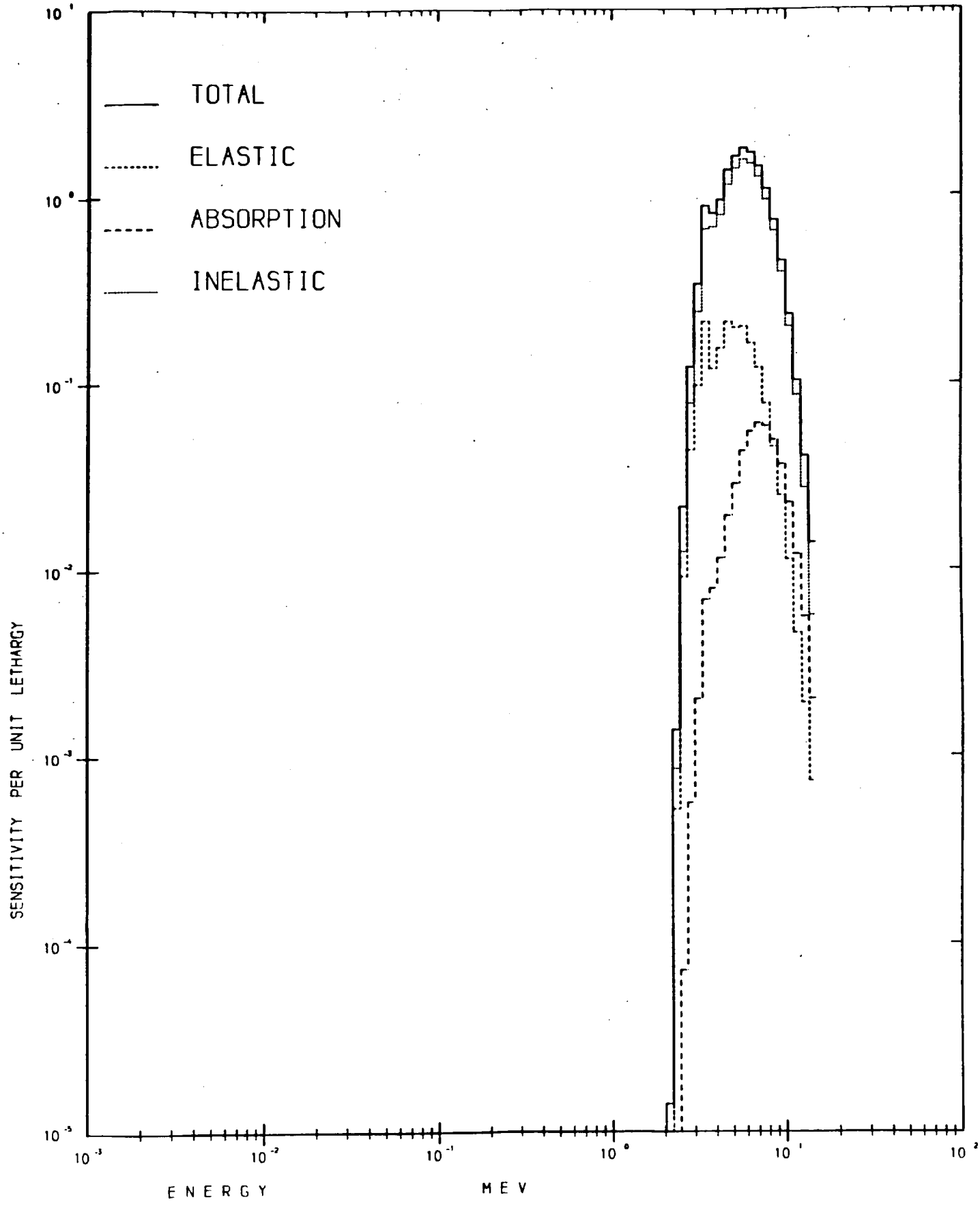
SENSITIVITY OF 238U(N,F)F.P TRANSMISSION TO IRON CROSS-SECTIONS, THICKNESS=4.11CM

FIGURE 51



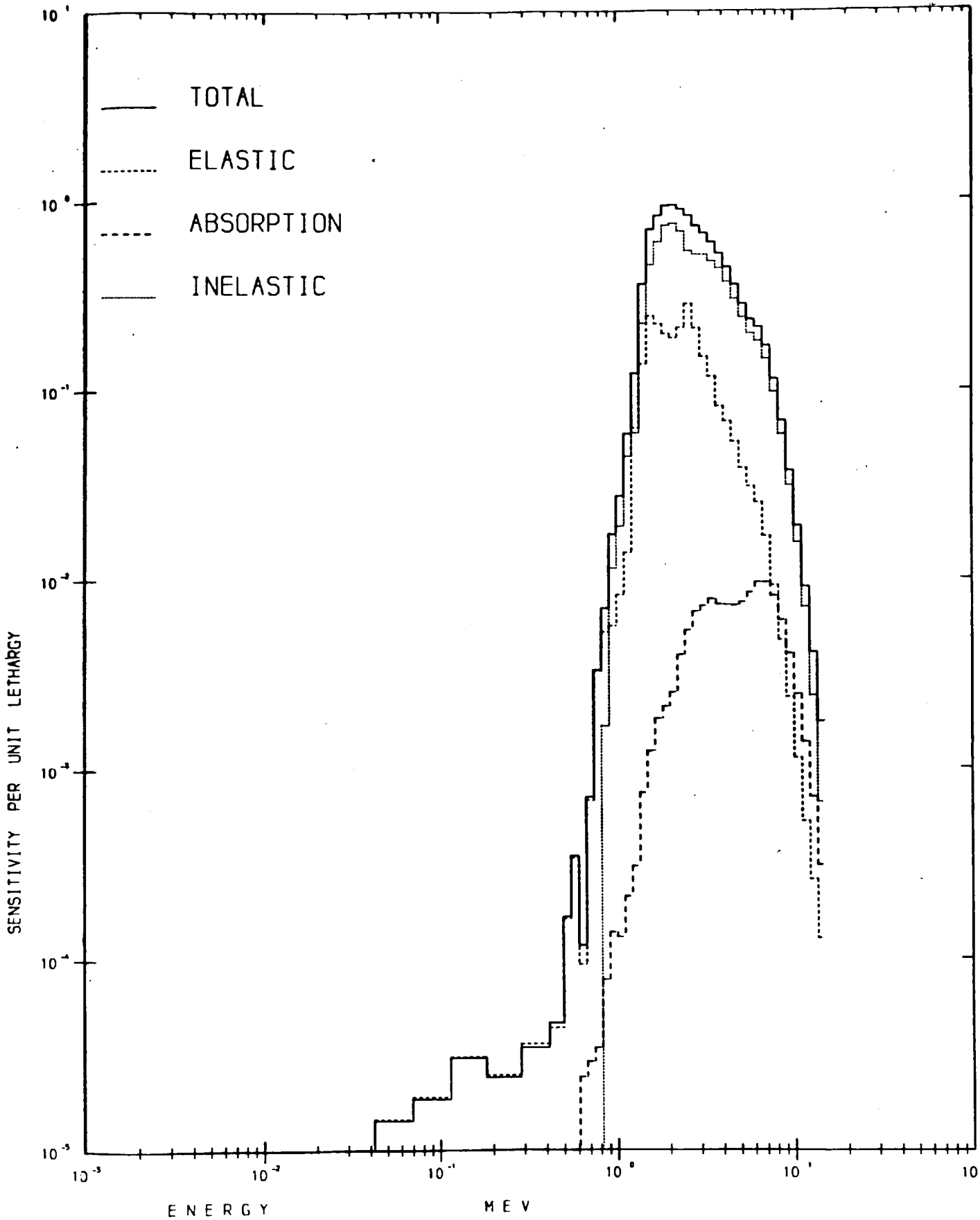
SENSITIVITY OF 237NP(N,F)F.P TRANSMISSION TO IRON CROSS-SECTIONS, THICKNESS=4.11CM

FIGURE 52



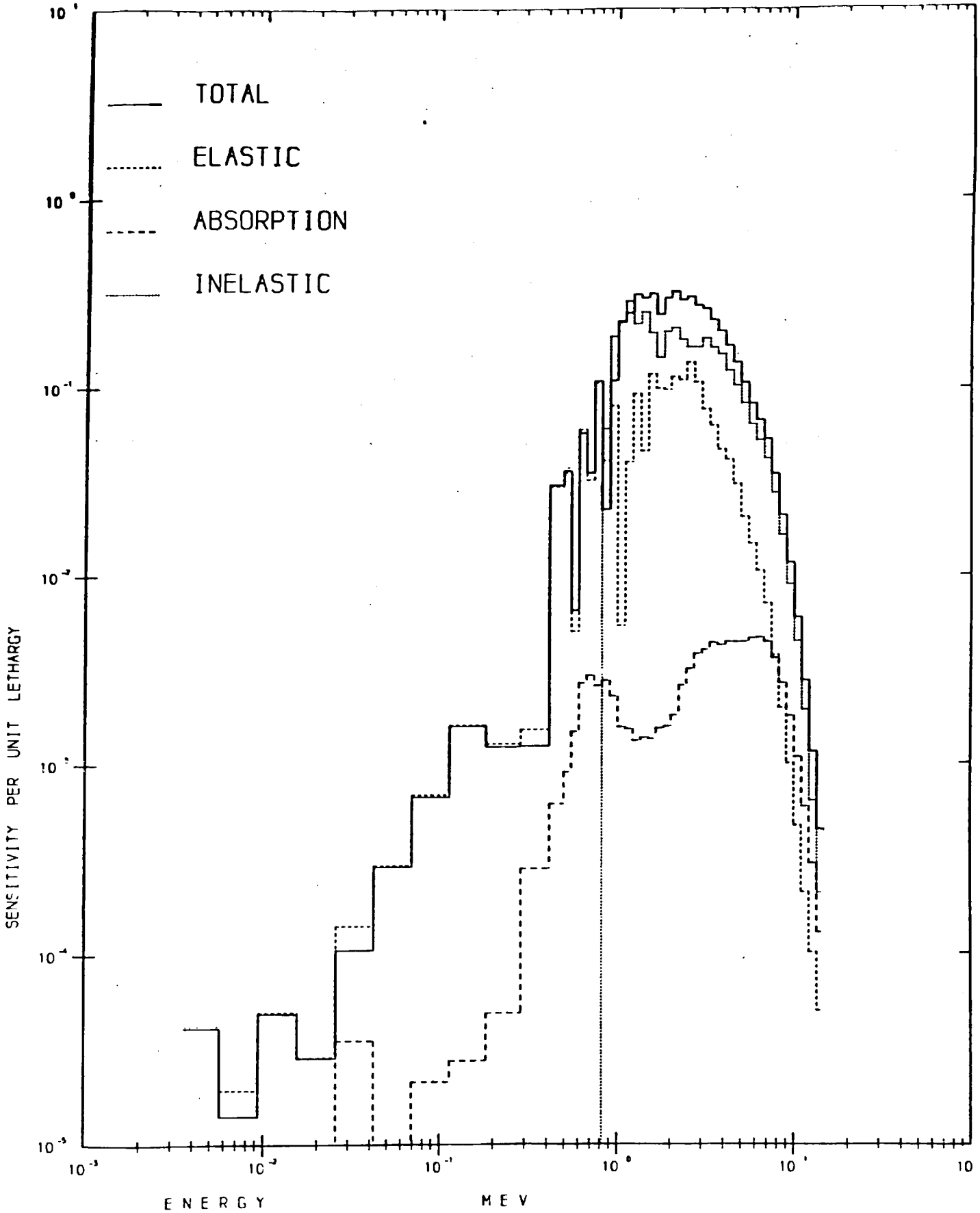
SENSITIVITY OF 27AL (N,P) 27MG TRANSMISSION TO IRON CROSS-SECTIONS, THICKNESS=9.16CM

FIGURE 53



SENSITIVITY OF 238U(N,F)F.P TRANSMISSION TO IRON CROSS-SECTIONS, THICKNESS=9.16CM

FIGURE 54

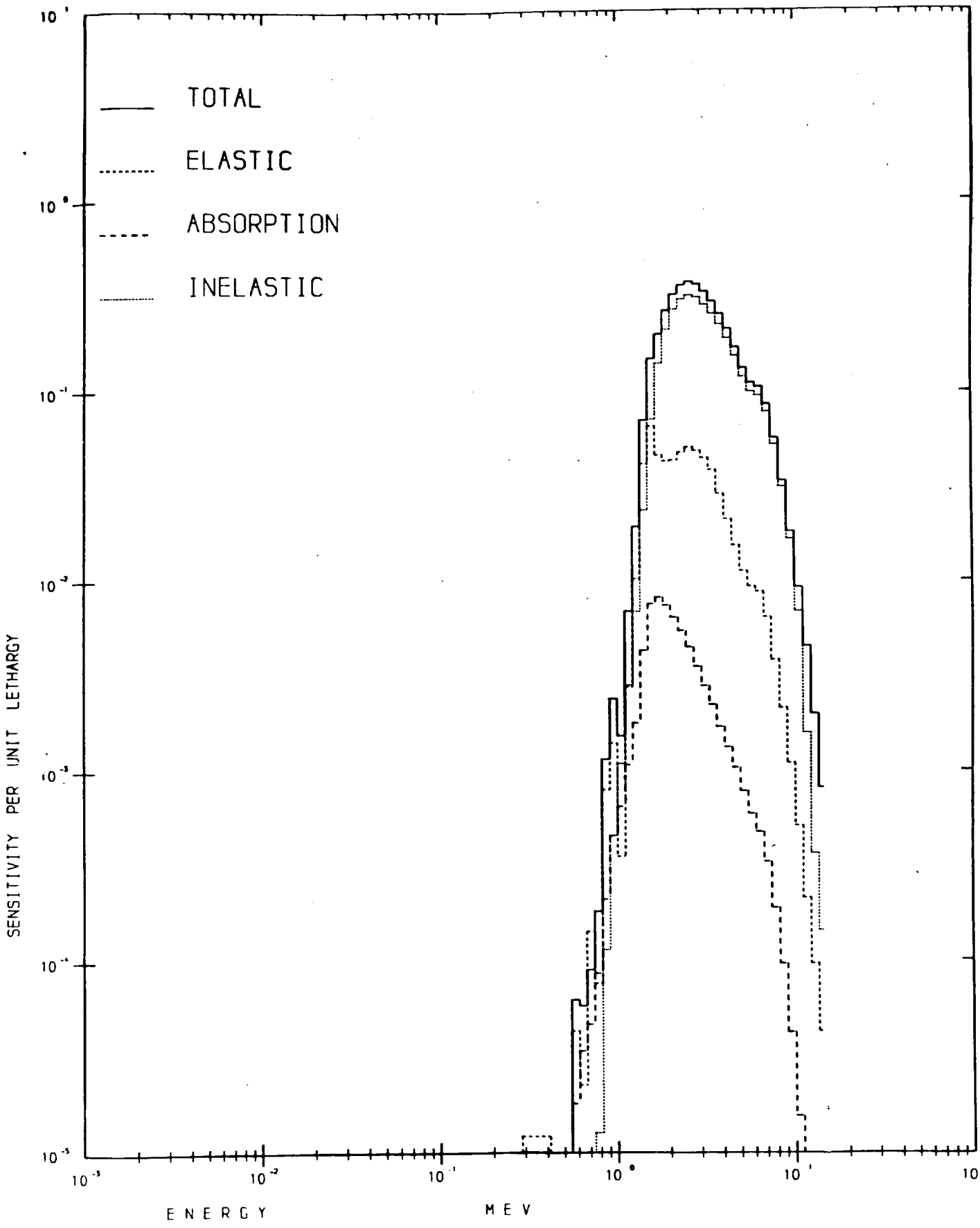


SENSITIVITY OF 237NP(N,F)F.P TRANSMISSION TO IRON CROSS-SECTIONS, THICKNESS=9.16CM

FIGURE 55

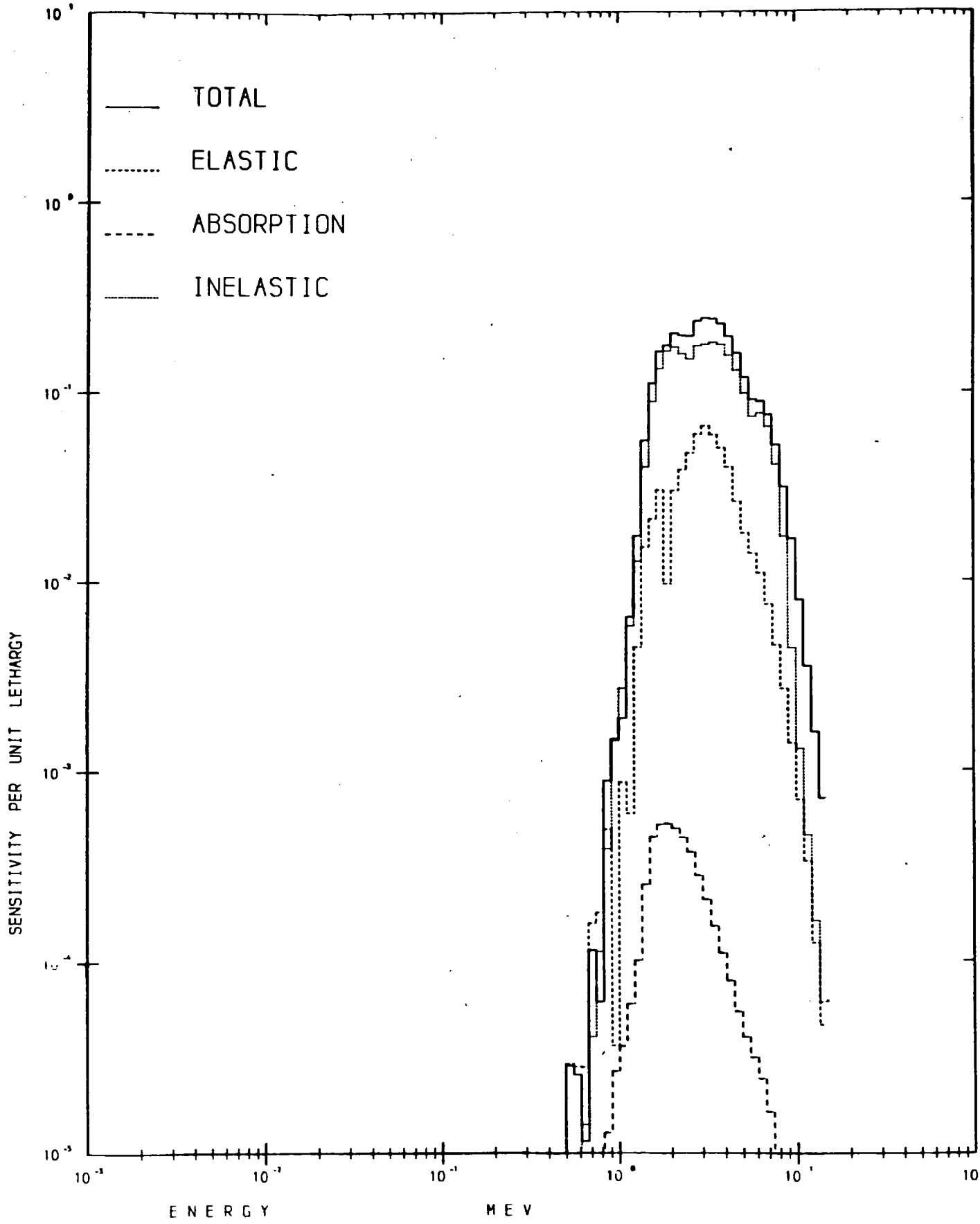
negative, although for some reactions and in low energy ranges they change sign. We consider it unnecessary and also inconvenient to differentiate between positive and negative values in these Figures. Instead, the following explanatory notes unambigously determine the sign of all the sensitivity profiles: The sensitivities to absorption and inelastic cross-sections are always negative at all neutron energies, thicknesses and detectors for obvious reasons. Above the inelastic threshold, if the sensitivity to inelastic is higher than the sensitivity to total, a positive sensitivity to elastic is implied with the sensitivity to total being negative. Below the inelastic threshold, higher sensitivities to elastic than to total imply positive values for both of them; the only negative component in these energy ranges is the sensitivity to absorption which is responsible for the lower values of the total as compared to elastic.

In all these Figures the predominant role of the inelastic cross-section is noticeable. Naturally, the sensitivity to inelastic cross-section is expected to be higher than the sensitivity to elastic in any energy range (provided that the cross-sections do not differ a lot in magnitude), since the average energy loss in an inelastic collision is, in general, much higher than the average energy loss in an elastic one. It can be argued, therefore, that for a certain threshold detector the majority of inelastic collisions render the neutron undetectable while the opposite is valid for the elastic ones. This is particularly true for intermediate and heavy nuclei since the maximum fractional energy loss in a single elastic collision decreases with increasing mass of the struck nucleus (Ref. 33, page 168). At high neutron energies where the elastic scattering in the C.M system is forward peaked, the aforementioned trend is reinforced since, as will be seen later, this implies the scattering of a lot more neutrons to the



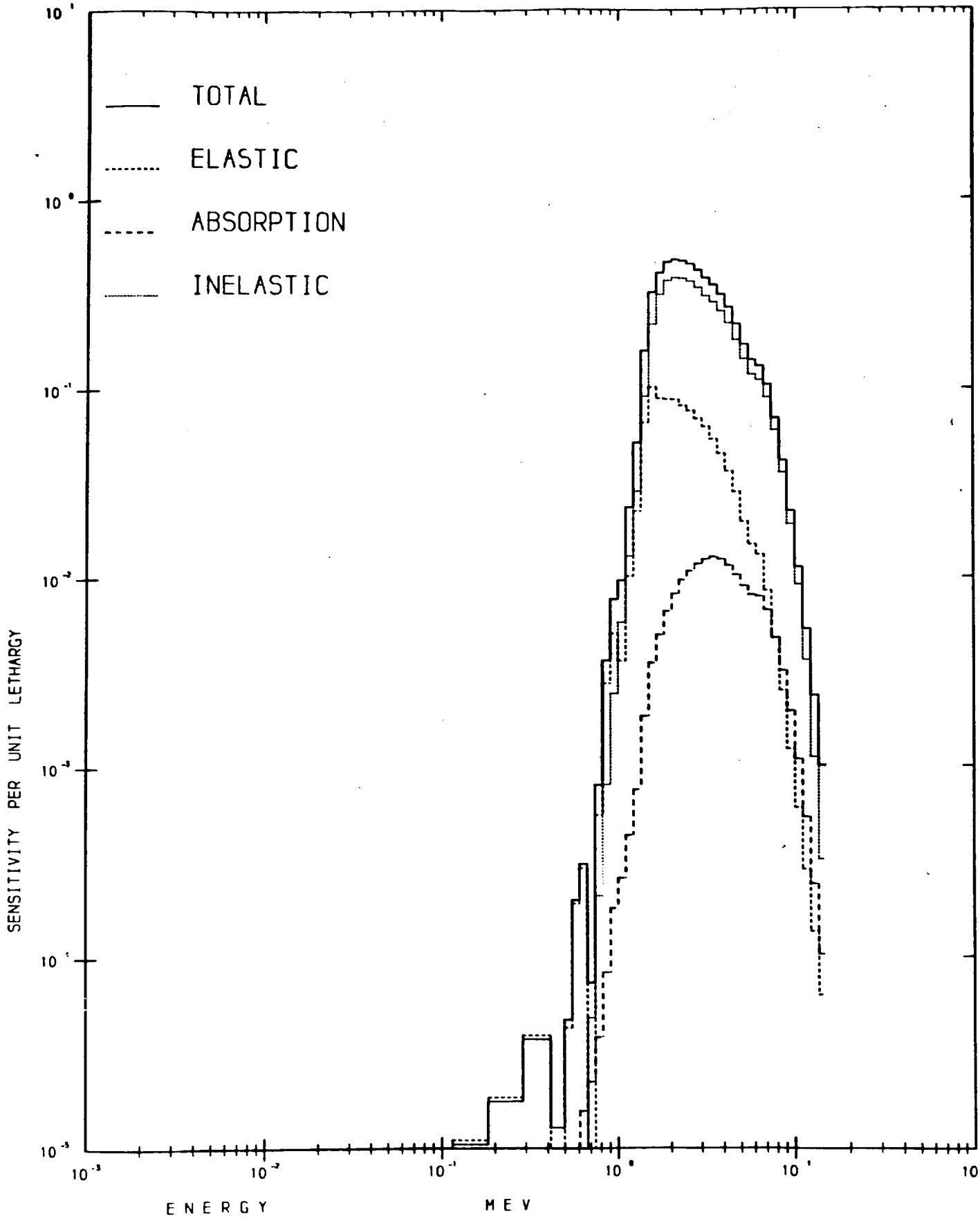
SENSITIVITY OF 238U(N,F)F.P TRANSMISSION TO TIN CROSS-SECTIONS, THICKNESS=7.01CM

FIGURE 56



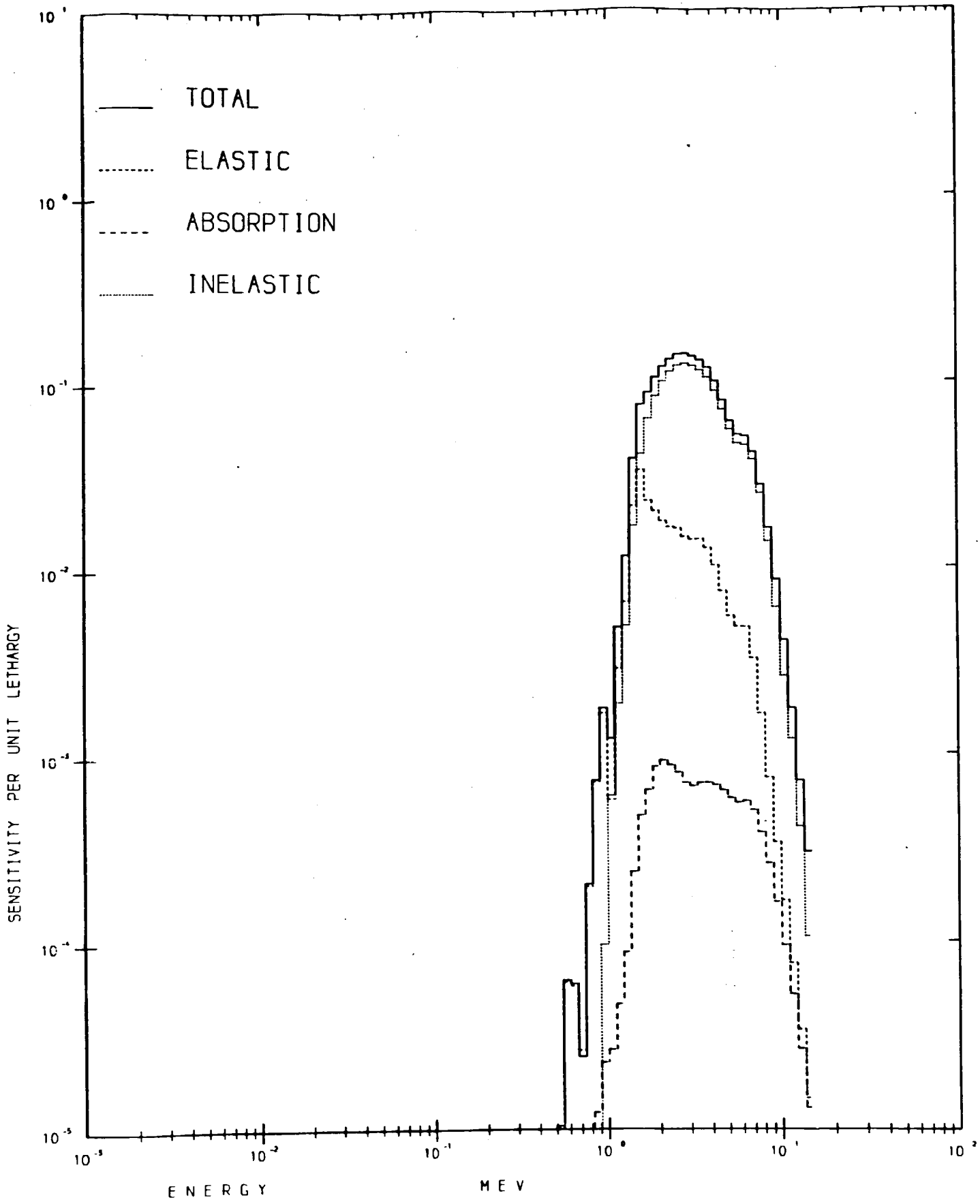
SENSITIVITY OF 238U(N,F)F.P TRANSMISSION TO LEAD CROSS-SECTIONS. THICKNESS=6.24CM

FIGURE 57



SENSITIVITY OF 238U(N,F)F.P TRANSMISSION TO COPPER CROSS-SECTIONS, THICKNESS=4.12CM

FIGURE 58



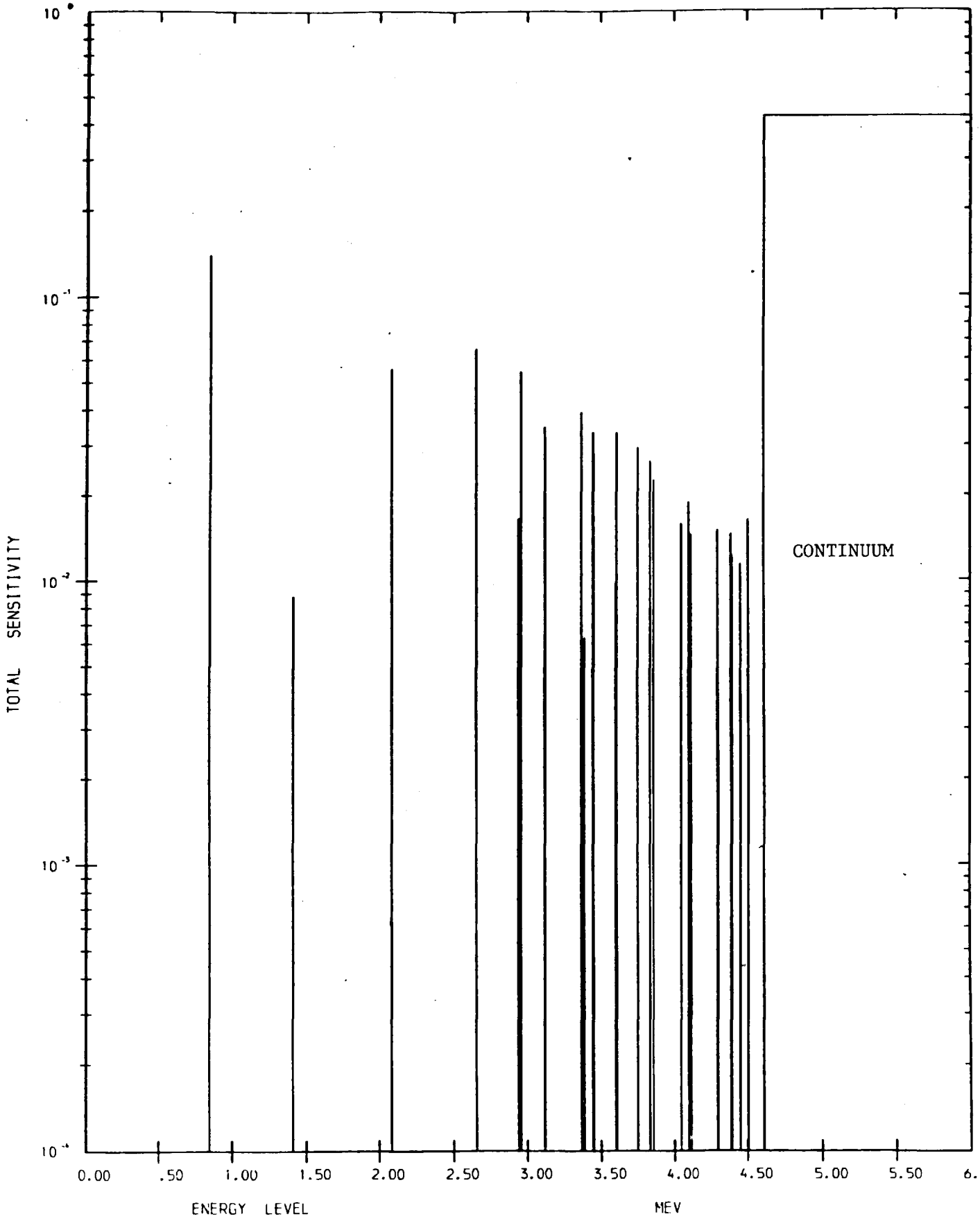
SENSITIVITY OF 238U(N,F) TRANSMISSION TO ZIRCONIUM CROSS-SECTIONS, THICK.=3.30CM

FIGURE 59

neighbourhood of the incident energy than to lower values.
In the same graphs it can be seen that, for a given shell, the relative importance of the elastic scattering increases as the detector threshold decreases, and approaches that of the inelastic scattering for the ^{237}Np(n.f)F.P detector. This happens mainly because the relative importance of the inelastic scattering for a given shell decreases with decreasing detector threshold since the proportion of the inelastic collisions rendering neutrons undetectable becomes smaller as the detector threshold falls. In other words and as far as the detection of a neutron is concerned, the inelastic scattering tends to behave more and more like the elastic one, as the energy range along which the detection system is sensitive extends to lower values.
Finally the small contribution of the absorption cross-section to the sensitivity of Transmission to the total cross-section is due to its minor role in describing the neutron interaction with iron shells in the energy range of interest (see Figure 43). The variations in the fine structure of the sensitivity profile to absorption cross-section in terms of the detector threshold originate from the absorption cross-section curve itself. (Compare Figure 43 with Figures 47 - 55). Figures 56, 57, 58 and 59 show the sensitivity profiles of the ^{238}U(n,f)F.P Transmission for the tin, lead, copper, and zirconium shells, respectively. These sensitivity profiles have a similar structure with the corresponding ones of the iron shells.

Total sensitivities

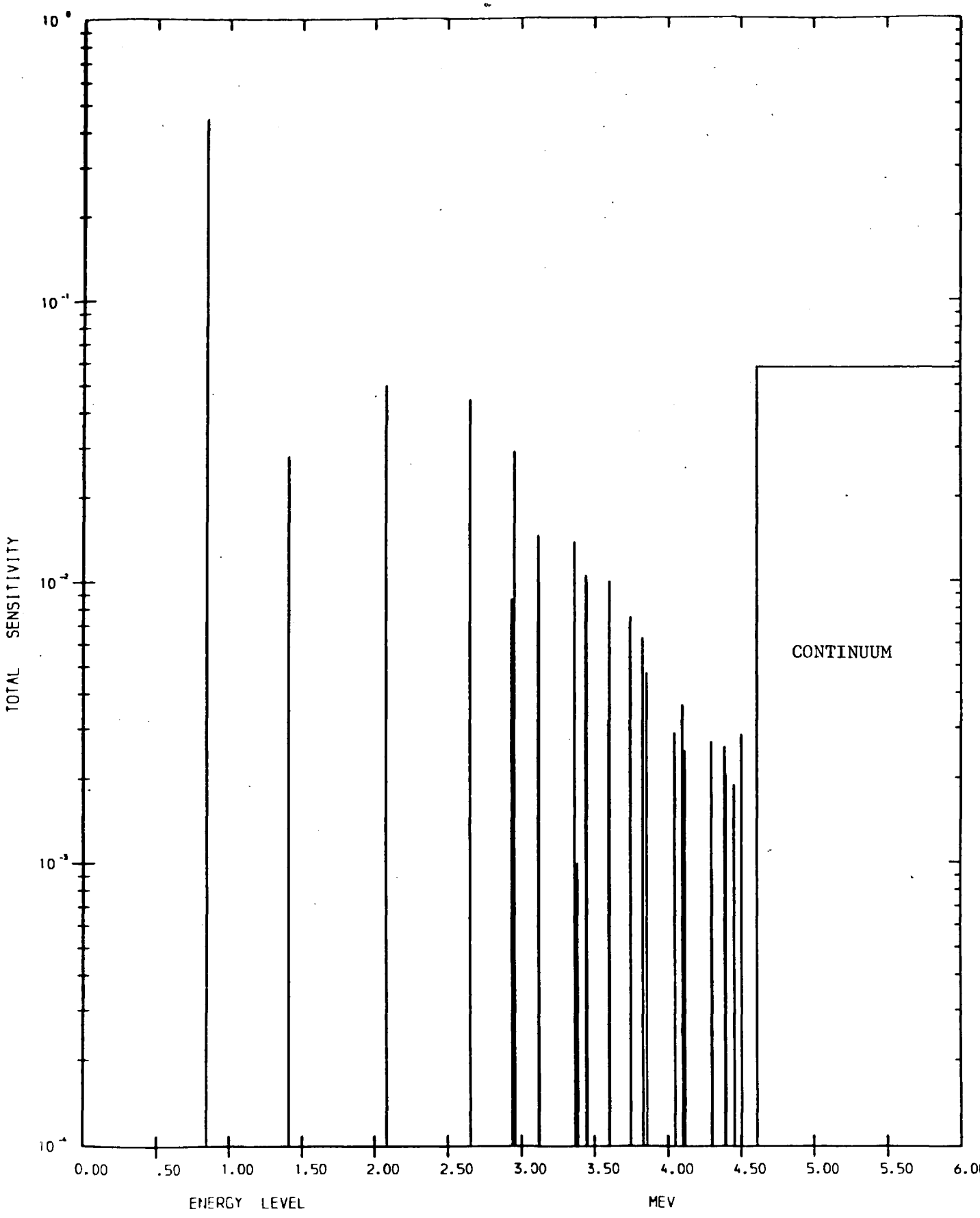
While the sensitivity profile for a certain cross-section x contains much valuable information, it is also convenient and useful to define a total (integral) cross-section sensitivity for reaction x



TOTAL SENSITIVITY TO DIFFERENT EXCITED LEVELS. IRON SHELL OF THICNESS = 9.16 CM

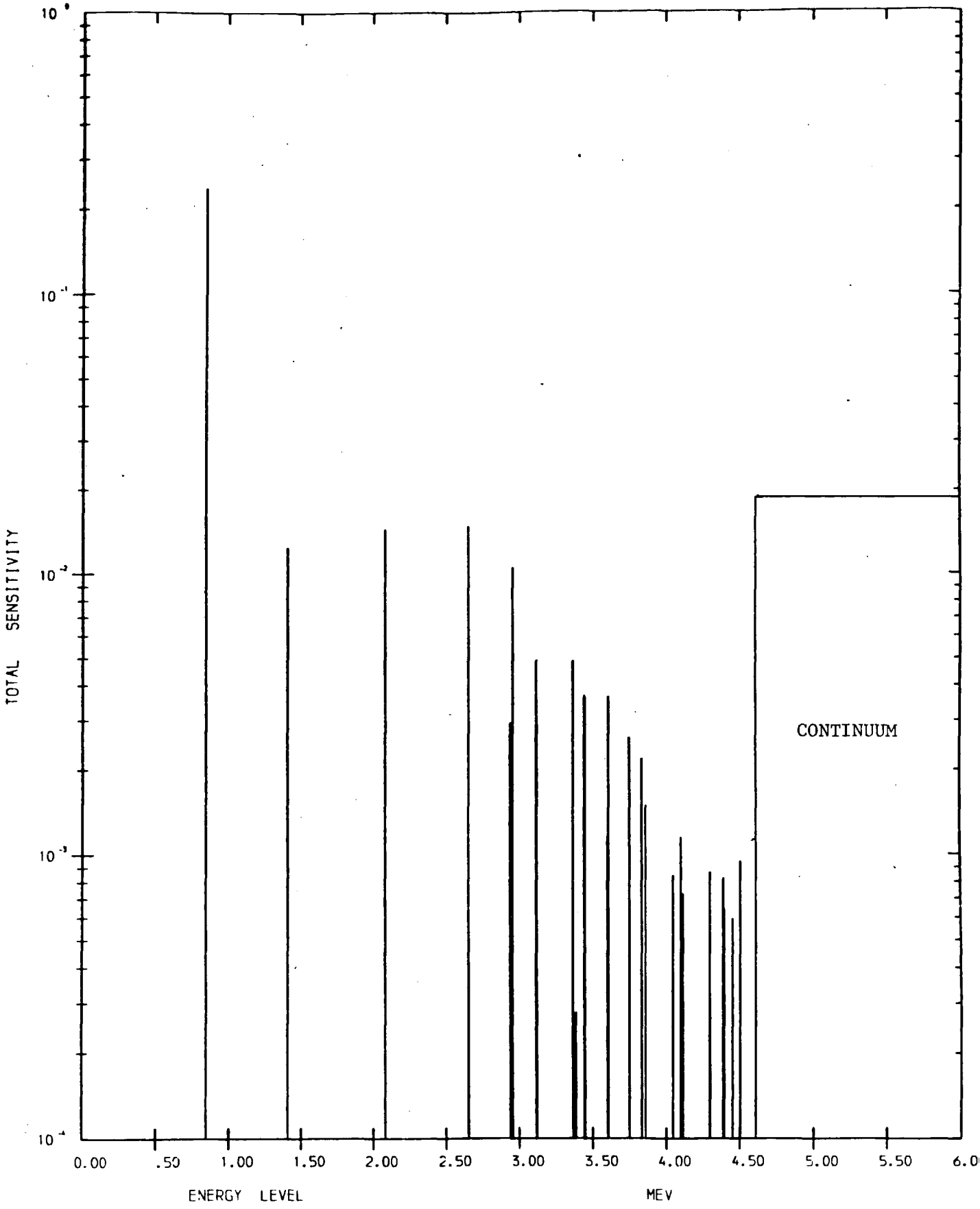
$^{27}Al(n, p)^{27}Mg$ DETECTOR

FIGURE 60



TOTAL SENSITIVITY TO DIFFERENT EXCITED LEVELS. IRON SHELL OF THICNESS = 9.16 CM
$^{238}U(n,f)$F.P DETECTOR

FIGURE 61



TOTAL SENSITIVITY TO DIFFERENT EXCITED LEVELS, IRON SHELL OF THICKNESS = 9.16 CM

$^{237}Np(n,f)$ F.P DETECTOR

FIGURE 62

by:

$$S_x \equiv \sum_{I=1}^{IGM} P_x(I) = \sum_{I=1}^{IGM} \frac{\delta T}{T} \frac{\Sigma_x(I)}{\delta \Sigma_x(I)} \qquad (4.16)$$

which reduces the sensitivity information about the whole cross-section set $\Sigma_x(I)$ to one number. S_x can be interpreted as the percentage change in Transmission resulting from a simultaneous 1% increase of the group cross-sections $\Sigma_x(I)$ in all energy groups I.

Total sensitivities have been calculated for the following reactions: total, elastic, absorption and inelastic for all the cases of Table 15 and are tabulated in Table 17.

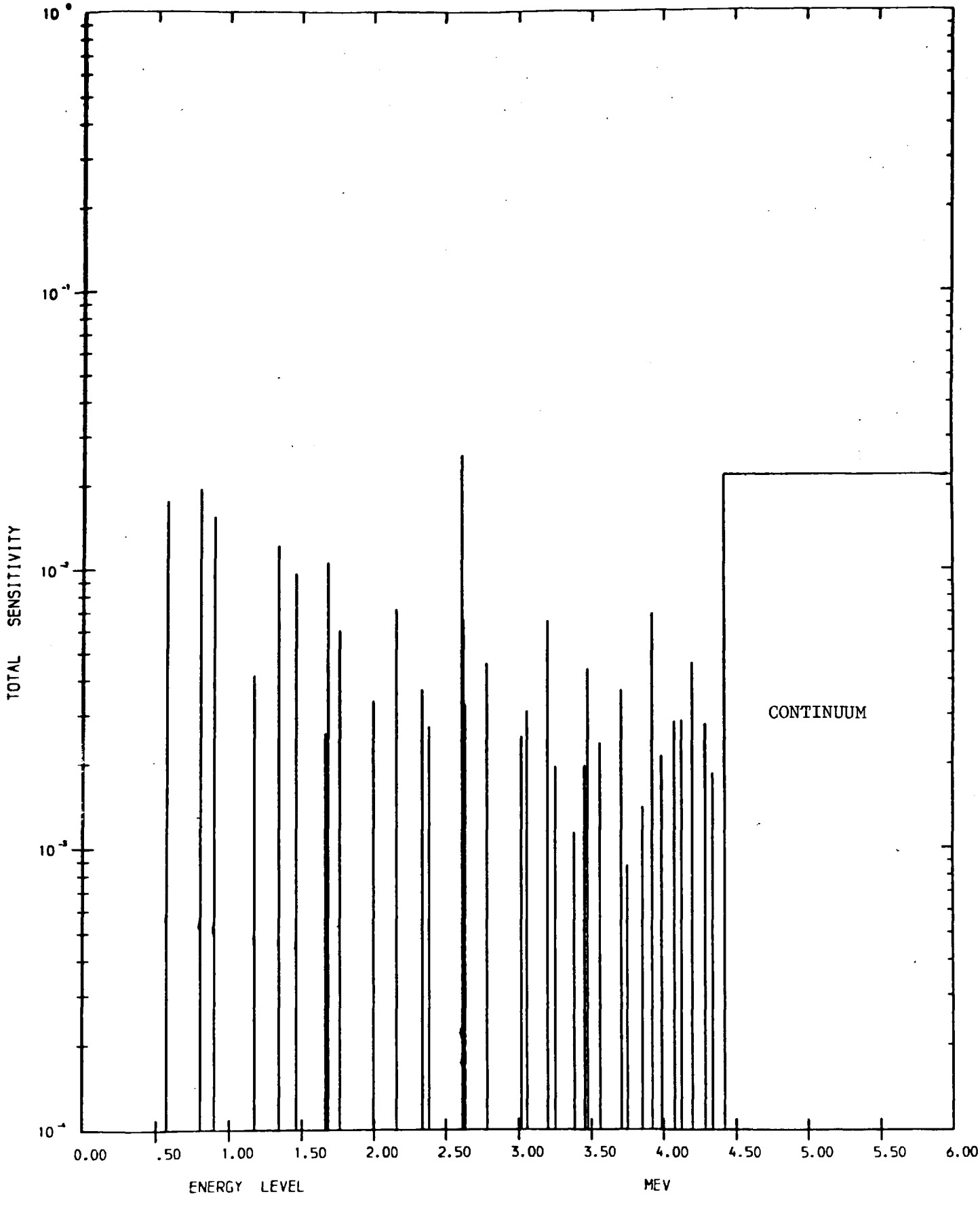
Total sensitivities were also calculated for all the cross-section sets describing the inelastic scattering to different excited levels and to the continuum for all isotopes of Table 15 (for iron the thickest shell was employed). Cross-section sets for inelastic scattering to different excited levels were not available for tin.

Figure 60, 61 and 62 give the total sensitivities of Transmission of the thickest iron shell to different excited levels and to the continuum for the three threshold detectors in terms of the level energy and continuum threshold. Similarly, Figures 63, 64 and 65 show the total sensitivities of the $^{238}U(n,f)F.P$ Transmission for lead, copper, and zirconium shells, respectively.

Table 17 reveals that the sensitivity of Transmission to inelastic cross-section is the predominant component of the sensitivity to total cross-section for all the cases included. (This was also demonstrated in the sensitivity profiles). More precisely, the sensitivity to inelastic amounts on average to about 80% of the sensitivity to total. The sensitivity to absorption is very small (1 - 3%) while the remaining refers to elastic, for all the cases of Table 17. It is also noticed in this Table that the sensitivity to total iron cross-

TABLE 17. TOTAL SENSITIVITIES OF TRANSMISSION TO TOTAL, ELASTIC ABSORPTION AND INELASTIC CROSS SECTIONS.

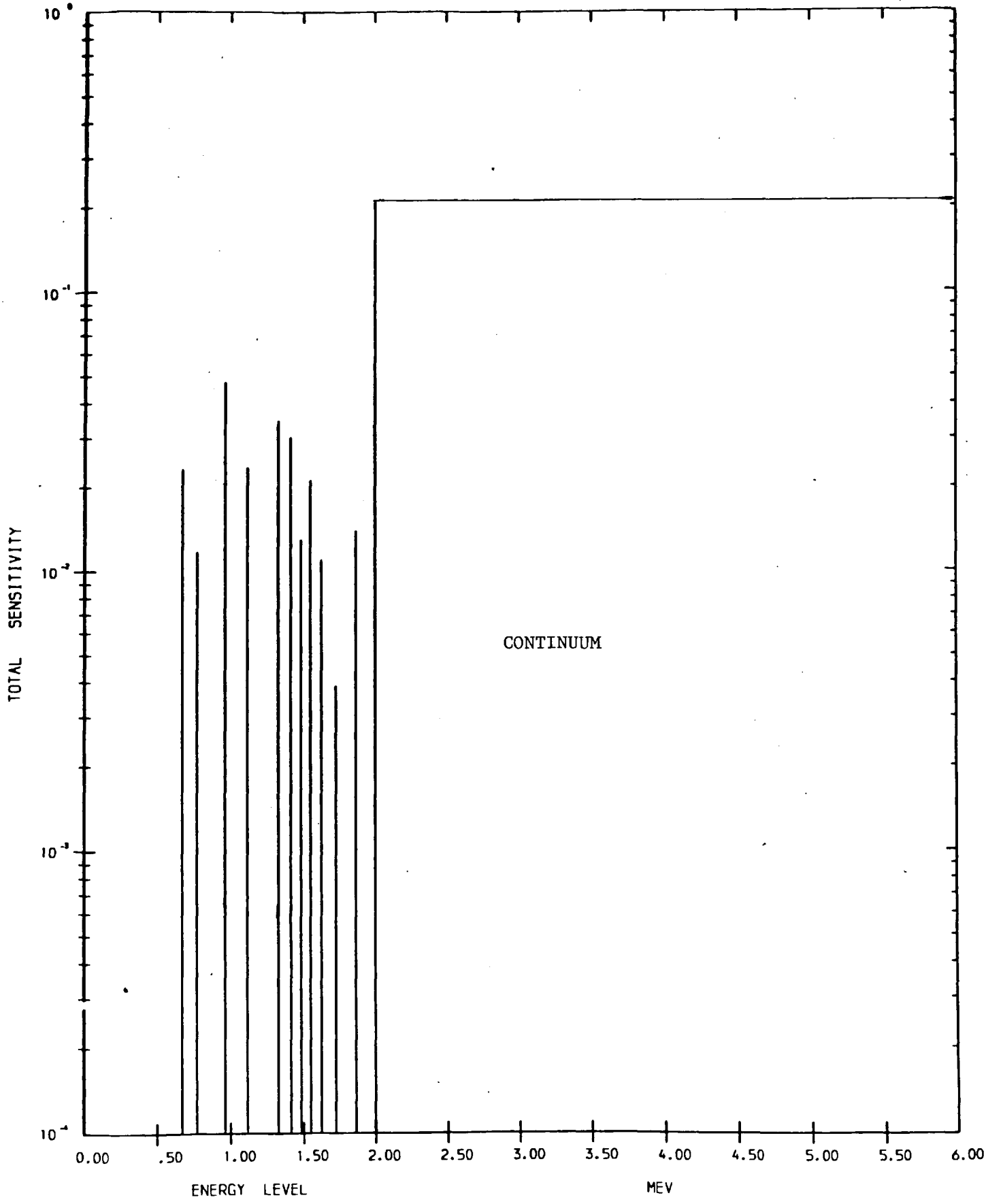
CASE	MATERIAL	THICKNESS cm	TOTAL SENSITIVITIES											
			$^{27}Al(n, P)^{27}Mg$				$^{238}U(n, f)F.P.$				^{237}Np n, f)F.P.			
			TOTAL	ELASTIC	ABSORPTION	INELASTIC	TOTAL	ELASTIC	ABSORPTION	INELASTIC	TOTAL	ELASTIC	ABSORPTION	INELASTIC
1	Fe	1.90	-2.851 E-01	-2.502 E-02	-8.929 E-03	-2.513 E-01	-1.801 E-01	-2.743 E-02	-2.780 E-03	-1.502 E-01	-7.246 E-02	-8.950 E-03	-2.001 E-03	-6.173 E-02
2	Fe	4.11	-6.226 E-01	-6.794 E-02	-1.901 E-02	-5.367 E-01	-4.534 E-01	-9.150 E-02	-6.000 E-03	-3.573 E-01	-2.043 E-01	-3.698 E-02	-4.558 E-03	-1.636 E-01
3	Fe	9.16	-1.389 E+00	-1.705 E-01	-4.237 E-02	-1.178 E+00	-1.030 E+00	-2.417 E-01	-1.209 E-02	-7.804 E-01	-4.740 E-01	-1.186 E-01	-9.019 E-03	-3.484 E-01
4	Sn	7.01					-3.943 E-01	-5.910 E-02	-6.323 E-03	-3.255 E-01				
5	Pb	6.24					-2.922 E-01	-5.590 E-02	-4.348 E-04	-2.302 E-01				
6	Cu	4.12					-5.589 E-01	-1.005 E-01	-1.635 E-02	-4.417 E-01				
7	Zr	3.30					-1.739 E-01	-2.627 E-02	-1.245 E-03	-1.448 E-01				



TOTAL SENSITIVITY TO DIFFERENT EXCITED LEVELS, LEAD SHELL OF THICKNESS = 6.24CM

$^{238}U(n,f)$F.P DETECTOR

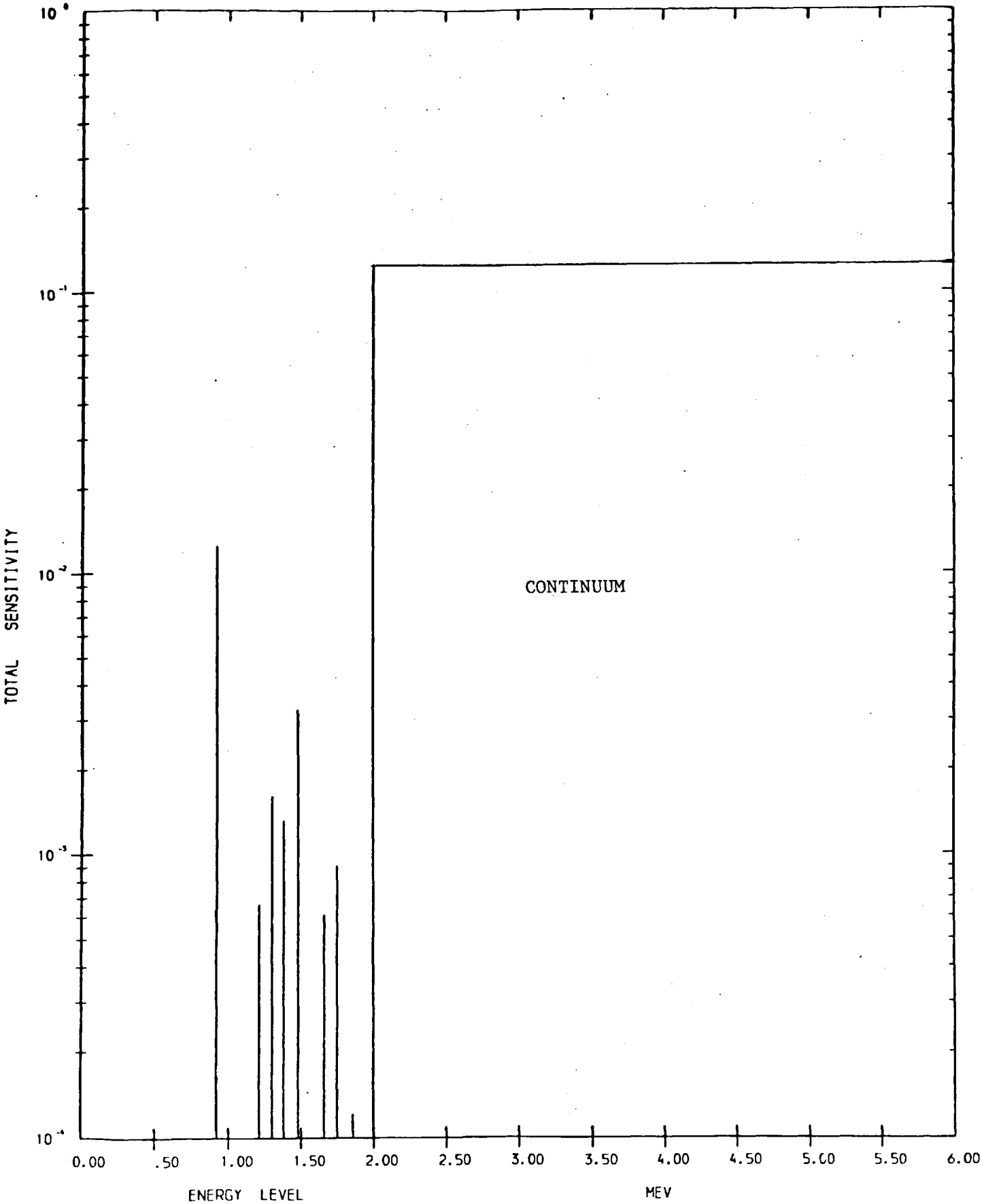
FIGURE 63



TOTAL SENSITIVITY TO DIFFERENT EXCITED LEVELS. COPPER SHELL OF THICKNESS=4.12CM

$^{238}U(n,f)$F.P DETECTOR

FIGURE 64



TOTAL SENSITIVITY TO DIFFERENT EXCITED LEVELS, ZIRCONIUM SHELL OF THICKNESS=3.30 CM

$^{238}U(n,f)$ F.P DETECTOR

FIGURE 65

section is an increasing function of both the detector threshold and shell thickness for reasons we have discussed earlier. The same behaviour is also presented by all its components, except that, in terms of the detector threshold, the sensitivity to elastic shows a maximum for the $^{238}U(n,f)F.P$ detector. This is due to the fact that the general trend of a decreasing sensitivity as the detector threshold falls is altered by the higher relative importance of the elastic scattering as we move to lower thresholds. So, according to Table 18, the sensitivity to elastic is on average only 10% of that to total for the $^{27}A\ell(n,p)^{27}Mg$ detector while it is around 20% for the other two detectors.

Table 18 gives the relative importances of the total sensitivities to elastic, absorption and inelastic for the three iron shells. This Table shows that the elastic scattering becomes more and more important as the shell thickness increases. This result is in full agreement with the B.B.C. conclusion that the effect on Transmission of the multiple (elastic) scattering in the shells cannot be neglected except for very thin shells. (Ref 1, pages 209, 214).

Comparing the total sensitivities to different excited levels and to the continuum of the thickest iron shell for the three detectors, (Figures 60, 61 and 63) it is noticed that although they follow the same pattern in terms of the level energy, the absolute values are higher for higher thresholds, as expected, and that the sensitivity to the 1^{st} excited level and to the continuum are of more interest. In particular, the predominant role of the continuum is noticeable for the $^{27}A\ell(n,p)^{27}Mg$ detector and of the 1^{st} excited level for the other two detectors.

The pattern of the total sensitivities versus level energy seems to be, more or less, the same for all the detectors. This happens mainly because it reflects the magnitude of the corresponding cross-section

TABLE 18. RELATIVE IMPORTANCES OF THE PARTIAL CROSS SECTION SENSITIVITIES FOR THE IRON SHELLS.

CASE	THICKNESS cm	RELATIVE IMPORTANCES (%)								
		$^{27}Al(n, P)^{27}Mg$			$^{238}U(n, f)F.P.$			$^{237}Np(n, f)F.P.$		
		ELASTIC	ABSORPTION	INELASTIC	ELASTIC	ABSORPTION	INELASTIC	ELASTIC	ABSORPTION	INELASTIC
1	1.90	8.9	3.1	88.0	15.2	1.5	83.3	12.3	2.7	85.0
2	4.11	10.8	3.0	86.2	20.1	1.3	78.6	18.0	2.0	80.0
3	9.12	12.2	3.0	84.8	23.3	1.1	75.6	24.8	1.9	73.3

set, that is, high inelastic group constants for a certain level imply high sensitivity and vice-versa.

In going from high to low threshold sensitivities a gradual decrease in their values is observed except from the first two levels which have higher values for the $^{238}U(n,f)F.P$ detector than for the $^{27}Al(n,f)F.P$. This happens because for the first few excited levels the cross-section "peaks" lie well below or adjacent to $^{27}Al(n,p)F.P$ threshold (4.4 MeV) and consequently they do not fully contribute to the corresponding sensitivities for this detector. As the threshold reduces from 4.4 to 1.5 MeV they are fully included in the sensitive energy range and increase the total sensitivity. This also explains why in going from the $^{238}U(n,1)F.P$ to $^{237}Np(n,f)F.P$ detector this anomaly disappears and all the sensitivities fall, as expected.

For the lead shell the sensitivity to inelastic is essentially shared by a relatively small number of excited levels (9 out of 35) and the continuum, while for the copper and zirconium shells the sensitivity to continuum is the main component (47% of the total inelastic for Cu, and 85% for Zr). However low continuum thresholds and small numbers of excited levels generally contribute to high sensitivities to the continuum for a given detector, as depicted in Figures 63, 64 and 65.

Effect of the scattering anisotropy on Transmissions, sensitivity and flux profiles.

In the optimisation procedure it was demonstrated that the anisotropy of the scattering processes has a considerable impact on the calculated Transmissions (Table 6, section 3.4.3). In this paragraph we will shed more light on this effect, based on SWANLAKE results.

SWANLAKE calculates the percentage changes in the result both by group and the total (integrated over energy) in going from P_N calculations to P_{N-1}, P_{N-2}, , P_o, where N is the order of scattering kernel expansion employed. For our calculations N = 3, and it has been found that the difference between P_3 and P_o Transmissions is essentially that between P_1 and P_o, that is, the percentage change of Transmission in going from P_1 to higher order approximations is negligibly small. Conversely, the "energy" profiles of these changes have a similar structure with the corresponding sensitivity profiles and are not included or discussed in this work. Therefore we will focus our attention only on the total percentage change of Transmission in going from P_3 to P_o calculations, which essentially gives a measure of the effect of the anisotropy of a neutron producing reaction on the calculated Transmission.

Table 19 presents the percentage differences between P_3, P_o calculations for total and elastic, for all the cases of Table 15.

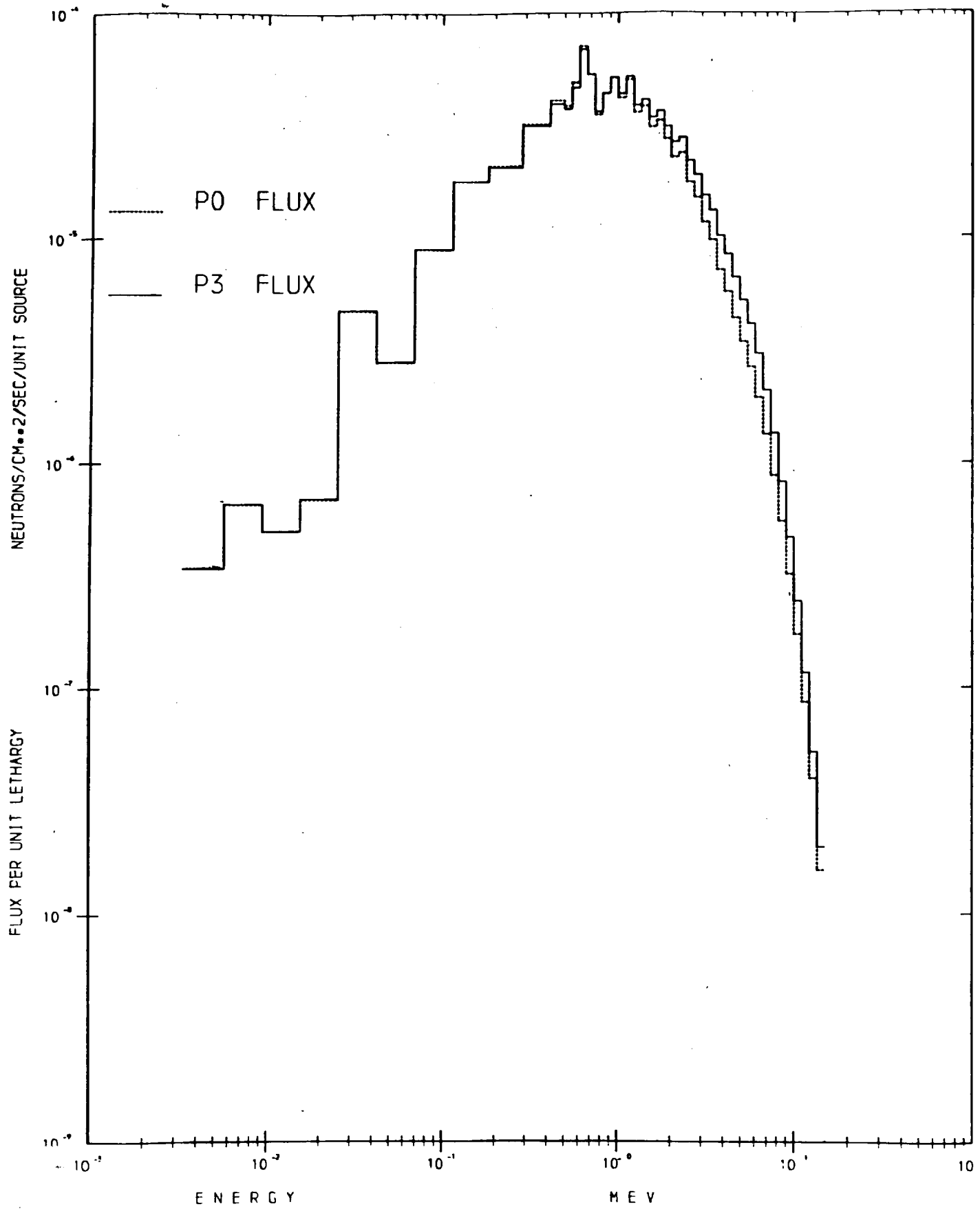
Before proceeding to any comments and conclusions drawn from this Table, it must be emphasized that these numbers are not sensitivities caused by, say, increasing the Legendre expansion coefficients (see Eqn. (3.7), page 75) by 1%, but percentage changes caused by completely omitting them. (100% reduction). Although the sensitivity of the result to Legendre expansion coefficients is a very important quantity in relating uncertainties in the angular distribution (and in most cases, energy distribution) of secondary neutrons to the final, nuclear data - originated error of the calculated quantity, it cannot be calculated by SWANLAKE.

The results of Table 19 are generally in a good agreement with P_o and P_3 ANISN calculations. Three important results emerge from this Table:

I. The anisotropy of the inelastic scattering is unimportant for

TABLE 19. PERCENTAGE CHANGES IN TRANSMISSIONS FOR P_3, P_0 CALCULATIONS.

CASE	MATERIAL	THICKNESS cm	PERCENTAGE CHANGES					
			$^{27}Al(n, P)^{27}Mg$		$^{238}U(n, f)F.P.$		$^{237}Np(n, f)F.P.$	
			TOTAL	ELASTIC	TOTAL	ELASTIC	TOTAL	ELASTIC
1	Fe	1.90	- 5.13	- 5.07	- 2.48	- 2.42	-1.13	-1.10
2	Fe	4.11	-16.88	-16.68	- 8.58	- 8.40	-4.02	-3.91
3	Fe	9.16	-39.86	-39.41	-19.88	-19.45	-9.02	-8.76
4	Sn	7.01			- 5.89	- 5.89		
5	Pb	6.24			- 5.63	- 5.63		
6	Cu	4.12			- 9.88	- 9.88		
7	Zr	3.30			- 1.92	- 1.92		



P0 AND P3 NEUTRON SPECTRA AT THE CENTRE OF THE IRON SHELL. THICKNESS=9.16CM

FIGURE 66

the iron shells. (For the other shells the inelastic scattering was isotropically represented in our calculations).

II. The effect on Transmission of elastic scattering anisotropy is substantial for all the cases studied, and a rapidly increasing function of both the detector threshold and shell thickness.

III. Isotropic (P_o) calculations greatly under-estimate the Transmissions for all the cases studied (see also Table 20).

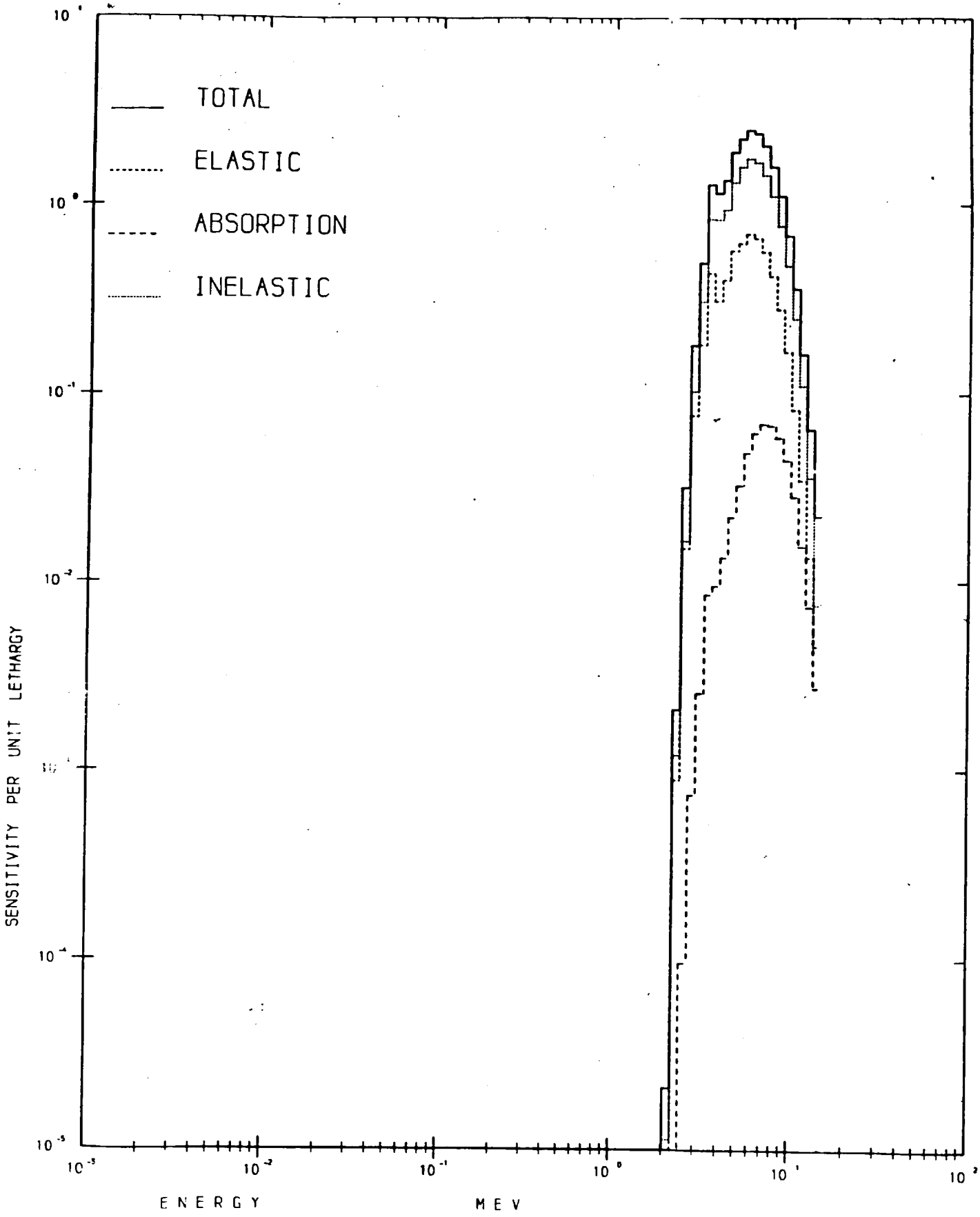
The negligibly small effect of the angular anisotropy of inelastic scattering on T stems from the fact that this anisotropy becomes important above approximately 10 MeV where the number of neutrons having these energies is very small (Ref. 33, p 61). The second result can easily be justified in the light of the arguments of the previous paragraph, while the third one will become clear in the following.

Figure 66 shows the P_o and P_3 neutron spectra at the centre of the iron shell of thickness 9.16 cm.

Figures 67, 68 and 69 present the P_o sensitivity profiles to total, elastic, absorption and inelastic for the same case, while Table 20 gives the corresponding P_o and P_3 total sensitivities.

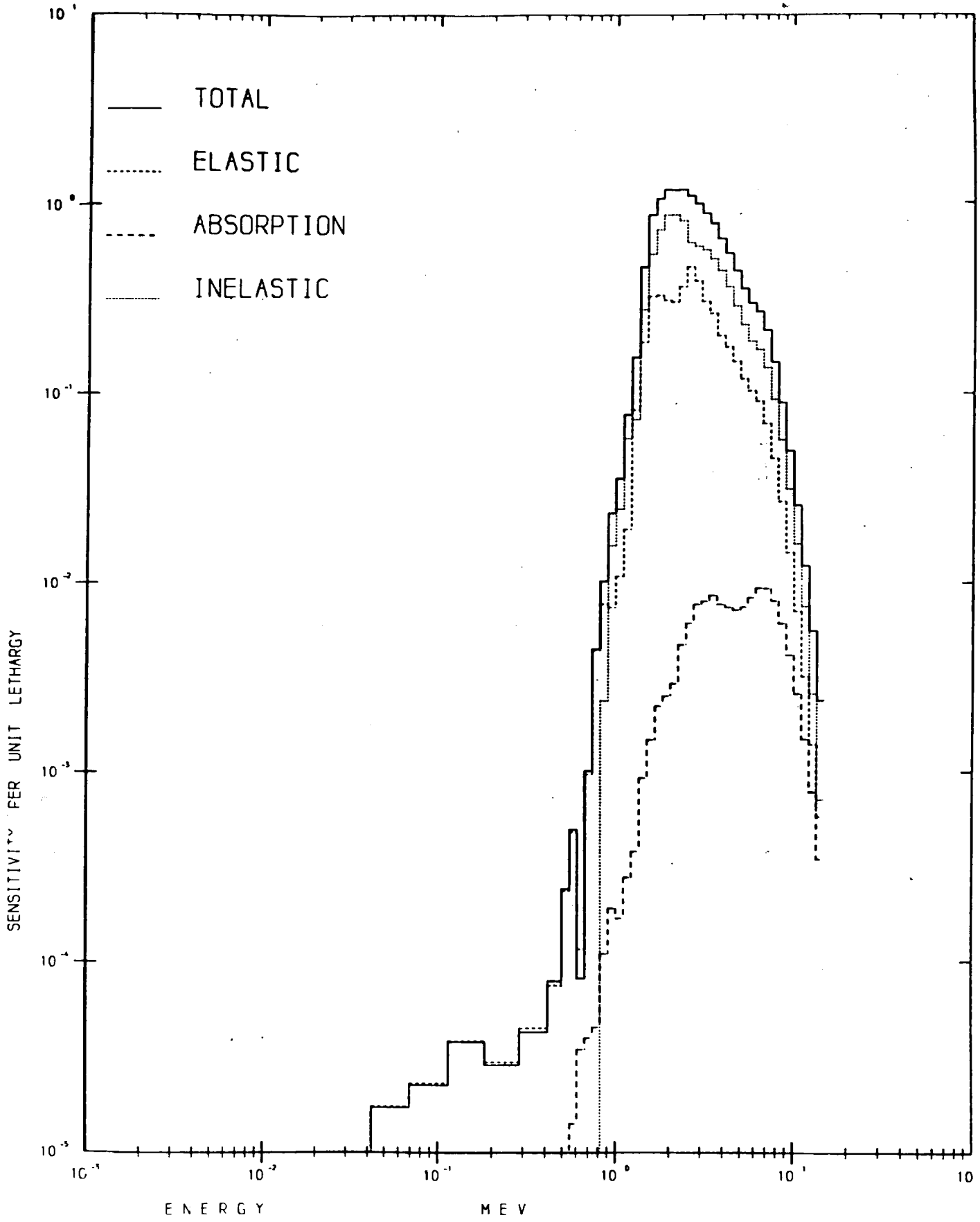
For a given source spectrum and shell thickness the flux profile is determined by the material cross-sections for different interactions, the angular and energy distributions of secondary neutrons. According to Figure 66 the omission of the elastic scattering anisotropy underestimates the neutron flux in the energy range of approximately 1.5 - 15.0 MeV, while it does not affect the fine structure of the flux profile.

In order to explain this effect and the energy range in which it occurs we must refer to the wave representation of neutrons and to the description of the shape elastic scattering (as opposed to compound elastic scattering) in terms of the interactions of the partial neutron waves



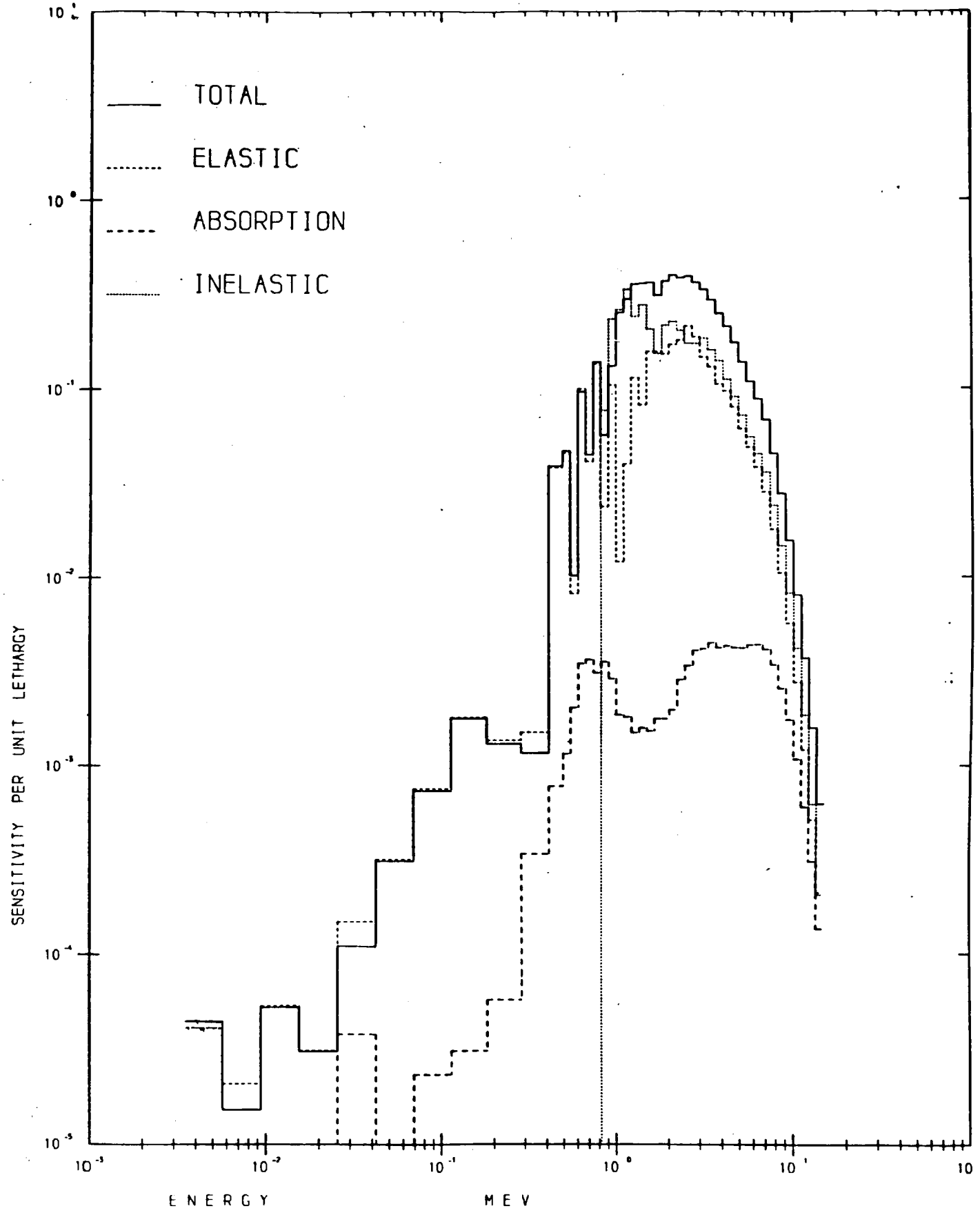
PO SENSITIVITY OF 27AL(N,P)27MG TRANSMISSION TO IRON CROSS-SECTIONS, THICKNESS=9.16CM

FIGURE 67



PO SENSITIVITY OF 238U(N,F)F.P TRANSMISSION TO IRON CROSS-SECTIONS, THICKNESS=9.16CM

FIGURE 68



PO SENSITIVITY OF 237NP(N,F)F.P TRANSMISSION TO IRON CROSS-SECTIONS, THICKNESS=9.16CM

FIGURE 69

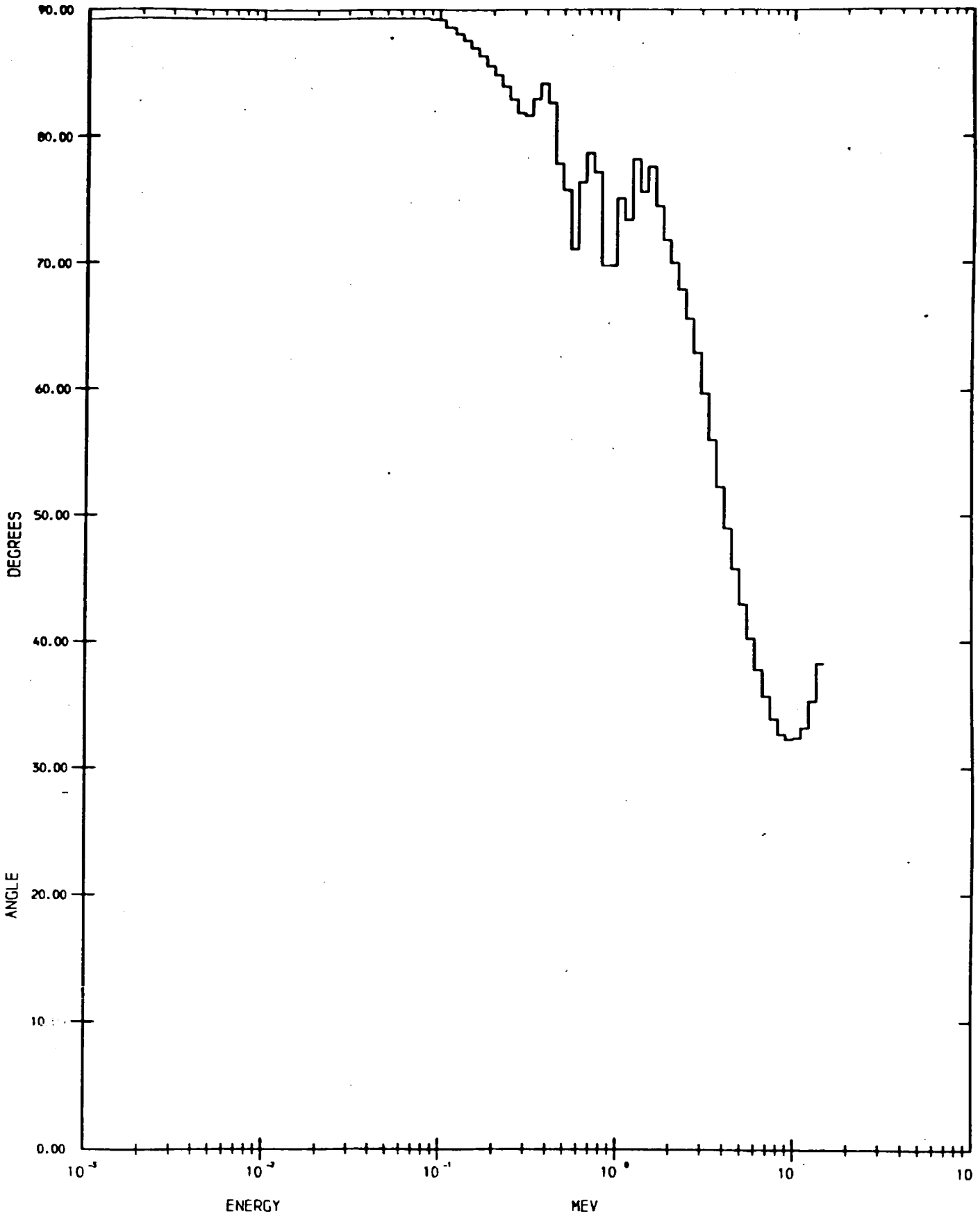
with the target nucleus. Without going into details, it has been found experimentally and it can also be shown theoretically that the scattering of s - wave neutrons is always isotropic in the centre-of-mass system (Ref 33 , page 50) (it must be mentioned here that Laboratory and C.M. systems tend to become identical with increasing mass of the target nucleus and it is not usually necessary to make a distinction between them for nuclei heavier than nitrogen or oxygen). It is also known that s-wave scattering is the only mode of potential scattering possible when kR<<1. (Ref 33 , pages 39-42) k is the wave number of a neutron and is given by:

$$k = \frac{P}{\hbar} = \frac{\sqrt{E}}{4.55\ 10^{-10}} \quad cm^{-1} \tag{4.17}$$

where: P is the neutron momentum, $\hbar$ is Planck's constant divided by 2π and E the neutron energy in eV. R is the nuclear radius given, approximately, by:

$$R = \frac{r_e}{2} A^{1/3} = 1.41\ 10^{-13} A^{1/3} \text{ cm} \tag{4.18}$$

where: A is the atomic mass number and r_e the electron radius. Introducing Eqns (4.17) and (4.18) into the condition $kR \simeq 1$, an energy boundary can be established above which the p - waves begin to interact with the nucleus and the scattering ceases to be isotropic in the C.M. system. The angular distribution in this case tends to become forward peaked; that is, the neutrons are most frequently scattered through small angles. As the value of kR is increased still further by moving to heavier nuclei and/or higher neutron energies, more partial waves interact and the scattering becomes increasingly forward peaked. For iron this energy boundary is found to be about 0.71 MeV. This energy value is compatible with Figure 70 which gives the mean angle of elastic scatter in terms of neutron energy. According to this



MEAN ANGLE OF ELASTIC SCATTER VERSUS ENERGY FOR IRON

FIGURE 70

Figure the elastic scattering cannot any longer be considered isotropic for neutron energies exceeding 0.7 MeV, while it is truely isotropic for neutron energies falling below 0.1 MeV.

Now in trying to relate angular with energy distributions of elastically scattered neutrons so as to explain the effect of the angular anisotropy on both Transmission and flux, we also make use of the fact that the energy distribution of elastically scattered neutrons is directly proportional to the differential elastic scattering cross-section given by the formula: (Ref 33 pages 166, 171)

$$P(E\rightarrow E') = \begin{cases} \dfrac{4\pi\sigma_{e\ell}(\theta)}{E(1-a)\sigma_{e\ell}} & , \quad aE<E'<E \\ 0 & \quad E<E'<aE \end{cases} \tag{4.19}$$

where: E is the incident neutron energy, E' the energy of the elastically scattered neutron, $\sigma_{e\ell}(\theta)$ the differential elastic scattering cross-section, θ the angle between direction of incidence and direction of scatter in either system for iron and a is given by:

$$a = \left(\frac{A-1}{A+1}\right)^2 \tag{4.20}$$

In the case where elastic scattering is isotropic then $\sigma_{e\ell}(\theta)$ is constant, namely:

$$\sigma_{e\ell}(\theta) = \frac{\sigma_{e\ell}}{4\pi} \tag{4.21}$$

and Eqn. (4.19) becomes:

$$P(E\rightarrow E') = \begin{cases} \dfrac{1}{E(1-a)} & , \quad aE<E'<E, \\ 0 & , \quad E<E'<aE \end{cases} \tag{4.22}$$

Eqn. (4.22) says that when the elastic scattering is isotropic the energy distribution of the scattered neutrons is a constant, independent

of E' (i.e. the energy of a scattered neutron will be found with equal probability in any interval dE' between E' = aE and E' = E). If the scattering is forward peaked, that is, neutrons are preferentially scattered through small angles, P(E→E') is larger near E' = E than near E' = aE, since neutrons lose comparatively little energy in small angle scattering, according to the formula (Ref 33, page 168).

$$\cos\theta = 1 - \left(\frac{A+1}{A}\right)^2\left(1 - \frac{E'}{E}\right) \qquad (4.23)$$

However, if $\sigma_{el}(\theta)$ is peaked in the backward direction, P(E→E') is larger near E' = aE. The function P(E→E') is shown in Figure 71 for these cases and also for isotropic scattering.

For iron a = 0.931 which implies a maximum lethargy width for the elastic energy losses of 0.07. Since the first 35 energy groups of the 55 - group structure are of equal lethargy of 0.1, it is perceived that elastic scattering contributes mainly to within group scatter and to downscatter to next group only.

Figures 70 and 71 explain why the P_o calculations substantially under-estimate the neutron flux in the energy range of approximately 1.5 MeV - 14.9 MeV. In this energy range, according to Figure 70, the elastic scattering is strongly forward peaked; this implies from Figure 71 very small energy losses compared to that of isotropic elastic scattering which corresponds to P_o calculations. The fact that the elastic cross-section is high in this energy range (see Figure 43) makes the P_3 fluxes noticeably higher than those of P_o calculations and therefore the Transmissions. It is also noticeable in Figure 66 that P_o and P_3 fluxes coincide in energy ranges where the elastic scattering is isotropic (below 0.2 MeV) and that there are energy groups where the P_3 fluxes are lower than the P_o ones to compensate for the higher

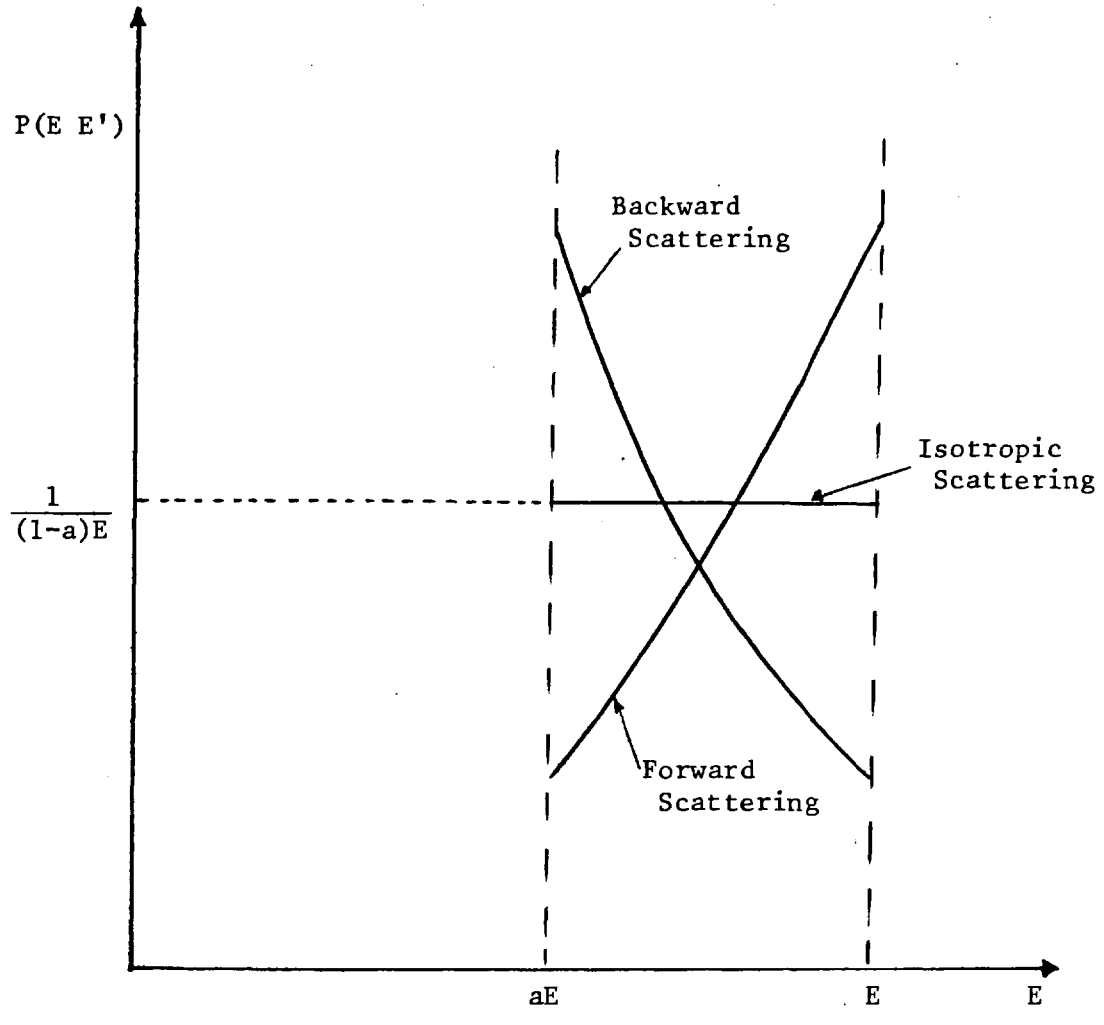


FIGURE 71 ELASTIC SCATTERING DISTRIBUTION FUNCTIONS FOR VARIOUS FORMS OF SCATTERING.

values observed in the energy range 1.5 - 14.9 MeV. The same Figure can also be used to explain why the percentage difference in Transmission between P_o and P_3 calculations is much higher for the $^{27}A\ell(n,p)^{27}Mg$ detector, with an effective threshold at 4.4 MeV, than for the $^{237}Np(n,f)F.P$ one whose sensitivity extends down to 0.5 MeV. Comparing P_o and P_3 sensitivity profiles (Figures 67, 68, 69 and Figures 53, 54, 55, respectively) and total sensitivities given in Table 20

TABLE 20. P_0, P_3 TRANSMISSIONS AND TOTAL SENSITIVITIES FOR THE IRON SHELL OF THICKNESS = 9.16 cm.

DETECTOR	TRANSMISSIONS			TOTAL SENSITIVITIES							
				P_0				P_3			
	P_0	P_3	EXPERIMENTAL	TOTAL	ELASTIC	ABSORPTION	INELASTIC	TOTAL	ELASTIC	ABSORPTION	INELASTIC
$^{27}Al(n, P)^{27}Mg$	0.1854	0.2778	-	-1.985 E+00	-5.597 E-01	-4.973 E-02	-1.373 E+00	-1.389 E+00	-1.705 E-01	-4.237 E-02	-1.178 E+00
$^{238}U(n, f)F.P.$	0.3705	0.4495	0.4694	-1.334 E+00	-4.454 E-01	-1.272 E-02	-8.750 E-01	-1.030 E+00	-2.417 E-01	-1.209 E-02	-7.804 E-01
$^{237}Np(n, f)F.P.$	0.6686	0.7272	0.7250	-6.042 E-01	-2.171 E-01	-9.599 E-03	-3.768 E-01	-4.740 E-01	-1.186 E-01	-9.019 E-03	-3.484 E-01

for the d = 9.16 cm iron shell, we observe a substantial shift of the P_o sensitivity profile to elastic cross-section to higher values for all the detectors, and much higher total sensitivities for the elastic, while the values for absorption remain essentially unchanged; for inelastic a considerably lower increase is noticed. In particular, in comparing Figures 55 and 69 it is noticed that in the energy range of about 2.0 - 10.0MeV the P_o sensitivity profiles to elastic and inelastic coincide while they do not differ at all from the corresponding P_3 ones below 2 MeV.

The same arguments can be used to explain the much higher sensitivity to elastic cross-sections in P_o calculations. A 1% increase of a certain elastic group constant $\sigma_{el,g}$ in the energy range of strongly forward peaked scattering is expected to have a considerably higher effect on Transmission in P_o calculations where the elastically scattered neutrons are uniformly distributed between the energies E and aE with $E_{g-}<E<E_{g+1}$, than it has for P_3 calculations. In the latter case and according to Figure 71 the scattered neutrons are accumulated in the vicinity of the incident energy E and hence for most of these neutrons the elastic scattering has a negligible effect.

The combination of Figures 66 and 70 can also explain why the increase in the total sensitivity to elastic in going from P_3 to P_o calculations is much higher for the $^{27}Al(n,p)^{27}Mg$ detector (228%) while for the other two detectors is at the same level (84%). Indeed, the $^{27}Al(n,p)^{27}Mg$ detector is sensitive only in the energy range where the elastic scattering is strongly forward peaked, whereas the other two detectors cover energy ranges where the angular anisotropy is less important.

The substantial difference between P_o and P_3 Transmissions in Table 20 and the fact that the P_3 values approach the measured ones demonstrate

the importance of the elastic scattering anisotropy in our calculations. Finally, comparing Figures 66 and 43 we note that the very fine structure of the neutron spectra in the energy range of about 0.5 - 1.5 MeV mirrors the structure of the cross-section in the same energy range. This shows that the fine structure of the neutron spectra is mainly determined by the group cross-sections than any other nuclear data parameters.

4.2.4 SWANLAKE Results and Conclusions.

The following conclusions summarize the sensitivity analysis of the calculated Transmissions in terms of the material cross-sections:

I. The Transmissions strongly depend on the material cross-sections over relatively short energy intervals within the energy range of about 0.5 - 11.0 MeV. These energy intervals define the "sensitivity peaks" within the sensitive energy range determined by the convolution of source spectrum and detector response and, approximately, are: 3.0 - 10 MeV for the $^{27}A\ell(n,p)^{27}Mg$ detector, 1.1 - 5.0 MeV for the $^{238}U(n,f)$F.P one, and 0.8 - 5.0 MeV for $^{237}Np(n,f)$F.P. The energy integrated sensitivity to total cross-section is an increasing function of both detector threshold and shell thickness.

II. The sensitivity to inelastic cross-section is the paramount component of the sensitivity to total, amounting to about 75 - 90% for all the materials, detectors and thicknesses studied. Sharing this high sensitivity to inelastic cross-section amongst its partials for different excited levels and the continuum, the first excited level and the continuum are the main components for the $^{237}A\ell(n,f)^{27}Mg$ detector. For the other two detectors the sensitivity to the 1^{st} excited level contributes the most for the iron shells. For lead it appears that some energy levels and the continuum are equally important, while for copper and zirconium the continuum plays a predominant role.

III. The anisotropy of the inelastic scattering has negligible effect on Transmission for the iron shells, while it is very important to account of elastic scattering anisotropy, especially for high thresholds and thicknesses.

An isotropic treatment of the elastic scattering greatly under-estimates the Transmissions.

4.3 SENSITIVITY OF TRANSMISSION TO LEGENDRE COEFFICIENTS OF THE SCATTERING KERNEL

We saw in the previous section that (a) SWANLAKE gives only the effect on Transmission by completely omitting the first and higher order Legendre coefficients of the scattering kernel expansion, (b) the angular anisotropy of the secondary neutrons is confined to that of the elastic processes and (c) a first order expansion is considered adequate for all the cases studied.

Actually the P_o sensitivity matrix calculated by SWANLAKE contains real sensitivities, that is, the change in the result caused by 1% increase of that particular element of the scattering matrix with the scattering being considered isotropic (This perturbation is implied by the 1% increase of the corresponding scattering cross-section σ_g and is the same for all $\sigma_{g\to g'}$ with $g' \geq g$). Sensitivity matrices of order higher than zero simply comprise correction terms applicable to corresponding P_o values and account for the anisotropy of the scattering. This different interpretation of P_o and higher order elements of the SWANLAKE sensitivity matrices stems from the fact that the P_o coefficients of the scattering kernel expansion coincide with the group transfers, that is:

$$\sigma_{g\to g'}(\mu_o) = \sum_{\ell=o}^{\infty} \frac{2\ell+1}{2\pi} \sigma^{\ell}_{g\to g'} P_{\ell}(\mu_o) \tag{4.24}$$

$$\sigma^{\ell}_{g\to g'} = 2\pi \int_{-1}^{+1} \sigma_{g\to g'}(\mu_o) P_{\ell}(\mu_o) d\mu_o \tag{4.25}$$

from which, since $P_o(\mu_o) = 1$

$$\sigma^{o}_{g\to g} = \sigma_{g\to g'} \tag{4.26}$$

In this section a quantitative assessment of the total sensitivity of Transmission to the first order expansion coefficient

of the elastic scattering, averaged over the fission spectrum and detector response, viz:

$$\sigma^1_{e\ell} = \frac{\sum_{g=1}^{IGM} N_g \sigma_{D,g} \sum_{g=g'}^{IGM} \sigma^1_{e\ell,g\to g'}}{\sum_{g=1}^{IGM} N_g \sigma_{D,g}} \qquad (4.27)$$

will be attempted, using B.B.C. theory, data and results. This exercise will be undertaken only for iron, assuming that the results and conclusions reached will approximately be valid and for other materials.

First of all, the simplified form of the Transmission formula, Eqn. (2.7), can easily be expressed in terms of the mean cosine $\bar{\mu}_o$ of the elastic scattering angle, averaged over the fission spectrum and detector response. Indeed, the elastic transport cross-section σ_{et} in Eqn. (2.7) can be written as: (Ref 1, page 221)

$$\sigma_{et} = \sigma_{e\ell}(1-\bar{\mu}_o) = \sigma_{e\ell} S \qquad (4.28)$$

Values of S are given in B.B.C. work for all the detectors and isotopes used. According to this information (Ref 4, pages 149, 153, 155) the values of $\bar{\mu}_o$ for iron and the three detectors are:

$$\bar{\mu}_o = \begin{cases} 0.69 & \text{for the } {}^{27}A\ell(n,p){}^{28}Mg \text{ DETECTOR} \\ 0.42 & \text{for the } {}^{238}U(n,f)F.P. \text{ DETECTOR} \\ 0.30 & \text{for the } {}^{237}Np(n,f)F.P. \text{ DETECTOR} \end{cases}$$

We observe that as the detector threshold decreases the elastic scattering becomes less anisotropic (forward peaked) in accordance with Figure 70.

Eqn. (2.7) can now be rewritten as:

$$T = 1-\left[1-e^{-N(\sigma_{in}+\sigma_{e\ell}(1-\bar{\mu}_o)x)}\right]\left(\frac{\sigma_{in}}{\sigma_{in}+\sigma_{e\ell}(1-\bar{\mu}_o)P_m}\right) \tag{4.29}$$

The relation between $\bar{\mu}_o$ and $\sigma^1_{e\ell}$ can easily be found from Eqn. (4.25), viz:

$$\sigma^1_{e\ell,g\to g'}=2\pi\int_{-1}^{+1}\sigma_{e\ell,g\to g'}(\mu_o)\mu_o d\mu_o \equiv \sigma_{e\ell,g\to g'}\bar{\mu}_{o,g\to g'} \tag{4.30}$$

and therefore, according to Eqn (4.27):

$$\sigma^1_{e\ell} = \frac{\sum_{g=1}^{IGM} N_g\sigma_{D,g}\sum_{g=g'}^{IGM}\sigma_{e\ell,g\to g'}\bar{\mu}_{o,g\to g'}}{\sum_{g=1}^{IGM} N_g\sigma_{D,g}} = \sigma_{e\ell}\bar{\mu}_o$$

that is,

$$\sigma^1_{e\ell} = \sigma_{e\ell}\bar{\mu}_o \tag{4.31}$$

Eqns. (4.30), (4.31) show that the Legendre coefficients can vary independently from the corresponding group transfers or total (averaged) scattering cross-sections and this can be interpreted as different angular distributions of secondary neutrons.

Now the (total) sensitivity of Transmission to the 1st order expansion coefficient is defined, in the usual way, as

$$S_{L,1} \equiv \frac{\partial T}{\partial\sigma^1_{e\ell}}\frac{\sigma^1_{e\ell}}{T} \tag{4.32}$$

and coincides with the sensitivity of Transmission to $\bar{\mu}_o$, as is easily verified using Eqn (4.2), viz:

$$S_{L,1} = \frac{\partial T}{\partial\sigma^1_{e\ell}}\frac{\sigma^1_{e\ell}}{T} = \frac{\partial T}{\partial\bar{\mu}_o}\frac{\bar{\mu}_o}{T} \tag{4.33}$$

The R.H.S. of Eqn. (4.31) can be estimated using Eqn. (4.29) and data listed in the result Tables of Ref. 4. More precisely, the

differentiation of Eqn. (4.29) with respect to $\bar{\mu}_o$ gives the following formula for the sensitivity $S_{L,1}$:

$$S_{L,1} = \frac{\bar{\mu}_o}{T} \cdot \frac{\sigma_{in}\sigma_{e\ell}}{R_1} \left[x\, e^{-R_2} - \frac{R_3(1-e^{-R_2})}{R_1} \right] \qquad (4.34)$$

where: x is the shell thickness

$$R_1 = \sigma_{in} + \sigma_{e\ell}\,(1-\bar{\mu}_o)\,P_m$$

$$R_2 = N(\sigma_{in} + \sigma_{e\ell}\,(1-\bar{\mu}_o))x$$

$$R_3 = P_m - (1-\bar{\mu}_o) \cdot \frac{\partial P_m}{\partial \bar{\mu}_o}$$

$$\frac{\partial P_m}{\partial \bar{\mu}_o} = -\sigma_{e\ell}\, x \, \frac{\partial P_m}{\partial (\Sigma_{tr} x)}$$

$\frac{\partial P_m}{\partial (\Sigma_{tr} x)}$ is found as the slope (dimensionless) of the curves $P_m = f(\Sigma_{tr} x)$ for various $K = r_2/r_1$ ratios (see Table 2) plotted in Figure 7. The relation between $\Sigma_{tr} x$ and $\bar{\mu}_o$ needed is given by the expression:

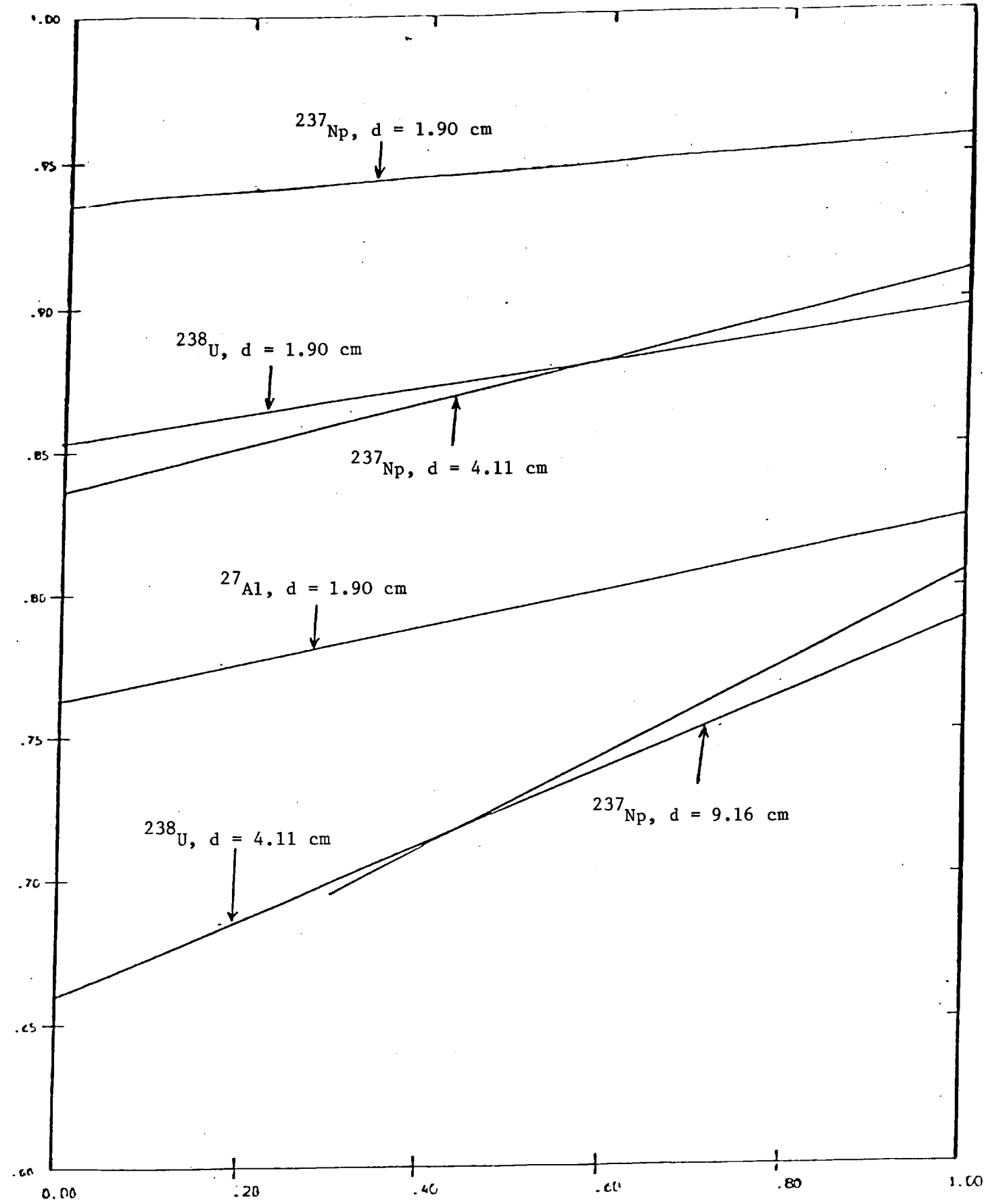
$$\Sigma_{tr} x = N(\sigma_{in} + \sigma_{e\ell}\,(1-\bar{\mu}_o))x$$

Table 21 presents the sensitivities to $\sigma^1_{e\ell}$ as given by Eqn. (4.3.4) together with the input data required and the corresponding total sensitivities to elastic cross-section as calculated by SWANLAKE, for all the iron cases for which experimental Transmissions were available. Two important remarks can be made according to the results of Table 21: The total sensitivities to elastic cross-section and to 1^{st}-order expansion coefficient follow the same trend in terms of shell thickness and detector threshold, as expected from what has been discussed so far and that they are of opposite sign and of the same order of magnitude.

However, we cannot accept the same reliability level for sensitivities

TABLE 21. TOTAL SENSITIVITY TO 1st ORDER EXPANSION COEFFICIENT OF THE SCATTERING KERNEL FOR VARIOUS IRON CASES.

	CASE		INPUT DATA							
	DETECTOR	THICKNESS cm	σ_{el}	σ_{in}	$\bar{\mu}_o$	P_m	$\frac{dP_m}{d(\Sigma_{tr}x)}$	T_E	$S_{L,1}$ (Eqn. 4.34)	S_{EL} (Swanlake)
1	^{27}Al	1.90	2.400	1.200	0.69	0.620	-0.780	0.793	4.938 E-02	-2.502 E-02
2	^{238}U	1.90	2.484	0.686	0.42	0.590	-0.700	0.868	1.801 E-02	-2.743 E-02
3	^{237}Np	1.90	2.474	0.276	0.30	0.610	-0.739	0.945	5.329 E-03	-8.950 E-03
4	^{238}U	4.11	2.484	0.686	0.42	0.390	-0.424	0.712	7.377 E-02	-9.150 E-02
5	^{237}Np	4.11	2.474	0.276	0.30	0.410	-0.450	0.861	2.467 E-02	-3.698 E-02
6	^{238}U	9.16	2.484	0.686	0.42	0.250	-0.193	0.467	1.790 E-01	-2.417 E-01
7	^{237}Np	9.16	2.474	0.276	0.30	0.300	-0.238	0.723	6.514 E-02	-1.186 E-01



TRANSMISSION VARIATION IN TERMS OF MEAN COSINE OF ELASTIC SCATTER FOR IRON SHELLS

FIGURE 72

calculated by SWANLAKE and those based on B.B.C. work, where both the method of analysis and the data used are much simpler and of poorer quality. So, although the $S_{L,1}$ sensitivities must be thought of as being accompanied by large uncertainties, the fact that they follow the expected trend in terms of shell thickness and detector threshold implies that they are not unrealistic and can be, at least qualitatively, used.

A further indication of how well Eqn. (4.34) describes the sensitivity of Transmission to $\sigma^1_{e\ell}$ can be acquired by examining the compatibility of Transmission changes between P_o, P_1 calculations as predicted by SWANLAKE and calculated from Eqn. (4.29). The same equation can also be used to study the variation of Transmission in terms of $\bar{\mu}_o$ for a given iron shell and detector which, of course, corresponds to different angular distributions of the elastically scattered neutrons.

Table 22 gives the percentage Transmission differences between P_1, P_o calculations estimated by both SWANLAKE and Eqn. (4.29). Figure 72 shows the dependence of T on $\bar{\mu}_o$, for some of the cases of Table 21. P_o Transmissions could not be calculated for the thickest iron shell (cases 6, 7 in Table 22) because the value of $\Sigma_{tr}x$, for these cases, was found out of the range over which P_m values are given in Figure 7. It is noticed in Table 22 that the B.B.C. method gives compatible results with SWANLAKE, at least as far as their variation in terms of detector threshold and shell thickness is concerned. The B.B.C. results in Table 22 tend to under-estimate the percentage Transmission differences as predicted by SWANLAKE for the ^{238}U and $^{237}N_p$ detectors and therefore, the $S_{L,1}$ sensitivities given in Table 21 are expected to do the same. However, the fact that the dependence of Transmission on $\bar{\mu}_o$ is linear, as seen in Figure 72 for all thicknesses and detectors, explains

TABLE 22. PERCENTAGE TRANSMISSION DIFFERENCES BETWEEN P_1, P_0 CALCULATIONS FOR VARIOUS IRON CASES.

	CASE		PERCENTAGE DIFFERENCES	
	DETECTOR	THICKNESS cm	B.B.C. METHOD	SWANLAKE
1	^{27}Al	1.90	- 4.97	- 5.07
2	^{238}U	1.90	- 2.01	- 2.42
3	^{237}Np	1.90	- 0.61	- 1.10
4	^{238}U	4.11	- 7.05	- 8.40
5	^{237}Np	4.11	- 2.58	- 3.91
6	^{238}U	9.16	— (- 17.90)	- 19.45
7	^{237}Np	9.16	— (- 6.51)	- 8.76

why the percentage differences in Transmissions between P_1, P_o calculations are about 100 times the corresponding $S_{L,1}$ sensitivities. The values for cases 6 and 7 in Table 22 (enclosed within parentheses) were found in this way.

From the analysis undertaken in this section it was accepted that one hundredth of the percentage change in Transmission between P_3 (essentially P_1) and P_o calculations given by SWANLAKE constitutes a good estimate of the sensitivity of Transmission to the 1^{st}-order expansion coefficient of the scattering kernel.

Since the anisotropy of the inelastic scattering is unimportant and a 1^{st}-order approximation is adequate for the elastic scattering, it is perceived that the sensitivity to the 1^{st} order expansion coefficient is sufficient in describing the effect on Transmission of uncertainties in the angular distribution and consequently energy distribution of neutrons scattered elastically and inelastically to different excited levels. (The energy distribution of inelastically scattered neutrons to different excited levels also depends on the energy level, and for scattering to continuum on the nuclear temperature and continuum threshold). The sensitivities to the 1^{st}-order expansion coefficient of the scattering kernel, so deduced, are found to be of about the same magnitude as the total sensitivities to elastic for the ^{238}U and $^{237}N_p$ detectors and twice as much for the $^{27}A\ell$ one, for all the iron shells. They are given together with the sensitivities to total and elastic in Table 23.

TABLE 23. SENSITIVITIES TO TOTAL, ELASTIC AND 1st ORDER EXPANSION COEFFICIENT FOR IRON SHELLS.

CASE	SHELL THICKNESS cm	TOTAL SENSITIVITIES											
		$^{27}Al(n, P)^{27}Mg$				$^{238}U(n, f)F.P.$				$^{237}Np(n, f)F.P.$			
		S_T	S_{EL}	$S_{L,1}$	$\frac{S_{L,1}}{S_T}$ %	S_T	S_{EL}	$S_{L,1}$	$\frac{S_{L,1}}{S_T}$ %	S_T	S_{EL}	$S_{L,1}$	$\frac{S_{L,1}}{S_T}$ %
1	1.90	-2.851 E-01	-2.502 E-02	5.070 E-02	17.7	-1.801 E-01	-2.743 E-02	2.420 E-02	13.4	-7.246 E-02	-8.950 E-03	1.100 E-02	15.2
2	4.11	-6.226 E-01	-6.794 E-02	1.660 E-01	26.6	-4.534 E-01	-9.150 E-02	8.400 E-02	18.5	-2.043 E-01	-3.698 E-02	3.910 E-02	19.1
3	9.16	-1.389 E+00	-1.705 E-01	3.940 E-01	28.3	-1.030 E+00	-2.417 E-01	1.945 E-01	18.8	-4.740 E-01	-1.186 E-01	8.760 E-02	18.4

4.4 SENSITIVITY OF TRANSMISSION TO DOSIMETRY CROSS-SECTIONS.

The sensitivity profiles of Transmission to dosimetry cross-sections can easily be obtained since the reaction rates depend linearly on the dosimetry data.

Specifically, the definition of the sensitivity profile, (Eqn.(4.3)):

$$P_{D,I} = \frac{\partial T}{\partial \sigma_{D,I}} \frac{\sigma_{D,I}}{T} \tag{4.35}$$

the definition of Transmission:

$$T = \frac{R'}{R} \tag{4.36}$$

and the expressions giving the reaction rates R', R with and without the presence of the material shell, respectively, in terms of the macroscopic dosimetry cross-section $\Sigma_{D,I}$ and the corresponding zone integrated scalar fluxes Φ'_I, Φ_I, viz:

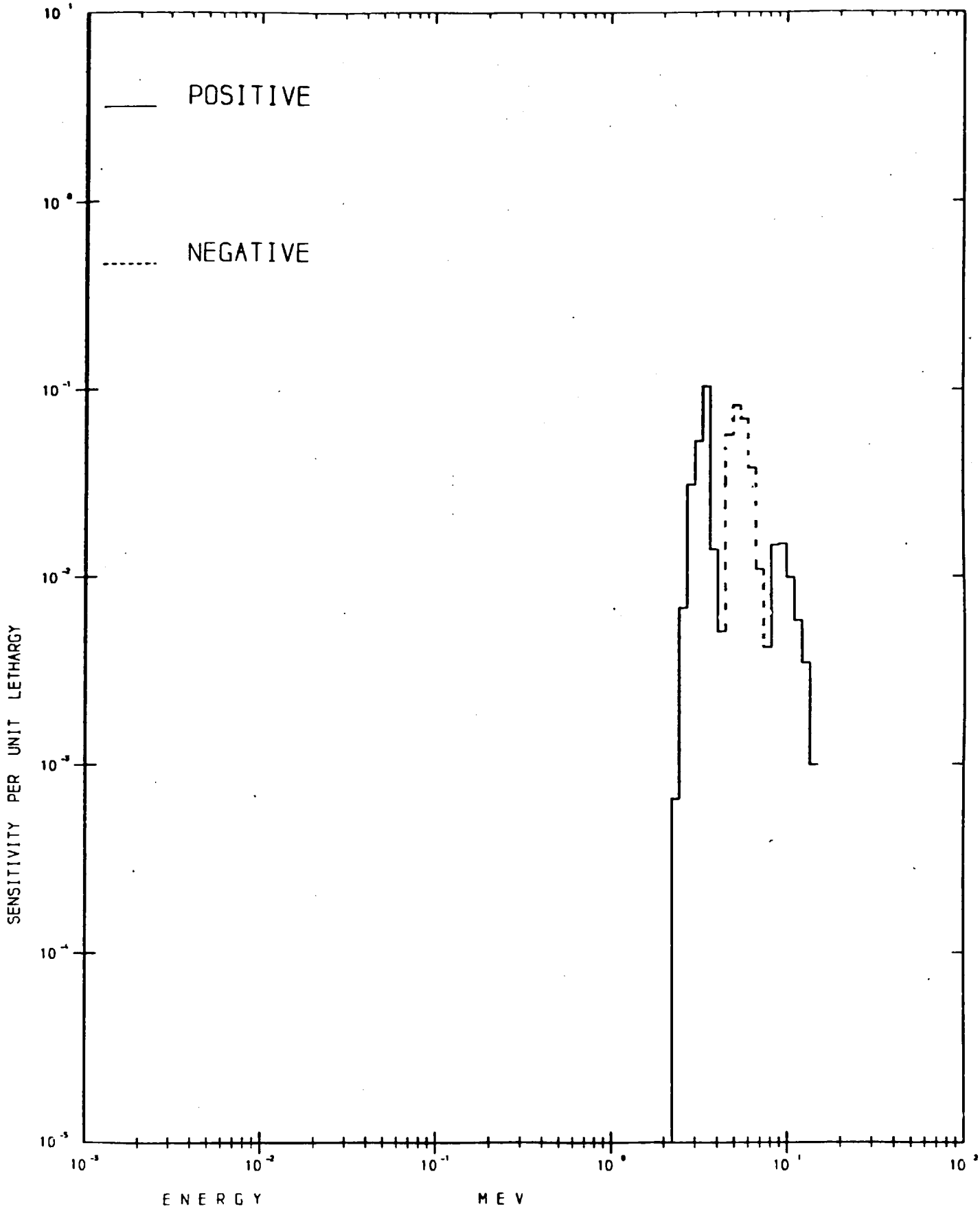
$$R' = \sum_{I=1}^{IGM} \Sigma_{D,I} \Phi'_I \tag{4.37}$$

$$R = \sum_{I=1}^{IGM} \Sigma_{D,I} \Phi_I \tag{4.38}$$

yield the following simple formula for $P_{D,I}$:

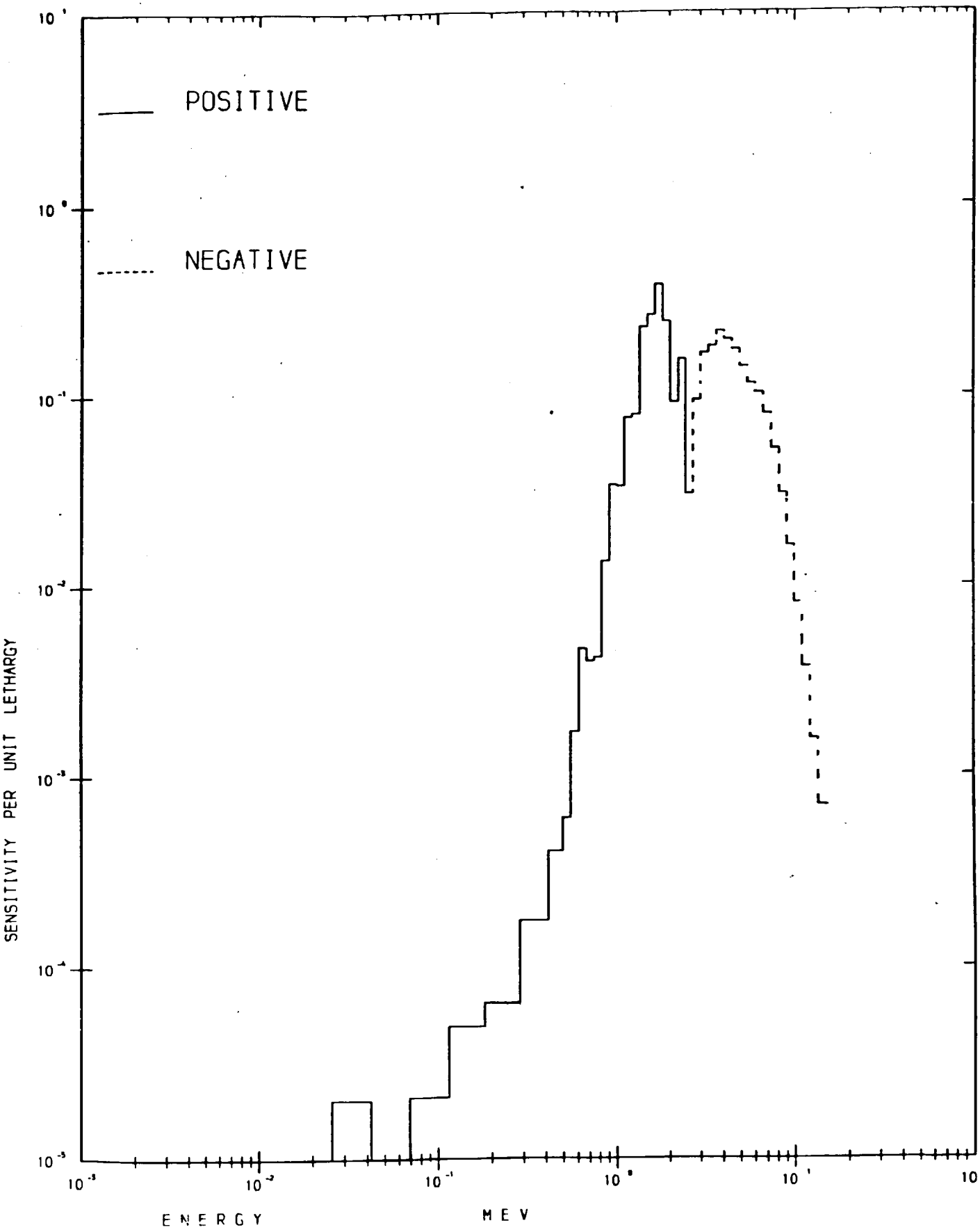
$$P_{D,I} = \Sigma_{D,I} \left(\frac{\Phi'_I}{R'} - \frac{\Phi_I}{R}\right) \tag{4.39}$$

Figures 73, 74 and 75 present the sensitivity profiles per unit lethargy, $\frac{P_{D,I}}{\Delta U_I}$, for the three threshold detectors and the thickest iron shell. We observe that positive and negative ranges are equally important as contrasted to sensitivity profiles to material cross-sections where the sensitivities were generally negative in the important energy regions. Also, higher dosimetry cross-sections imply according to Eqn. (4.39), larger sensitivity coefficients to dosimetry data while the opposite was valid for the sensitivity profiles to



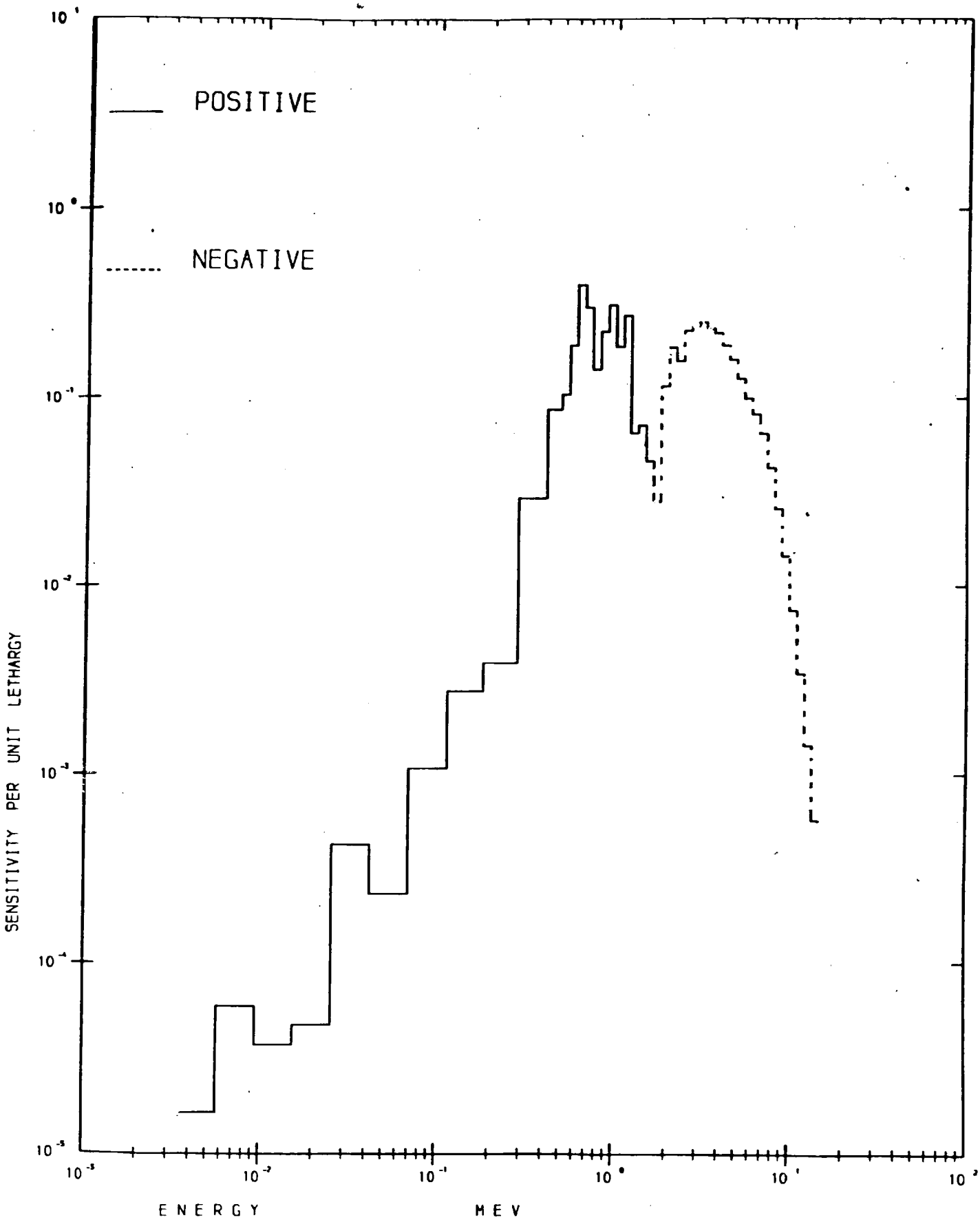
SENSITIVITY OF TRANSMISSION TO 27AL (N,P) 27MG DOSIMETRY DATA, THICKNESS = 9.16CM

FIGURE 73



SENSITIVITY OF TRANSMISSION TO 238U(N,F)F.P DOSIMETRY DATA, THICKNESS = 9=16CM

FIGURE 74



SENSITIVITY OF TRANSMISSION TO 237NP(N,F)F.P DOSIMETRY DATA. THICKNESS = 9=16CM

FIGURE 75

material cross-sections for reasons discussed in previous sections. In the high energy range where $\Phi'_I << \Phi_I$, $\Phi'_I/_{R'} < \Phi_I/_R$ holds for ^{238}U and $^{237}N_p$ detectors though R'< R. This explains why the sensitivities are negative at high energies, reach a minimum as Φ'_I approaches Φ_I, and then take positive values. For the $^{27}A\ell$ detector the relation R' < R prevails for fluxes at very high energies and therefore $\Phi'_I/_{R'} > \Phi_I/R$ in this energy range; this explains the positive values experienced in the sensitivity profile for the $^{27}A\ell(n,p)^{27}Mg$ reaction from 15.0MeV down to 8.0MeV.

The total sensitivity to dosimetry cross-section data is found to be:

$$S_D = \sum_{I=1}^{IGM} P_{D,I} = \sum_{I=1}^{IGM} \Sigma_{D,I} \left(\frac{\Phi'_I}{R'} - \frac{\Phi_I}{R}\right) = 0$$

This is as expected since, according to Eqns. (4.37) and (4.38), a 1% increase in all the dosimetry group constants implies the same percentage increase for both reaction rates and, consequently, it does not affect the Transmission. The above result also demonstrates that the condensation of the sensitivity information concerning a certain cross-section set to a single number, though it means what it represents, is not always a useful and sufficient measure of the dependence of a integral quantity on the cross-section set being investigated. In the case of material cross-sections the fact that we knew the sensitive energy region and that the sensitivity coefficients had the same sign allowed us to use the total sensitivity (in parallel with the sensitivity profiles) as a "sensitivity" measure for the cross-section set under discussion. Additionally, the sensitivity coefficient has the physical interpretation of determining the effect of the error accompanying a certain group constant on the uncertainty associated with the integral quantity; the total sensitivity hardly lends itself to such an inter-

pretation.

The total sensitivity to dosimetry cross-sections is zero for all the detectors and shell thicknesses. In contrast, the uncertainty of Transmission due to errors accompanying the dosimetry data is not zero, as will be seen in the following chapter.

Finally, it should be noted that in cases where the dosimetry reaction also describes part of the neutron interaction with the material shell, a term calculated via Eqn. (4.7) must be added to Eqn. (4.39). However in our case this problem does not arise and in most practical cases where it does this additional term is negligible compared to the contribution from Eqn. (4.39).

4.5 SENSITIVITY OF TRANSMISSION TO SOURCE SPECTRUM.

Although an analytical sensitivity function for the input source spectrum can, in principle, be derived according to the neutron transport equation, in the present work the sensitivity profile of Transmission to fission spectrum was calculated by simply applying small variations on its multi-group representation and recording the effect on the calculated Transmission.

We considered it unnecessary and expensive in computing time to maintain the fine 55-group structure in these calculations. A 1% increase was simultaneously applied to all group constants representing the fission spectrum within a certain energy range; the "sphere off" and "sphere on" reaction rates were then obtained from ANISN and the sensitivity coefficients and profiles per unit lethargy were subsequently estimated. This exercise was undertaken only for iron and for the medium thickness shell. The results are summarised in Table 24.

In Figures 76, 77 and 78 the sensitivity profiles of Transmission to fission spectrum are presented together with the sensitivity profiles to iron total cross-section and to dosimetry reaction for the three threshold detectors and for the shell of thickness 4.11 cm. According to these graphs the sensitivity to the fission spectrum is very small compared to the sensitivity to iron total cross-section, especially for the $^{27}A\ell(n,p)^{27}Mg$ detector; with respect to the sensitivity to dosimetry cross-sections the local minima presented by their sensitivity profiles form energy intervals where the sensitivity to the fission spectrum is much higher from that to dosimetry data and vice-versa. Nevertheless, it is clear from these graphs that the absolute sensitivity to dosimetry data is in general higher from that to fission spectrum, especially for the low threshold detector.

TABLE 24. SENSITIVITY OF TRANSMISSION TO FISSION SPECTRUM IRON SHELL OF THICKNESS 4.11 cm.

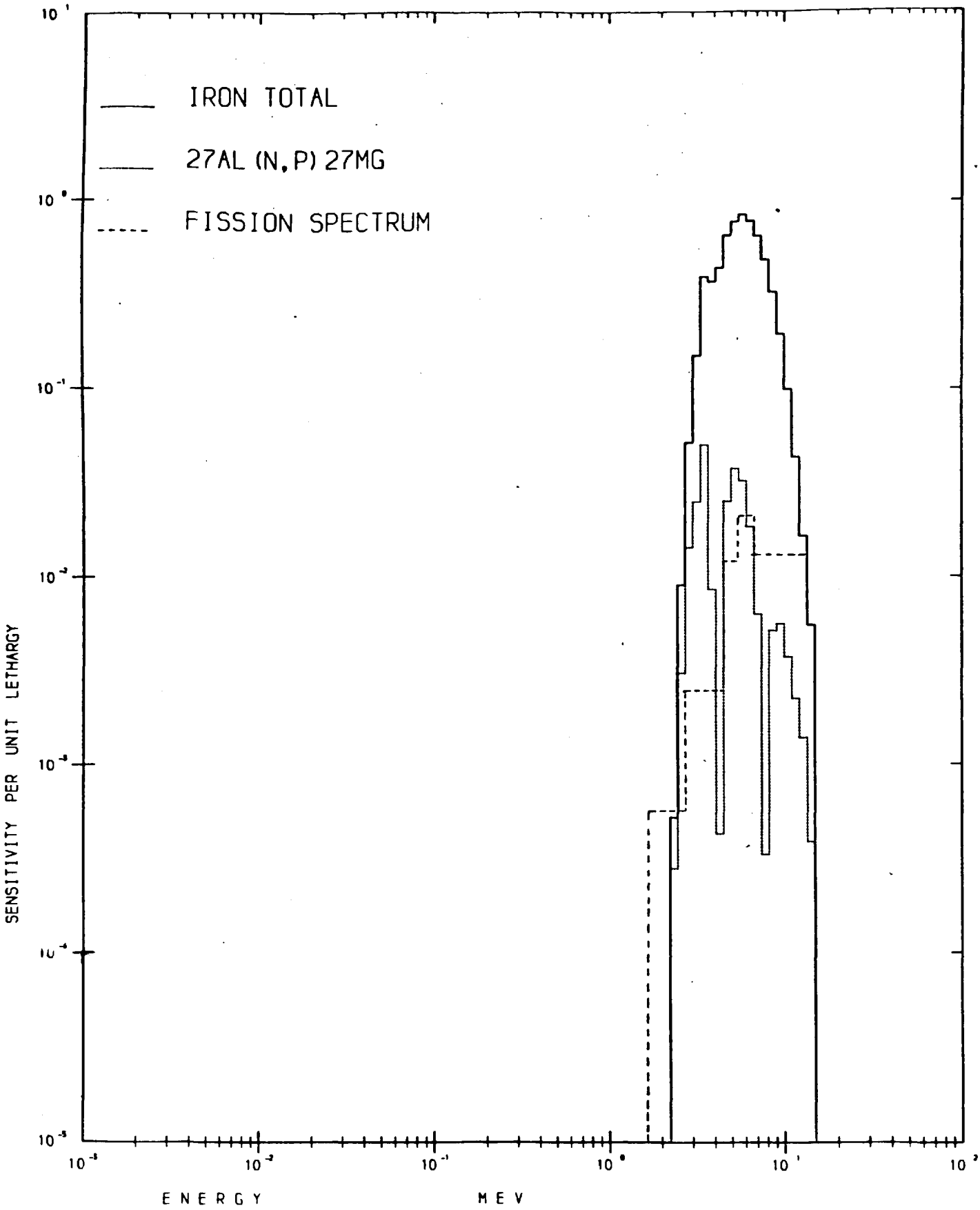
CASE	ENERGY RANGE MeV	ENERGY GROUPS INCLUDED	LETHARGY WIDTH	DETECTOR	REACTION RATES "ON"	REACTION RATES "OFF"	TRANSMISSION	SENSITIVITY COEFFICIENTS	SENSITIVITY PER UNIT LETHARGY
1	1.49 E+01 - 6.71 E+00	1-8	0.79	^{27}Al	2.83992 E-31	5.03985 E-31	0.563492	1.18 E-02	1.50 E-02
				^{238}U	2.54744 E-29	3.60870 E-29	0.705916	-1.84 E-03	-2.33 E-03
				^{237}Np	1.41198 E-28	1.61051 E-28	0.876728	-2.05 E-03	-2.60 E-03
2	6.71 E+00 - 4.96 E+00	9-11	0.30	^{27}Al	2.84076 E-31	5.04227 E-31	0.563389	-6.38 E-03	-2.10 E-02
				^{238}U	2.54771 E-29	3.60906 E-29	0.705920	-1.27 E-03	-4.20 E-03
				^{237}Np	1.41198 E-28	1.61047 E-28	0.876750	4.56 E-04	1.50 E-03
3	4.96 E+00 - 3.67 E+00	12-14	0.30	^{27}Al	2.83534 E-31	5.03254 E-31	0.563401	-4.25 E-03	-1.41 E-02
				^{238}U	2.54823 E-29	3.60998 E-29	0.705884	-6.37 E-03	-2.12 E-02
				^{237}Np	1.41204 E-28	1.61056 E-28	0.876738	-9.12 E-04	-3.04 E-03
4	3.67 E+00 - 2.46 E+00	15-18	0.40	^{27}Al	2.82935 E-31	5.02175 E-31	0.563419	-1.06 E-03	-2.65 E-03
				^{238}U	2.55073 E-29	3.61231 E-29	0.706121	2.72 E-02	6.79 E-02
				^{237}Np	1.41252 E-28	1.61100 E-28	0.876797	5.81 E-03	1.45 E-02

TABLE 24. Continued.

CASE	ENERGY RANGE MeV	ENERGY GROUPS INCLUDED	LETHARGY WIDTH	DETECTOR	REACTION RATES "ON"	REACTION RATES "OFF"	TRANSMISSION	SENSITIVITY COEFFICIENTS	SENSITIVITY PER UNIT LETHARGY
5	2.46 E+00 - 1.65 E+00	19-22	0.39	^{27}Al	2.82618 E-31	5.01606 E-31	0.563426	1.77 E-04	4.55 E-04
				^{238}U	2.54981 E-29	3.61233 E-29	0.705862	-9.49 E-03	-2.43 E-02
				^{237}Np	1.41253 E-28	1.61112 E-28	0.876799	6.04 E-03	1.55 E-02
6	1.65 E+00 - 1.10 E+00	23-26	0.40	^{27}Al	2.82666 E-31	5.01692 E-31	0.563425	0.0	0.0
				^{238}U	2.54453 E-29	3.60486 E-29	0.705861	-9.63 E-03	-2.40 E-02
				^{237}Np	1.41212 E-28	1.61086 E-28	0.876625	-1.38 E-02	-3.40 E-02
7	1.10 E+00 - 7.42 E-01	27-30	0.39	^{27}Al	2.82778 E-31	5.01890 E-31	0.563425	0.0	0.0
				^{238}U	2.54352 E-29	3.60306 E-29	0.705933	5.66 E-04	1.45 E-03
				^{237}Np	1.41195 E-28	1.61043 E-28	0.876753	7.98 E-04	2.04 E-03
8	7.42 E-01 - 4.97 E-01	31-34	0.40	^{27}Al	2.82881 E-31	5.02074 E-31	0.563425	0.0	0.0
				^{238}U	2.54432 E-29	3.60421 E-29	0.705930	1.41 E-04	3.54 E-04
				^{237}Np	1.41142 E-28	1.60981 E-28	0.876761	1.71 E-03	4.27 E-03

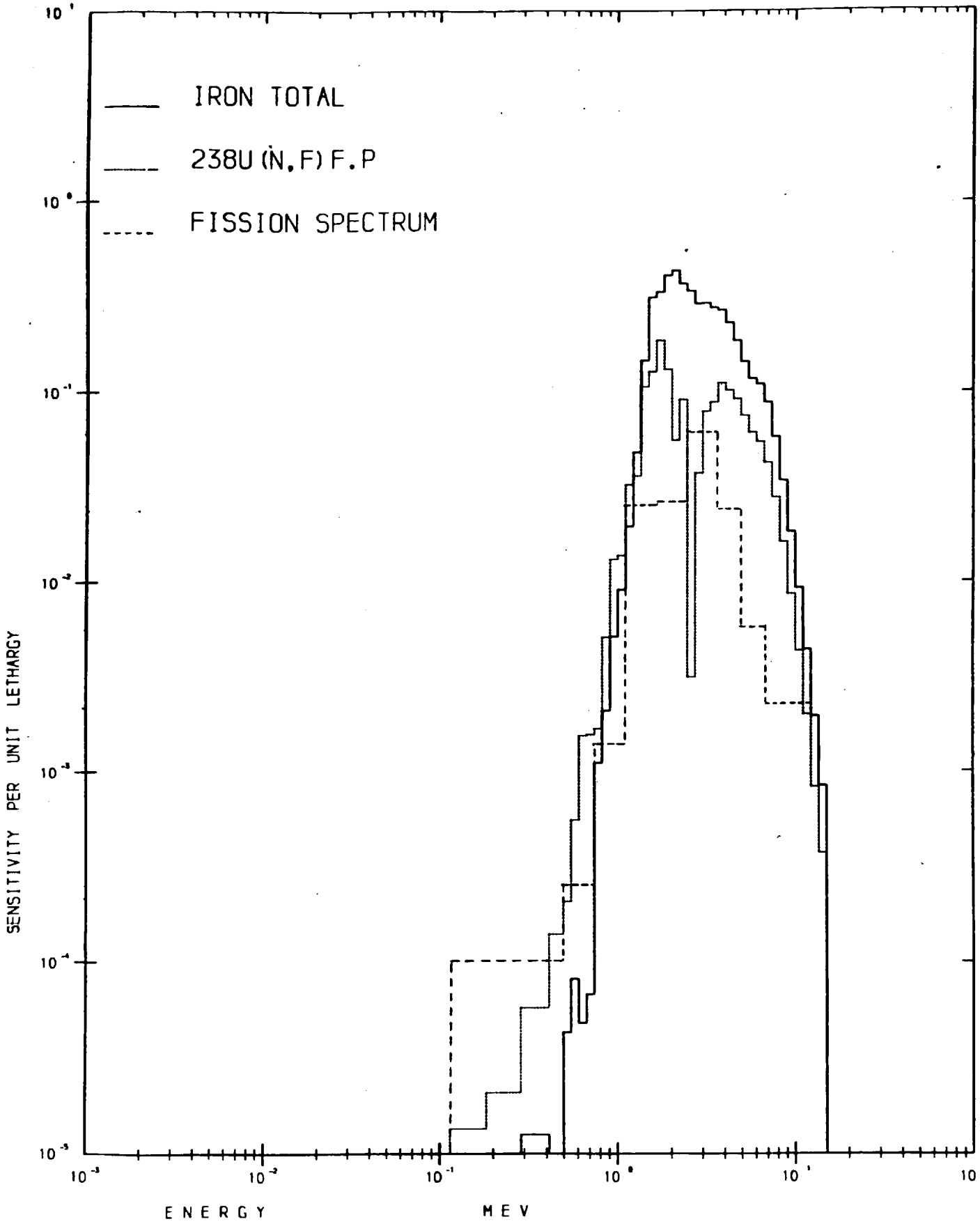
TABLE 24. Continued.

CASE	ENERGY RANGE MeV	ENERGY GROUPS INCLUDED	LETHARGY WIDTH	DETECTOR	REACTION RATES "ON"	REACTION RATES "OFF"	TRANSMISSION	SENSITIVITY COEFFICIENTS	SENSITIVITY PER UNIT LETHARGY
9	4.97 E-01 - 1.11 E-01	35-38	1.49	^{27}Al	2.82781 E-31	5.01896 E-31	0.563425	0.0	0.0
				^{238}U	2.54341 E-29	3.60292 E-29	0.705930	1.41 E-04	1.00 E-04
				^{237}Np	1.41028 E-28	1.60854 E-28	0.876745	-1.14 E-04	-7.65 E-05
10	1.11 E-01 - 1.00 E-10	39-55	20.1	^{27}Al	2.83090 E-31	5.02444 E-31	0.563425	0.0	0.0
				^{238}U	2.54618 E-29	3.60686 E-29	0.705929	0.0	0.0
				^{237}Np	1.41164 E-28	1.61009 E-28	0.876746	0.0	0.0
UNPERTURBED FISSION SPECTRUM				^{27}Al	2.83135 E-31	5.02524 E-31	0.563425	-	-
				^{238}U	2.54659 E-29	3.60743 E-29	6.705929	-	-
				^{237}Np	1.41186 E-28	1.61034 E-28	0.876746	-	-



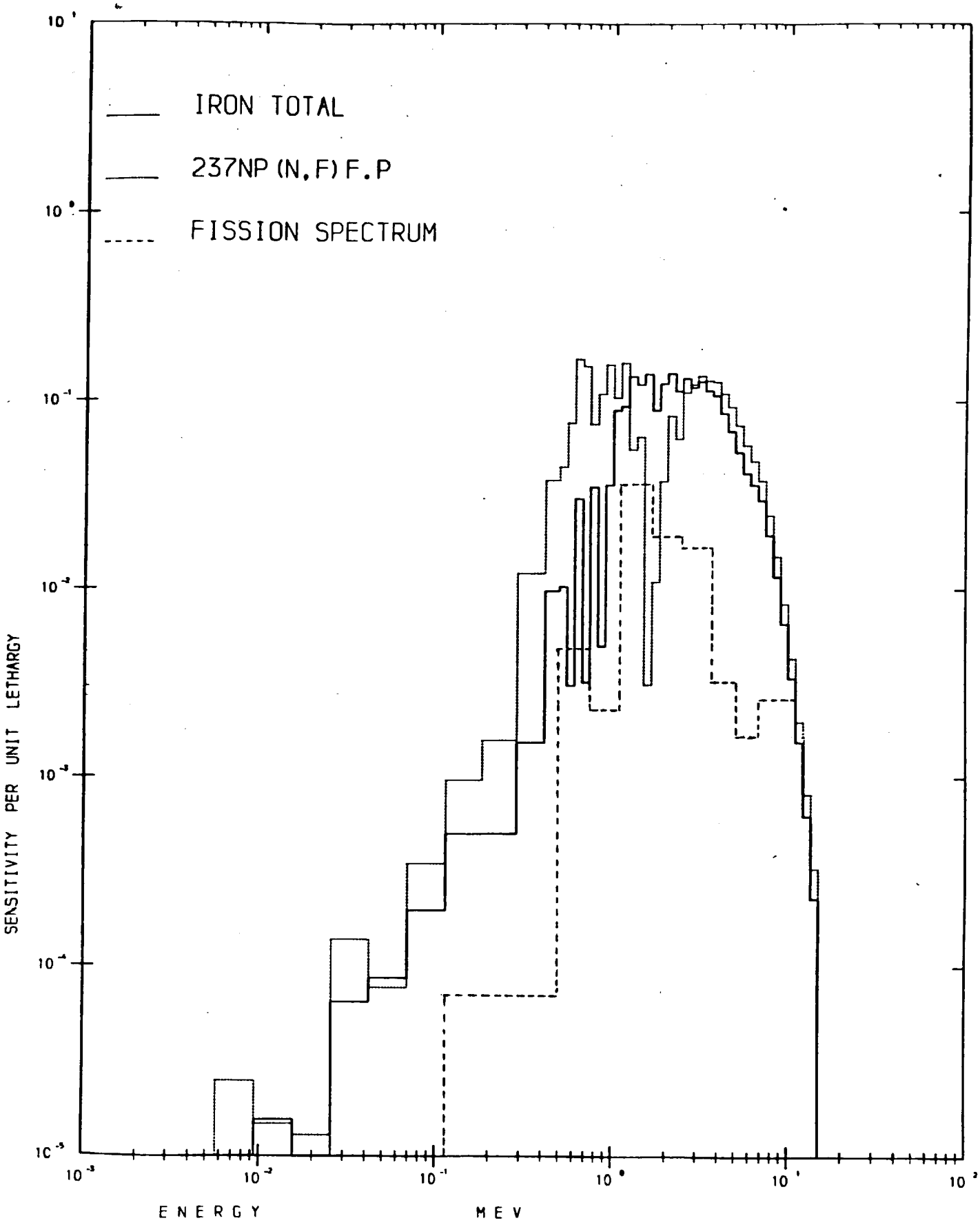
SENTIVITY OF TRANSMISSION TO VARIOUS INPUT DATA, IRON SHELL OF THICKNESS = 4.11 CM

FIGURE 76



SENSITIVITY OF TRANSMISSION TO VARIOUS INPUT DATA,
IRON SHELL OF THICKNESS = 4.11 CM

FIGURE 77



SENSITIVITY OF TRANSMISSION TO VARIOUS INPUT DATA, IRON SHELL OF THICKNESS = 4.11 CM

FIGURE 78

4.6 SUMMARY

Figures 76, 77 and 78 summarize the sensitivity results of Transmission to the three main categories of input data, namely, material cross-sections, dosimetry cross-sections and fission spectrum. For all the Transmissions the sensitivity to fission spectrum is very small over the whole sensitive energy range as compared with the sensitivity to total cross-section of the material of the shell. As far as the sensitivity to dosimetry cross-sections is concerned, for the $^{27}Al(n,p)^{27}Mg$ Transmissions this sensitivity is very small, for the $^{238}U(n,f)F.P$ ones cannot be neglected and for the $^{237}Np(n,f)F.P$ is of equal importance with that to material cross-sections.
The results and conclusions concerning the sharing of the sensitivity of the total cross-section amongst its partials and the effect of the angular anisotropy of elastic scattering on Transmission have been given in section 4.2.4 and therefore are not repeated here.
There are additional parameters and quantities on which the Transmission depends which have not been studied in this chapter. Such quantities are the energy levels and continuum threshold for inelastic scattering and parameters determining the energy distribution of inelastically scattered neutrons to continuum. The sensitivity of Transmission to these quantities is expected to be very low and this is the reason for avoiding their analysis.

It must be pointed out here that high sensitivity coefficients for a certain data set do not necessarily imply that large discrepancies between experimental and calculated Transmissions are due to inadequacies of the input data set in the sensitive energy region. It is possible for input data characterized by high sensitivity coefficients to have a minor contribution to both the uncertainty of the calculated integral quantity and the observed discrepancy between experimental and calculated

values; this is because they are meant to be known with high accuracy and vice-versa. Hence, in case that error information about the input data is unknown or unavailable the sensitivity profiles simply reveal which data sets and energy ranges are more likely to be responsible for the observed discrepancies.

If "error files" are available in a suitable form the contribution of each input data set to the total uncertainty accompanying the integral quantity can be estimated and the compatibility of the observed discrepancies with this uncertainty examined.

Furthermore an improvement of our knowledge about both certain data sets and the measured integral quantities can be attained by combining these two pieces of information. Both these important courses of further investigation, made possible by the existence of suitable multigroup error files for both the iron cross-sections and dosimetry data, are addressed, discussed and pursued in detail in the following chapters.

CHAPTER FIVE

UNCERTAINTY ANALYSIS OF CALCULATED TRANSMISSIONS

5.1 INTRODUCTION

Nuclear design calculations have always been limited in their accuracy by both computational methods and uncertainties in nuclear data. After a period of extensive refinements in calculational methods and computer codes, more emphasis in recent years has been directed toward improving nuclear data bases. Because quantitative and complete estimates of cross-section errors were not available in most cases, several ad hoc systems of nuclear design uncertainty analysis have evolved. One of the most fruitful for reactor core parameters has been the employment of integral experiments to measure directly such quantities as effective multiplication, central reactivity worths, etc., to compare with calculated results. However, the expense involved in such integral experiments normally precludes all but the most vital programmatic measurements.

Even when such experiments are available, the designer is faced with an indeterminate problem of attributing the errors in his analysis of the experiment to individual cross sections (assuming he is confident of the precision of his analytical tools).

An alternative approach to the problem of determining accuracy of design calculations greatly reduces the need for integral experiments. Although this approach, using results of sensitivity studies for the problem under consideration, never answers the absolute question of how computational results compare with experimental truth, it allows one to place quantitative error bands on these results. This method, called uncertainty analysis, does require that nuclear data errors are quantified and formatted to the best of the evaluator's ability, but in return it allows one to analyze errors in calculated design parameters which would

be extremely difficult and expensive to measure directly in any integral experiment.

A quantitative analysis of cross section uncertainties and their effects on design parameters has been possible since nuclear analysis was first attempted. In fact, there is a literature based upon direct recomputation with alternate data sets.
This approach can be characterized as one based upon "credibly deviant" cross section data sets, starting with some estimates of the probable range of values, either at the pointwise or multigroup stage of energy dependance.
However, such methods are limited in their information content, furnishing at best the magnitude of "typical" errors. But to make a truly quantitative estimate of cross-section errors, one must have considered in detail the variance of the cross-section data at all energies of interest. Just as importantly, one must consider correlations among energy bands and among partial cross sections.
When such detailed evaluations of cross-section errors have been performed, the next logical step is to format them in computer-accessible files, as has been done for a few reactor materials (34).
The versatile and powerful tools of generalized perturbation tneory can be used, as already has been demonstrated in the preceding chapter, to determine the sensitivity of design parameters to unit fractional changes in a cross-section and across a certain energy range.
The sensitivity profiles,so obtained,can then be combined with correlated error estimates, or covariances, to quantify the variance in integral design parameters.

Uncertainty analysis of calculated integral quantities in terms of the nuclear data used gives an estimate of the confidence which can be placed in such calculations provided that uncertainties caused by

the calculational method are considerably smaller than those attributable to data uncertainties.

Furthermore, uncertainty analysis can be used to identify areas of ill-defined data or those cross-sections which merit refinement, re-evaluation or remeasurement.

In these cases the measurement sensitivity coefficient, defined by: (35)

$$M^{R}_{x,I} \equiv \frac{\delta(\Delta R/R)}{(\Delta R/R)} \Big/ \frac{\delta(\Delta\sigma^{x}_{I}/\sigma^{x}_{I})}{(\Delta\sigma^{x}_{I}/\sigma^{x}_{I})} = \frac{\delta\Delta R}{\Delta R} \Big/ \frac{\delta\Delta\sigma^{x}_{I}}{\sigma^{x}_{I}}$$

(Here Δ stands for standard deviation since the symbol σ is used for the microscopic cross-section) gives directly the fractional improvement in total uncertainty estimate per unit fractional improvement in the relative accuracy of an item of data. This type of profile focusses the attention much more sharply than the conventional sensitivity profiles on areas of significant data weakness - its accurate calculation, however requires information on correlations between the group data. Also target accuracies for some important shielding or reactor core quantities can, through uncertainty analysis, establish accuracy requirements for nuclear data, after of course allowance for any other source of uncertainty (source data, modelling, approximations in the calculational method, conversion factors) has been made. Such a list of requirements for non-existent or improved nuclear data needed for nuclear energy programms is the WRENDA (36).

Finally in cases where experimental information concerning a certain integral calculated quantity exists, uncertainty analysis is used to examine the consistency of measured and calculated values; this process can, under the new name of consistency analysis, go further to the reconciliation of discrepant calculation and experiment for their mutual

benefit, and is analysed, documented and demonstrated in the following chapter.

A basic multigroup formulation of the uncertainty analysis problem follows and a simple equation giving the fractional uncertainty of the calculated integral quantity in terms of sensitivity profiles and appropriate covariance information is derived.

The sources of errors and correlations in the multigroup nuclear data are discussed next; a broad-group structure version of the derived uncertainty equation is given next compatible with the available multigroup covariance information, and the assumptions and approximations under which the results of the present analysis will be meaningful are clearly stated and assessed.

The chapter concludes with the uncertainties of the calculated Transmissions due to nuclear data used. A comparison with the uncertainty due to calculational procedure is also made and the effect of the partial and energy-dependent correlations on the calculated uncertainty is studied.

Finally the consistency between these uncertainties and the observed discrepancies of measured and calculated Transmissions is examined and the basis for a further consistency investigation is founded.

5.2 BASIC MULTIGROUP FORMULATION OF UNCERTAINTY ANALYSIS

In the following derivation of the uncertainty function the contributions from errors in modelling, in group-averaging of cross-sections or of other nuclear data parameters and in the implementation of the algorithm itself are not considered. Since a collective quantitative assessment of their magnitude has already been given in Chapter 3, it remains to be seen how this error is compared with that due to input data.

In accordance with the multigroup calculation of both Transmissions and sensitivity profiles, the various input data can adequately be represented by vector parameters $\vec{P}_k$ where the number of components for each of those vectors coincide with the number of energy groups, IGM, employed in the calculations, viz:

$$\vec{P}_k = (P_{k,1}, P_{k,2}, P_{k,3}, \ldots, P_{k,IGM})$$

The index k may refer to the multigroup representation of fission spectrum, to a certain reaction describing part of the neutron interaction with the material shells, to a dosimetry reaction or to a certain quantity describing the energy or angular distributions of secondary neutrons.

Our goal is to calculate the effect of a given nuclear data uncertainty $\delta P_{k,i}$ on Transmission; or in other words, to predict the uncertainty δT due to a given nuclear data uncertainty $\delta P_{k,i}$.

In the following we assume that first order perturbation theory is sufficiently accurate for our purposes.

Since

$$T = T(\vec{P}_k) \qquad k = 1.2 \ldots NOP$$

Where NOP = number of parameters, we can calculate any change in T due to small changes $\delta P_{k,i}$ in $P_{k,i}$ as:

$$\delta T \simeq \sum_{k=1}^{NOP} \sum_{i=1}^{IGM} \frac{\partial T}{\partial P_{k,i}} \delta P_{k,i} \qquad (5.1)$$

However, what we really want is the standard deviation of T derived from the statistical population of possible nuclear data parameter values, which is defined as the positive square root:

$$\Delta T = \sqrt{E\{(\delta T)^2\}} = \sqrt{var(T)} \qquad (5.2)$$

where var (T) denotes the variance of the calculated T. Var (T) is formally obtained as the expectation value of $(\delta T)^2$ and may be written as:

$$var(T) = E\left[(\delta T)^2\right] = E\left[\sum_{k,\ell}^{NOP} \sum_{i,j}^{IGM} \frac{\partial T}{\partial P_{k,i}} \frac{\partial T}{\partial P_{\ell,j}} \delta P_{k,i} \delta P_{\ell,j}\right] \qquad (5.3)$$

using Eqn. (5.1). Since $\partial T/\partial P_{k,i}$ and $\partial T/\partial P_{\ell,j}$ are constants over the considered statistical ensemble, we can rewrite Eqn. (5.3) as:

$$var\ (T) = \sum_{k,\ell}^{NOP} \sum_{i,j}^{IGM} \frac{\partial T}{\partial P_{k,i}} \frac{\partial T}{\partial P_{\ell,j}} E\ (\delta P_{k,i}\ \delta P_{\ell,j}) \qquad (5.4)$$

The expectation value of the product $\delta P_{k,i}\ \delta P_{\ell,j}$ is the definition of matrix element of the covariance matrix for the input data over a joint probability density function of $f(\vec{P})$ where $\vec{P} = (\vec{P}_1\ \vec{P}_2, \ldots \vec{P}_k, \vec{P}_{NOP})$, viz:

$$cov\ (P_{k,i},\ P_{\ell,j}) \equiv E\ (\delta P_{k,i}\ \delta P_{\ell,j}) =$$

$$= \int_{-\infty}^{+\infty} \int_{-\infty}^{+\infty} (P_{k,i} - \hat{P}_{k,i})\ (P_{\ell,j} - \hat{P}_{\ell,j})\ f\ (\vec{P}) \prod_{k=1}^{NOP} \prod_{i=1}^{IGM} d\ P_{k,i} \qquad (5.5)$$

where $\hat{P}_{k,i}$, $\hat{P}_{\ell,j}$ are the expectation values of $P_{k,i}$ and $P_{\ell,j}$, respectively.

Inserting this definition (Eqn (5.5)) into Eqn (5.4) we obtain our final result:

$$var(T) = \sum_{k,\ell}^{NOP} \sum_{i,j}^{IGM} \frac{\partial T}{\partial P_{k,i}} \frac{\partial T}{\partial P_{\ell,j}} cov\ (P_{k,i},\ P_{\ell,j}) \qquad (5.6)$$

A more rigorous and general definition of the concept of the covariance matrix of a certain number of continuous random variables $\vec{X}$ is given in Appendix B. We simply state here that the covariance in-

formation of the input data in a multigroup form comprises a (NOP x IGM) x (NOP x IGM) symmetric matrix which describes in an abstract but analytically manageable manner the uncertainties accompanying the input data and any inter-relationships (correlations) which exist between them. An outline of possible sources of both data uncertainties and their correlations is given in the following section.

The form of such a covariance matrix is shown in Figure 79. The matrix has been divided into square partitions, each corresponding to a certain combination of k,ℓ values. The partitions for which $k = \ell$ go along the main diagonal and attribute the uncertainties of the group parameters and the correlations between group constants of the same parameter, that is, the energy-dependent correlations. Indeed the diagonal elements of these partitions of the covariance matrix are the usual (uncorrelated) nuclear data uncertainties expressed as the variance of $P_{k,i}$

$$\underset{\substack{k=\ell \\ i=j}}{\text{cov}}\ (P_{k,i},P_{\ell,j}) = \text{cov}\ (P_{k,i},P_{k,i}) = \text{var}\ (P_{k,i}) = E\left[(\delta P_{k,i})^2\right] = (\Delta P_{k,i})^2$$

The off-diagonal partitions describe generally correlations between group constants of different parameters; they can arise in reality for a variety of reasons, they are known as partial correlations and may have either positive or negative values.

It is convenient and useful to work in terms of fractional quantities in our uncertainty studies. Eqn (5.6) can easily be transformed into a fractional form using Eqn (5.2), viz:

$$\left(\frac{\Delta T}{T}\right)^2 = \sum_{k,\ell}^{NOP} \sum_{i,j}^{IGM} \frac{\partial T}{\partial P_{k,i}} \frac{P_{k,i}}{T} \frac{\partial T}{\partial P_{\ell,j}} \frac{P_{\ell,j}}{T} \frac{\text{cov}\ (P_{k,i}, P_{\ell,j})}{P_{k,i}\ P_{\ell,j}}$$

or, in an abbreviated final form:

$$\left(\frac{\Delta T}{T}\right)^2 = \sum_{k,\ell}^{NOP} \sum_{i,j}^{IGM} U_{k,i}\ U_{\ell j} \frac{\text{cov}\ (P_{k,i},P_{\ell,j})}{P_{k,i}\ P_{\ell,j}} \qquad (5.7)$$

where:

$$U_{k,i} = \frac{\partial T}{\partial P_{k,i}} \frac{P_{k,i}}{T} \tag{5.8}$$

$$U_{\ell,j} = \frac{\partial T}{\partial P_{\ell,j}} \frac{P_{\ell,j}}{T} \tag{5.9}$$

Eqns (5.8) and (5.9) are the familiar sensitivity coefficients of Transmission to various input data, defined and studied in the previous chapter, at least for the most important input data.

It must be pointed out here that the quantities $P_{k,i}$, $P_{\ell,j}$ appearing in Eqn (5.7) are not meant to be random variables but their expectation values.

As will become clear in both Appendix B and following Chapter estimates of these values are usually used and at these estimates the constant, over the statistical ensemble, values of the fractional sensitivity coefficients (Eqns (5.8), and (5.9)) are calculated.

Eqn (5.7) shows that the only ingredients of an uncertainty analysis problem are the highly problem-dependent sensitivity coefficients and the problem-independent nuclear data error information in a suitable form. Although some satisfactory and relatively accurate techniques have been developed for obtaining the sensitivity profiles of an integral quantity to various input data, at least in the domain of 1st-order perturbation theory and for one-dimensional problems, the same can not be said for the status of the error information of the nuclear data.

Only recently the need for a detailed study of nuclear data uncertainties and correlations and their presentation in a form suitable for both uncertainty and consistency studies has been fully appreciated. A very brief description of the status of both the evaluated nuclear data files and their covariance information is given next.

5.3 SOURCES OF ERRORS AND CORRELATIONS IN NUCLEAR CROSS SECTION DATA

In the present section we shall be mainly concerned with the Evaluated Nuclear Data File (ENDF/B) because it represents today the most complete library of evaluated data for neutronics calculations and is widely used for many transport applications. Although primarily intended to be used in various neutronics calculations, the library aims at providing our best current knowledge of the microscopic data. The U K N D L data for iron, also used in the present work,is originating from this library.

5.3.1 ENDF Libraries

The process of analyzing experimentally measured cross-section data, combining it with the predictions from nuclear model calculations, and attempting to extract the true value of a cross-section is referred to as "evaluation". The parameterization and reduction of the data to a tabular form produces an evaluated data set.

The ENDF format was developed to store these evaluated data sets. This system comprises two libraries; the ENDF/A library acts as a storage for new data as they come in from various laboratories in an incomplete form. The ENDF/B system contains complete data sets for each material in a form more suitable for reactor calculations. Periodically, the ENDF/B tapes are updated and new information is taken from ENDF/A and transferred to ENDF/B.

The special formats and procedures by which the various nuclear data sets are represented in ENDF files are not discussed here. (see Ref. 37)

The evaluated data set for each material is divided into files. Each file contains data of a certain class as neutron cross-sections, resonance parameter data, angular and energy distributions of secondary neutrons, thermal neutron scattering law data, photon production cross-sections from both neutron and photon reactions, angular and energy distributions of these photons etc.

The transport codes that perform neutronic calculations require data libraries in various different forms and quite different from the ENDF/B library. Therefore, processing codes have been written which read the ENDF/B library as input and generate secondary cross-section libraries. These secondary libraries, in turn, are read as input into a spectrum-generating code, and generally broad group-averaged cross-sections are obtained for use in the neutronics calculations. Both DLC-37/D and DLC-37/F versions of the multigroup ANISN - formated library DLC-37/EPR were obtained from the version ENDF/B-IV of the ENDF library in this way, using selected modules from the AMPX modular code system.

5.3.2 Point Data Errors

Measured nuclear data are observables. The data given in a nuclear data file (the evaluated point data) represent single points extracted from a population of possible values. The uncertainties on the scalar cross-sections can arise either from uncertainties in the measurement of the cross-section itself or from uncertainties in the measurements of the composite cross-sections. For example

$$\text{var}\ (\sigma^{A}) = \text{var}\ (\sigma^{(n,a)}) + \text{var}\ (\sigma^{(n,p)}) + \text{var}\ (\sigma^{(n,a)}) + \text{etc.}$$

Using the limited population of measured data and the associated quoted experimental errors, the evaluator can select, using some statistical artifice, the best estimate of the cross-section and place upper and lower confidence bounds or quote a standard error on the value. This practice has been adopted by evaluators for some data files in ENDF/B-IV (viz C^{12}, O^{16} and N^{14}) and for many more in ENDF/B-V (38). In most cases the frequency distribution for the measurements is approximately normal.

In threshold regions, however, the frequency distribution is skew since cross-sections cannot be negative. In these cases, although the

confidence bound approach would be more meaningful, the evaluators of ENDF/B have chosen, for reasons of consistency, to replace the skew distribution with a normal distribution with the same mean and approximately the same shape.

5.3.3 Correlations Between Point Data

The simplest identifiable correlation is the partial correlation that exists between derived and measured cross sections at the same energy. Until recently,measurements of the elastic cross-section in all but the simplest nuclei have been fraught with difficulty, and evaluated data for elastic scattering has been inferred from measurements of the absorption,inelastic (or in some cases non-elastic) and total cross-sections. The elastic cross section is therefore a redundant piece of information which is positively correlated with the total cross-section and negatively correlated with the other partial cross-sections.

Cross-section measurements are frequently conducted over a range of energies and this can lead naturally to the appearance of an energy dependent correlation. In the simplest form it is inherent in the measurements by way of a systematic error common to all the measurements such as the uncertainties in the source intensity of an accelerator or the detection efficiency of a counter. A correlation which is energy-dependent can also arise from the frequently used technique of measuring cross-sections over a range of energies relative to the cross-section at some fixed energy Eo and then subsequently normalizing the data by an absolute measurement of the cross-section at Eo. Any later revision of the cross-section at Eo would cause the re-normalisation of the complete set of measurements. Another common experimental practice which leads to an energy-dependent correlation is the use of cross-section standards. In many cases accurate nuclear data can be obtained by measurement of a sample cross-section relative

to that of some well-defined standard such as ^{235}U (n,f), ^{10}B(n,a), H (n,p). The energy-dependent correlation, in this case also known as materials correlation, arises in that any revision of the standard cross-section naturally leads to a revision of the sample cross-sections.

The energy-dependent correlation is not merely a trait of measured data; it can also be introduced in the evaluation process. For instance,in energy regions where the physics is well understood and suitable theories exist, nuclear models are often fitted to the measurement and to the evaluated data calculated from the model. The uncertainties in the model parameters can introduce an energy-dependent correlation in the evaluated data. Models frequently used in nuclear data evaluation include the optical potential, the Breit-Wigner resonance approximation, R-matrix theory and the Weiskopf evaporation model. The energy-dependent correlation is usually positive, although in fitting resonances positive or negative correlations can exist.

The evaluator not only uses nuclear theory to fit measured data in areas with good measurement coverage; it can also be used to interpolate data in sparsely measured energy regions and to extrapolate to energies above the measured data. For example,there are very few neutron sources capable of providing sufficient flux in the energy range 8 to 14 MeV for cross-section determination; nuclear data in this region has often to be evaluated by nuclear model fitting or by graphical interpolation. If subsequently one of the end point of the fit is re-assessed,the indermidiate data will be perturbed by an amount dependent upon the energy displacement from the end point.

5.3.4 Group Processing Errors

Nuclear data in an evaluated data file can only be used in transport calculations by sophisticated point energy Monte Carlo and discrete ordinates codes, as has already been demonstrated. For more routine methods of solution, group averaging of the data is necessary. The errors that arise in the processing of nuclear data into multi-

group format derive either from the use of an inappropriate weighting function or the choice of an unsuitable fitting algorithm.

The appropriate weighting function for nuclear data is the point angular differential energy flux. (see Eqns (3.6) and (3.7), page 75). Since this is the quantity desired from the solution of the transport equation, or at least some discrete representation of it, an approximation to the flux, usually called the weighting spectrum is required for group collapsing. The weighting function is usually a simple function of energy, which is isotropic and spatially independent. Two common global weighting spectra are the Fermi slowing down spectrum used for thin media and the narrow resonance weighting function used for deep penetration.

However these weighting spectra are only approximations and although in smooth regions of the cross-section the errors are small, for regions containing resonances, thresholds or interference minima the errors can be large, especially if the group width is not sufficiently small for either the group collapsing to be independent of the chosen spectrum or the selected global weighting spectrum to be a good approximation of the scalar flux.

At present no suitable method appears to be available for quantifying both the magnitude and the distribution of the uncertainty introduced into the group cross-section data by the choice of an inappropriate weighting function.

In summary therefore, nuclear data errors can arise from a multiplicity of sources which include the process of measurement, the fitting of nuclear models or evaluator's eye-guides for the purposes of extrapolation or interpolation and from the multi-group averaging of the data so necessary for rapid solution of the transport equation. The measurement uncertainties and the correlations introduced by nature of the experiment and by evaluation can in general be assessed in the strictest statistical sense, but the errors injected by data processing

cannot, as yet, be suitably quantified.

5.3.5 Evaluated Data Covariance Files

The construction of a covariance matrix based upon all the possible sources of uncertainties and correlations outlined in the preceding section is a nice admixture of science, art and insight and of course lies beyond the scope of this thesis.

We shall strictly place outselves as users of a covariance matrix which in its final form, comprises elements describing the covariance of cross-section A at energy E_1 and cross-section B at energy E_2. A and B may refer to the same cross-section (energy-dependent covariance) and E_1, E_2 may represent the same energy value (variance of a certain cross-section at a given energy). It should be noted here that two important classes of nuclear data viz. energy distributions and angular distributions of secondary neutrons are, as yet, not accompanied by proper and trustworthy covariance information, suitable for practical applications (uncertainty and consistency studies).

Covariance files for neutron cross-sections and resonance parameters are incorporated in the latest version of ENDF/B-V under special formats and procedures which are discussed in Ref 38.

However this covariance information is usually required in a multigroup form, as has already been demonstrated. Only recently have standard formats and procedures been established within the ENDF/B system for the processing of evaluated and correlated energy-dependent uncertainty information into a multigroup covariance matrix formulation (34). Unfortunately, multigroup covariance matrices in very broad energy group structures and for very few reactions are only available from ENDF/B file, for a limited number of materials. This broad group scheme together with their condensed structure impose some severe limitations on both uncertainty and consistency analysis of the calculated Transmissions which, as will be seen in following chapters, have a crucial impact on the correctness and acceptability of the final results

and conclusions.

By their very nature the ENDF/B covariance files in either "pointwise" or multigroup form contain approximate quantities whose magnitudes, even under the best of circumstances, are not known better than about 30%, the distribution law was assumed to be normal and the evaluated data files contain the mean value of the distribution. The above remarks will be very useful in the subsequent manipulation of both ENDF/B data and covariance files.

An independent source of multigroup covariance information which is also used in the present work are Orphan's multigroup covariance matrices for the partial cross-sections of some nuclei (39).

These covariance matrices were constructed on the basis of conservative error assignments and fitting of correlations functions to the data; their advantages are the very fine group structure employed and that various reaction types are represented separately; as drawbacks we can quote the fact that they lack the statistical rigor of ENDF/B evaluations, partial correlations between different reactions are not considered and that they only cover the energy range from 2.0 to 14.9 MeV.

Concluding this section we note that the energy-dependent covariance matrix of a certain cross-section describes in an abstract but analytically manageable and practically valuable manner how well this cross-section set is meant to be known; the higher the rank of the matrix and the smaller the absolute values of its elements the better the cross-section is known. The partial covariance matrices between different cross-sections show how their uncertainties are correlated over the whole energy range and are needed in problems where both these cross-sections appear (see Figure 79).

The covariance matrices were established to permit systematic sensitivity investigations, to propagate uncertainties in radiation transport

calculations and thereby to determine, in a credible fashion, what cross-section measurements, evaluations, or processing methods most need further refinement for specific applications. Moreover the existence of high quality covariance information permits the use of well-defined and accurately measured "benckmark" experiments in improving our knowledge about basic nuclear data.

A great deal of work lies ahead in improving existing or acquiring new uncertainty information about cross-sections or other classes of basic nuclear data, and in processing it in a form suitable for practical applications.

5.4 UNCERTAINTY ANALYSIS OF CALCULATED TRANSMISSIONS

The uncertainty Equation (5.7) can be applied to any nuclear design problem and is sufficiently accurate in the domain of 1st-order perturbation theory, provided that the necessary sensitivity and input data uncertainty information is available in the required multigroup form.

In the uncertainty analysis of Transmissions apart from the fission spectrum and dosimetry cross-sections, a list of parameters adequately describing the material cross-section data could be the following: scalar cross-sections for absorption, elastic scattering, inelastic scattering to different excited levels and to continuum; energy levels and continuum threshold; nuclear temperature determining the energy distribution of secondary neutrons from the continuum; Legendre coefficients describing the angular distributions of elastically and inelastically scattered neutrons.

Hence a proper and trustworthy uncertainty analysis of Transmissions would require sensitivity and uncertainty information in the multigroup structure used for all these parameters.

5.4.1 Status of the Uncertainty Information of Input Data.

As far as the uncertainty information of the input data is concerned what are at present available are broad-group structure covariance matrices for elastic and non-elastic cross-sections of iron, a multigroup covariance matrix of the $^{238}U(n,f)$ F.P reaction in a broad 6-group scheme and a multigroup covariance matrix for the $^{27}A\ell(n,P)^{27}$ Mg reaction in the group structure used in the calculations and covering the energy range 2 to 15 MeV.

The uncertainty information for iron and for the $^{238}U(n,f)$F.P reaction was taken from the ORNL-5318 report (34). These covariance matrices were obtained from ENDF/B "pointwise" uncertainty files using 1/E and the fission spectrum as weighting functions, respectively.

The $^{27}A\ell(n,P)^{27}Mg$ covariance matrix was extracted from ORPHAN'S compilation. Although more reactions and materials from those investigated in the present study are included in this compilation than in the ORNL-5318 report, the fact that it does not cover the whole sensitive energy range for all the detectors renders it rather inappropriate.

The covariance matrices for the reactions mentioned above are given in Tables 25, 26, 27, 28 and 29 in a fractional form as required by Eqn (5.7), together with the group boundaries.

In the ORNL-5318 report the multigroup covariance matrices were given in terms of relative standard deviations and correlation matrices. The re-construction of the relative covariance matrices as given in the above Tables was accomplished via the relation:

$$\frac{cov(P_i,P_j)}{P_iP_j} = \frac{\Delta P_i}{P_i} \frac{\Delta P_j}{P_j} r_{ij} \qquad (5.10)$$

where $\Delta P_i/P_j, \Delta P_j/P_j$ are the relative standard deviations of group cross-sections P_i, P_j, respectively and r_{ij} the corresponding correlation coefficient.

Comparing the uncertainty information available with that required according to the number of parameters involved and leaving aside additional difficulties concerning the sensitivity determination for some of these parameters, it is realized that our uncertainty analysis could easily be considered a piece of art rather than a well defined, thoroughly scientific investigation.

However, this strictly judged and pessimistic view can be rebuffed with some arguments drawn from both the sensitivity analysis of Transmissions and general considerations which indicate that the proposed uncertainty analysis is worth considering and that it can give very useful and reliable results. The most important of these arguments are:

TABLE 25. RELATIVE MULTIGROUP COVARIANCE MATRIX OF ELASTIC CROSS SECTION FOR IRON. (FROM ORNL-5138 REPORT, 1/E WEIGHTING)

BROAD GROUP BOUNDARIES (MeV)		ELASTIC								
	GROUP	1	2	3	4	5	6	7	8	9
1.492 E+01 - 4.400 E+00	1	1.440 E-02	2.382 E-04	6.185 E-05	0	0	0	0	0	0
4.400 E+00 - 2.600 E+00	2		8.649 E-03	2.245 E-03	0	0	0	0	0	0
2.600 E+00 - 1.350 E+00	3			1.521 E-03	1.312 E-04	0	0	0	0	0
1.350 E+00 - 7.080 E-01	4				3.246 E-04	2.213 E-04	0	0	0	0
7.030 E-01 - 5.800 E-01	5					6.760 E-04	9.724 E-05	0	0	0
5.800 E-01 - 4.100 E-01	6						4.840 E-04	3.009 E-04	2.210 E-05	0
4.100 E-01 - 3.095 E-01	7							9.000 E-04	6.636 E-05	0
3.095 E-01 - 2.620 E-01	8								7.840 E-04	1.545 E-05
2.620 E-01 - 6.200 E-02	9									1.440 E-04

ELASTIC

TABLE 26. RELATIVE MULTIGROUP COVARIANCE MATRIX OF NON-ELASTIC CROSS SECTION FOR IRON (FROM ORNL-5318 REPORT, 1/E WEIGHTING).

NON-ELASTIC	GROUP	1	2	3	4	5	6	7	8	9
	1	1.988 E-02	4.371 E-04	1.893 E-04	0	0	0	0	0	0
	2		2.402 E-02	1.034 E-02	0	0	0	0	0	0
	3			6.241 E-03	1.493 E-03	0	0	0	0	0
	4				3.364 E-03	2.204 E-04	1.628 E-04	0	0	0
	5					4.000 E-02	2.935 E-02	0	0	0
	6						2.433 E-02	1.054 E-02	1.054 E-02	4.745 E-03
	7							4.000 E-02	4.000 E-02	1.796 E-02
	8								4.000 E-02	1.796 E-02
	9									1.690 E-02

TABLE 27. RELATIVE MULTIGROUP COVARIANCE MATRIX OF ELASTIC TO NON-ELASTIC CROSS SECTION FOR IRON (FROM ORNL-5318 REPORT, 1/E WEIGHTING).

		NON-ELASTIC								
ELASTIC	GROUP	1	2	3	4	5	6	7	8	9
	1	-1.684 E-02	-3.403 E-04	-1.252 E-04	0	0	0	0	0	0
	2	-2.262 E-04	-1.326 E-02	-4.856 E-03	0	0	0	0	0	0
	3	-8.798 E-04	-4.696 E-03	-2.409 E-03	-2.442 E-04	0	0	0	0	0
	4			-3.626 E-04	-3.466 E-04	0	0	0	0	0
	5				-9.048 E-06	-9.360 E-05	-3.650 E-05	0	0	0
	6				-7.656 E-06	-7.480 E-05	-3.432 E-05	-1.320 E-05	-2.200 E-05	-1.114 E-05
	7						-1.404 E-05	-5.400 E-05	-8.400 E-05	-4.290 E-05
	8						-1.310 E-05	-5.040 E-05	-7.840 E-05	-4.000 E-05
	9						-3.744 E-06	-1.440 E-05	-2.440 E-05	-2.652 E-05

TABLE 28. RELATIVE MULTIGROUP COVARIANCE MATRIX FOR $^{238}U(n, f)F.P.$ REACTION (FROM ORNL-5318 REPORT, FISSION SPECTRUM WEIGHTING).

BROAD GROUP BOUNDARIES (MeV)	$^{238}U(n, f)F.P.$ REACTION	$^{238}U(n, f)F.P.$ REACTION					
	GROUP	1	2	3	4	5	6
2.00 E+01 - 3.679 E+00	1	9.610 E-04	4.200 E-04	2.192 E-04	5.093 E-05	-4.836 E-06	0
3.679 E+00 - 1.353 E+00	2		6.250 E-04	4.036 E-04	1.867 E-04	6.240 E-05	0
1.353 E+00 - 4.979 E-01	3			6.760 E-04	2.837 E-04	8.112 E-05	0
4.979 E-01 - 1.832 E-01	4				9.610 E-04	1.148 E-03	2.320 E-04
1.832 E-01 - 4.087 E-02	5					6.084 E-03	6.683 E-04
4.087 E-02 - 1.000 E-11	6						1.147 E+00

TABLE 29. RELATIVE MULTIGROUP COVARIANCE MATRIX FOR $^{27}Al(n, P)^{27}Mg$ REACTION (FROM ORPHAN'S COMPILATION).

GROUP BOUNDARIES (MeV)	$^{27}Al(n, P)^{27}Mg$ REACTION	$^{27}Al(n, P)^{27}Mg$ REACTION																				
	GROUP	1	2	3	4	5	6	7	8	9	10	11	12	13	14	15	16	17	18	19	20
1.49 E+01 - 1.34 E+01	1	1.00 E-02	0	0	0	0	0	0	0	0	0	0	0	0	0	0	0	0	0	0	0
1.34 E+01 - 1.22 E+01	2		1.00 E-02	2.50 E-03	9.00 E-04	3.00 E-04	1.00 E-04	0	0	0	0	0	0	0	0	0	0	0	0	0	0
1.22 E+01 - 1.10 E+01	3			1.00 E-02	3.30 E-03	1.20 E-03	5.00 E-04	0	0	0	0	0	0	0	0	0	0	0	0	0	0
1.10 E+01 - 1.00 E+01	4				1.00 E-02	3.70 E-03	1.50 E-03	0	0	0	0	0	0	0	0	0	0	0	0	0	0
1.00 E+01 - 9.04 E+00	5					1.00 E-02	4.10 E-03	0	0	0	0	0	0	0	0	0	0	0	0	0	0
9.04 E+00 - 8.18 E+00	6						1.00 E-02	0	0	0	0	0	0	0	0	0	0	0	0	0	0
8.18 E+00 - 7.40 E+00	7							1.00 E-02	5.80 E-03	3.70 E-03	2.60 E-03	1.90 E-03	1.50 E-03	1.30 E-03	1.10 E-03	9.00 E-04	8.00 E-04	7.00 E-04	1.90 E-03	1.60 E-03	1.30 E-03
7.40 E+00 - 6.70 E+00	8								1.00 E-02	7.00 E-03	5.30 E-03	4.10 E-03	3.60 E-03	3.20 E-03	2.90 E-03	2.60 E-03	2.30 E-03	2.10 E-03	6.00 E-03	5.30 E-03	4.70 E-03
6.70 E+00 - 6.06 E+00	9									1.00 E-02	6.50 E-03	5.90 E-03	5.20 E-03	4.60 E-03	4.20 E-03	3.80 E-03	3.40 E-03	3.10 E-03	9.10 E-03	8.00 E-03	7.10 E-03
6.06 E+00 - 5.48 E+00	10										1.00 E-02	7.80 E-03	7.00 E-03	6.20 E-03	5.60 E-03	5.10 E-03	4.60 E-03	4.30 E-03	1.25 E-02	1.11 E-02	9.90 E-03
5.48 E+00 - 4.96 E+00	11											1.00 E-02	8.90 E-03	8.00 E-03	7.20 E-03	6.60 E-03	6.00 E-03	5.50 E-03	1.62 E-02	1.44 E-02	1.29 E-02
4.96 E+00 - 4.49 E+00	12												1.21 E-02	1.09 E-02	9.80 E-03	9.00 E-03	8.20 E-03	7.60 E-03	2.23 E-02	1.99 E-02	1.78 E-02
4.49 E+00 - 4.06 E+00	13													1.42 E-02	1.28 E-02	1.17 E-02	1.07 E-02	9.90 E-03	2.93 E-02	2.61 E-02	2.35 E-02
4.06 E+00 - 3.67 E+00	14														1.62 E-02	1.48 E-02	1.36 E-02	1.26 E-02	3.72 E-02	3.32 E-02	2.99 E-02
3.67 E+00 - 3.32 E+00	15															1.83 E-02	1.68 E-02	1.56 E-02	4.60 E-02	4.12 E-02	3.71 E-02
3.32 E+00 - 3.01 E+00	16																2.04 E-02	1.89 E-02	5.58 E-02	5.00 E-02	4.50 E-02
3.01 E+00 - 2.72 E+00	17																	2.25 E-02	6.66 E-02	5.97 E-02	5.38 E-02
2.72 E+00 - 2.46 E+00	18																		2.50 E-01	2.24 E-01	2.04 E-01
2.46 E+00 - 2.23 E+00	19																			2.50 E-01	2.25 E-01
2.23 E+00 - 2.01 E+00	20																				2.50 E-01

1. The sensitivity of Transmission to thermal fission spectrum has been found to be very small compared to the sensitivity to total iron cross-section for all the detectors, and generally smaller than that to dosimetry data. (See Figures 76, 77 and 78).

Bearing in mind that this spectrum is at present meant to be known not less than the iron cross-section data, it is understood that the uncertainty of Transmission originated in fission spectrum errors can be considered as negligibly small[1].

2. The Transmissions have been found to be insensitive to the angular ansisotropy of the inelastically scattered neutrons.

3. The excited energy levels and continuum threshold of inelastic scattering are usually better known than the cross-sections for different reactions.

4. Uncertainties in the energy distribution of inelastically scattered neutrons to continuum are expected to affect mainly the $^{27}Al(n,p)^{27}Mg$ Transmission (see Figures 60, 61 and 62). Only one experimental value exists for this detector corresponding to the thinest shell; consequently this sort of uncertainty becomes unimportant at least in examining the consistency of measured and calculated values.

5. The fact that the sensitivity of Transmission to the 1st order expansion coefficient of the scattering kernel for elastic scattering is of the same order of magnitude as that to elastic cross-section must also be taken into consideration.

Moreover the ENDF/B-IV nuclear data for iron has been evaluated according

---

1. Watt's formula:

$$\phi(E) = 0.453 \exp(-AE)\sinh\sqrt{BE}$$

with
$$A = 1.0123 \pm 0.0111 \text{ MeV}^{-1}$$
$$B = 2.1893 \pm 0.1552 \text{ MeV}^{-1}$$

used in uncertainty calculations for the fission spectrum gave fractional errors of 10-20% in the sensitive energy region (40).

to new experimental information concerning the angular and energy distributions of secondary neutrons.

6. Elastic and non-elastic cross-sections undergo two types of neutron interaction which are distinguished as far as the detection of a neutron in the B.B.C. experiments is concerned. This happens because the majority of non-elastic collisions render the neutrons undetectable while the opposite is valid for the elastic scattering. Hence the fact that these two basic modes of neutron interaction are treated separately in the uncertainty information available reinforces its suitability in our analysis (for example, it would be unwise to undertake the uncertainty analysis in terms of only the total iron cross-section for which covariance information is also included in the same report).

In the light of the above arguments it is perceived that (a) undertaking the uncertainty analysis in terms of only material and dosimetry cross-sections is a good approximation and (b) the covariance information available, condensed for both reaction-type and energy resolution, does not allow the full exploitation of the detailed sensitivity wealth calculated in the previous chapter, but still permits a meaningful and useful uncertainty calculation. An independent and appropriate yardstick against which all the above reasoning can be assessed will be the degree of consistency between calculated uncertainties in Transmissions and the observed discrepancies of experimental and calculated values.

5.4.2 Uncertainty Analysis Results

Broad group formulation

The uncertainty Equation (5.7) can be written in a matrix form as:

$$\left(\frac{\Delta T}{T}\right)^2 = U^T C U \qquad (5.11)$$

where: U is a vector comprising NOP x IGM fractional sensitivity components, viz

$$U = \begin{bmatrix} \vec{U}_1 \\ \vec{U}_2 \\ \vdots \\ \vec{U}_{NOP} \end{bmatrix} = \begin{bmatrix} U_{1,1} \\ U_{2,2} \\ \vdots \\ U_{1,IGM} \\ U_{2,1} \\ U_{2,2} \\ \vdots \\ U_{2,IGM} \\ \vdots \\ U_{NOP,1} \\ U_{NOP,2} \\ U_{NOP,IGM} \end{bmatrix}$$

and C is a (NOP x IGM) x (NOP x IGM) symmetric matrix comprising the multigroup covariance information of the input data, viz:

$$C = (C_{k,\ell,i,j}) \qquad k,\ell = 1,2 \ldots\ NOP \qquad i,j = 1,2 \ldots\ IGM$$

A pictorial view of Eqn (5.11) is given in Figure 79, with NOP = 3 and IGM = 4.

In accordance with the analysis in the previous paragraph, the number of parameters in our uncertainty analysis problem is 3. (elastic and non-elastic iron cross-sections and the dosimetry reaction for either of $^{27}A\ell$ and ^{238}U (n,f)F.P detectors).

For the $^{237}N_p$(n,f)F.P Transmissions only two parameters will be included since uncertainty information in a suitable form for this dosimetry reaction was not available.

As far as the determination of the sensitivity vectors is concerned, it is noticed that they cannot simply be taken from the results of the previous chapter since the group structures of the sensitivity profiles and covariance matrices do not coincide.

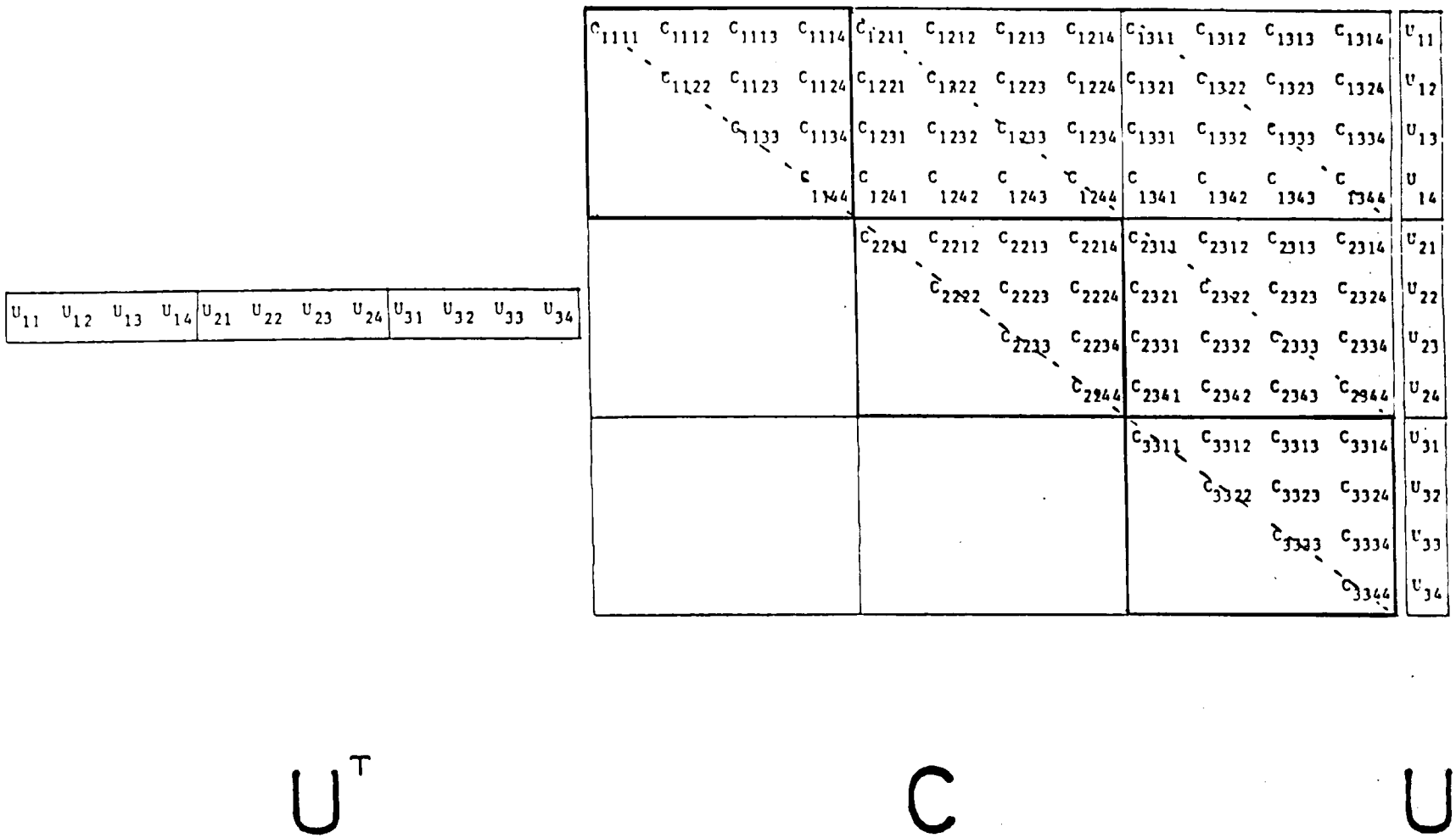


FIGURE 79

PICTORIAL VIEW OF THE UNCERTAINTY EQUATION

Furthermore the fact that the group structures of the iron and dosimetry data covariance matrices are not the same, in conjunction with the fact that they are uncorrelated prompt us to establish a more convenient form of Eqn (5.11) by splitting it into two major components, viz:

$$\left(\frac{\Delta T}{T}\right)^2 = U^T \begin{bmatrix} C_M & o \\ o & C_D \end{bmatrix} U =$$

$$= U_M^T \; C_M \; U_M + U_D^T \; C_D \; U_D = \left(\frac{\Delta T}{T}\right)^2_M + \left(\frac{\Delta T}{T}\right)^2_D \qquad (5.12)$$

where U_M, C_M refer to sensitivity and uncertainty information of the iron cross-sections, while U_D, C_D to that of dosimetry data.

However the problem of determining the broad group sensitivity coefficients required in Eqn (5.12) from the fine structure sensitivity information of the previous chapter still remains.

One possible way of getting around this problem is as follows:

Starting from Eqn (5.7) and working on either component of Eqn (5.12) we have:

$$\left(\frac{\Delta T}{T}\right)^2_M = \sum_{k,\ell}^{NOP} \sum_{I,J}^{NBG} \sum_{i=i(I)}^{i(I+1)-1} \sum_{j=j(J)}^{j(J+1)-1} U_{k,i} \; U_{\ell,j} \; \frac{\mathrm{cov}(P_{k,i}, P_{\ell,j})}{P_{k,i} P_{\ell,j}} \qquad (5.13)$$

where: NBG is the number of broad energy groups in which the covariance information is given and i(I), j(J) denote the group number in the fine energy structure which starts a new broad group, as shown in Figure 80.

It is obvious that this notation is valid only if fine and broad group boundaries coincide, something which is approximately true for our case.

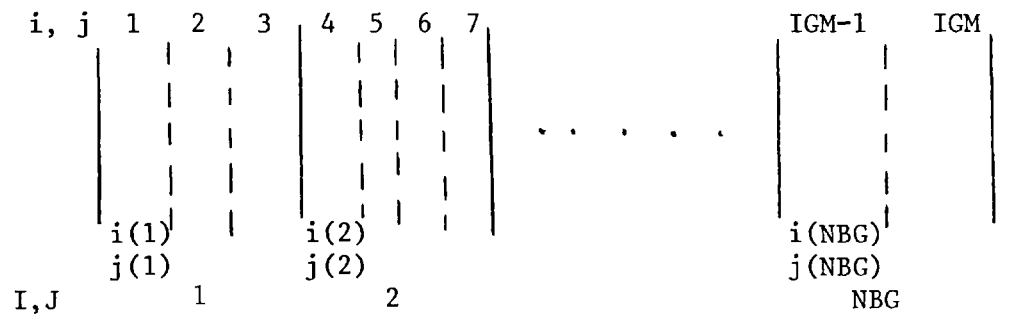


FIGURE 80

FINE AND BROAD GROUP STRUCTURES IN UNCERTAINTY CALCULATIONS.

However what is available is the broad group fractional covariances

$$\mathrm{Cov}(P_{k,I},P_{\ell,J})/P_{\ell,I}P_{k,J}\,.$$

A good and conservative assumption in establishing the unknown relation between the fine fractional covariances appearing in Eqn (5.13) and those given in Tables 25-29 is that the fine group cross-sections comprising a broad group are fully correlated, viz:

$$\frac{\mathrm{cov}(P_{k,i},P_{\ell,j})}{P_{k,i}\,P_{\ell,j}} = \frac{\mathrm{cov}(P_{k,I},P_{\ell,J})}{P_{k,I}\,P_{\ell,J}}\,, \quad \begin{matrix} i\varepsilon(i(I),\ i(I+1)-1) \\ j\varepsilon(j(J),\ j(J+1)-1) \end{matrix} \tag{5.14}$$

and therefore Eqn (5.13) becomes:

$$\left(\frac{\Delta T}{T}\right)^2_M = \sum_{k,\ell}^{NOP}\ \sum_{I,J}^{NBG} \frac{\mathrm{cov}(P_{k,I},P_{\ell,J})}{P_{k,J}\,P_{\ell,J}} \sum_{i=i(1)}^{i(I+1)-1} U_{k,i} \sum_{j=j(J)}^{j(J+1)-1} U_{\ell,j} \tag{5.15}$$

Defining the broad group sensitivities as:

$$U_{k,I} \equiv \sum_{i=i(I)}^{i(I+1)-1} U_{k,i} \tag{5.16}$$

$$U_{\ell,J} \equiv \sum_{j=j(J)}^{j(J+1)-1} U_{\ell,j} \tag{5.17}$$

Eqn (5.15) takes the final form:

$$\left(\frac{\Delta T}{T}\right)^2_M = \sum_{k,\ell}^{NOP}\ \sum_{I,J}^{NBG} U_{k,I}\,U_{\ell,J}\,\frac{\mathrm{cov}(P_{k,I},P_{\ell,J})}{P_{k,I}P_{\ell,J}} \tag{5.18}$$

Three important remarks can be made at this point:

1. The broad group sensitivities given as the sum of the fine group ones (Eqns (5.16), (5.17)) do not necessarily coincide with those obtained if the whole procedure of Transmission calculation and sensitivity analysis had been undertaken in this broad group structure. Despite the fact that the uncertainty information is available in a condensed energy scheme the calculation and sensitivity analysis of Transmissions must be carried out in a fine energy group structure to guarantee that the systematic errors introduced by the group collapsing are kept at

minimum. The comparison between pointwise and multigroup MONTE - CARLO calculations in Chapter 3 is very persuasive in this respect.

2. The broad group scheme of the multigroup covariance information taken from the ORWL-5318 report does not give the rank of the corresponding covariance matrices; that is,the uncertainty information in Tables 25 - 28 could have been given in a finer form, more appropriate to uncertainty and consistency studies. The broad energy structure of the covariance matrices degrades the sensitivity information (Eqns (5.10), (5.17)) and biases the uncertainty of the calculated quantity in an unknown fashion; the implications on the consistency analysis are more severe as will be seen in the following chapter.

3. An attempt to undertake the uncertainty analysis in the fine group structure used in the calculations would give different but meaningful results only if a different assumption was postulated in trying to create the fine group covariance matrices from the given broad group ones. Any sort of realistic and acceptable assumption concerning the uncertainties and correlations of the fine group cross-sections within a certain broad group, except that of the same uncertainty and full correlation, would require additional information in a suitable form which is not easily accessible and can not readily be processed.

Results and conclusions

Table 30 gives the percentage uncertainties of calculated Transmission for the three iron shells, obtained via Eqn (5.12), together with the percentage uncertainties of the measured values taken from Table 14.

A little FORTRAN program UNCERT was written to do the matrix operations of Eqn (5.12); the broad group sensitivity vectors required are tabulated in Tables 31, 32 and 33. The sensitivity to non-elastic was simply calculated as the difference between the sensitivities to total and to elastic, correspondingly.

The following conclusions emerge from the results of Table 30.

1. The uncertainty of the calculated Transmissions is generally higher than that of the measured values and much higher for large thicknesses and high thresholds.

2. The total uncertainty is an increasing function of both shell thickness and detector threshold; that is, it follows the same trend with the total sensitivity of Transmission to iron total cross-section.

3. The contribution of the dosimetry data to the total uncertainty is negligibly small for the ^{27}Al and ^{238}U detectors. The unavailability of reliable multigroup uncertainty information for the $^{237}N_p(n,f)F.P$ reaction in conjunction with the fact that the sensitivity profile for this reaction is of the same order of magnitude with that of the iron total cross-section (see Figure 78), and the relatively small uncertainties of the $^{237}N_p(n.f)F.P$ calculated Transmissions precludes the acceptance of the same conclusion for the $^{237}N_p(n.f)F.P$ Transmissions. Indeed, preliminary calculations of the $(\Delta T/T)_D$ uncertainty for the $^{237}N_p(n,f)F.P$ Transmissions with uncertainty information drawn from the error assignments to dosimetry reactions in the form of multigroup standard deviations by McErlroy (41) gave $(\Delta T/T)_D$ uncertainties

TABLE 30. PERCENTAGE UNCERTAINTIES OF EXPERIMENTAL AND CALCULATED TRANSMISSIONS IN IRON SHELLS.

DETECTOR	PERCENTAGE UNCERTAINTIES																	
	SHELL THICKNESS = 1.90 cm						SHELL THICKNESS = 4.11 cm						SHELL THICKNESS = 9.16 cm					
	EXPERIMENTAL	CALCULATED					EXPERIMENTAL	CALCULATED					EXPERIMENTAL	CALCULATED				
		$(\Delta T/T)_M$			$(\frac{\Delta T}{T})_D$	$\frac{\Delta T}{T}$		$(\Delta T/T)_M$			$(\frac{\Delta T}{T})_D$	$\frac{\Delta T}{T}$		$(\Delta T/T)_M$			$(\frac{\Delta T}{T})_D$	$\frac{\Delta T}{T}$
		PARTIAL AND ENERGY CORRELATIONS SUPPRESSED	PARTIAL CORRELATIONS SUPPRESSED	FULL COVARIANCE INFORMATION				PARTIAL AND ENERGY CORRELATIONS SUPPRESSED	PARTIAL CORRELATIONS SUPPRESSED	FULL COVARIANCE INFORMATION				PARTIAL AND ENERGY CORRELATIONS SUPPRESSED	PARTIAL CORRELATIONS SUPPRESSED	FULL COVARIANCE INFORMATION		
$^{27}Al(n, P)^{27}Mg$ (4.4 MeV)	0.89	3.21	3.22	3.00	0.07	3.00	-	6.84	6.89	6.27	0.12	6.27	-	15.07	15.12	13.56	0.26	13.56
$^{238}U(n, f)F.P.$ (1.5 MeV)	0.22	1.04	1.32	1.20	0.08	1.20	0.28	2.51	3.19	2.76	0.16	2.76	0.87	5.49	7.07	5.92	0.31	5.93
$^{237}Np(n, f)F.P.$ (0.6 MeV)	0.35	0.36	0.47	0.41	-		0.38	0.97	1.26	1.03	-		0.60	1.98	2.61	2.04	-	

TABLE 31. BROAD GROUP SENSITIVITY COEFFICIENTS TO IRON ELASTIC AND NON-ELASTIC CROSS SECTIONS.

SHELL THICKNESS cm	DETECTOR	BROAD GROUP SENSITIVITIES										TOTAL (ENERGY INTEGRATED) SENSITIVITY	SENSITIVITY TO TOTAL
		BROAD GROUP NUMBER	1	2	3	4	5	6	7	8	9		
		FINE GROUPS INVOLVED	1-13	14-18	19-25	26-28	29-32	33-34	35	36	37-55		
		REACTION											
1.90	$^{27}Al(n, P)^{27}Mg$	ELASTIC	-1.751 E-02	-7.489 E-03	-7.420 E-06	0	0	0	0	0	0	-2.502 E-02	-2.851 E-01
		NON-ELASTIC	-2.244 E-01	-3.451 E-02	-1.388 E-05	0	0	0	0	0	0	-2.600 E-01	
	$^{238}U(n, f)F.P.$	ELASTIC	-3.567 E-03	-8.695 E-03	-1.480 E-02	-3.581 E-04	-4.800 E-06	7.840 E-07	5.351 E-07	5.803 E-07	5.600 E-07	-2.743 E-02	-1.801 E-01
		NON-ELASTIC	-4.075 E-02	-4.537 E-02	-6.562 E-02	-9.369 E-04	-1.000 E-07	-6.200 E-08	-1.420 E-08	-7.200 E-09	-1.000 E-08	-1.526 E-01	
	$^{237}Np(n, f)F.P.$	ELASTIC	-2.014 E-03	-5.074 E-03	-4.540 E-03	3.252 E-03	-4.000 E-04	-2.400 E-04	4.490 E-05	4.996 E-05	2.600 E-05	-9.006 E-03	-7.246 E-02
		NON-ELASTIC	-1.217 E-02	-1.592 E-02	-2.346 E-02	-1.191 E-02	-2.100 E-05	-4.000 E-05	0	0	0	-6.346 E-02	
4.11	$^{27}Al(n, P)^{27}Mg$	ELASTIC	-4.797 E-02	-1.975 E-02	0	0	0	0	0	0	0	-6.772 E-02	-6.224 E-01
		NON-ELASTIC	-4.777 E-01	-7.699 E-02	0	0	0	0	0	0	0	-5.547 E-01	
	$^{238}U(n, f)F.P.$	ELASTIC	-1.100 E-02	-3.254 E-02	-4.695 E-02	-9.910 E-04	-1.207 E-05	5.602 E-06	2.778 E-06	3.445 E-06	3.413 E-06	-9.150 E-02	-4.534 E-01
		NON-ELASTIC	-8.843 E-02	-1.133 E-01	-1.573 E-01	-2.669 E-03	-3.700 E-07	-2.580 E-07	-6.500 E-08	-4.100 E-08	-5.300 E-08	-3.619 E-01	
	$^{237}Np(n, f)F.P.$	ELASTIC	-6.248 E-03	-1.849 E-02	-2.260 E-02	1.112 E-02	-1.940 E-03	8.141 E-04	2.070 E-04	2.536 E-04	1.441 E-04	-3.673 E-02	-2.123 E-01
		NON-ELASTIC										-1.755 E-01	
9.16	$^{27}Al(n, P)^{27}Mg$	ELASTIC	-1.219 E-01	-4.834 E-02	0	0	0	0	0	0	0	-1.702 E-01	-1.388 E+00
		NON-ELASTIC	-1.047 E+00	-1.715 E-01	-1.390 E-04	0	0	0	0	0	0	-1.218 E+00	
	$^{238}U(n, f)F.P.$	ELASTIC	-2.527 E-02	-8.521 E-02	-1.275 E-01	-3.721 E-03	-5.032 E-05	1.364 E-05	9.935 E-06	1.545 E-05	1.675 E-05	-2.417 E-01	-1.030 E+00
		NON-ELASTIC	-1.721 E-01	-2.534 E-01	-3.557 E-01	-7.749 E-03	-1.330 E-06	-1.050 E-06	-3.000 E-07	-2.300 E-07	-3.300 E-07	-7.883 E-01	
	$^{237}Np(n, f)F.P.$	ELASTIC	-1.315 E-02	-4.261 E-02	-6.729 E-02	8.893 E-03	-4.006 E-03	-2.187 E-03	5.154 E-04	8.099 E-04	4.900 E-04	-1.185 E-01	-4.737 E-01
		NON-ELASTIC	-5.518 E-02	-8.309 E-02	-1.393 E-01	-7.720 E-02	-2.400 E-04	-2.020 E-04	-2.040 E-05	-1.350 E-05	-1.000 E-05	-3.552 E-01	

TABLE 32. BROAD GROUP SENSITIVITY COEFFICIENTS OF TRANSMISSION TO $^{27}Al(n, P)^{27}Mg$ DOSIMETRY DATA.

GROUP STRUCTURES		SENSITIVITY COEFFICIENTS		
BROAD GROUP	FINE GROUPS INCLUDED	SHELL THICKNESS = 1.90 cm	SHELL THICKNESS = 4.11 cm	SHELL THICKNESS = 9.16 cm
1	1	1.105 E-05	3.868 E-05	9.945 E-05
2	2	4.514 E-05	1.379 E-04	3.471 E-04
3	3	5.595 E-05	2.223 E-04	5.842 E-04
4	4	6.936 E-05	3.704 E-04	9.915 E-04
5	5	7.396 E-05	5.554 E-04	1.497 E-03
6	6	-4.062 E-05	5.091 E-04	1.472 E-03
7	7	-3.251 E-04	3.305 E-05	4.204 E-04
8	8	-6.625 E-04	-6.224 E-04	-1.097 E-03
9	9	-1.150 E-03	-1.815 E-03	-3.796 E-03
10	10	-1.644 E-03	-3.189 E-03	-6.899 E-03
11	11	-1.654 E-03	-3.707 E-03	-8.128 E-03
12	12	-9.090 E-04	-2.480 E-03	-5.661 E-03
13	13	3.059 E-04	-4.248 E-05	-5.089 E-04
14	14	7.665 E-04	8.447 E-04	1.395 E-03
15	15	2.787 E-03	4.955 E-03	1.026 E-02
16	16	1.374 E-03	2.463 E-03	5.239 E-03
17	17	7.404 E-04	1.407 E-03	3.086 E-03
18	18	1.553 E-04	3.019 E-04	6.809 E-04
19	19	1.349 E-05	2.780 E-05	6.550 E-05
20	20	0.0	0.0	0.0
TOTAL SENSITIVITY		1.208 E-05	8.976 E-06	5.227 E-05

TABLE 33. BROAD GROUP SENSITIVITY COEFFICIENTS OF TRANSMISSION TO $^{238}U(n, f)$ F.P. DOSIMETRY DATA.

SHELL THICKNESS cm	SENSITIVITY COEFFICIENTS						TOTAL SENSITIVITY
	BROAD GROUP	1	2	3	4	5	6	
	FINE GROUPS INCLUDED	1-14	15-24	25-34	35-37	38-40	41-55	
1.90		-3.107 E-02	2.660 E-02	4.434 E-03	1.600 E-05	2.600 E-06	7.200 E-07	-1.446 E-05
4.11		-5.931 E-02	4.876 E-02	1.049 E-02	3.900 E-05	1.000 E-05	3.200 E-06	6.305 E-06
9.16		-1.124 E-01	8.773 E-02	2.473 E-02	1.500 E-04	3.700 E-05	1.300 E-05	5.740 E-06

comparable with the $(\Delta T/T)_M$ ones. However these values were not included in Table 30 mainly because of lack of reliability for this source of uncertainty information.

4. The suppression of the negative partial correlations between elastic and non-elastic iron cross-sections (see Table 27) overestimates the uncertainty while the opposite is valid for the energy-dependent positive correlations of the two reactions. (Tables 25, 26). This is more-strongly felt in the low threshold detectors where these correlations play a more important role, as expected.

Neglecting the partial correlations between elastic and non-elastic cross-sections of iron it is possible and interesting to examine how the "partial uncertainties" due to elastic and non-elastic components of the total are compared. This is done in Table 34.

TABLE 34

ELASTIC AND NON-ELASTIC PARTIAL UNCERTAINTIES OF THE CALCULATED TRANSMISSIONS IN IRON SHELLS

DETECTOR	PARTIAL PERCENTAGE UNCERTAINTIES								
	SHELL THICKNESS = 1.90cm			SHELL THICKNESS = 4.11cm			SHELL THICKNESS = 9.16cm		
	ELASTIC	NON ELASTIC	TOTAL	ELASTIC	NON ELASTIC	TOTAL	ELASTIC	NON ELASTIC	TOTAL
$^{27}A\ell(n,p)^{27}Mg$	0.22	3.21	3.22	0.61	6.86	6.89	1.53	15.05	15.12
$^{238}U(n,f)F.P$	0.13	1.31	1.32	0.46	3.16	3.19	1.21	6.96	7.07
$^{237}N_p(n,f)F.P$	0.06	0.46	0.47	0.25	1.24	1.26	0.62	2.54	2.61

From Table 34 it is seen that the uncertainty of Transmission due to elastic cross-section is very small compared to that originated in the non-elastic cross-section.

Tables 25, 26, and 31 reveal that lower values of the covariance matrix

elements and much lower sensitivities for the elastic cross-section than that characterizing the non-elastic one are responsible for this result.

Consequently the analysis and results undertaken so far prompt us to accept that the uncertainty accompanying the calculated Transmissions and originating from the input data can practically be considered as that due to non-elastic cross-section data only, at least for the $^{27}A\ell$ and ^{238}U detectors.

It was demonstrated in Chapter 3 that the statistical uncertainty accompanying the MCBEND - multigroup Transmissions could adequately attribute the error due to both calculational method and modelling of the experiments. (However, the uncertainty due to group collapsing is not incorporated in this value since it is very difficult to quantify this sort of error).

Table 35 compares the two major components of the total uncertainty in Transmission, that is, the uncertainty originating from the input data and that due to calculational procedure, for the two thin iron shells for which this information exists. (The fact that the "calculational uncertainty"refers to a larger detection region than the actual size of the detectors used does not complicate the comparison since the fractional uncertainty of Transmission due to input data is expected to be approximately the same for both cases).

The results of Table 35 show that the uncertainty of Transmissions due to both the algorithm employed and the modelling of the experiments is negligibly small compared with that originating from the input data used. We do not expect this picture to be largely distorted should the unknown errors due to group collapsing have been included. But even if this does happen the above conclusion and the further analysis in the following chapter will be valid at least for the multigroup representation of the nuclear data.

TABLE 35

A COMPARISON BETWEEN "CALCULATIONAL" AND "DATA" UNCERTAINTIES OF TRANSMISSIONS IN IRON SHELLS

DETECTOR	SHELL THICKNESS = 1.90cm			SHELL THICKNESS = 4.11cm		
	CALCULATIONAL UNCERTAINTY (%)	DATA UNCERTAINTY (%)	TOTAL UNCERTAINTY (%)	CALCULATIONAL UNCERTAINTY (%)	DATA UNCERTAINTY (%)	TOTAL UNCERTAINTY (%)
$^{27}Al(n,p)^{27}Mg$	0.85	3.00	3.11	1.50	6.27	6.44
$^{238}U(n,f)F.P$	0.35	1.20	1.25	0.49	2.76	2.80
$^{237}Np(n,f)F.P$	0.22	0.41*	0.46	0.36	1.03*	1.09

*In these values the uncertainty due to dosimetry data has not been included.

The systematic nature of calculational and modelling errors together with their, very often, unknown distributions make the above conclusion of crucial importance in the comparison between experimental and calculated Transmissions and permits further investigation based on these two independent pieces of information for their mutual benefit.

The fact that the multigroup cross-section data are meant to follow multivariate normal distributions in conjunction with the 1st-order perturbation theory adopted in the present analysis allowed the fractional uncertainties of the calculated Transmissions to be interpreted as normally distributed. This implies that the calculated Transmissions are taken to be random variables following univariate normal distributions in the context, of course, of the above assumptions. Figure 81 depicts the relation between observed discrepancies and standard deviations of calculated and measured Transmissions. This Figure shows that these discrepancies are consistent with the standard deviations of the calculated Transmissions determined essentially in terms of the uncertainties of the non-elastic cross-section.

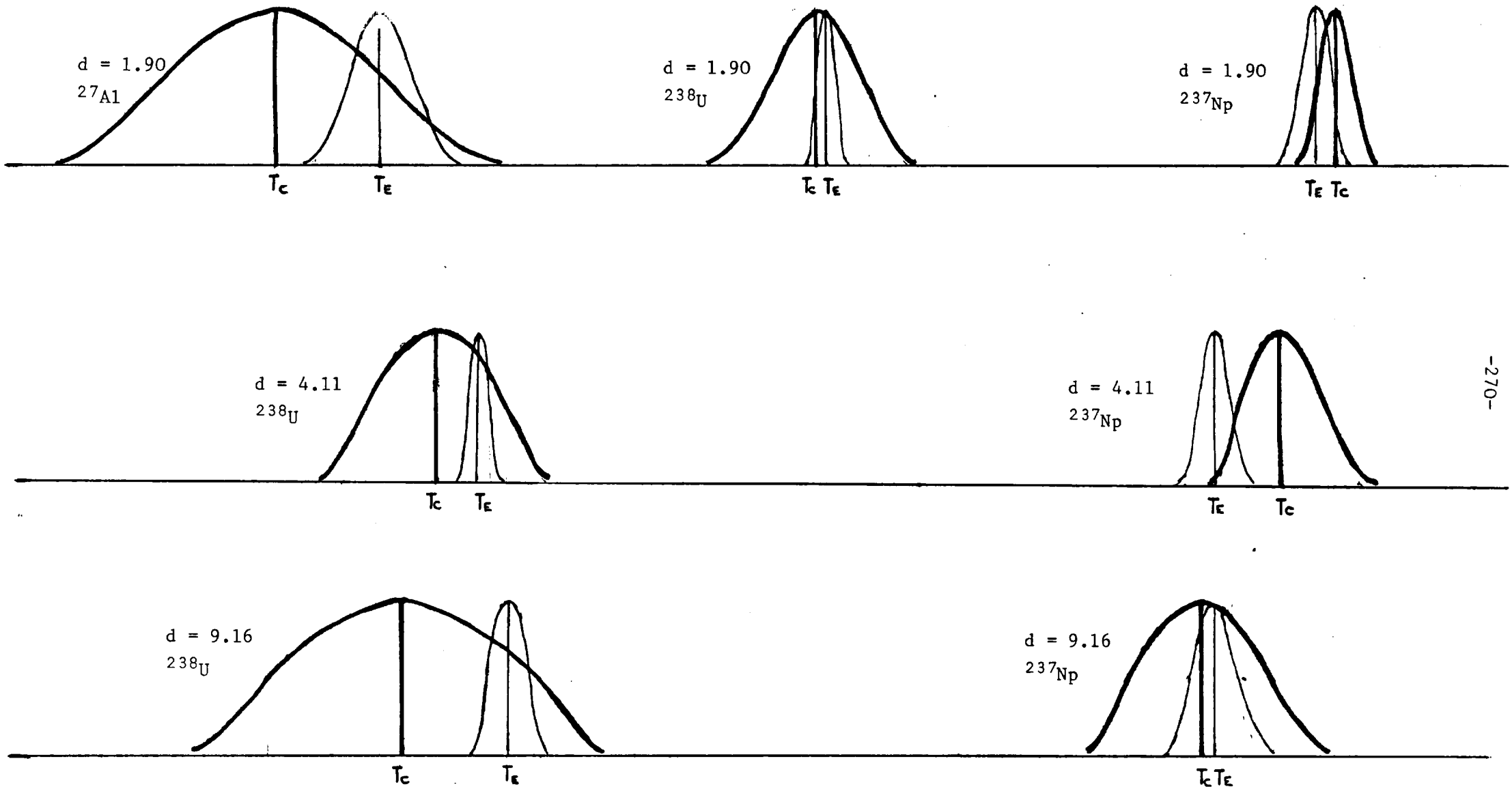


FIGURE 81. EXPERIMENTAL AND CALCULATED TRANSMISSIONS AND THEIR STANDARD DEVIATIONS FOR IRON SHELLS.

This consistency is an additional factor reinforcing the validity of the conclusion about the unimportance of the calculational uncertainty in the present study and shedding more light on the statement adopted earlier - that all classes of input, to calculational procedure, data except the non-elastic cross-section have negligible effect on the final uncertainty of $^{27}A\ell$ and ^{238}U Transmissions.

The considerable overlapping of the Te and Tc normal distributions in Figure 81 allows the interpretation of the observed discrepancy as that of pure statistical nature and therefore the calculated Transmissions can be considered as a new independent set of experimental measurements of the same physical quantity. Superposing these two normal distributions would lead to an improved estimate of this quantity corresponding to a larger data ensemble (measured Transmissions, evaluated cross-section data). This improved estimate of Transmission could then generate better cross-section data than the original one. The fact that the experimental Transmissions are much better known that the calculated ones favour such a line of further investigation. This kind of data analysis, formally known as consistency analysis, is mathematically formulated in Appendix B and fully studied in Chapter 6.

CHAPTER SIX

CROSS-SECTION ADJUSTMENTS

6.1 INTRODUCTION

Nuclear data adjustment was born out of the requirement for reduced uncertainty margins in commercial reactor designs. In the reactor physics domain discrepancies between prediction and observation were derived from both inadequacies in the calculational method and errors in the nuclear data used in the calculation. The assessment of the adequacy of rival methods and data sets was conducted through theoretical intercomparison exercises and by the performance of integral experiments. Initially the integral experiments were used simply to identify the best existing evaluated nuclear data file and to indicate areas of the evaluated cross-section data where better quality measurements were required. The guidance given by these integral experiments helped designers and reactor physicists to formulate some of the more important requests for accurate nuclear data; the mechanism for making such requests known to evaluators and measurers was, and still is, the WRENDA list.

In general, therefore, the feedback to the nuclear data from these technical assessment exercises was either non-existent, as in the case of the UKNDL, or only over the time scale for a complete re-evaluation of the library, as was the case for the ENDF/B library. Moreover, requests for more accurate nuclear data measurements had to await the development of new detection systems and better neutron sources. The time required for the satisfaction of nuclear data requests became so long that the direct feedback of the results of integral experiments into design calculations appeared to be the only expedient way of significantly reducing the uncertainties on reactor design parameters. It was at this stage that the adjustment of nuclear

data, on the basis of some statistical model, to obtain consistency with experimental observations was first advocated and in order to assist in this process a special class of integral experiments, designated benchmarks, were identified.

It is useful at this point to comment on the different approaches to the cross-section adjustment problem followed in the reactor physics and reactor shielding areas.

In fast reactor physics the integral experiments mounted have been "mock-up" versions of design study cores. Indeed the assembly is made to resemble as closely as possible the clean reactor core. During the conduct of the experiment, fission rates, leakage, critical sizes and Keff are measured and compared with calculations using design tools viz. diffusion theory. The cross-section data can then be adjusted according to some prescription in order to obtain closer agreement with experiment. It is often argued that the adjustments do not represent purely data-related uncertainties (errors in the evaluated data and inappropriate group condensation), but also account for errors arising out of the inappropriate use of diffusion theory in quasi-heterogeneous systems. Since in the reactor core situation the measured responses are those desired by the designer and the calculational method and data are simple and appropriate to design work, the adjustment of the cross-section data, for whatever reason, will produce a data set which is optimised for that type of reactor core.

This type of pragmatic approach has been adopted by the reactor physics community as an expedient to better quality design calculations, whilst awaiting the arrival of high quality nuclear data and the emergence of more rapid techniques for the accurate solution of the neutron transport equation (e.g. better DS_n methods and developments in finite element techniques). Trying to peer through the mist of calculational uncertainties into the basic nuclear data itself is a more difficult

matter; a reasonable hope is that the adjustment of group cross-sections may give at least some useful broad clues to the evaluator or measurer of basic data. Use of such derived data sets in very different environments may not improve calculational performance and could indeed degrade it.

The situation in reactor shielding is very different. The design quantities of interest such as nuclear heating, biological dose-rates and material damage-rates cannot be measured in integral experiments; instead neutron spectra and/or foil activation measurements have to be made. Uncertainties are therefore injected into the calculation - to - measurement comparison through unfolding schemes, counting techniques and flux - to - response conversion factors. Moreover, from the design viewpoint full scale reactor shield "mock-ups", with many duct and instrumentation penetrations, are rarely possible so that methods and data have to be tested in much simpler experimental situations. These clean-source, simple-geometry, single-material experiments which may be wholly unrelated to design situations have sometimes been referred to as DATAM experiments in that their purpose is to check data and methods. The data related effects are assessed using nominally exact methods of solution of the transport equation such as MONTE - CARLO or discrete ordinate techniques; the performance of simple design oriented codes such as removal-diffusion theory can subsequently be tested using, where possible, the same nuclear data. Since the DATAM experiments can rarely be extrapolated to provide bias factors for design calculations, the performance of the method and data must be accurately and independently assessed.

In this class of experiments therefore, provided that measurement can be made at all energies of practical interest, one might hope to generate cross-section sets which represent a "good average" for the material in most environments, although they would be rather less good

in specific configurations than those generated from the appropriate experiments.

So far the provision of reliable working adjusted data sets either "general" or "specific" for practical calculations giving useful clues to measurers has been seen as an end in itself. Use of recently developed nuclear data adjustment methods (see page 280) which seek adjustment of basic nuclear model parameters may enable one to look partly through the group structure into the basic nuclear data itself. However, neutron transport in shields after a few mean free paths is frequently dominated by resonance maxima, inteference minima and inelastic cross-section thresholds; it is in these rapidly varying regions of the cross-section that the group - averaging technique is least accurate. An expression of the dichotomy that can exist in the mind of the shielding benchmark analyst might be thus: is it better to optimise the multigroup data set irrespective of the source of the errors in the group constants and use the adjusted data in the restricted design context for which it has been modified, or should some effort be made to quantify the accuracy of the group condensation mechanism in order to delve into and modify the contents of the evaluated nuclear data library itself and so generalise the applicability of the optimised data set?

The concept of the direct adjustment of an evaluated library on the basis of the results of consistency analysis has represented a major philosophical problem in the domain of nuclear data quantification. To adjust or not to adjust is still a controversial question in the field of nuclear data evaluation. In this chapter an effort is made to establish the conditions and requirements which will allow suitable and precise integral experiments to have a direct and problem-independent role in permanently improving fine-multigroup or even pointwise basic nuclear data libraries.

A review of cross-section adjustment methods follows and their advantages and drawbacks are clearly stated. The assumptions under which a linear least-squares model incorporating parameter evaluations as additional observations gives meaningful results in non-linear problems are cited next and a comparison with the real conditions of our consistency analysis problem is undertaken. Broad-group cross-section adjustments are derived next for both ENDF/B-IV and UKNDL iron cross-section data and the a' priori and a' posteriori relative multi-group covariance matrices are also compared. The adjusted data sets are then assessed both on the basis of how well they predict Transmissions, whether or not they are included in the adjustment procedure, and in terms of their absolute broad group elastic and non-elastic components. The physical interpretation of the deduced adjustment follows, the shortcomings of the present adjustment method and their causes are stated and the requirements for a problem-independent feedback of integral measurements into basic nuclear data libraries are also outlined. Finally a comparison with the Winfrith iron benchmark experiment is attempted.

6.2 A REVIEW OF NUCLEAR DATA ADJUSTMENT METHODS

The history of the adjustment of multigroup neutron interaction parameters by fitting integral measurements stems in the U.K. from the work of Pendlebury et al (42) and later by McDougall and Rowlands (43). In parallel with this work has been the development of methods by Gandini (44), Barre et al (45), Pazy et al (46) and Mitani and Kuroi (47). The methods basically disagree on the treatment of the energy-dependent correlation in the nuclear data and of the systematic errors in the cross-section data and the integral measurements.

The algorithm used by MacDougall and Rowlands required a least-squares fit to both the integral and nuclear data parameters:

$$\text{Min}F = \sum_{p=1}^{p} \sum_{k=1}^{q} \left(\frac{f_k^p}{g_k^p}\right)^2 + \sum_{i=1}^{n} \left(\frac{d_i}{e_i}\right)^2 \qquad (6.1)$$

and

$$d_i = \frac{M_i - R_i'}{R_i} = \frac{M_i}{R_i} - 1 - \sum_{p=1}^{p} \sum_{k=1}^{q} U_k^{p,R} \, f_k^p \qquad (6.2)$$

where:

f_k^p: is the fractional group cross-section adjustment.

g_k^p: is the fractional standard deviation of the differential cross-section which is assumed to be normally distributed.

e_i: is the fractional standard deviation of the normally distributed part of the integral experiment.

M_i, R_i: are the measured and calculated values of the response, respectively

R_i' : is the calculated response for a fractional change f_k^p in the k^{th} group of the reaction cross-section x^p.

$U_k^{p,R}$: is the k^{th}-element of the sensitivity vector.

The method by which correlations in the integral measurements were

treated was to assume that they arise largely from systematic errors and to redefine the variable d_i to include a discrepancy from this source.

The energy-dependent correlations in the cross-section data were deemed to be known a priori and were included by defining f_k^p in such a way that it is related to the adjustment of the adjacent lower energy group. This method relies essentially on correcting the integral measurements for systematic errors prior to adjustment and transforming the correlated cross-section variables to a mapping where they can be considered independent. The adjustments are determined by minimization of the least-squares function and allows the determination of the covariance matrix of the adjustments through the use of expectation theory. Moreover, the adjustment factors can be shown to depend only upon the relative values of the assumed standard deviations e_i and g_k^p, whereas the covariance matrix of the adjusted data is dependent upon the absolute values (see Appendix B). To obtain an appropriate final matrix, a goodness-of-fit χ^2 test has been performed and the final variances scaled indiscriminately a posteriori by χ^2/n.

It is important that all the systematics on the integral measurements be identified and removed in the adjustment process otherwise the expected chi-squared per measurement degree of freedom would not be close to unity; this practice of a posteriori scaling must be undertaken with caution since it is only applicable when the error information of the input data has been under-estimated. In general, scaling factors can arise from a variety of reasons such as inadequacies in the calculational methods, improper account of the energy-dependent correlations of the nuclear data etc.

Pendlebury (48) chose to allow for correlations in the cross-section data by a rather crude method of using a weight factor of q^{-1} on the cross-section adjustment penalty, viz:

$$\text{MinF} = \sum_{p=1}^{p} \sum_{k=1}^{q} \frac{1}{q} \left(\frac{f_k^p}{g_k}\right)^2 + \sum_{i=1}^{n} \left(\frac{d_i}{e_i}\right)^2 \qquad (6.3)$$

He also proposed a method of adjusting basic cross-section data from adjustments calculated for group cross-sections.

In the treatment of systematics in the integral data, Cecchini et al (49) chose an equiprobable distribution for the integral measurements and the normal error distribution for the group cross-section data:

$$\text{MinF} = \sum_{p=1}^{p} \sum_{k=1}^{q} \left(\frac{f_k^p}{g_k^p}\right)^2 \quad \text{subject to } |d_i| < e_i \text{ for all } i$$

whilst Barre and his collaborators chose the reverse, adopting a square distribution for the cross-section data and allowing the integral measurements to be randomly distributed, viz:

$$\text{MinF} = \sum_{i=1}^{n} \left(\frac{d_i}{e_i}\right)^2 \quad \text{subject to } |f_k^p| < g_k^p \text{ for all } k \text{ and } p$$

Pazy et al, however, constructed their adjustment method on the basis of a continuous energy formulation in which group adjustment parameters were defined by:

$$x(E) = (1 + f_k^p)\, x^p(E) \quad E_k < E \leqslant E_{k+1}$$

and the minimization of the least squares integral reduced to the solution of a symmetric Fredholm equation with a degenerate kernel. No account was taken of nuclear data correlations other than that between the total cross-section and its components.

Mitani and Kuroi (50) developed a method quantifying cross-section energy-dependent correlations and systematics in absolute cross-section data. The uncertainties in absolutely measured cross-

section data have been assessed by fitting nuclear models to the experimental data and defining the errors in the group constants in terms of the standard deviations of the parameters of the fitted theory. This line of approach is in sharp contrast to the empirical approach proposed by Perey (51) and used in the evaluation of ENDF/B correlated error files.

A limitation of the multi-group data adjustment approach is the dependence of the cross-section modification factors upon the selected group scheme and condensation weighting function. The consistent method developed by Gandini and Salvatores (52) relates the sensitivity of an integral response directly to the parameters of a nuclear model either as specified in the nuclear data file or as a fitting algorithm in a data file processing code. Thus if $\hat{x}_k$ is the estimated value of the k^{th} group cross-section and $\hat{q}_m$ is the most likely value of the m^{th} parameter of the nuclear model, then for small changes:

$$\hat{x}_k - x_k = \sum_m \frac{\partial x_k}{\partial q_m} (\hat{q}_m - q_m) \tag{6.4}$$

The Taylor expansion of the integral response in terms of the group cross-sections may be written as:

$$R' - R = \sum_k \frac{\partial R}{\partial x_k} (x_k' - x_k) \tag{6.5}$$

and therefore:

$$\delta R = \sum_k \frac{\partial R}{\partial x_k} \sum_m \frac{\partial x_k}{\partial q_m} (q_m' - q_m) \tag{6.6}$$

The derivative $\partial R/\partial x_k$ can be found by normal sensitivity analysis and the function $\partial x_k/\partial q_m$ can usually be determined analytically from the nuclear model. Thus using the correlation matrix for the nuclear model parameters, a least-squares fit to the integral data can furnish estimates of correction factors to be applied to the nuclear model

parameters. Examples of nuclear models to which the theory has been extended include the ABBN approach to resonance self-shielding, the Porter Thomas distribution for unresolved resonances, Breit-Wigner formalism for resolved resonances and the Weiskopf evaporation model. The method essentially removes part of the problem dependence of the data adjustment technique. Moreover it allows access to the parameters such as energy transfer cross-sections which it would be impractical to treat systematically in the multi-group form. Furthermore the method allows for the evaluation of basic nuclear data parameters from extensive measurements; in some cases this method can lead to a more accurate estimator of a nuclear parameter than the corresponding differential microscopic measurement. Indeed, the method represents the opposite end of the spectrum as regards cross-section measurement techniques. Microscopic measurements are often performed on the thinest material samples that the detector efficiency will allow, in order to mitigate the effect of multiple scattering. In a single material integral benchmark, on the other hand, it is the equilibrium distribution of a population of neutrons derived from a well defined source that is being modelled.

A new approach to the adjustment of group cross sections fitting integral measurements has been proposed by Y.A.Chao (53). The adjustment is viewed as a process of estimating theoretical and/or experimental negligence errors to bring statistical consistency to the integral and differential data so that they can be combined to form an enlarged ensemble, based on which an improved estimation of the physical constants can be made. In this method the discrepancy between measured and calculated values of the integral quantity is considered as consisting of two components: the statistical component due to statistical uncertainties arising from the finiteness of the data ensemble and the negligence component due to negligence errors

arising from some negligence in experiments (e.g. calibration) or in theory (e.g. approximations). Given the situation of no information on the sources of any discrepancy between the data, it seems reasonable to regard a large discrepancy (in the χ^2 sense) as indicating a high likelihood for a negligence discrepancy, while regarding a small discrepancy as indicating that for a statistical one. A statistical discrepancy may appear among the affected parameters in an uncorrelated or correlated way and can be handled in a well-defined and straightforward way via the standard methods of statistics for combination and propagation of uncertainties.

In contrast, a negligence discrepancy due to a single source of error necessarily appears among the affected parameters in a completely correlated (systematic) manner; its treatment bears ambiguity and is often disputable. It is in the presence of negligence discrepancy that the original data sets should be adjusted while in the case of statistical discrepancy the two data sets are simply combined into a larger unified ensemble and the physical constants are re-estimated. A three-step approach is suggested in the presence of a negligence discrepancy and its formalism of general validity is developed. In step-one, the data of negligence error are extracted from the given integral and differential data. The method of extraction is based on the concepts of prior probability and information entropy. It automatically leads to vanishing negligence error as the two sets of data are statistically consistent. The second step is to identify the sources of negligence error and adjust the data by an amount compensating for the extracted negligence discrepancy. In the last step, the two data sets already adjusted to mutual consistency, are combined as a single unified ensemble. Standard methods of statistics can then be applied to re-estimate the physical constants.

A finite element basis for cross-section adjustment and

evaluation has been recently proposed by F. Schmittroth and R. Schenter (54). The method is especially appropriate for cross-sections that are well represented by continuous functions. The algorithm is based on least-squares techniques that use complete covariance information and prior values. Nuclear model calculations, microscopic and integral data, and the results of prior multigroup adjustments can be combined in a single consistent evaluation.

6.3 STATISTICAL FORMULATION OF THE CONSISTENCY PROBLEM

The statistical consistency between measured and calculated Transmissions in iron shells depicted in Figure 81 allows the formulation of our cross-section adjustment problem as that of data combination and the use of relatively simple and well-established statistical methods.

The existence of multigroup covariance information for iron and dosimetry cross-sections permits the use of simple adjustment methods which do not require or incorporate schemes for generating covariance information in a suitable form prior to adjustment. On the other hand the lack of resolution in both energy and reaction types of the multigroup covariance matrices available precludes the continuous energy treatment of the adjustment problem and imposes, as well be demonstrated later, a broad multigroup adjustment scheme determined by the ranks of the covariance matrices.

In the light of the above arguments an adjustment procedure based on the well-known least-squares method of statistical inference seems very appropriate to our problem. The method of least-squares is an application of minimum variance estimators and is widely used in situations where a functional form is known (or assumed) to exist between the observed quantities and the parameters to be estimated.

However, the formulation of the adjustment procedure as a least-squares problem will be undertaken in terms of multigroup cross-sections (parameters) and Transmissions (observed quantities). The fact that the number of parameters to be estimated is higher than the number of observed quantities, as often happens, necessitates the use of previous parameter measurements or evaluations as additional observations to make the set of equations over-determined. The functional form between observations and parameters required by the least-squares

method is that of Eqn (2.8) which, of course, will be approximated by a linear form based on a first-order expansion in Taylor series of the function. The mathematical formulation of the least-squares problem with the particular features outlined above is given in Appendix B. We simply state here the basic assumptions undertaken and the solution reached.

Given:

1. A set of measurements or evaluations of the parameters $\vec{x}_p = (x_{p1}, x_{p2}, \cdots x_{pr} = \text{NBGxNOP})$ comprising a random sample of size one from a multivariate distribution $\vec{X}_p$.

2. A matrix N_p. This matrix, or a constant multiple of it $\sigma^2 N_p$, is the covariance matrix of $\vec{X}_p$.

3. A set of measurements of integral quantities $\vec{x}_o = (x_{o1}, x_{o2} \cdots x_{on-r})$ comprising a random sample of size one from a multivariate distribution $\vec{X}_o$.

4. A matrix N_o. This matrix, or a constant multiple of it $\sigma^2 N_o$, is the covariance matrix of $\vec{X}_o$.

5. That, the random variables $\vec{X}_p$ and $\vec{X}_o$ are stochastically independent.

6. That, the function $\vec{X}_o = \vec{x}_o (\vec{X}_p)$, relating observed integral quantities to parameters, can be approximated by a linear model:

$$\vec{X}_o = \vec{x}^*_o + C (\vec{X}_p - \vec{x}_p) \tag{6.7}$$

where:

$$\vec{x}^*_o = \vec{x}_o (\vec{x}_p)$$

that is, the value of the function at the sample point of parameters calculated by a certain method (analytical or numerical techniques) and:

C: a matrix comprising the derivatives of the function $\vec{X}_o = \vec{x}_o (\vec{X}_p)$ with respect to parameters and calculated by also analytical or numerical methods at the sample point of the parameter vector, $\vec{x}_p$, viz:

$$C_{ij} = \left| \frac{\partial x_{oi}(\vec{X}_p)}{\partial X_{pj}} \right|_{X_{pj}=x_{pj}} \qquad \begin{matrix} j = 1,2...r \\ i = 1,2...n-r \end{matrix} \qquad (6.8)$$

Then the most likely values $\vec{x}_p'$, $\vec{x}_o'$ of $E(\vec{X}_p)$, $E(\vec{X}_o)$ and estimates N_p', N_o' of the covariance matrices N_p, N_o based on the enlarged data ensemble $(\vec{x}_p, \vec{x}_o)$ can be obtained through the formulae:

$$\vec{P}' = RS^T(L + N)^{-1}\vec{D} \qquad (6.9)$$

$$R' = \sigma^2[R - RS^T(L + N)^{-1}SR] \qquad (6.10)$$

$$\vec{D}' = N(L + N)^{-1}\vec{D} \qquad (6.11)$$

$$L' = \sigma^2[N - N(L + N)^{-1}N] \qquad (6.12)$$

$$\chi^2 = g_E(\vec{D}, (L + N)^{-1}\vec{D}) \qquad (6.13)$$

$$\hat{\sigma}^2 = \chi^2/n-r \qquad (6.14)$$

where:

$$P_j' = \frac{x_{pj}' - x_{pj}}{x_{pj}} \qquad j = 1,2...r \qquad (6.15)$$

$$S_{ij} = \frac{x_{pj}}{x_{oi}^*} \left| \frac{\partial x_{oi}(\vec{X}_p)}{\partial X_{pj}} \right|_{X_{pj}=x_{pj}} \qquad \begin{matrix} j = 1,2...r \\ i = 1,2...n-r \end{matrix} \qquad (6.16)$$

$$L_{k\ell} = \frac{N_{ok\ell}}{x_{ok}^* x_{o\ell}^*} \qquad k,\ell = 1,2...n-r \qquad (6.17)$$

$$R_{k\ell} = \frac{N_{pk\ell}}{x_{pk} x_{p\ell}} \qquad k,\ell = 1,2...r \qquad (6.18)$$

$$N = S R S^T \qquad (6.19)$$

$$D_i = \frac{x_{oi} - x_{oi}^*}{x_{oi}^*} \qquad i = 1,2...n-r \qquad (6.20)$$

$$D_i' = \frac{x_{oi}' - x_{oi}^*}{x_{oi}^*} \qquad i = 1,2...n-r \qquad (6.21)$$

$$L_{k\ell}' = \frac{N_o'}{x_{ok}^* x_{o\ell}^*} \qquad k,\ell = 1,2...n-r \qquad (6.22)$$

$$R_{k\ell}' = \frac{N_p'}{x_{pk} x_{p\ell}} \qquad k,\ell = 1,2...r \qquad (6.23)$$

Working in terms of fractional quantities is both convenient in that it allows the adjustment factors, calculated via Eqn (6.15), to be applied indiscriminately to all fine group constants comprising a certain broad group without having to evaluate an average (i.e. spectrally dependent) value and compatible with the covariance matrices available.

An important characteristic of the least-squares method is that it does not require the multi-variate distributions to be normal, only that their first and second moments exist. (This implies the existence of the covariance matrix, see Appendix B).

However if we make the further assumptions that:

7. The multivariate distributions of both parameter evaluations and observed quantities are normal, and

8. The constant factor σ^2 in Eqns (6.10), (6.12) is unity, viz $\sigma^2 = 1$ (this amounts to accepting that the covariance matrices N_p, N_o are completely known).

Then we can test the "likelihood"of the input data prior to obtaining the solution by means of a chi-square test on χ^2 in terms of the input data only. Since in obtaining the value of χ^2 from Eqn (6.13) the linear approximation between observed quantities and parameters is used the chi-square test examines collectively both the consistency of the input data and the adequacy of the theory (1st order approximation). Consequently values of χ^2 significantly greater than expected may originate in inprecissions (random errors) and inaccuracies (systematic errors) in the input data unaccounted for, and/or in a failure of the linear model to describe the unknown relation between observed quantities and parameters.

Before proceeding to applying Eqns (6.9/14) to our cross-section adjustment problem it is worth examining how well the assumptions of the least squares method given above match the real situation concerning Transmissions and multigroup cross-sections.

We do not think that there is a need to comment upon assumptions 1, 3, 5 and 7 either because they are reasonable or because they have previously been discussed. For example, it has already been explained why Transmissions and cross-section evaluations can be considered stochastically independent (see page 63) or why they are meant to follow normal distributions.

Assumptions 2, 4, 6 and 8 are rather dubious and require some further explanation. First of all to accept that the covariance matrices of the multigroup cross-sections are either completely known or known with infite precision within a scalar factor σ^2contradicts both experimental information and theoretical reasoning. It has already been mentioned that the covariance matrices of the ENDF/B library contain approximate quantities whose magnitudes, even under the best of circumstances, are not known to better than about 30% (see page 240). It is also known that the variance terms of the covariance matrix are generally known with greater precision that the covariance terms but, even here, there will be considerable variation, as some quantities will be measured with far greater precision than others. Therefore to scale all the elements of a covariance matrix by an unknown factor and seek improvements of the error information in terms of estimates of this common factor, which some statistical methods may give, is far away from an objective and well-established technique in the field of statistical inference.

If the estimate $\hat{\sigma}^2$ of the scaling factor σ^2 is to have any meaning,the high value of χ^2 from which it arises (see Eqn. 6.14) must reflect an under-estimation of the error information of the input data rather than originate from any other deficiency of the whole procedure (e.g. omission of parameters, inadequate representation of existing correlations or of the function etc.). In most practical cases this cannot unequivocally be demonstrated and in our problem it does not happen.

However, very high values of χ^2 do not satisfy the chi-square test and consequently the subsequent $\hat{\sigma}^2$ estimates will be in fact meaningless. Another problem with the $\hat{\sigma}^2$ estimates, which arises from the use of parameter evaluations as additional observations, is that the scaling factor σ^2 should be the same for both N_p and N_o covariance matrices. Since $\vec{X}_p$ and $\vec{X}_o$ are stochastically independent random variables being measured by different processes, it is obvious that this assumption cannot safely be accommodated.

In the light of all the above reasoning we decided not to employ the capability of the least-squares method to provide an unbiased estimate of the scalar factor σ^2; setting in Eqns (6.10), (6.12) $\sigma^2=1$, we shall interpret high values of χ^2 not satisfying the chi-square test as proving inconsistency of the input data and/or incompatibility of the input data with theory (linear model). In such a case, the adjustment procedure will come to a halt and the possible sources of the inconsistences and/or incompatibilities will be carefully examined and, if possible, removed. On the other hand if the value of χ^2 is compatible with the pre-established significance level on the central chi-square distribution, the cross-section adjustment procedure will be carried on and new mean values and covariance estimates of both parameters and observed quantities, based on the enlarged data ensemble $(\vec{x}_p, \vec{x}_o)$, will be derived according to Eqns (6.9/ 12). The statistical consistency between measured and calculated Transmissions experienced in Chapter 5 indicates that this must be the case.

The adequacy of the linearization of the functional form between Transmission and multigroup cross-sections is also questionable. It is evident that the smaller the difference $X_{pi} - x_{pi}$, $i = 1,2....r$ in Eqn. (6.7), the better the linear approximation of the function $\vec{X}_o = \vec{x}_o(\vec{X}_p)$. The relatively small differences between measured and

and calculated Transmissions, presented in Table 14, generally imply small cross-section adjustments and therefore Eqn (6.7) is expected to be adequately valid. However, calculational errors in the determination of both the expansion point $\vec{x}_o^* = \vec{x}_o(\vec{x}_p)$ and the elements of the design matrix C_{ij} (see Eqns (6.7), (6.8)) through proper numerical techniques should be kept at minimum if the linear model is to be of any use. Finally high values of χ^2 and alternative general methods of calculating the Transmissions at the new estimates of the multigroup cross-sections can be used in judging the efficiency and adequacy of the linear model.

Another point which deserves some consideration is the choice of Transmissions to be finally used in the adjustment procedure and the choice of parameters (multigroup cross-sections etc.) for adjustment. According to what has been discussed so far, it is evident that only multigroup cross-sections can be included in the adjustment procedure. Furthermore, the analysis undertaken in Chapter 5 excludes the use of the $^{237}N_p(n,f)F.P$ Transmissions for the following reasons:

1. The relatively high sensitivity of these Transmissions to the $^{237}N_p(n,f)F.P$ reaction in conjunction with the relatively low uncertainty of the calculated values due to the iron cross-section data used (see Figure 78 and Table 30) make the inclusion of the $^{237}N_p(n,f)F.P$ dosimetry data in any uncertainty and consistency studies unavoidable.

2. At the time the present work was undertaken, reliable multigroup covariance information concerning the above dosimetry reaction was not available.

3. Inclusion of the $^{237}N_p$ Transmissions in the adjustment procedure without considering the $^{237}N_p(n,f)F.P$ cross-section data as adjustable parameters gave unacceptably high values of χ^2 (around

5 per degree of freedom).

Therefore we are left with the $^{27}A\ell$ and ^{238}U Transmissions, and multigroup iron and dosimetry cross-sections as observed integral quantities and adjustable parameters, respectively.

The adjustment procedure developed in Appendix B requires the adjustable multigroup parameters to have the same energy group structure. For the multigroup covariance information available and concerning iron and dosimetry cross-section data this is not the case, as is easily seen in Tables 25 - 29. Moreover, it has already been demonstrated that the calculated Transmissions are much more sensitive to iron than to $^{27}A\ell(n,p)^{27}Mg$ and $^{238}U(n,f)$F.P dosimetry cross-sections, and that these reaction cross-sections are not, at least, less known than those of iron; it has also been found that the uncertainty of calculated Transmissions due to dosimetry data is negligibly small compared with that originating from the iron cross-sections. (see Table 30). All these reasons prompt us to exclude the $^{27}A\ell(n,p)^{27}Mg$ and $^{238}U(n,f)$ F.P dosimetry data from the adjustment procedure. Hence, $^{27}A\ell$ and ^{238}U Transmissions will constitute the observed quantities, while broad-group elastic and non-elastic iron cross-sections will be the adjustable parameters.

6.4 CROSS-SECTION ADJUSTMENTS

The formulae:

$$\chi^2 = g_E(\vec{D}, (L+N)^{-1}\vec{D}) \quad (6.24)$$

$$\vec{P}' = RS^T(L+N)^{-1}\vec{D} \quad (6.25)$$

$$R' = R - RS^T(L+N)^{-1} SR \quad (6.26)$$

with:

$$N = S \; R \; S^T$$

were finally used in examining both the consistency of the input data and the adequacy of the linear model, and in obtaining the fractional cross-section adjustments of elastic and non-elastic broad-group iron cross-sections and their new covariance matrices, based on the enlarged data ensemble of experimental Transmissions and cross-section evaluations.

A FORTRAN programme, called ATHENE, was written to make the matrix manipulations involved in the above equations.

Both ENDF/B-IV (DLC-37F version) and UKNDL(2) iron multigroup cross-sections were used enabling thus to study the convergence of the adjusted sets towards a better final library.

The relative broad group covariance matrix of iron cross-sections required in Eqns (6.25) and (6.26) (matrix R) was constructed from Tables 25, 26 and 27. The same matrix was obviously used for both libraries.

The relative covariance matrix of the measured Transmissions was taken to be diagonal. Its variance terms were calculated from the standard deviations and experimental values given in Table 14. Any correlations between experimental Transmissions could only be introduced by uncertainties in the corrections applied to measured values and accounting for the deviations of source spectrum from ^{235}U-fission and the counter assymetry. (see pages 47-55). The analysis followed in Chapter 2 and the fact that the total uncertainty of experimental Transmissions

almost coincides with the statistical error (see Table 2A) justifies the diagonal representation of Transmission covariance matrix. This is given in Table 36.

The elements of the fractional design matrix (see Eqn (6.16)) were taken from Table 31 for the ENDF/B-IV library and from Table 37 for the UKNDL. Note that the broad-group sensitivity coefficients are approximately the same for both libraries, something which reinforces the validity of the linear model.

Finally, the vectors of fractional differences between experimental and calculated Transmissions for both libraries (see Eqn. (6.20))are given in Table 38 and have been calculated from Table 14.

Eqn (6.24) gave the following values for χ^2

$$\chi^2 = \begin{cases} 7.44 & \text{for E N D F/B-IV} \\ 7.05 & \text{for U K N D L} \end{cases}$$

The total number of input quantities to the cross-section adjustment problem is n = the number of broad group cross-sections (r parameters) + the number of experimental Transmissions (n-r observed integral quantities), that is, n = 18 + 4 = 22. Since we solve for the broad

TABLE 38 FRACTIONAL DIFFERENCES BETWEEN EXPERIMENTAL AND CALCULATED TRANSMISSIONS IN IRON SHELLS.

DATA LIBRARY \ D_i	D_1	D_2	D_3	D_4
ENDF/B-IV	2.624E-02	3.001E-03	1.091E-02	4.427E-02
U K N D L	1.340E-02	-7.539E-03	-1.300E-02	-7.820E-03

group cross-sections, the number of degrees of freedom will be n-r = 22-18 = 4. The probability that $\chi^2 \geq 7.4$ (or 7.05) is found, from statistical Tables (11), to be approximately 0.15 which is a very good value,taking into consideration the various approximations made.

TABLE 36. RELATIVE COVARIANCE MATRIX OF EXPERIMENTAL TRANSMISSIONS IN IRON SHELLS.

TRANSMISSION		T_1	T_2	T_3	T_4
		d = 1.9 cm $^{27}Al(n, P)^{27}Mg$	d = 1.9 cm $^{238}U(n, f)F.P.$	d = 4.11 cm $^{238}U(n, f)F.P.$	d = 9.16 cm $^{238}U(n, f)F.P.$
T_1	d = 1.9 cm $^{27}Al(n, P)^{27}Mg$	8.000 E-05	0	0	0
T_2	d = 1.9 cm $^{238}U(n, f)F.P.$	0	4.782 E-06	0	0
T_3	d = 4.11 cm $^{238}U(n, f)F.P.$	0	0	7.863 E-06	0
T_4	d = 9.16 cm $^{238}U(n, f)F.P.$	0	0	0	7.629 E-05

TABLE 37. BROAD GROUP SENSITIVITY COEFFICIENTS OF TRANSMISSIONS TO IRON ELASTIC AND NON-ELASTIC CROSS SECTIONS (U K N D L (2)).

SHELL THICKNESS cm	DETECTOR	BROAD GROUP SENSITIVITIES									TOTAL (ENERGY INTEGRATED) SENSITIVITY	SENSITIVITY TO TOTAL
		BROAD GROUP NUMBER	1	2	3	4	5	6	7	8	9	
		FINE GROUPS INVOLVED	1-13	14-18	19-25	26-28	29-32	33-34	35	36	37-55	
		REACTION										
1.90	$^{27}Al(n, P)^{27}Mg$	ELASTIC	-1.838 E-02	-7.423 E-03	-7.645 E-06	0	0	0	0	0	0	-2.580 E-02	-2.728 E-01
		NON-ELASTIC	-2.129 E-01	-3.394 E-02	-1.355 E-05	0	0	0	0	0	0	-2.470 E-01	
	$^{238}U(n, f)F.P.$	ELASTIC	-3.679 E-03	-8.351 E-03	-1.413 E-02	-4.300 E-04	-6.085 E-06	1.501 E-07	5.870 E-07	6.172 E-07	5.920 E-07	-2.660 E-02	-1.683 E-01
		NON-ELASTIC	-3.674 E-02	-4.357 E-02	-6.022 E-02	-1.154 E-03	-1.180 E-07	-5.690 E-08	-1.150 E-08	-1.010 E-08	-9.400 E-09	-1.417 E-01	
4.11	$^{238}U(n, f)F.P.$	ELASTIC	-1.160 E-02	-3.139 E-02	-4.540 E-02	-1.154 E-03	-1.670 E-05	2.938 E-06	2.818 E-06	3.732 E-06	3.700 E-06	-8.966 E-02	-4.291 E-01
		NON-ELASTIC	-8.168 E-02	-1.081 E-01	-1.466 E-01	-3.059 E-03	-3.800 E-07	-2.260 E-07	-5.400 E-08	-5.900 E-08	-2.000 E-07	-3.394 E-01	
9.16	$^{238}U(n, f)F.P.$	ELASTIC	-2.721 E-02	-8.193 E-02	-1.259 E-01	-3.681 E-03	-6.483 E-05	4.187 E-06	8.995 E-06	1.663 E-05	1.850 E-05	-2.388 E-01	-9.811 E-01
		NON-ELASTIC	-1.619 E-01	-2.388 E-01	-3.332 E-01	-8.009 E-03	-1.300 E-06	-8.690 E-07	-2.390 E-07	-3.300 E-07	-4.200 E-07	-7.423 E-01	

Consequently we can confidently proceed to the next stage of adjusting the cross-sections and re-estimating their covariance information, since the assumptions and approximations made are judged reasonable by the chi-square test. We contend that the relatively high value of χ^2 obtained reflects rather the omission of other nuclear data parameters from the least-squares model than an under-estimation of the variance and/or covariance terms of the a priori covariance information used.

Table 39 gives the percentage adjustments applicable to iron broad-group elastic and non-elastic cross-sections for both libraries; the a priori and a posteriori percentage standard deviations of these cross-sections are also included in this Table. They have been calculated from the variance terms of the new covariance matrix R' which is presented in Tables 40, 41, 42 for the ENDF/B-IV library only. The results of Table 39 show that:

1. The adjustment procedure essentially affects the first three broad energy groups, as expected from the broad-group sensitivity profiles.

2. Both the magnitude and the sign of the adjustments differ greatly for the two data libraries. This is a consequence of the relatively large differences between the two sets of calculated Transmissions, as seen in Table 14.

3. The adjustments for both reactions are relatively small and are within the corresponding standard deviations of the broad group cross-sections for both libraries. This is not a surprising result since it verifies the statistical consistency between experimental Transmissions and cross-section evaluations; this has already been demonstrated both in Figure 81 and by the meaningful values of χ^2.

4. Significant improvements (up to 200%) in the standard deviations of the iron broad-group elastic and non-elastic cross-sections

TABLE 39. PERCENTAGE ADJUSTMENT FACTORS AND STANDARD DEVIATIONS FOR IRON BROAD GROUP ELASTIC AND NON-ELASTIC CROSS SECTIONS. (ENDF/B-IV and U K N D L.)

GROUP NUMBER	ENERGY RANGE (MeV)	ELASTIC					NON-ELASTIC				
		ADJUSTMENT FACTOR (%)		S.D. BEFORE ADJUSTMENT (%)	S.D. AFTER ADJUSTMENT (%)		ADJUSTMENT FACTOR (%)		S.D. BEFORE ADJUSTMENT (%)	S.D. AFTER ADJUSTMENT. (%)	
		ENDF/B-IV	U.K.N.D.L.		ENDF/B-IV	U.K.N.D.L.	ENDF/B-IV	U.K.N.D.L.		ENDF/B-IV	U.K.N.D.L.
1	14.9 - 0.71	8.77	5.51	12.2	4.0	4.2	-9.79	- 6.00	14.1	4.3	4.6
2	4.4 - 2.6	0.49	-6.25	9.3	5.6	5.6	-2.43	10.06	15.5	5.2	5.2
3	2.6 - 1.35	0.88	-1.97	3.9	2.3	2.3	-1.95	4.52	7.9	2.4	2.4
4	1.35 - 0.71	0.01	-0.13	1.8	1.8	1.8	-0.45	0.23	5.8	5.7	5.7
5	0.71 - 0.58	0	0	2.6	2.6	2.6	-0.01	0	20.0	20.0	20.0
6	0.58 - 0.41	0	0	2.2	2.2	2.2	0	0	15.6	15.6	15.6
7	0.41 - 0.30	0	0	3.0	3.0	3.0	0	0	20.0	20.0	20.0
8	0.30 - 0.26	0	0	2.8	2.8	2.8	0	0	20.0	20.0	20.0
9	0.26 - 0.06	0	0	1.2	1.2	1.2	0	0	13.0	13.0	13.0

TABLE 40. RELATIVE BROAD GROUP COVARIANCE MATRIX OF IRON ELASTIC CROSS SECTION AFTER ADJUSTMENT.

ELASTIC	GROUP	1	2	3	4	5	6	7	8	9
	1	1.616 E-03	-5.926 E-04	-8.587 E-04	2.314 E-05	-1.836 E-07	1.521 E-08	3.711 E-09	3.489 E-09	6.956 E-10
	2		3.119 E-03	-6.593 E-05	-1.619 E-04	6.358 E-07	-6.658 E-08	-1.129 E-08	-8.188 E-09	-1.485 E-09
	3			5.307 E-04	6.558 E-05	2.845 E-07	-2.902 E-08	-5.391 E-09	-4.112 E-09	-7.624 E-10
	4				3.191 E-04	2.213 E-04	-2.231 E-09	-4.120 E-10	-3.407 E-10	-6.503 E-11
	5					6.760 E-04	9.724 E-05	2.274 E-11	2.776 E-11	5.905 E-12
	6						4.840 E-04	3.009 E-04	2.210 E-05	-3.406 E-13
	7							9.000 E-04	6.638 E-05	-1.166 E-13
	8								7.840 E-04	1.545 E-05
	9									1.440 E-04

TABLE 41. RELATIVE BROAD GROUP COVARIANCE MATRIX OF IRON NON-ELASTIC CROSS SECTION AFTER ADJUSTMENT.

NON-ELASTIC	GROUP	1	2	3	4	5	6	7	8	9
	1	1.862 E-03	-1.128 E-03	-3.225 E-04	1.431 E-04	6.419 E-07	4.806 E-07	1.811 E-08	1.857 E-08	9.917 E-09
	2		2.737 E-03	-6.551 E-04	-1.432 E-03	-3.910 E-06	-2.914 E-06	-6.067 E-08	-6.238 E-08	-3.253 E-08
	3			5.794 E-04	7.432 E-04	-2.201 E-06	-1.641 E-06	-3.933 E-08	-4.041 E-08	-2.122 E-08
	4				3.258 E-03	2.196 E-04	1.627 E-04	-8.241 E-09	-8.453 E-09	-4.490 E-09
	5					4.000 E-02	2.935 E-02	-1.348 E-10	-1.380 E-10	-7.439 E-11
	6						2.433 E-02	1.054 E-02	1.054 E-02	4.745 E-03
	7							4.000 E-02	4.000 E-02	1.796 E-02
	8								4.000 E-02	1.796 E-02
	9									1.690 E-02

TABLE 42. RELATIVE BROAD GROUP COVARIANCE MATRIX OF IRON ELASTIC TO IRON NON-ELASTIC CROSS SECTION AFTER ADJUSTMENT.

ELASTIC \ NON-ELASTIC	GROUP	1	2	3	4	5	6	7	8	9
	1	-1.618 E-03	1.112 E-03	3.821 E-04	-1.081 E-04	-4.119 E-07	-3.080 E-07	-1.018 E-08	-1.045 E-08	-5.555 E-09
	2	6.873 E-04	-2.468 E-03	7.077 E-04	7.229 E-04	1.825 E-06	1.359 E-06	2.356 E-08	2.424 E-08	1.252 E-08
	3	1.802 E-04	-1.827 E-04	-9.467 E-05	4.988 E-05	7.891 E-07	5.879 E-07	1.175 E-08	1.209 E-08	6.289 E-09
	4	-2.989 E-05	3.182 E-04	-1.982 E-04	-3.248 E-04	6.161 E-08	4.593 E-08	1.005 E-09	1.032 E-09	5.406 E-10
	5	3.048 E-07	-1.438 E-06	-8.521 E-07	-9.208 E-06	-9.360 E-05	-3.650 E-05	-8.522 E-11	-8.715 E-11	-4.716 E-11
	6	-2.378 E-08	1.435 E-07	8.094 E-08	-7.647 E-06	-7.480 E-05	-3.432 E-05	-1.320 E-05	-2.200 E-05	-1.114 E-05
	7	-6.317 E-09	2.696 E-08	1.641 E-08	2.975 E-09	4.002 E-11	-1.404 E-05	-5.400 E-05	-8.400 E-05	-4.290 E-05
	8	-6.194 E-09	2.109 E-08	1.362 E-08	2.792 E-09	4.500 E-11	-1.310 E-05	-5.040 E-05	-7.840 E-05	-4.000 E-05
	9	-1.250 E-09	3.947 E-09	2.606 E-09	5.559 E-10	9.407 E-12	-3.744 E-06	-1.440 E-05	-2.400 E-05	-2.652 E-05

in the sensitive energy region have been deduced by the adjustment model applied. This is a much more important result in practical terms than the adjusted optimised data sets themselves, as will be demonstrated later.

Comparing the relative multigroup covariance matrices of elastic and non-elastic iron cross-sections before and after the adjustment (Tables 25, 26, 27 and Tables 40, 41 and 42, respectively), the existence of non-zero correlations between all the groups and reactions in the a posteriori matrices is the first thing to note. The statistical model used has injected correlations in places where they did not exist before (though in most cases these injected correlations are negligibly small and have no practical significance) and has largely modified existing correlations in the sensitive energy region. More precisely, it is noted that in the sensitive energy region where the adjustments are not zero (the first four energy groups) the a priori positive energy-dependent correlations in both reactions (covariance terms in Tables 25, 26 and Tables 40 and 41, respectively) have changed both in sign and magnitude to such an extent that the initial covariance information, based on cross-section measurements and evaluations, has been totally replaced by mathematical, non-observational correlations introduced by the statistical model. Moreover, relatively high correlations have been generated by the model between groups in the sensitive energy region whose a priori correlations were zero. (Covariance terms between groups 1, 4 and 2, 4 in Tables 40 and 41). In the non-sensitive energy region (energy groups 5 to 9) both variance and covariance terms have been left almost intact by the model, with the non-zero terms - replacing the zero ones in the a priori matrices- having no practical meaning.

With respect to the partial correlations between elastic and non-elastic

cross-sections (Tables 27 and 42), it is noticed that the diagonal terms of the a posteriori covariance matrix are of the same sign and smaller magnitude, while the off-diagonal terms are of opposite sign and are larger.

Mathematical, non-observational correlations injected by the statistical model used can swamp the original information based on measurements and evaluations, and therefore consistency analysis constitutes an alternative method for generating reliable covariance information suitable, at least, for those design situations whose environment resembles that of the consistency analysis experiment. The effect of these correlations on the uncertainty of a certain calculated integral quantity in terms of the adjusted data set will be examined in the following section.

6.5 ASSESSMENT OF THE ADJUSTED CROSS-SECTION DATA SETS

The adjusted cross-section sets which incorporate more experimental information are expected to be better than the original data libraries. However, the condensed form in which the a priori covariance information was available required the adjustment procedure to be accomplished in terms of broad-groups for the elastic and non-elastic components of the total neutron cross-section. This is a severe drawback of the method since all the fine group cross-sections comprising a certain broad group are adjusted by the same factor, although the sensitivity of the integral quantity to these constants varies significantly, as has already been demonstrated. Something analogous happens with the different components of the non-elastic cross section. For example, the absorption cross-section is adjusted by the same factor as the inelastic,although the Transmission is practically insensitive to absorption.

For the above reasons we expect the adjusted data sets to give good results in situations characterized by sensitivity profiles similar to that of the consistency analysis problem. It can therefore be said that the poor quality of the a priori covariance information available renders the deduced cross-section adjustments problem-dependent and that the adjusted data sets may give erroneous results if applied to substantially different environments.

In the light of the above arguments we intend to check the superiority of the adjusted sets over the corresponding data libraries using the following criteria:

I. How well the adjusted sets predict the Transmissions used in the adjustment procedure.

II. How well the adjusted sets predict Transmissions which have not been included in the adjustment procedure.

III. How well the adjusted sets are compared to each other,

that is, are they in better agreement than the original libraries not only in predicting a certain integral quantity but also in terms of their elastic and non-elastic components?

6.5.1 New Estimates of Transmissions and their Uncertainties.

The formulae:

$$\vec{D}' = N(L+N)^{-1}\vec{D} \qquad (6.27)$$

$$L' = N - N(L+N)^{-1}N \qquad (6.28)$$

were used in calculating the new values of Transmissions and their covariance matrix based on the enlarged data ensemble of experimental Transmissions and cross-section evaluations.

Table 43 presents the new values of Transmissions calculated via Eqn. (6.27) (linear model) and their percentage standard deviations estimated from the variance terms of the covariance matrix L'. Also included in the Table are the experimental and ANISN-calculated Transmissions using both the original ENDF/B-IV and U K N D L files, and the adjusted data sets. The percentage standard deviations of both experimental and calculated Transmissions prior to adjustment also appear. (It should be mentioned here that the standard deviations of Transmissions calculated in terms of the U K N D L adjusted set are almost the same as those of the ENDF/B-IV adjusted set for obvious reasons; that is why they have been omitted in Table 43. Also the variance terms of the L' matrix are approximately the same as those found separately for each Transmission by using the new covariance matrix of the cross-sections R' in the programme UNCERT (see pages 262-263)).

The following conclusions can be drawn from the results of Table 43.

1. The two adjusted data sets give essentially the same values of calculated Transmissions. Indeed the re-estimated Transmissions, obtained via the linear model, are almost identical for the two libraries

TABLE 43. IRON TRANSMISSIONS AND THEIR UNCERTAINTIES BEFORE AND AFTER ADJUSTMENT

CASE	TRANSMISSIONS					PERCENTAGE STANDARD DEVIATIONS		
	EXPERIMENTAL	ANISN-CALCULATED BEFORE ADJUSTMENT	CALCULATED VIA LINEAR MODEL (Eqn. 6.27)	ANISN-CALCULATED AFTER ADJUSTMENT	DATA SET	EXPERIMENTAL TRANSMISSION	CALCULATED TRANSMISSION BEFORE ADJUSTMENT	CALCULATED TRANSMISSION AFTER ADJUSTMENT
$^{27}Al(n, P)^{27}Mg$ d = 1.9 cm	0.7938	0.7735	0.7899	0.7889	ENDF/B-IV	0.89	3.00	0.83
		0.7833	0.7899	0.7897	U.K.N.D.L.			
$^{238}U(n, f)F.P.$ d = 1.9 cm	0.8688	0.8662	0.8713	0.8710	ENDF/B-IV	0.22	1.20	0.09
		0.8754	0.8714	0.8718	U.K.N.D.L.			
$^{238}U(n, f)F.P.$ d = 4.11 cm	0.7132	0.7055	0.7146	0.7145	ENDF/B-IV	0.28	2.76	0.21
		0.7226	0.7146	0.7155	U.K.N.D.L.			
$^{238}U(n, f)F.P.$ d = 9.16 cm	0.4694	0.4495	0.4613	0.4614	ENDF/B-IV	0.87	5.92	0.47
		0.4731	0.4614	0.4624	U.K.N.D.L.			

while the ANISN-recalculated ones present negligibly small differences compared with that of the initially calculated values. However, it remains to be seen how the broad group elastic and non-elastic iron cross-sections of the two adjusted sets actually compare.

2. The re-estimated Transmissions are generally closer to the corresponding experimental values than those calculated from the unadjusted data libraries. It is noticed, however, that some re-estimated values depart from that approach to the corresponding experimental Transmissions. This is not unexpected since the statistical combination of the experimental and calculated Transmissions (corresponding to cross-section evaluations) was undertaken simultaneously for all of them and not for each one separately. Consequently we expect the re-calculated Transmission vectors $\vec{T}'_{C,ENDF}$, $\vec{T}'_{C,UKNDL}$ to lie closer to experimental $\vec{T}_E$ than the initially calculated $\vec{T}_{C,ENDF}$, $\vec{T}_{C,UKNDL}$, something which does not exclude the possibility of some of their individual components not following this behaviour. Figure 82 was constructed by considering the experimental and calculated Transmission sets as vectors in a four-dimensional orthonormal space. The angles shown were obtained from the definition of the inner product between any two vectors of that space. It is clearly shown in this Figure that the re-calculated Transmission vectors $\vec{T}'_{C,ENDF}$, $\vec{T}'_{C,UKNDL}$ are closer to each other and also to the experimental vector $\vec{T}_E$ than were $\vec{T}_{C,ENDF}$ and $\vec{T}_{C,UKNDL}$. (Looking at this Figure bear in mind that the vectors shown are not meant to lie in the same plane).

3. The very small discrepancies between the linear model and ANISN re-calculated Transmissions demonstrate the adequacy and effectiveness of the linear approximation in our problem. Had not this been the case, higher values of χ^2 could have been obtained and an iterative scheme (Eqns (B.66/68), Appendix B) would have been unavoidable.

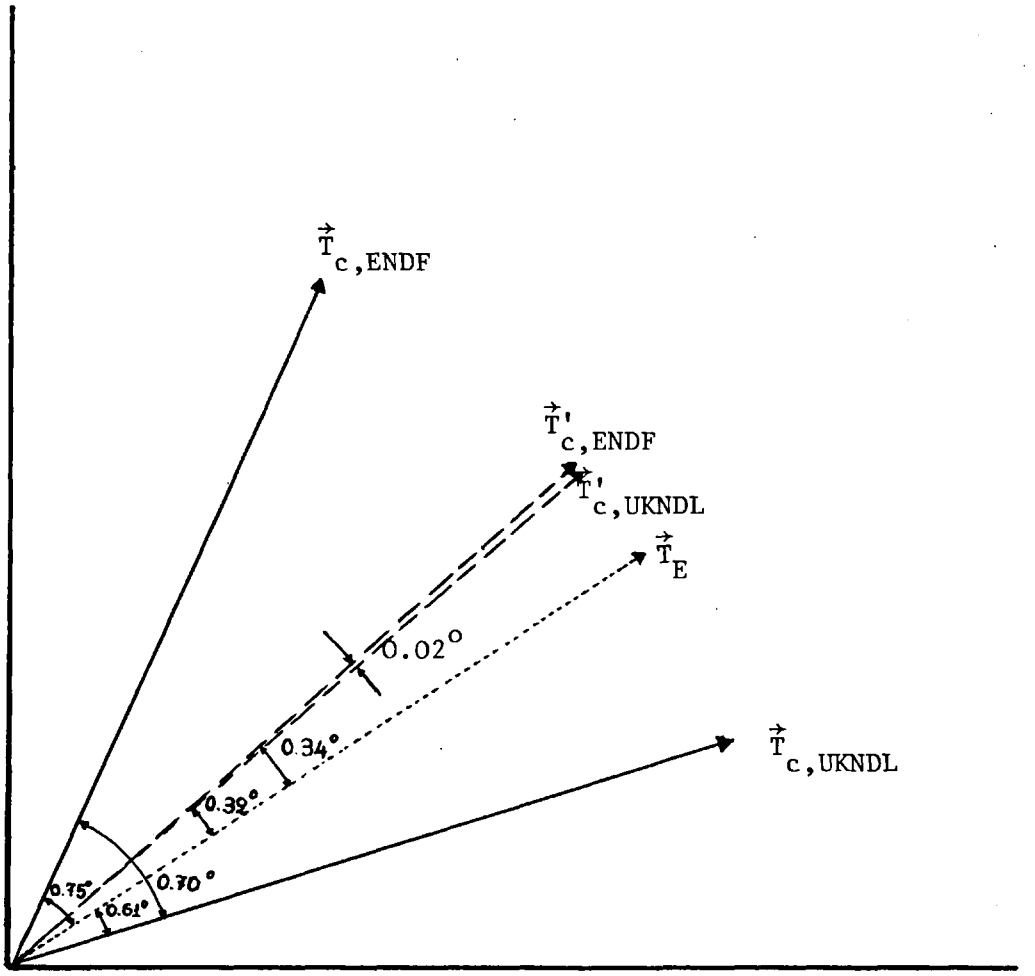
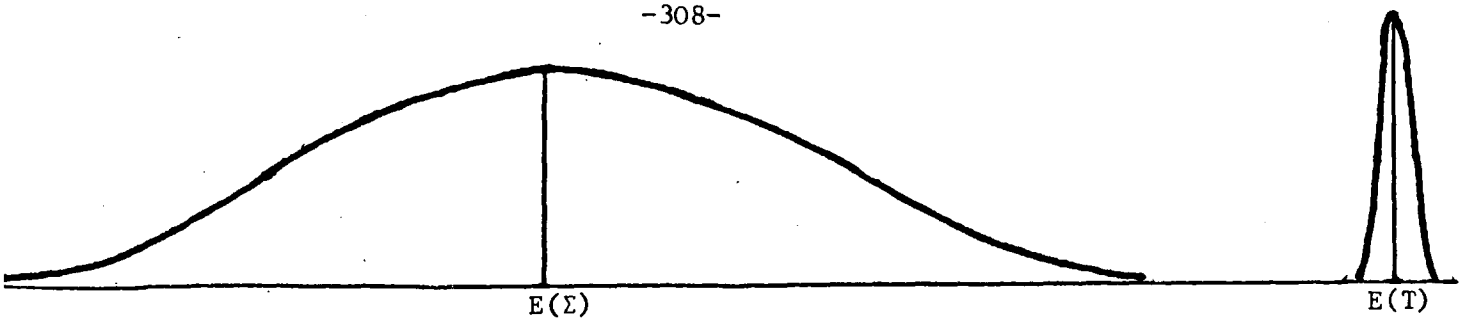
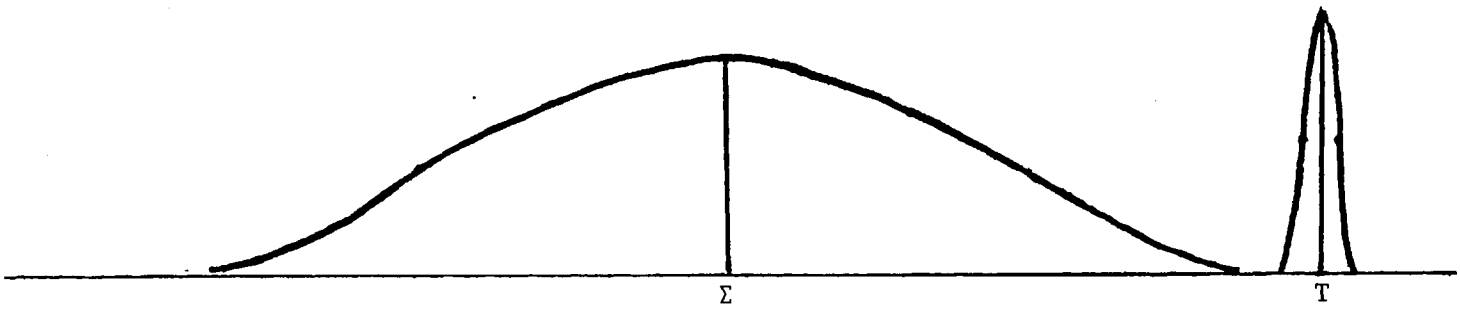


FIGURE 82. RELATION BETWEEN EXPERIMENTAL, CALCULATED AND RE-ESTIMATED TRANSMISSION VECTORS.

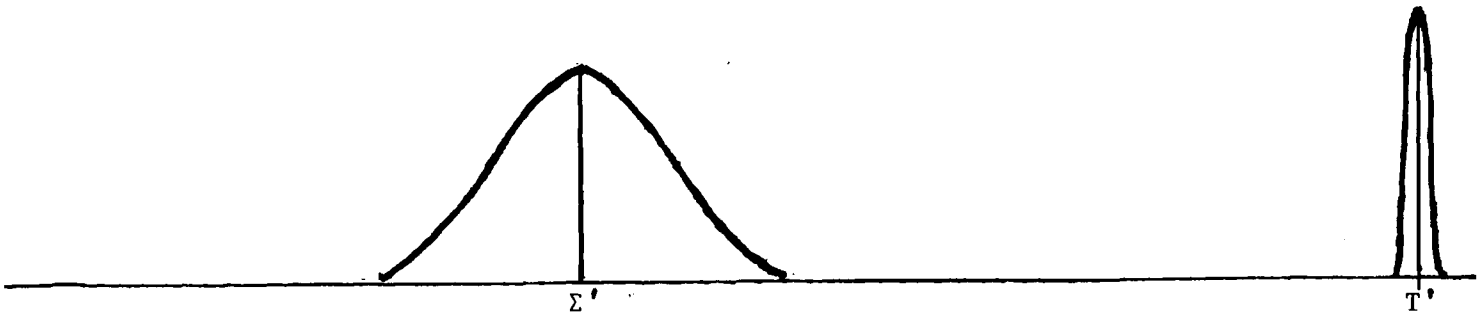
4. The standard error of the re-estimated Transmissions is much smaller than that based on the a priori covariance information and lower than that of the experimental value for all the cases. This noticeable difference indicates that in the process of statistical combination of the two sets of observations (experimental Transmissions and cross-section evaluations), more information is passed from Transmissions to cross-sections than that in the opposite direction. The above relations are depicted in Figure 83 where one Transmission (^{238}U(n,f)F.P, d = 9.16) and one broad group cross-section (non-elastic, 2nd broad group) are picked up from the corresponding vectors



I. True distributions with unknown means and fully known variances.
$\Delta\Sigma/\Sigma = 0.155$, $\Delta T/T = 0.0087$



II. Sample points of the two distributions.
$\Delta\Sigma/\Sigma = 0.155$, $\Delta T/T = 0.0087$ (before adjustment)



III. Estimates of the means and new variances based on the sample points and the linear relationship connecting the two distributions.
$(\Delta\Sigma/\Sigma)' = 0.052$, $(\Delta T/T)' = 0.0047$ (after adjustment)

FIGURE 83. NORMAL DISTRIBUTIONS OF MEASURED TRANSMISSIONS AND CROSS-SECTION EVALUATIONS BEFORE AND AFTER ADJUSTMENT.

and presented as if they were following uni-variate normal distributions. The greater improvement in terms of cross-sections than Transmissions depicted in this Figure and originating from the fact that the experimental Transmissions are better known than the cross-sections (or, equivalently, the calculated Transmissions), demonstrates the important role that suitable and precise integral experiments can play in improving our current knowledge of nuclear data.

6.5.2 Calculation of Transmissions and their Uncertainties in Terms of both Unadjusted and Adjusted Data Sets

The ^{238}U(n,f)F.P Transmission in the iron shell of thickness 3.795 cm (case 9 in Table 1) was used to assess the improvement of the adjusted data sets (both values and error information) over the original data files. Table 44 gives the ANISN calculated and re-calculated (in terms of the adjusted data file) values of this Transmission for both libraries together with its experimental value. The percentage standard deviations estimated via Eqn (5.18) and the effect of various correlations in both the adjusted and unadjusted covariance matrices on that uncertainty are also included.

The superiority of the adjusted data sets in predicting integral quantities of the same sensitivity profile as that of the adjustment procedure is very clear in this Table. The adjusted data sets, though derived from different libraries, essentially give the same calculated value which also lies nearer the experimental than that of the original data libraries. Hence, as far as the calculation of these integral quantities is concerned the original data libraries converge through the adjustment procedure to a better final library which yields much better results than themselves.

Not only are the re-calculated values in better agreement with the measured ones but also their uncertainties are significantly reduced

TABLE 44. CALCULATED VALUES AND STANDARD DEVIATIONS OF A TRANSMISSION BEFORE AND AFTER ADJUSTMENT.

EXPERIMENTAL		CALCULATED								
			PRIOR TO ADJUSTMENT				AFTER ADJUSTMENT			
TRANSMISSION	STANDARD DEVIATION (%)	DATA SET	TRANSMISSION	S.D. WITH FULL COVARIANCE INFORMATION (%)	S.D. WITH PARTIAL CORRELATIONS SUPPRESSED (%)	S.D. WITH ALL CORRELATIONS SUPPRESSED (%)	TRANSMISSION	S.D. WITH FULL COVARIANCE INFORMATION (%)	S.D. WITH PARTIAL CORRELATIONS SUPPRESSED (%)	S.D. WITH ALL CORRELATIONS SUPPRESSED (%)
0.7424	0.24	ENDF/B-IV	0.7370	2.42 or (± 0.018)	2.78	2.19	0.7452	0.18 or (± 0.0013)	0.28	0.75
		U.K.N.D.L.	0.7529				0.7464			

compared with those of the original libraries. For instance, it is noticed in Table 44 that the fractional uncertainty of Transmission is reduced by a factor 13 in going from the original to adjusted data set. Note that both calculated Transmissions are consistent within the uncertainty accompanying them both before and after the adjustment.

The role of both partial and energy-dependent correlations of the cross-section covariance matrix is significantly different between unadjusted and adjusted data sets in determining the uncertainty of an integral quantity. However, the reduction of the standard deviations of the broad group iron cross-sections in going from the original to the adjusted data set, shown in Table 39, is largely responsible for the resulting improvement in the calculated uncertainty of Transmission. This is easily seen in Table 44 by comparing the calculated uncertainties before and after adjustment with all correlations suppressed. But the effects and relative importance of both kinds of correlations in the adjusted and unadjusted sets are not the same at all. The omission of the energy-dependent correlations underestimates the uncertainty of Transmission by 21% in the unadjusted data set, while it over-estimates it by 167% in the adjusted one. Similarly the omission of partial correlations, though in both cases it over-estimates the Transmission uncertainty, is relatively more important for the adjusted set than it is for the original library. The above conclusions are compatible with the replacement of the observational, positive, energy-dependent correlations of the a priori covariance matrix by mathematical, negative ones in the a posteriori covariance matrix injected by the statistical model used. This very fact explains why it is sometimes preferable and more convenient to simulate a certain design situation by a suitable experiment and reliably deduce the appropriate covariance information needed by

employing consistency analysis techniques and informed guesses of the a' priori covariance matrix, than to embark on a detailed study and assessment of all possible correlations underlying the basic nuclear data, group collapsing etc.

6.5.3 Comparison of the Adjusted Data Sets.

In the present section the two adjusted libraries will be compared and the convergence towards a better final library will be examined.

Broad group elastic and non-elastic iron cross-sections were generated from the ENDF/B-IV and U K N D L files for the first three broad groups (for the rest of the groups the adjustments are practically zero) using the fission spectrum as a weighting function. (Any reasonable weighting function can be used in this process since the only assumption made in formulating the adjustment problem in a broad-group scheme was that the fine-group cross-sections within a certain broad group are fully correlated and have the same fractional uncertainty, see Eqn. (5.14)).

Table 45 presents the unadjusted and adjusted broad-group elastic and non-elastic iron cross-sections for both libraries together with the a' priori and a'posteriori standard deviations. Fission spectrum - averaged elastic and non-elastic cross-sections over the energy range covered by the first three broad groups are also included for both the adjusted and unadjusted data sets.

It is noticed in this Table that adjusted broad group constants are generally closer than their unadjusted counterparts. The 2nd broad-group does not follow this trend but this does not destroy the tendency of the two libraries to approach each other after adjustment, as can be seen by comparing the fission spectrum-averaged elastic and non-elastic cross-sections before and after adjustment. What is more

TABLE 45. ADJUSTED AND UNADJUSTED BROAD GROUP ELASTIC AND NON-ELASTIC IRON CROSS SECTIONS.

BROAD GROUP	DATA SET	UNADJUSTED SETS				ADJUSTED SETS			
		ELASTIC		NON-ELASTIC		ELASTIC		NON-ELASTIC	
		σ_E barns	S.D. barns	σ_{NON} barns	S.D. barns	σ_E barns	S.D. barns	σ_{NON} barns	S.D. barns
1 (1-13)	ENDF/B-IV	2.112	± 0.26	1.533	± 0.22	2.297	± 0.09	1.383	± 0.06
	U.K.N.D.L.	2.209	± 0.27	1.435	± 0.20	2.330	± 0.09	1.349	± 0.06
2 (14-18)	ENDF/B-IV	2.317	± 0.21	1.140	± 0.17	2.328	± 0.13	1.112	± 0.06
	U.K.N.D.L.	2.371	± 0.22	1.090	± 0.17	2.222	± 0.12	1.199	± 0.06
3 (19-25)	ENDF/B-IV	2.310	± 0.09	0.740	± 0.06	2.328	± 0.05	0.726	± 0.02
	U.K.N.D.L.	2.349	± 0.09	0.691	± 0.05	2.303	± 0.05	0.722	± 0.02
Average	ENDF/B-IV	2.277		1.001		2.322		0.960	
	U.K.N.D.L.	2.331		0.943		2.282		0.979	

important is that the unadjusted broad-group elastic and non-elastic values for the two libraries, which were consistent within one standard deviation (viz, a certain broad group constant from one library lies within the corresponding value from the other library $\pm$ one standard deviation), remain consistent and after adjustment despite the significant reduction of the standard error. What, therefore, is shown in Table 45 is that the broad-group constants of the two libraries get closer after adjustment, while simultaneously the error bounds are significantly reduced.

6.6 PHYSICAL INTERPRETATION OF THE OBSERVED ADJUSTMENTS

The only interpretation which can, so far, unambigiously be given to the cross-section adjustments deduced by the least-squares method and within the domain of 1st order approximation is that they create "artificial" data libraries whose common characteristic is that they give approximately the same calculated values for some integral quantities; the starting point for the adjustment procedure could be any data library provided that the 1st-order approximation is sufficient and that experimental and calculated integral quantities are statistically consistent. These integral quantities calculated in terms of the "artificial data libraries" are meant to lie nearer the true value and to be better known than their counterparts calculated in terms of the starting libraries, provided of course that they refer to an environment very similar to that of the consistency experiment.

It has repeatedly been pointed out so far that these important findings quite often constitute a worthwhile goal themselves regardless of any possible improvements in the basic nuclear data the deduced adjustments may contain or indicate.

Do the adjustments of Table 39 contain any useful information concerning the multigroup and, even further, the pointwise versions of the basic nuclear data libraries used? If they do what does it amount to?

The most important feature of the deduced adjustments for both libraries is that their absolute magnitudes are smaller than the corresponding standard deviations of the broad-group constants. This implies that the integral test undertaken in the present study for both libraries has validated our current knowledge (both values and uncertainty information) about those items of the two libraries to which the integral quantity used was sensitive. Had relatively larger adjustments been

obtained, say 2-3 times the corresponding standard deviations or more, the consistency of measured Transmissions and cross-section evaluations would have been at stake and the elimination of all other possible sources for their explanation (e.g. omission of vital adjustable parameters from the statistical model) would have resulted in questioning the appropriateness of the weighting function or even the correctness of the basic scalar cross-section data itself. Hence, the consistency of measured Transmissions and multigroup data libraries and the relatively small, with respect to corresponding standard deviations, cross-section adjustments demonstrate both the good shape of the basic pointwise nuclear data in the sensitive energy region and the adequacy of the multigroup libraries in the calculation of Transmissions.

It has been proposed by some workers (53) and it would be more appropriate for the term "adjustment" to be kept for those consistency and data evaluation problems where negligence errors and therefore strong inconsistencies exist or, at least, cannot be excluded. If the two data samplings are statistically consistent they are simply combined and re-estimated by standard statistical methods, and not adjusted or corrected. In this context it is perceived that cross-section changes, deduced in either reactor physics "mock up" experiments or shielding "benchmark" experiments(where the statistical model used cannot include,for various reasons,all the important parameters), can be called adjustments. They very rarely accept a physical interpretation and certainly only in cases where the reason causing them has been identified and isolated.

Our consistency analysis problem is that of data combination and re-estimation and not of data adjustment. Therefore the only simple physical interpretation which can freely and unequivocally be given to the observed cross-section adjustments is that t h e y y i e l d

the new optimised broad group cross - section values which together with the re-estimated standard deviations constitute our current knowledge of these quantities based on the enlarged data ensemble of cross-section evaluations and experimental Transmissions.

The consistency analysis undertaken in this chapter did not reveal reactions and energy ranges where re-evaluation or re-measurement of basic nuclear data are required, as might have been expected before embarking on the re-evaluation of B.B.C. experiments. Instead the present study validated both libraries and showed the way along which improvements in basic nuclear data libraries can be acquired by the exploitation of suitable and precise integral experiments. We emphasize the potential of this use of integral experiments mainly because what can finally be achieved does not only depend on the quality and appropriateness of the integral experiment. The correct and full exploitation of the useful information an integral experiment may give about certain nuclear data parameters strongly depends on their correct, detailed and analytical representation in the statistical model. If we had available detailed, in both energy and reaction type, covariance information for the iron scalar cross-sections (elastic, inelastic to different levels etc.) as well as for any other nuclear data considered necessary to include (e.g. the angular and energy distributions of secondary neutrons, dosimetry cross-sections etc.) and an appropriate method for sensitivity calculations, we would argue that the improvements attained would be problem-independent - an alternative, to the differential measurement, method of constantly and consistently updating nuclear data files. We improved our knowledge about iron cross-sections in terms of broad group elastic and non-

elastic cross-sections simply because in this condensed form the covariance information was available. But the neutron interaction with iron and with any other material cannot generally and adequately be described in terms of these quantities. Adjusting, therefore, either the basic cross-section data or the fine multigroup cross-sections comprising a certain broad group constant by the same factor (imposed by the lack of energy and reaction type resolution in the covariance matrix), we mis-interpret the integral experiment (by ignoring the sensitivity variation) and we may degrade instead of improving our current knowledge of cross-sections represented by the data file.

Until complete, detailed and reliable covariance information becomes available for the basic nuclear data, and methods of quantifying both the magnitude and distribution of group-averaging errors are formally established, integral experiments can only be used in assessing the appropriateness of nuclear data libraries for various types of calculations and in producing optimised data sets for specific applications. Recent developments in MONTE - CARLO perturbation theory (55) allow the adjustment procedure to be carried out in terms of pointwise nuclear data libraries; however this more realistic approach has certain drawbacks and the formidable task of identifying, assessing and formulating the various correlations between basic nuclear data still remains.

6.7 COMPARISON WITH THE WINFRITH IRON BENCHMARK EXPERIMENT

Iron cross-section adjustments have been undertaken at A.E.E Winfrith based on the ASPIS iron benchmark experiment conducted during the period 1974 - 75.

A full description of the experimental arrangement and results obtained can be found in Ref. 56 . The iron was in the form of rectangular plates separated by voids over a distance of approximately 1m and bombarded by fission-spectrum neutrons generated in a converter plate which was located near the thermal colomn of the NESTOR experimental reactor. Threshold, proton recoil and resonance sandwich counters were used at various distances inside the shield thus furnishing many channels of high quality signal information.

Two different approaches were followed in the consistency analysis of this experiment: M.M.Chestnutt (57) used a multigroup version of U K N D L iron data file ($1/E\Sigma_T(E)$ weighting), ANISN/SWANLAKE as calculational tools, the two tier hycrid statistical model developed by A.K. McCracken (58) and ORPHAN'S compilation of multigroup iron cross-sections (see page 246) in deducing his adjustments.

In contrast, M.C. Hall (55) used pointwise U K N D L iron data (thousand-group "Dice" data processed from the U K N D L basic data file), the MONTE - CARLO code DUCKPOND (MCBEND + sensitivity calculation option) in the calculations, an iterative least-squares estimator and the ORNL-5318 broad group covariance information in determining his fractional adjustments for the iron elastic and non-elastic cross-sections. Their results in the common energy range between B.B.C. and Winfrith iron benchmark experiments are given in Table 46 together with ours and the standard deviations (those obtained from ORNL-5318 report) prior to and after adjustment.

Needless to say we do not seek in Table 46 quantitative agreement

TABLE 46. A COMPARISON BETWEEN WINFRITH AND B.B.C. IRON BENCHMARK EXPERIMENTS.

BROAD GROUP/ FINE GROUPS INVOLVED/ ENERGY RANGE MeV	WINFRITH IRON BENCHMARK EXPERIMENT								B.B.C. EXPERIMENT			
	MULTIGROUP ADJUSTMENTS		POINTWISE ADJUSTMENTS		STANDARD DEVIATIONS				MULTIGROUP ADJUSTMENTS		STANDARD DEVIATIONS	
					ORNL-5318		AFTER ADJUSTMENT				AFTER ADJUSTMENT	
	ELASTIC (%)	NON-ELASTIC (%)	ELASTIC (%)	NON-ELASTIC (%)	ELASTIC	NON-ELASTIC	ELASTIC	NON-ELASTIC	ELASTIC (%)	NON-ELASTIC (%)	ELASTIC	NON-ELASTIC
1 (1-13) 14.9-4.4	-3.0	5.0	-5.0	6.0	12.2	14.1	4.3	4.3	5.0	- 6.0	4.2	4.6
2 (14-18) 4.4-2.6	-6.0	16.0	-3.0	2.0	9.3	15.5	4.5	5.5	-6.0	10.0	5.6	5.2
3 (19-25) 2.6-1.35	-1.0	9.0	6.0	-17.0	3.9	7.9	2.3	2.7	-2.0	4.0	2.3	2.4

between the adjustments in the two experiments, but only the absence of strong inconsistencies attributable to the method of estimation and/or to the basic iron nuclear data. And such inconsistences do exist in this Table. As has already been demonstrated in the preceding section, any cross-section adjustment factors deduced from various integral experiments are acceptable provided they do not exceed certain limits determined by a pre-fixed significance level on the distribution (e.g. 1 standard deviation for a 65% significance level). In such cases, varying adjustment factors simply reflect the different composition of the enlarged data ensemble (cross-section evaluations + integral experiment) on which the optimised re-estimated cross-sections are based. Looking at Table 46 from this angle we realize that there is nothing wrong with the fact that our adjustment factors for the 1st broad-group elastic and non-elastic cross-sections are of the opposite sign to that of Winfrith benchmark experiment, since both experiments gave adjustment factors considerably smaller than the corresponding a priori standard deviations. Severe disagreement exists between the two adjustment procedures of the Winfrith iron benchmark experiment especially in the energy range 1.35-2.60MeV where the adjustments to pointwise elastic and non-elastic cross-section data are incompatible with their multi-group counterparts and largely exceed the corresponding standard deviations. Is the incompatibility between "multigroup" and "pointwise" adjustment factors due to the different representation of neutron interaction with iron or to the different calculational tools used or, even more, to different covariance information used in the two methods? We cannot be specific about this point. On the other hand the inclusion of all sensitive nuclear data parameters in the "pointwise" consistency analysis of the same experiment would validate the large adjustments deduced and

constitute an incentive for measurers and evaluators to re-examine the basic scalar cross-section data in this energy range. This has not been done and therefore it is quite possible that these adjustments may be partly ficticious, because of the omission of important nuclear data parameters.

The adjustments to iron cross-sections deduced from B.B.C. experiments in the energy range 1.35 - 2.6 MeV are consistent with the corresponding standard errors and appear to have a reconciliatory influence on the comparison between "multigroup" and "pointwise" adjustment factors of the Winfrith benchmark experiment in the same energy range.

Another important result of Table 46 is that the a' posteriori standard deviation of the iron cross-sections are approximately the same for both experiments despite the large differences which exist between them (material thickness, experimental arrangements, amount and quality of integral information measured etc.).

Concluding this section we note that the cross-section adjustments to iron elastic and non-elastic broad group cross-sections deduced in the present study are in a broad agreement with those obtained from a multigroup treatment of the Winfrith iron benchmark experiment while they are incompatible with the adjustments deduced from a MONTE - CARLO pointwise analysis of the same experiment. The only way to validate the large, compared to standard deviations, adjustments obtained in the more realistic "pointwise" approach is the inclusion of all important nuclear data parameters in the statistical model. The consistent method (see page 280) together with reliable covariance information for the nuclear data parameters (in this case determining the angular and energy distributions of secondary neutrons) look very promising in this respect, and indeed it has given good preliminary results based on a subset of measurements from this experiment (59).

CHAPTER SEVEN

RECAPITULATION - CONCLUSIONS

The present study has examined and demonstrated the feasibility of integral measurements to improve basic nuclear data files. This was considered a very important exercise and a worthwhile goal in itself since improved basic nuclear data are urgently needed in a variety of fast reactor core and shield design calculations and differential measurements alone are very unlikely to satisfy the high priorities established within the required time scale.
The generation of improved data sets based on integral measurements and appropriate only to a certain category of design environments has been appreciated, established and widely used for the last two decades, particularly in the domain of fast reactor physics.
The permanent, problem-independent improvement of fine-multigroup or basic nuclear data libraries based on integral measurements is a more difficult problem and requires the validity of many conditions which, so far, can very rarely be met simultaneously in practice.
We summarize these requirements:

1. A geometrically well-defined experiment in a single material with precise integral measurements appropriate to the nuclear data we seek to improve. The uncertainties of the measured integral quantities and their correlations must carefully be assessed and quantified. Their presentation in the form of a covariance matrix is required.

2. A calculational scheme for determining the measured integral quantity in terms of the basic nuclear and other data required, which guarantees that modelling and calculational method errors are relatively unimportant. In cases where multigroup representation of the basic nuclear data is employed in the calculations the appropriateness and adequacy of the group-averaging procedure must be examined and the

uncertainties introduced properly evaluated.

3. Analytical or numerical tools to calculate the sensitivity of the integral quantity to each item of input data. (source strength and spectrum, material cross-section and response data as functions of energy). In cases where huge quantities of input data are derived according to a certain theoretical model (as, for instance, the group transfers from the elastic and inelastic scattering laws and evaporation model), the sensitivity of the integral quantity to model parameters can preferably be considered instead, and used thereafter.

4. Detailed error information of the input data in the analytically manageable form of covariance matrices. It is of crucial importance that these covariance matrices represent our current knowledge of the input data as minutely as possible with all sources of error and correlations being accounted for. Fine-energy structure, separate covariance matrices for various input data and the existence of covariance matrices describing the correlations between different input data categories, difficult to identify, assess and quantify though, are extremely important features of the input data covariance information in any attempt to improve permanently the input data from measurements of calculated integral quantities.

5. A statistical method and a functional form (usually linear) relating integral quantities to input data, to combine the two independent pieces of experimental information, that is, input data measurements or evaluations and measured integral quantities. In this last stage of the process better values and/or higher accuracies of the input quantities are obtained.

In pursuing the above course we first recognised the appropriateness of the B.B.C. experiments for such analysis. Indeed the B.B.C. work fulfilled the first requirement, and the detailed documentation together with their method of analysis permitted the

correction of the measured Transmissions for differences between real and ideal experimental conditions, and the construction of a diagonal covariance matrix describing how well the experimental Transmissions, finally included in the consistency analysis, were meant to be known.

The use in B.B.C. work of a fission-spectrum source and threshold reactions as detectors greatly facilitated the fulfilment of the second requirement. The uncertainties due both to the transformation of the ideal experimental arrangement into a one-dimensional model and to the calculational algorithm itself were shown to be unimportant compared with those originating from the nuclear data. Moreover, the relatively small thicknesses of the material shells employed in conjunction with the high-energy threshold of the detectors and the fine energy group structure used contributed to the satisfactory representation of the neutron flux by 1/E weighting, as the comparison between MCBEND-pointwise and MCBEND-multigroup calculations demonstrated. However, this comparison did not show that the group-averaging uncertainties were unimportant or how they could be quantified. Strong inconsistencies or incompatibilities between measured and calculated Transmissions for various elements, shell thicknesses, threshold detectors and nuclear data libraries were not observed.

In dealing with the sensitivity problem, three main categories of input data were identified: material cross-section data, dosimetry cross-sections and fission spectrum representation. The one-dimensional first-order perturbation code SWANLAKE gave detailed negative sensitivity profiles of Transmission to scalar cross-sections describing the various modes of neutron interaction with the material shell. The sensitive energy range was entirely determined from the convolution of fission-spectrum and detector's response, while the total (energy integrated) sensitivity was found to be an increasing

function of both shell thickness and detector threshold. The predominant role of the inelastic processes was revealed from these sensitivity profiles; in particular, the importance of inelastic scattering to the 1st excited level and to the continuum for the iron shells was clearly demonstrated. Approximate methods were employed in determining the sensitivity of Transmission to other important nuclear data parameters. It was shown that the 1st order expansion coefficient of the scattering kernel could adequately be used in evaluating the effect on Transmission of the angular and energy distributions of elastically scattered neutrons. The importance of the elastic scattering angular anisotropy and the unimportance of the inelastic one for our calculations were also demonstrated. The sensitivity of Transmission to the 1st order expansion coefficient was found to be of the same order of magnitude as that to the elastic cross-section (about 20% of that to the total cross-section) for ^{238}U and ^{237}Np detectors and twice as much for the $^{27}A\ell$ one.

The sensitivities to other important nuclear data parameters such as excited level energies, continuum threshold, nucleus temperature etc. were not studied, but an effort was made to show their unimportance for the present study.

The sensitivity profiles to dosimetry cross-sections were derived analytically, and showed negative and positive regions of equal importance with a tendency to fall with increasing detector threshold. The exactly opposite behaviour of the sensitivity to material cross-sections explained why the dosimetry data could have a very important role in interpreting discrepancies between measured and calculated Transmissions for the ^{237}Np detector while they would be of minor significance for the other two.

The sensitivity to fission spectrum was empirically found to be very

small compared with that of material total cross-sections, especially for the high-energy threshold detectors.

In discussing the validity of the fourth requirement in our problem, we can only deplore the huge gap between the input data covariance information actually used and that required. It is the lack of complete and detailed covariance information for the input data, more than any other weakness or deficiency in the whole procedure, which deprives our final results and conclusions of having the meaning and validity they were supposed to have. This gives a rather instructive value to the present attempt of improving basic nuclear data files on the basis of experimental integral information. Despite the insufficiency and condensed form of the covariance information used the uncertainty analysis of calculated Transmissions showed that the experimental values were consistent with those calculated to well within their standard deviations, especially for the $^{27}A\ell$ and ^{238}U detectors. The negligibly small contribution of dosimetry data errors to the final uncertainty of the calculated Transmissions was demonstrated for $^{27}A\ell$ and ^{238}U detectors, while the absence of reliable multigroup covariance information for the $^{237}Np(n,f)F.P$ reaction and the relatively high sensitivities to this reaction precluded the acceptance of the same conclusion for ^{237}Np Transmissions.

The statistical consistency between experimental and calculated Transmissions verified collectively the minor role of uncertainties in nuclear data parameters and other input data omitted from the uncertainty analysis, the reliability of the covariance information used and the adequacy of the calculational model employed.

The statistical method used and the results and conclusions reached in the last stage of our investigation were to a large extent predetermined from the condensed and inappropriate form of the covariance information used for such a kind of analysis. Only $^{27}A\ell$ and

^{238}U Transmissions and broad group elastic and non-elastic iron cross-sections were finally used in the adjustment procedure for reasons we discussed above. A first order Taylor's series expansion of the unknown relation between Transmissions and broad group cross-sections about the sample point (eg. broad-group cross-section evaluations) was shown to be adequate. Linear least-squares estimators were subsequently used in deducing the new values of broad group cross-sections and their covariance information based on the enlarged data ensemble of experimental Transmissions and cross-section evaluations. Any effort to overcome the constraint of undertaking the adjustment procedure in terms of broad group elastic and non-elastic cross-sections, entirely imposed by the rank and structure of the covariance matrices used, would require additional error information concerning energy-dependent fine group and partial correlations of various reactions which was not available.

A chi-square test to check the likelihood of the input data prior to adjustment verified collectively both their consistency and the adequacy of the linear model.

Improved adjusted data sets were derived for both the ENDF/B-IV and UKNDL(2) data files. These adjusted data sets demonstrated their superiority over the corresponding original libraries both by predicting more accurately Transmissions, whether or not these were included in the adjustment procedure, and by the fact that the broad group constants got closer to each other than they were in the original libraries and their accuracy increased significantly. In constrast, the fine multigroup or pointwise nuclear data libraries may have not been improved due to the condensed and inappropriate form of the covariance information employed.

I believe that the present thesis has demonstrated the important role integral measurements can play in the field of nuclear

data evaluation and the crucial importance attached to the structure and quality of nuclear data covariance information for such a use of integral experiments. In this respect, the systematic efforts for the development of special formats and procedures in ENDF/B-V for representing nuclear data covariances in an analytically manageable form are mostly welcome, though the restricted accessibility to the first neutron cross-section covariances included in this library is regretted.

I hope that the ENDF/B-V file, representing today the most complete library of evaluated data and providing our best current knowledge of the microscopic data, will soon be equipped with covariance information concerning energy and angular distributions of secondary neutrons and that integral measurements of nuclear data will play a vital role in improving its valuable content.

REFERENCES

1. J. Nuclear Energy, I, 1956, Vol. 3, p. 207.
2. J. Nuclear Energy, I, 1956, Vol. 3, p. 273.
3. J. Nuclear Energy, I, 1957, Vol. 4, p. 3.
4. J. Nuclear Energy, I, 1957, Vol. 4, p. 147.
5. GITTINGS, BARCHALL, and EVERHART, Phys. Rev. 75, 1610 (1949.
6. PHILLIPS, DAVIS, and GRAVES, Phys. Rev. 88, 600 (1952).
7. POZE, Kh.R., and GLAZKOV, N.P., J. Exptl. Theoret. Phys. (U.S.S.R.) 3, 745 (1956).
8. MACGREGOR, BALL and BOOTH, Phys. Rev. 108, 726 (1957).
9. NUclear Science and Engineering, 28, 111-113 (1967).
10. Nuclear Science and Engineering, 51, 278-295 (1973).
11. MARTIN, B.R., Statistics for Physicists, Academic Press, London, 1971.
12. ENGLE, W.W. "A Users Manual for ANISN, a One-Dimensional Discrete Ordinates Transport Code with Anisotropic Scattering", K-1673, Oak Ridge (1967).
13. ZIJP, W.L., "On the consistency between integral and differential cross-section data", ECN-78-160, Petten (1978).
14. SIGMA, a code for group collapsing, University of London Reactor Centre, Ascot, Berkshire.
15. DAVISON, B., "Neutron Transport Theory", Oxford University Press, 1957 (Section 10.3.4).
16. KAHN, H., "Applications of Monte-Carlo, AECU-3259 (1954).
17. PARKER, J.B., DICE Mk V (edited by J.B. Parker), AWRE O 27/66 (1966).
18. PARKER, K., "The Aldermaston Nuclear Data Library, AWRE O 70/63 (1963).
19. STRAKER, E.A., et al. "The Morse Code - A Multigroup Neutron and Gamma Ray Monte-Carlo Transport Code. ORNL 4585 (1970).
20. BENDALL, D.E., and BRISSENDEN, R.J., "McBEND programme users guide", Winfrith (1980).

21. PRICE, J.A., "A guide to Galaxy 6 part 1", AWRE O1k3/75, Aldermaston (1975).

22. GREENE, N.M., et al. "AMPX A modular Code System for Generating Coupled Multigroup Neutron Gamma Libraries from ENDF/B. ORNL-TM-3206 (1975).

23. EDGERTON, J. Unpublished.

24. STACEY, W.M. Jr., "Variational Estimates and Generalised Perturbation Theory for the Ratios of Linear and Bilinear Functionals". J. Math. Phys. 13 (8) 1119 (1972).

25. GANDINI, A. "A Generalised Perturbation Method for Bi-Linear Functionals of the Real and Adjoint Neutron Fluxes". J. Nuclear Energy, 21, 755 (1967).

26. OBLOW, E.M., "General Sensitivity Theory for Radiation Transport". ORNL-TM-4110 (1973).

27. Nuclear Science and Engineering, 51, 339 (1973).

28. Trans. Am. Nuc. Soc. 21, 543 (1975).

29. RIEF, H., "Three dimensional Effects in Sensitivity Studies", Paper B4. Proc. of the 5th Int. Conf. on Reactor Shielding, Knoxsville (1977).

30. BARTINE, D.E., OBLOW, E.M., and MYNATT, F.R., "SWANLAKE - A Computer Code Utilising ANISN Radiation Transport Calculations for Cross-Section Sensitivity Analysis". ORNL-TM-3809 (1973).

31. LYMPANY, S.D., McCRACKEN, A.K., and PACKWOOD, A., "Contribution to the Exercise of Sensitivity Studies for the NEA Theoretical Fast Reactor Benchmark". Paper C4. ibid. (22).

32. Private communication from R.W. Roussin, EPIC, ORNL.

33. LAMARSH, J.R., "Introduction to Nuclear Reactor Theory", Addison-Wesley (1966).

34. DRISCHLER, J.D., WEISBIN, C.R., "Compilation of Multigroup Cross-Section Covariance Matrices for Several Important Reactor Materials". ORNL-5318, 1977.

35. Private communication from Mr. A.K. McCracken, AEE-Winfrith.

36. WRENDA 76/77 Ed. Lessler, R.M. "World Request List for Nuclear Data". INDC (SEC)-55/URSF IAEA Vienna (1976).

37. DRAKE, M.K., (Ed.) "Data Formats and Procedures for the ENDF Neutron Cross-Section Library". BNL-50274 (1970).

38 PEREY, F.G., "Data Covariance Files for ENDF/B-V" ORNL-TM-5938 (1977).

39. GERSTL, S.A.W., DUDZIAK, D.J. and MUIT, D.W. "Application of Sensitivity Analysis to a Quantitative Assessment of Neutron Cross-Section Requirements for the TFTR". LA-6118-MS Appendix A. (1975).

40. McCRACKEN, A.K., Private communication, WNDG/164(RPD/JSS/134).

41 McELROY, W.N., and KELLOGG, L.S., "Fuels and Materials Fast Reactor Dosimetry Data Development and Testing". Nuclear Technology 25 (1975) No. 2 p. 180.

42. HEMMENT, P.G.E., and PENDLEBURY, E.D. "The Optimisation of Neutron Cross-Section Data Adjustments to give Agreement with Experimental Critical Sizes". Int. Conf. on Fast Critical Exp. and their Analysis, ANL 7320 (1966)

43. MACDOUGAL, J.D. and ROWLANDS, J.L. "The Use of Integral Measurements to Adjust Cross-Sections and Predict Reactor Properties". Paper 1-6 Proc. of BNES Int. Conf. on the Physics of Fast Reactor Operation and Design (1969).

44. GANDINI, A., "Nuclear Data and Integral Measurements Correlation for Fast Reactors. Part 1. CNEN Report RT/FI(73)5 (1973).

45. BARRE, J.Y., and RAVIER, J., "Imprecisions des Parametres Carateristiques d'un Reactuer Rapide de Puissance deus aux Incertitudes Actuelles Concernant les Donnees Neutroniques". Proc. of a Symp. on Fast Reactor Physics. Vol. I SM-101/58 Karlsruhe (1968).

46. PAZY, A., RAKAVY, G., REISS, Y., and YEIVIN, Y., "Integral Measurements as Supplementary Data in Neutron Cross-Section Evaluation". Proc. of IAEA Conf. on Nuclear Data for Reactors. Vol. II. CN-23/15 Paris (1966).

47 MITANI, H., and KUROI, H., "Adjustment of Group Cross-Sections by Means of Integral Data-(I) Theoretical Study". J. Nucl. Sci. and Technol. 9 (7) (1972).

48. BALLANCE, B.M.O., PENDLEBURY, E.D., PRICE, J.A., and WEST, P.H., "The Optimisation of Neutron Cross-Section Adjustments to give Agreement with Spectrum Measurements at the Centre of Critical Systems". Paper 1.13 ibid. 43.

49. CECCHINI, G., FARINELLI, V., GANDINI, A., and SALVATORES, M., "Analysis of Integral Data for Few-Group Parameter Evaluation of Fast Reactors". A/Conf. 28/P/627 Vol. 2 388 Geneva (1964).

50. J. Nucl. Sci. and Technol. 12, (11) (1975).

51. PEREY, F.G., "Estimated Uncertainties in Nuclear Data - An Approach". Paper IA3 Proc. of Conf. on Nuclear Cross-Sections and Technology NBS-425 Vol. I Washington D.C. (1975).

52. GANDINI, A., and SALVATORES, M. "Nuclear Data and Integral Measurements Correlation for Fast Reactors. Part 3: The Consistent Method". CNEN Report RT/FI(74)3 (1974).

53. CHAO, Y.A., "A New Approach to the Adjustment of Group Cross-Sections Fitting Integral Measurements". Nucl. Sci. and Eng. 72 1-8 (1979).

54. SCHMITTROTH, F., and SCHENTER, R.E., "Finite Element Basis in Data Adjustment". Nucl. Sci. and Eng. 74 168-177 (1980).

55. HALL, M.G. "Mont-Carlo Perturbation Theory in Neutron Transport Calculations". Ph.D. Thesis, University of London (1980).

56. CARTER, M.D., and PACKWOOD, A. "The Winfrith Benchmark Experiment in Iron-Experimental Results". Proc. Specialists' Meeting, Sensitivity and Shielding Benchmarks, Paris (1975).

57. CHESTNUTT, M.M., "A Maximum Likelihood Adjustment Philosophy for Observational Consistency between Nuclear Physics and Reactor Technology". Ph.D. Thesis, University of London (1979).

58. CHESTNUTT, M.M., and McCRACKEN, A.K., "Resulsts of the Analysis of the Winfrith Iron Benchmark". Winfrith (1980).

59. D'ANGELO, A., OLIVA, A., PALMIOTTI, G., SALVATORES, M., and ZERO, S. "Consistent Utilisation of Shielding Benchmark Experiments". Nucl. Sci. Eng. 65, 477 (1978).

APPENDIX A

CALCULATION OF FLUXES INSIDE SPHERICAL SHELL SOURCES

In this Appendix the formulae giving the scalar flux inside uniformly distributed isotropic spherical surface and shell sources are derived.

The flux in the space inside the shell source is shown to converge to that of a spherical surface source when the shell thickness tends to zero.

Finally the equivalence of spherical surface and shell sources is examined in flux calculations at the centre of the shell.

A1. SCALAR FLUX INSIDE A SPHERICAL SURFACE SOURCE

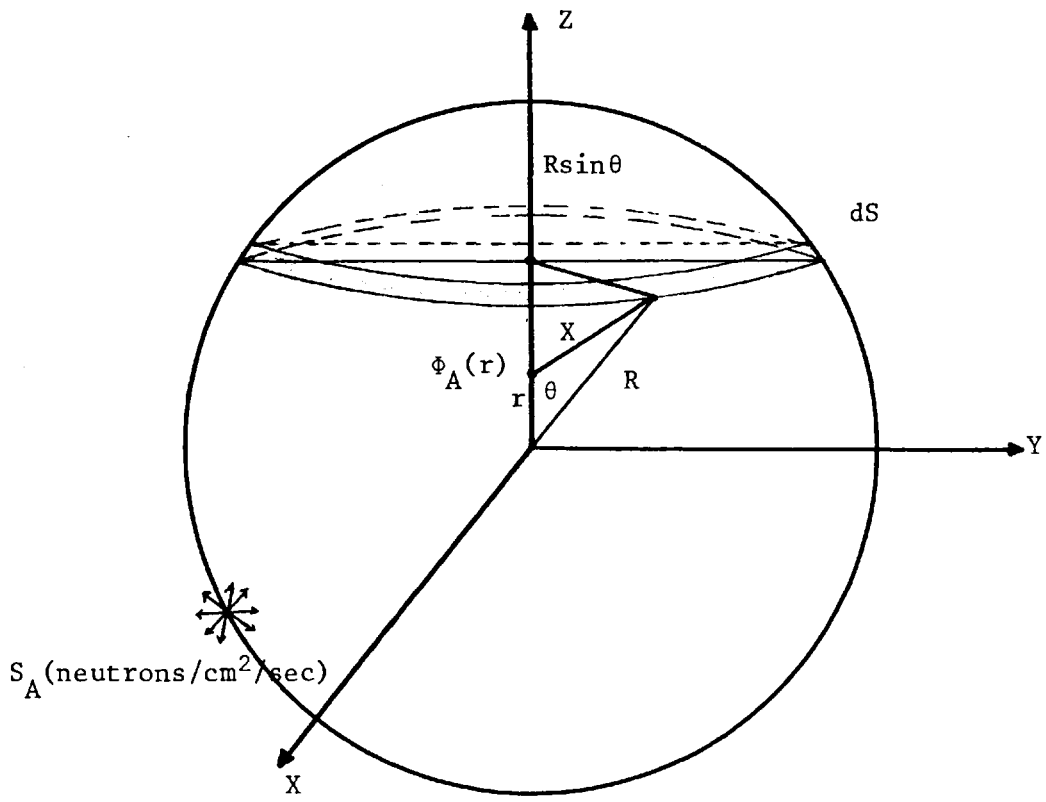


FIGURE A1

In Figure (A1) a spherical surface source of radius R isotropically emits S_A neutrons/cm^2/sec. According to this Figure the following relations hold:

$$dS = 2\pi R \sin\theta \, R d\theta \tag{A1}$$

$$X^2 = r^2 + R^2 - 2rR\cos\theta \tag{A2}$$

$$d\Phi_A(r) = \frac{S_A \, d\,S}{4\pi \; X^2} \tag{A3}$$

From Eqn. (A2) we get:

$$2\,X\,d\,X = 2rR\sin\theta d\theta \tag{A4}$$

and therefore, Eqn. (A3) becomes:

$$d\Phi_A(r) = \frac{S_A\,R}{2r}\;\frac{dX}{X} \tag{A5}$$

from which:

$$\Phi_A(r) = \frac{S_A\,R}{2r}\int_{R-r}^{R+r}\frac{dX}{X} \tag{A6}$$

or, finally:

$$\Phi_A(r) = \frac{S_A\,R}{2r}\;\ln\left(\frac{R+r}{R-r}\right) \qquad \text{for } r<R \tag{A7}$$

Eqn. (A7) gives the scalar flux inside a spherical surface source in terms of the distance from the centre, the source radius and strength. At the centre the flux is found to be:

$$\Phi_A(r=o) = \frac{S_A}{4\pi R^2} \int dS = \frac{S_A 4\pi R^2}{4\pi R^2} = S_A$$

that is:

$$\Phi_A(o) = S_A \tag{A8}$$

a result which can also be found as:

$$\Phi_A(o) = \lim_{r\to o} \Phi_A(r) = \lim_{r\to o} \left| \frac{S_A R}{2r} \ell n \left(\frac{R+r}{R-r}\right) \right| \tag{A9}$$

Since for $r/R << 1, \ell n(\frac{R+r}{R-r}) = \frac{2r}{R} + O\,(\frac{r}{R})^3$, Eqn. (A9) can be written as:

$$\Phi_A(o) = \lim_{r\to o} \frac{S_A R}{2r} \frac{2r}{R} = S_A$$

Eqn. (A9) shows that the scalar flux at the centre of a spherical surface source coincides with its strength.

A2. SCALAR FLUX IN THE SPACE INSIDE A SHELL SOURCE

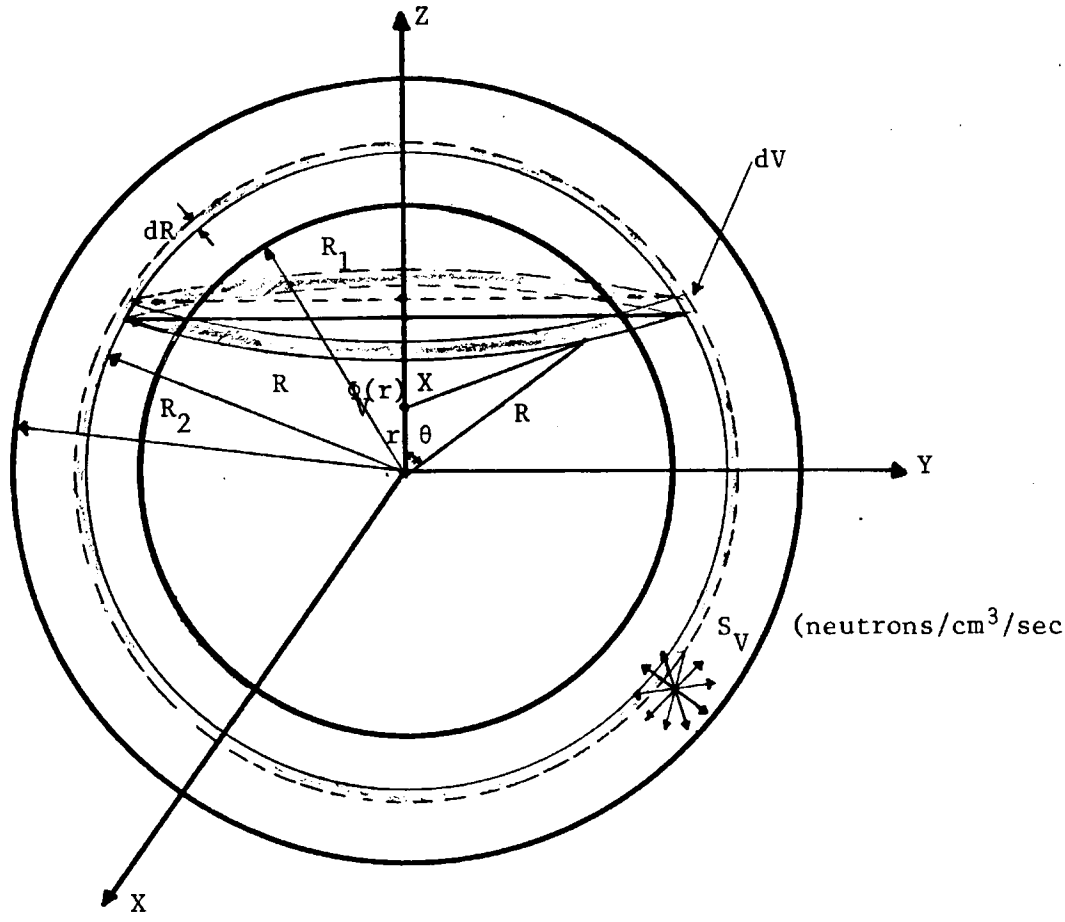


FIGURE A2

The shell source at Figure (A2) has thickness $d = R_2 - R_1$ and isotropically emits S_V neutrons/cm^3/sec. We are interested in the flux $\Phi_V(r)$ at a certain point $\vec{r}$ in the space inside the source. According to this Figure the following relations hold:

$$dV = 2\pi R^2 \sin\theta d\theta dR \qquad (A10)$$

$$d\Phi_V(r) = \frac{S_V \, d\,V}{4\pi\, X^2} \tag{A11}$$

Taking into account Eqns. (A2) and (A10), Eqn. (A11) becomes:

$$d\Phi_V(r) = \frac{S_V \, 2\pi R^2 \sin\theta d\theta dR}{4\pi(R^2 + r^2 - 2Rr\cos\theta)} \tag{A12}$$

from which:

$$\Phi_V(r) = \frac{S_V}{2} \int_{R_1}^{R_2} dR \int_{+1}^{-1} \frac{\sin\theta d\theta}{R^2 + r^2 - 2Rr\cos\theta} =$$

$$= \frac{S_V}{2r} \int_{R_1}^{R_2} \ell n \left(\frac{R+r}{R-r}\right) dR \tag{A13}$$

After the integration we end in the following final for the flux:

$$\Phi_V(r) = \frac{S_V}{4r}\left[(R_2^2 - r^2)\,\ell n\left(\frac{R_2+r}{R_2-r}\right) - (R_1^2 - r^2)\,\ell n\left(\frac{R_1+r}{R_1-r}\right) + 2r(R_2 - R_1)\right] \tag{A14}$$

with $r<R_1<R_2$

Expression (A14) gives the scalar flux in the space inside a shell source in terms of the source strength, inside and outside radii and the distance from the centre.

It can easily be proved that the flux at the centre of the shells is given by:

$$\Phi_V(o) = S_V(R_2 - R_1) \tag{A15}$$

A3. SOME USEFUL RELATIONS BETWEEN $\Phi_A(r)$ AND $\Phi_V(r)$ SCALAR FLUXES

In this section we first prove that the flux inside a spherical surface source is the limit-case of a shell source when its thickness tends to zero. According to Fig. A3 we shall show that:

$$\lim_{R_1 \to R_2} \Phi_V(r) = \Phi_A(r) \tag{A16}$$

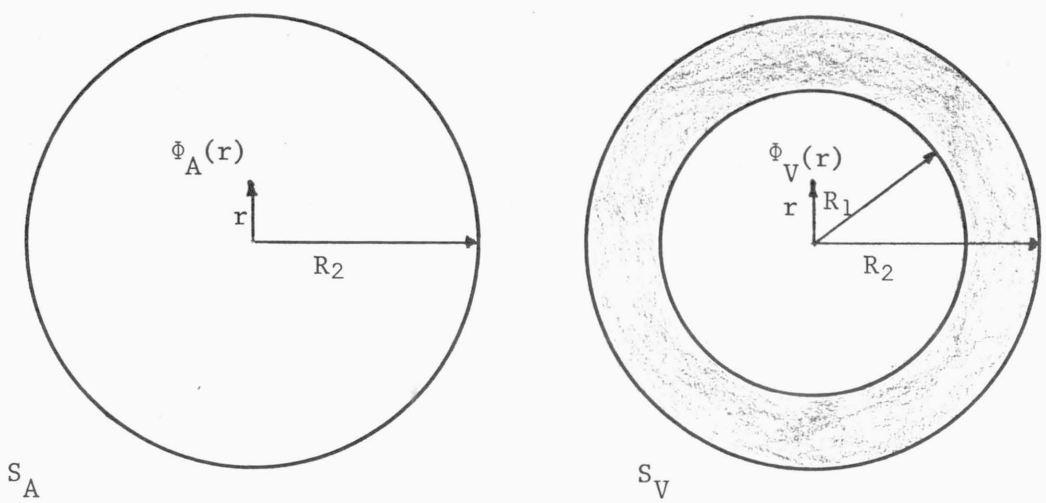


FIGURE A3

PROOF:

First we normalize the surface and volume sources, that is:

$$4\pi R_2^2 S_A = 1 \tag{A17}$$

$$\frac{4\pi}{3}(R_2^3 - R_1^3)S_V = 1 \tag{A18}$$

from which:

$$S_V = \frac{3\,R_2^2\,S_A}{(R_2^3 - R_1^3)} \tag{A19}$$

In the light of Eqn. (A19), Eqn. (A14) becomes:

$$\Phi_V(r) = \frac{3\,R_2^3\,S_A}{4r(R_2^3 - R_1^3)}\left[(R_2^2 - r^2)\ln\left(\frac{R_2+r}{R_2-r}\right) - (R_1^2 - r^2)\ln\left(\frac{R_1+r}{R_1-r}\right) + 2r(R_2 - R_1)\right] \tag{A20}$$

from which:

$$\lim_{R_1\to R_2}\Phi_V(r) = \lim_{R_1\to R_2}\frac{3\,R_2^2 S_A\left[(R_2^2-r^2)\ln\left(\frac{R_2+r}{R_2-r}\right)-(R_1^2-r^2)\ln\left(\frac{R_1+r}{R_1-r}\right)+2r(R_2-R_1)\right]}{4r(R_2^3-R_1^3)}$$

$$= \lim_{R_1\to R_2}\frac{3\,R_2^2 S_A}{4r}\,\frac{d/dR_1\left[(R_2^2-r^2)\ln\left(\frac{R_2+r}{R_2-r}\right)-(R_1^2-r^2)\ln\left(\frac{R_1+r}{R_1-r}\right)+2r(R_2-R_1)\right]}{d/dR_1\left[(R_2^3 - R_1^3)\right]}$$

$$= \frac{3\,R_2^2\,S_A}{4r}\lim_{R_1\to R_2}\frac{\left[-2R_1\ln\left(\frac{R_1+r}{R_1-r}\right)+(R_1^2-r^2)\,\frac{R_1-r}{R_1+r}\,\frac{2r}{(R_1-r)^2}-2r\right]}{-3R_1^2}$$

$$= \frac{3\,R_2^2\,S_A}{4r}\lim_{R_1\to R_2}\frac{2R_1\ln\left(\frac{R_1+r}{R_1-r}\right)}{3R_1^2} = \frac{3\,R_2^2\,S_A}{4r}\,\frac{2\ln\left(\frac{R_2+r}{R_2-r}\right)}{3R_2}$$

$$= \frac{S_A\,R_2}{2r}\ln\left(\frac{R_2+r}{R_2-r}\right) = \Phi_A(r)$$

That is, Eqn. (A16) has been proved.

Another interesting result is the relation amongst R, R_1, R_2 for which the $\Phi_A(o)$ and $\Phi_V(o)$ are equal.

As we have already seen $\Phi_A(o)$ and $\Phi_V(o)$ are given by the expressions:

$$\Phi_A(o) = S_A$$

$$\Phi_V(o) = S_V(R_2 - R_1)$$

Using Eqns. (A17), (A18) we easily find that the requirement $\Phi_A(o) = \Phi_V(o)$ yields the following Equation relating to R, R_1, R_2.

$$R = \frac{R_2^2 + R_1R_2 + R_1^2}{3} \qquad \text{(A21)}$$

For most of the cases Eqn. (A21) can be approximated by:

$$R = \frac{(R_1 + R_2)}{2} \qquad \text{(A22)}$$

Expression (A22) shows that, as far as the calculation of the flux at the centre of a shell source is concerned, the shell source can be replaced by a spherical surface emitting the same number of neutrons per sec and located at the mid-point of the shell.

APPENDIX B

LEAST - SQUARES METHOD

B1 INTRODUCTION

In this Appendix a rigorous statistical formulation of the least-squares estimation method is presented. The linear least-squares method is firstly treated, that is, the simple case where a linear functional form relates "observed quantities" and parameters". The linear least-squares method is subsequently expanded to include cases where the parameter space is a subset of the "observed quantities" space. Such cases arise in practice when the number of observations is smaller than the number of parameters to be estimated and therefore evaluation of the parameters can be used as additional observations to make the set of Equations overdetermined.

Finally the non-linear least-squares method is treated in cases where a linear form (e.g. Taylor's series expansion) can approximate the complicated and very often unknown relation between observables and parameters.

B2 LINEAR LEAST SQUARES

Basic Concepts - Definitions

DEFINITION 1. Let X be a non-empty set. By a σ-algebra on X is meant a class H of subset of X, such that:

(a) $\phi \in H$

(b) if $S \in H$, $X/S \in H$ (The complement of S is an element of H)

(c) if $\{S_i, i \in N\} \in H$ then $\underset{i \in N}{U} S_i \in H$

DEFINITION 2. A non-empty set X together with a σ-algebra H on X (X,H) is called a measurable space.

DEFINITION 3. A positive measure μ on the measurable space (X,H) consists of a function $\mu : H \to R^+$ such that

(a) $\mu(\phi) = o$

(b) if $\{S_i, i \in N\}$ is a sequence of mutually disjoint measurable sets from H, then $\mu\{\bigcup_{i\in N} S_i\} = \sum_{i\in N} \mu\{S_i\}$

DEFINITION 4. A triple (X,H,μ) is called a measured space if (X,H) is a measurable space, and μ is a positive measure on (X,H).

DEFINITION 5. A measure μ on a measurable space (X,H) is said to be a probability measure if $\mu(X) = 1$.

DEFINITION 6. A measure μ on a measurable space (X,H) is said to be complete, if given $T \subseteq S$, $S \in H$ and $\mu(S) = 0$, then $T \in H$ and $\mu(T) = 0$.

DEFINITION 7. A probability space consists of a triple (X, H, P) where X is a non-empty set, H is a σ-algebra of subsets of X and P is a complete probability measure on (X,H).

DEFINITION 8. Let (X,H) and (Y,K) be measurable spaces. A function $f : X \to Y$ is said to be measurable if given any $S \in K$, $f^{-1}(S) \in H$.

DEFINITION 9. If (Ω,H,P) is a probability space, (E,B) is a measured space, then a measurable function $X : \Omega \to E$ is called a random variable.

DEFINITION 10. If (Ω,H,P) is a probability space, (E,B) a measurable space, and $X : \Omega \to E$ a random variable then the expected or mean value of X is defined by:

$$\mu_X = E(X) = \int_\Omega X dP \tag{B1}$$

whenever the integral exists.

DEFINITION 11. Let E be an inner product space, and define the mapping

$\pi : E \to L(E,E)$ by

$$|\pi(X)|u = g(u,X)X \tag{B2}$$

where: X, u ϵ E and L(E,E) represents the set of all linear transformations from E into E and g stands for inner product.

DEFINITION 12. Let (Ω, H, P) be a probability space, $X : \Omega \to E$, a random variable taking values in a finite dimensional inner product space E, with inner product g. Then

$$\pi o(X-\mu) : \Omega \to L(E,E)$$

Define the variance - covariance transformation of X by:

$$\Sigma = E(\pi o(X-\mu)) = \int_\Omega \pi o(X-\mu) dP$$

whenever the integral exists.

THEOREM 1. If $(\vec{e}_i)$ is a basis (orthonormal) for E, and Σ_{ij} the matrix of the variance - covariance transformation Σ with respect to this basis, then (Ref 1):

$$\Sigma_{ij} = E[(X_i - \mu_i)(X_j - \mu_j)] \tag{B4}$$

THEOREM 2. If (Ω, H, P) is a probability space, $X : \Omega \to E$ a random variable into a finite dimensional inner product space E, $A : E \to F$ a linear transformation into an inner product space F, then the random variable $Y = AoX$ has mean given by:

$$\mu_Y = A\,\mu_X \tag{B5}$$

and variance - covariance transformation defined by:

$$\Sigma_Y = A\Sigma_X A^T \tag{B6}$$

where A^T is the adjoint of A (Ref 2)

DEFINITION 12. A linear transformation A is positive definite if A is self-adjoint, and $g(X,AX) > 0$, unless $X = 0$.

THEOREM 3. If Σ is the variance - covariance transformation of a random variable, then Σ is a positive transformation. If, in addition, the induced probability measure μ on E is such that no subspace S of E satisfies $\mu(S) = 1$ then Σ is positive definite. (Ref 1)
If A is positive definite A is also invertible.

Linear Model - Least-Squares Estimators

DEFINITION 13. A nr linear model consists of a set (E,F,A,P,X) where:

(1) E and F are inner product spaces with dim E = n, dim F = r.

(2) $A \in L(F,E)$

(3) $P = (\Omega, H, P)$ is a probability space

(4) X is a random variable taxing values in E, $(X:\Omega \to E)$ with mean μ and variance - covariance transformation Σ

(5) $\exists$ a $\lambda_o \in F$ such that $E(X) = A(\lambda_o)$

Note: To avoid unnecessary complications we will be using the same symbols for random variables and sample points; so X stands for a random variable as well as any sample point from E.

DEFINITION 14. The Least Squares Function of a nr linear model is a map $\ell : E \times F \to R$ given by:

$$\ell(X,\lambda) = g_E(X - A(\lambda), \Sigma^{-1}(X - A(\lambda))) \tag{B7}$$

THEOREM 4. Let $f : U \to F_1$ and $h : U \to F_2$ be differentiable; if $P : U \to F_1 \times F_2$ is defined by:

$$P(X) = (f(X), h(X))$$

then: (Ref 2)

$$(D(g\circ P)(X)(v) = g(f_X(v),h(X))+g(f(X),h_X(v))$$

where: $f_X = (Df)(X)$, $h_X = (Dh)(X)$

DEFINITION 15. Define the function $\ell_X : F \rightarrow R$ by

$$\ell_X(\lambda) = \ell(X,\lambda) \tag{B8}$$

THEOREM 5. If ℓ is the least-squares function of an nr linear model (E, F, A, P, X) then for any $X \in E$, $\exists\ \lambda_p \in F$ such that the function ℓ_X has a minimum at λ_p which satisfies the equation:

$$A^T W^{-1} A(\lambda_p) = A^T W^{-1} X \tag{B9}$$

where: $\Sigma = \sigma^2 W$

Proof: $\ell_X(\lambda) = g_E(X - A(\lambda), \frac{W^{-1}}{\sigma^2}(X - A(\lambda))$

We define the functions:

$$f : F \rightarrow E \quad \text{by} \quad f(\lambda) = X - A(\lambda)$$

$$h : F \rightarrow E \quad \text{by} \quad h(\lambda) = \frac{W^{-1}}{\sigma^2}(X - A(\lambda))$$

$$P : F \rightarrow E\text{x}E \text{ by } P(\lambda) = (f(\lambda), h(\lambda))$$

$$Q : E \text{ x } E \rightarrow R \quad \text{by} \quad Q = g_E \circ P$$

Then we easily get:

$$DQ(\lambda)(a) = g_E(Df(\lambda)(a), h(\lambda)) + g_E(f(\lambda), Dh(\lambda)(a))$$

We require $DQ(\lambda)(a) = 0 \quad \forall\, a \in F$

According to the definitions of f and h functions we have:

$$Df(\lambda) = -A$$

$$Dh(\lambda) = -\frac{W^{-1}}{\sigma^2} A$$

and consequently

$$DQ(\lambda)(a) = g_E(-A(a), \frac{W^{-1}}{\sigma^2}(X - A(\lambda))) + g_E(X - A(\lambda), \frac{W^{-1}}{\sigma^2} D(a))$$

$$= g_E(-A(a), \frac{W^{-1}}{\sigma^2}(X - D(\lambda))) + g_E(\frac{W^{-1}}{\sigma^2}(X - A(\lambda)), -A(a))$$

$$= -\frac{2}{\sigma^2} g_E(A(a), W^{-1}(X - A(\lambda)))$$

$$= -\frac{2}{\sigma^2} g_F(a, A^T W^{-1}(X - A(\lambda)))$$

and therefore:

$$-\frac{2}{\sigma^2} g_F(a, A^T W^{-1}(X - A(\lambda))) = 0 \quad \forall\, a \in F$$

from which:

$$A^T W^{-1} X = A^T W^{-1} A(\lambda)$$

if $A^T W^{-1} A$ is invertible :

$$\lambda_p = (A^T W^{-1} A)^{-1} A^T W^{-1} X$$

λp is called a least-squares estimate of λ_o

DEFINITION 16. A LEAST SQUARES ESTIMATOR is a function $\hat{\lambda} : E \to F$ defined by:

$$\hat{\lambda} = (A^T W^{-1} A)^{-1} A^T W^{-1} X \qquad \text{(B10)}$$

$$\forall\ X \in E.$$

REMARKS 1. The least-squares estimator $\hat{\lambda}$ is an unbiased estimator of λ_o. This can easily be seen from Eqn. (B10):

$E(\hat{\lambda}) = (A^T W^{-1} A)^{-1} A^T W^{-1} E(X)$

Since $E(X) = A(\lambda_o)$, we get:

$E(\hat{\lambda}) = \lambda_o$.

2. The importance of the least-squares estimates stems from their "minimum-variance" properties, that is, the least-squares estimator minimises the variance of any linear combination of the parameters. (Ref. 3)

3. The covariance matrix of the random variable $x \in E$ was split into a scalar factor σ^2 and a matrix W. This separation serves two goals:

(a) To show that the least-squares estimates can be expressed in terms of, a sort of, relative covariance matrix of the "observation vector".

(b) The least-squares method is capable of providing an unbiased estimate of σ^2 as will be seen in the following paragraph. This potentiality implies that the least-squares method can successfully be applied to linear models where the covariance matrix of the observations is supposed to be known within a scalar factor, and it provides an unbiased estimate of this scalar factor together with estimates of the parameters and their covariance matrix.

However in practical situations the correctness and reliability of these estimates will depend amongst other factors and on the validity of the above assumption concerning the knowledge of the covariance matrix of the observations.

THEOREM 6. An unbiased estimator of σ^2 is defined by the Equation:

$$\hat{\sigma}^2 = \frac{1}{n-r} g_E(X - A \circ \lambda, W^{-1}(X - A \circ \lambda)) \qquad \text{(B11)}$$

(Ref. 3)

Since:

$$\hat{\lambda} = (A^T W^{-1} A)^{-1} A^T W^{-1} X$$

and $\quad \text{var}(X) = \Sigma = \sigma^2 W$

the variance-covariance transformation of the least-squares estimator $\hat{\lambda}$ is given by: (Theorem 2)

$$\text{var}(\hat{\lambda}) = (A^T W^{-1} A)^{-1} A^T W^{-1} \sigma^2 W W^{-1} A (A^T W^{-1} A)^{-1}$$
$$= \sigma^2 (A^T W^{-1} A)^{-1}$$

and its estimator in terms of $\hat{\sigma}^2$:

$$\hat{\text{var}}(\hat{\lambda}) = \frac{1}{n-r} g_E(X - A_o\lambda, W^{-1}(X - A_o\lambda)) (A^T W^{-1} A)^{-1}$$

DEFINITION 17. The S^2 - function of a linear model is defined by:

$$S^2 = g_E(X - A(\lambda), W^{-1}(X - A(\lambda)))$$

It has been shown that the S^2 - function has a minimum S_m^2 at $\bar{\lambda} = \lambda(X)$ viz:

$$S_m^2 = g_E(X - A\bar{\lambda}, W^{-1}(X - A\bar{\lambda}))$$

Define:

$$\chi^2 = g_E(X - A_o\lambda, W^{-1}(X - A_o\lambda))$$

According to Eqn. (B10) this minimum can be expressed in terms of only X, A, W, that is, the observation vector, its relative covariance matrix and the linear constraint between observed quantities and parameters. The formulae:

$$\hat{\lambda} = (A^T W^{-1} A)^{-1} A^T W^{-1} X \tag{B12}$$

$$\text{var}(\lambda) = \sigma^2 (A^T W^{-1} A)^{-1} \tag{B13}$$

$$\chi^2 = g_E(X - A_o\hat{\lambda}, W^{-1}(X - A_o\hat{\lambda})) \tag{B14}$$

$$\hat{var}(\hat{\lambda}) = \frac{\chi^2}{n-r} (A^T W^{-1} A)^{-1} \tag{B15}$$

are our final Equations for the least-squares estimates of the parameters, and for their covariance matrices in cases where (a) the covariance matrix of the observed quantities is fully known Eqns. (B12) and (B13), (b) known to within a scalar factor Eqns. (B12) and (B15).

B3 LINEAR LEAST-SQUARES ESTIMATORS WITH THE PARAMETER SPACE A SUBSET OF THE OBSERVATION SPACE

The linear least-squares method developed so far requires the number of parameters to be smaller than the number of observed quantities available or, in other words,

$$r < n$$

One way to achieve this requirement is to expand the "observed quantities" space by considering previous measurements or evaluations of the parameters as additional observations and include them into the original "observed quantities" space. In this case we can consider the observation space E as consisting of two orthogonal subspaces S_p (parameters) and S_o (observed quantities).

Since $F = S_p$ and $E = S_p \cup S_o$ it is obvious that $F \subset E$.

Consequently any $X \in E$ can be expressed as:

$$X = \Pi_p X + \Pi_o X = X_p + X_o$$

(where Π_p and Π_o are the projection operators onto subspaces F and $F^\perp$, and $I = \Pi_p + \Pi_o$)

i.e. any X can be written as a unique combination of elements from S_p and S_o.

The linear transformation $A : F \rightarrow E$ can be expressed as:

$$A = I_p + G \tag{B16}$$

where:

$$A = S_p \rightarrow E$$

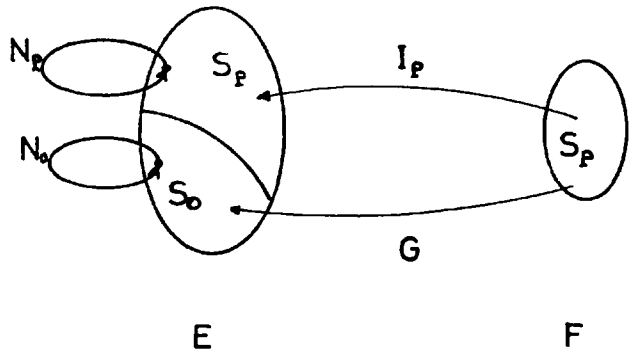
$$I_p : S_p \rightarrow S_p \qquad (I_p(X) = X)$$

$$G : S_p \rightarrow S_o$$

Let us suppose that the relative covariance matrix of the extended observation space E, W, has the property of leaving S_p and S_o invariant. This amounts to accepting that there are no correlations between parameter measurement or evaluations, and observations. In this case we can write:

$$W = N_p + N_o \tag{B17}$$

where N_p is the covariance matrix of the parameters and N_o is the covariance matrix of the observations (see Figure)



The following Equations are then evident:

$$A^T = I_p{}^T + G^T = I_p + G^T \tag{B18}$$

$$A^T W^{-1} = (I_p + G^T)(N_p^{-1} + N_o^{-1}) = N_p^{-1} + G^T N_o^{-1} \tag{B19}$$

$$A^T W^{-1} A = N_p^{-1} + G^T N_o^{-1} G \tag{B20}$$

In the light of Eqns. (B17/20) Eqn. (B9) can be written as:

$$(N_p^{-1} + G^T N_o^{-1} G)\hat{\lambda} = G^T N_o^{-1} X_o + N_p^{-1} X_p \tag{B21}$$

from which

$$N_p^{-1}(\hat{\lambda} - X_p) = G^T N_o^{-1}(X_o - G\hat{\lambda}) \tag{B22}$$

A very elegant way to proceed from (B22) is to introduce after Dragt et al. the auxiliary quantity:

$$X' = N_o^{-1}(X_o - G\hat{\lambda}) \tag{B23}$$

Eqn. (B22) can then be rewritten as:

$$\hat{\lambda} - X_p = N_p G^T X' \tag{B24}$$

or

$$G(\hat{\lambda} - X_p) = G N_p G^T X' \tag{B25}$$

Define:

$$N_b = G N_p G^T \tag{B26}$$

Then Eqn. (B25) becomes:

$$G(\hat{\lambda} - X_p) = N_b X' \tag{B27}$$

Using Eqn. (B27), Eqn. (B23) gives:

$$X' = N_o^{-1}(X_o - N_b X - GX_p) \tag{B28}$$

from which:

$$N_o X' + N_b X' = X_o - GX_p$$

Therefore:

$$X' = (N_o + N_b)^{-1}(X_o - GX_p) \tag{B29}$$

Substituting (B29) into (B24) we finally obtain:

$$\hat{\lambda} = X_p + N_p G^T (N_o + N_b)^{-1}(X_o - GX_p) \tag{B30}$$

The derivation of the corresponding formula for var($\hat{\lambda}$) can be done in a similar way:

Using Eqn. (B20) formula (B13) can be written as:

$$\text{var}(\hat{\lambda}) = \sigma^2 (N_p^{-1} + G^T N_o^{-1} G)^{-1} \tag{B31}$$

or

$$(N_p^{-1} + G^T N_o^{-1} G)\ \text{var}(\hat{\lambda}) = \sigma^2 I_p \tag{B32}$$

from which:

$$N_p^{-1}\text{var}(\hat{\lambda}) = \sigma^2 I_p - G^T N_o^{-1} G \text{ var}(\hat{\lambda}) \tag{B33}$$

we introduce the quantity:

$$X' = N_o^{-1} G \text{ var}(\hat{\lambda}) \tag{B34}$$

Eqn. (B33) then becomes:

$$\text{var}(\hat{\lambda}) = N_p \sigma^2 I_p - N_p G^T X' \tag{B35}$$

or

$$G \text{ var}(\hat{\lambda}) = G N_p \sigma^2 I_p - G N_p G^T X' \tag{B36}$$

Eqn. (B34) by virtue of Eqns. (B26) and (B36) takes the form:

$$X' = N_o^{-1}(G N_p \sigma^2 I_p - N_b X') \tag{B37}$$

from which:

$$N_o X' + N_b X' = G N_p \sigma^2 I_p$$

viz:

$$X' = (N_o + N_b)^{-1} G N_p \sigma^2 I_p \tag{B38}$$

Substituting into Eqn.(B31) we finally obtain:

$$\text{var}(\hat{\lambda}) = \sigma^2 [N_p - N_p G^T (N_o + N_b)^{-1} G N_p] \tag{B39}$$

In order to obtain the modified form of the χ^2 - statistics we first note:

$$X - A(\lambda) = (\Pi_p X + \Pi_o X) - (I_p + G)(\lambda)$$

$$= [X_o - G(\lambda)] + [X_p - \lambda]$$

$$W^{-1} = N_p^{-1} + N_o^{-1}$$

$$W^{-1}(X - A(\lambda)) = N_p^{-1}(X_p - \lambda) + N_o^{-1}(X_o - G(\lambda))$$

and consequently:

$$\chi^2 = g_E(X - A(\lambda), W^{-1}(X - A(\lambda)) = g_p(X_p - \hat{\lambda}, N_p^{-1}(X_p - \hat{\lambda})) + g_o$$

$$(X_o - Go\hat{\lambda}, N_o^{-1}(X_o - Go\hat{\lambda})) \qquad \text{(B40)}$$

The χ^2 is expressed in terms of only X_o, X_p, N_o, N_b, G as follows:
By defining the quantities:

$$\chi_p^2 = g_p(X_p - \hat{\lambda}, N_p^{-1}(X_p - \hat{\lambda})) \qquad \text{(B41)}$$

$$\chi_o^2 = g_o(X_o - Go\hat{\lambda}, N_o^{-1}(X_o - Go\hat{\lambda})) \qquad \text{(B42)}$$

we can write:

$$\chi^2 = \chi_p^2 + \chi_o^2 \qquad \text{(B43)}$$

By virtue of Eqn. (B24), Eqn (B41) can be written:

$$\chi_p^2 = g_p(N_p G^T X,\ N_p^{-1} N_p G^T X) = g_p(X,\ N_b X) \tag{B44}$$

Similarly in the light of Eqn. (B23), Eqn. (B42) gives:

$$\chi_o^2 = g_o(N_o X,\ N_o^{-1} N_o X) = g_o(X, N_o X) \tag{B45}$$

Combining Eqns. (B43/45) we get:

$$\chi^2 = g_p(X,\ N_b X) + g_o(X,\ N_o X) = g_E(X, (N_o+N_b)X) =$$

$$= g_E((N_o+N_b)^{-1}(X_o - GX_p),\ X_o - GX_p)$$

That is:

$$\chi^2 = g_E(X_o - GX_p, (N_o + N_b)^{-1}(X_o - GX_p)) \tag{B46}$$

New calculated values and covariance matrices of the "observed quantities-parameters" vector $X \in E$ can be obtained by operating the linear transformation A upon the least-squares estimator $\hat{\lambda}$ and using Eqns. (B30),(B39).

If we set $\hat{Y} = A \circ \hat{\lambda}$ and since $\hat{Y} = \hat{Y}_p + \hat{Y}_o$ with $Y_p \in S_p$ and $Y_o \in S_o$, we obtain:

$$Y = A \circ \hat{\lambda} = (I_p + G)(X_p + N_p G^T (N_o + N_b)^{-1}(X_o - GX_p))$$

$$= [X_p + N_p G^T (N_o + N_b)^{-1}(X_o - GX_p)] + [GX_p + N_b (N_o + N_b)^{-1}(X_o - GX_p)]$$

viz:

$$Y_p = X_p + N_p G^T (N_o + N_b)^{-1} (X_o - GX_p)$$

that is, the parameters-estimator we have already derived, and

$$Y_o = GX_p + N_b (N_o + N_b)^{-1} (X_o - GX_p) \tag{B47}$$

an estimator of the mean vector of the observed quantities based upon both X_p and X_o.

For the variance of $\hat{Y}$ we have:

$$\begin{aligned}
\text{var}(\hat{Y}) &= \sigma^2 \, A \, \text{var}(\hat{\lambda}) \, A^T = \sigma^2 (I_p + G) \text{var}(\hat{\lambda}) (I_p + G^T) \\
&= (I_p + G)(N_p - N_p G^T (N_o + N_b)^{-1} G N_p)(I_p + G^T)\sigma^2 \\
&= \sigma^2 [N_p - N_p G^T (N_o + N_b)^{-1} G N_p \\
&+ G N_p - N (N_o + N_b)^{-1} G N_p \\
&+ N_p G^T - N_p G^T (N_o + N_b)^{-1} N_b \\
&+ N_b - N_b (N_o + N_b)^{-1} N_b]
\end{aligned} \tag{B48}$$

We observe that though the covariance matrix of the "observations-parameters" vector was diagonal in space of N_p and N_o, that is:

$$W = \begin{bmatrix} N_p & 0 \\ 0 & N_o \end{bmatrix}$$

the covariance matrix of its estimator presents correlations between the two sub-spaces S_p and S_o of E. (Second and third terms in Eqn. B48)

Usually we are interested in the covariance matrix of the estimator of the observation vector itself, that is, the fourth term of Eqn. (B48).

$$\text{var}(\hat{Y}_o) = \sigma^2 [N_b - N_b(N_o + N_b)^{-1}N_b] \tag{B49}$$

An estimator of $\text{var}(y_o)$ in terms of $\hat{\sigma}^2 = \chi^2/n-r$ is then:

$$\hat{\text{var}}(\hat{Y}_o) = \frac{\chi^2}{n-r}[N_b - N_b(N_o + N_b)^{-1}N_b] \tag{B50}$$

Eqns. (B30), (B39), (B46), (B47), (B49), (B50) give the least-squares estimates of both parameters and observed quantities together with their covariance matrices, in the case where measurements or evaluations of the parameters accompanied by covariance matrices are considered additional observed quantities and are treated as such.

B4 NON-LINEAR LEAST-SQUARES METHOD

In most practical problems the constraint between observed quantities and parameters is not linear. In such cases a functional form is meant to relate observed quantities and parameters, that is

$$X_o = X_o(X_p) \tag{B51}$$

which may or may not be known.

An analytical solution to the general non-linear least-squares problem even in cases where the functional form is fully known has not yet been achieved. Approximate numerical methods are usually employed from which the most often used is that of linearizing the model by a Taylor series expansion of the function. The best expansion to make is about the

solution. Since we usually do not know the solution, such expansion must be made about some "trial value" from which a trial solution is obtained. This "trial solution" is then used as a "new point" about which the model is expanded again. Therefore an iterative procedure is developed and progress toward a "converged solution" is usually monitored by observing the successive improvements in χ^2 at each step. Let us transcribe in mathematical language the ideas discussed above. The first order Taylor series expansion of Eqn. (B51) gives:

$$X_o = X_o^* + C(X_p - X_p^*) \tag{B52}$$

where X_p^* = Taylor series expansion point

X_o^* = $X_o(X_p^*)$

C = is the design matrix made up from the partial derivatives of the model, $X_o(X_p)$, with respect to the parameter X_p and evaluated at $X_p = X_p^*$, that is:

$$C_{ij} = \left[\frac{\partial X_{oi}(X_p)}{\partial X_{pj}}\right]_{X_{pj} = X^*_{pj}} \qquad \begin{matrix} i = 1,2...n-r \\ j = 1,2...r \end{matrix}$$

If we redefine the random variables X_p and X_o as their fractional deviations from the expansion points X_p^* and $X_o^* = X_o(X_p^*)$ correspondingly, viz:

$$P_j = \frac{X_{pj} - X^*_{pj}}{X^*_{pj}} \qquad j = 1,2...r \tag{B54}$$

$$D_i = \frac{X_{oi} - X^*_{oi}}{X^*_{oi}} \qquad i = 1,2...n-r \qquad \text{(B55)}$$

then Eqn. (B52) can be rewritten as:

$$P = SD$$

where

$$S_{ij} = \frac{X^*_{pj}}{X^*_{oi}} C_{ij} = \frac{X^*_{pj}}{X^*_{oi}} \left[\frac{\partial X_{oi}}{\partial X_{pj}}\right]_{X_{pj} = X^*_{pj}} \qquad \text{(B56)}$$

It can be easily shown that the covariance matrices of the new random variables are given by:

$$R_{k\ell} = \frac{N_p}{X^*_{pk} X^*_{p\ell}} \qquad k,\ell = 1,2...r \qquad \text{(B57)}$$

and

$$L_{k\ell} = \frac{N_o}{X^*_{ok} X^*_{o\ell}} \qquad k,\ell = 1,2...n-r \qquad \text{(B58)}$$

It is now understood that the least-squares solution in terms of the new definition of the random variables can be simply obtained by replacing in Eqns. (B30), (B46), (B47) and (B50), X_p by P, X_o by D, G by S, N_p by R and N_o by L, viz:

$$P' = P + RS^T(L + N)^{-1}(D - SP) \qquad \text{(B59)}$$

$$R' = \sigma^2\left[R - RS^T(L + N)^{-1}SR\right] \qquad \text{(B60)}$$

$$D' = SP + N(L + N)^{-1}(D - SP) \qquad \text{(B61)}$$

$$L' = \sigma^2\left[N - N(L + N)^{-1}N\right] \qquad \text{(B62)}$$

An estimate for σ^2 is given by:

$$\sigma^2 = \chi^2/n-r \tag{B63}$$

where:

$$\chi^2 = g_E(D - SP,(L + N)^{-1}(D - SP)) \tag{B64}$$

In the above Equations N is defined as:

$$N = S\ R\ S^T \tag{B65}$$

In order to develop an iterative scheme giving the "converged solution", the model $X_o = X_o(X_p)$ is re-expanded about X_p' determined from the solution of Eqn. (B59) and successively about $X_{p,k}'$ where k shows the number of iterations.

The "converged solution" is then found according to the formulae:

$$P_{k+1}' = P + RS^T(L + N_k)^{-1}(D_k - S_kP_k) \tag{B66}$$

$$R_k' = \sigma^2\left[R - RS_k^T(L + N_k)^{-1}S_kR\right] \tag{B67}$$

$$\chi^2 = g_E(D_k - S_kP_k,(L + N_k)^{-1}(D_k - S_kP_k)) \tag{B68}$$

where:

$$P_{k+1,j}' = \frac{X_{p,(k+1),j}' - X_{p,j}^*}{X_{p,j}^*}$$

$$P_j = \frac{X_{p,j} - X^*_{p,j}}{X^*_{p,j}} \qquad j = 1,2...r$$

$$P_{k,j} = \frac{X_{p,j} - X'_{p,k,j}}{X'_{p,k,j}}$$

$$D_{k,i} = \frac{X_{o,i} - X^*_{o,k,i}}{X^*_{o,k,i}} \qquad i = 1,2...n-r$$

$$X^*_{o,k} = X_o(X'_{p,k})$$

S_k is the fractional design matrix defined by Eqn. (B56) and calculated at $X'_{p,k}$

$$N_k = S_k \, R \, S_k^T$$

It is important to note that the need to iterate is not an essential aspect of the method if the initial expansion point X^*_p yields a solution, through Eqn. (B59), which is close to it. Iterating is, however, necessary if the model is highly non-linear and X'_p is far from X^*_p. In this case the convergence of the process may or may not occur and when it does occur it may be at a "local minimum" which is a function of the starting value X^*_p. In cases where the initial expansion of the model is undertaken about the sample point, that it $X_p = X^*_p$ Eqns. (B59/64) take the simplified final form:

$$P' = R \, S^T(L + N)D \tag{B69}$$

$$R' = \sigma^2[R - R \, S^T(L + N)^{-1}SR] \tag{B70}$$

$$D' = N(L + N)^{-1}D \tag{B71}$$

$$L' = \sigma^2[N - N(L + N)^{-1}N] \tag{B72}$$

$$\chi^2 = g_E(D,(L + N)^{-1}D) \tag{B73}$$

$$\hat{\sigma}^2 = \chi^2/n-r \tag{B74}$$

Eqns. (B69/74) constitute our final solution to the non-linear least-squares problem in which an iteration scheme is note employed.

The least-squares estimates of both parameters and observed quantities are valid for any form of the corresponding joint density functions provided that the 1st and 2nd moments of the distributions exist.

This is a very important characteristic of the least-squares method which, together with its unbiased nature, renders it a very powerful tool in the statistical inference era.

However, if we make the assumption that the joint density functions of parameters and observations are multivariate normal then it can be shown that least-squares and maximum likelihood methods yield the same results. We can then test the likelihood of the input data (that is, parameter evaluations and observations) prior to obtaining the solution by means of a chi-square test on χ^2 using the number of observations as number of degrees of freedom.

REFERENCES OF APPENDIX B

1. GRAY, P.W., Private communication, ULRC, University of London.

2. LANG, S., "Real Analysis", Addison-Wesley, Vol. 2, (1966).

3. SEBER, G.A.F., "The Linear Hypothesis - A General Theory" Greffins Statistical Monographs No. 19, 1966.

100 - Energy Group Structure

Group	Energy Range (eV)		Group	Energy Range (eV)	
1	1.4918E 07*	1.3499E 07	51	8.6517E 04	6.7380E 04
2	1.3499E 07	1.2214E 07	52	6.7380E 04	5.2475E 04
3	1.2214E 07	1.1052E 07	53	5.2475E 04	4.0868E 04
4	1.1052E 07	1.0000E 07	54	4.0868E 04	3.1828E 04
5	1.0000E 07	9.0484E 06	55	3.1828E 04	2.4788E 04
6	9.0484E 06	8.1873E 06	56	2.4788E 04	1.9305E 04
7	8.1873E 06	7.4082E 06	57	1.9305E 04	1.5034E 04
8	7.4082E 06	6.7032E 06	58	1.5034E 04	1.1709E 04
9	6.7032E 06	6.0653E 06	59	1.1709E 04	9.1188E 03
10	6.0653E 06	5.4881E 06	60	9.1188E 03	7.1018E 03
11	5.4881E 06	4.9659E 06	61	7.1018E 03	5.5309E 03
12	4.9659E 06	4.4933E 06	62	5.5309E 03	4.3074E 03
13	4.4933E 06	4.0657E 06	63	4.3074E 03	3.3546E 03
14	4.0657E 06	3.6788E 06	64	3.3546E 03	2.6126E 03
15	3.6788E 06	3.3287E 06	65	2.6126E 03	2.0347E 03
16	3.3287E 06	3.0119E 06	66	2.0347E 03	1.5846E 03
17	3.0119E 06	2.7253E 06	67	1.5846E 03	1.2341E 03
18	2.7253E 06	2.4660E 06	68	1.2341E 03	9.6112E 02
19	2.4660E 06	2.2313E 06	69	9.6112E 02	7.4852E 02
20	2.2313E 06	2.0190E 06	70	7.4852E 02	5.8295E 02
21	2.0190E 06	1.8268E 06	71	5.8295E 02	4.5400E 02
22	1.8268E 06	1.6530E 06	72	4.5400E 02	3.5358E 02
23	1.6530E 06	1.4957E 06	73	3.5358E 02	2.7537E 02
24	1.4957E 06	1.3534E 06	74	2.7537E 02	2.1445E 02
25	1.3534E 06	1.2246E 06	75	2.1445E 02	1.6702E 02
26	1.2246E 06	1.1080E 06	76	1.6702E 02	1.3007E 02
27	1.1080E 06	1.0026E 06	77	1.3007E 02	1.0130E 02
28	1.0026E 06	9.0718E 05	78	1.0130E 02	7.8893E 01
29	9.0718E 05	8.2085E 05	79	7.8893E 01	6.1442E 01
30	8.2085E 05	7.4274E 05	80	6.1442E 01	4.7851E 01
31	7.4274E 05	6.7206E 05	81	4.7851E 01	3.7267E 01
32	6.7206E 05	6.0810E 05	82	3.7267E 01	2.9023E 01
33	6.0810E 05	5.5023E 05	83	2.9023E 01	2.2603E 01
34	5.5023E 05	4.9787E 05	84	2.2603E 01	1.7604E 01
35	4.9787E 05	4.5049E 05	85	1.7604E 01	1.3710E 01
36	4.5049E 05	4.0762E 05	86	1.3710E 01	1.0677E 01
37	4.0762E 05	3.6883E 05	87	1.0677E 01	8.3153E 00
38	3.6833E 05	3.3373E 05	88	8.3153E 00	6.4760E 00
39	3.3373E 05	3.0197E 05	89	6.4760E 00	5.0435E 00
40	3.0197E 05	2.7324E 05	90	5.0435E 00	3.9279E 00
41	2.7324E 05	2.4724E 05	91	3.9279E 00	3.0590E 00
42	2.4724E 05	2.2371E 05	92	3.0590E 00	2.3824E 00
43	2.2371E 05	2.0242E 05	93	2.3824E 00	1.8554E 00
44	2.0242E 05	1.8316E 05	94	1.8554E 00	1.4450E 00
45	1.8316E 05	1.6573E 05	95	1.4450E 00	1.1254E 00
46	1.6473E 05	1.4996E 05	96	1.1254E 00	8.7644E-01
47	1.4996E 05	1.3569E 05	97	8.7644E-01	6.8257E-01
48	1.3569E 05	1.2277E 05	98	6.8257E-01	5.3159E-01
49	1.2277E 05	1.1109E 05	99	5.3159E-01	4.1400E-01
50	1.1109E 05	8.6517E 04	100	4.1400E-01	1.0000E-04

*Read 1.4918×10^7.

55 - Energy Group Structure

Group No.	Energy interval (MeV)	Group No.	Energy interval (MeV)
1	1.3499E+01 - 1.4918E+01	31	6.7206E-01 - 7.4274E-01
2	1.2214E+01 - 1.3499E+01	32	6.0810E-01 - 6.7206E-01
3	1.1052E+01 - 1.2214E+01	33	5.5023E-01 - 6.0810E-01
4	1.0000E+01 - 1.1052E+01	34	4.9787E-01 - 5.5023E-01
5	9.0484E+00 - 1.0000E+01	35	4.5049E-01 - 4.9787E-01
6	8.1873E+00 - 9.0484E+00	36	2.7324E-01 - 4.5049E-01
7	7.4082E+00 - 8.1873E+00	37	1.8316E-01 - 2.7324E-01
8	6.7032E+00 - 7.4082E+00	38	1.1109E-01 - 1.8316E-01
9	6.0653E+00 - 6.7032E+00	39	6.7379E-02 - 1.1109E-01
10	5.4881E+00 - 6.0653E+00	40	4.0868E-02 - 6.7379E-02
11	4.9659E+00 - 5.4881E+00	41	2.4788E-02 - 4.0868E-02
12	4.4933E+00 - 4.9659E+00	42	1.5034E-02 - 2.4788E-02
13	4.0657E+00 - 4.4933E+00	43	9.1188E-03 - 1.5034E-02
14	3.6788E+00 - 4.0657E+00	44	5.5308E-03 - 9.1188E-03
15	3.3287E+00 - 3.6788E+00	45	3.3546E-03 - 5.5308E-03
16	3.0119E+00 - 3.3287E+00	46	1.2341E-03 - 3.3546E-03
17	2.7253E+00 - 3.0119E+00	47	4.4500E-04 - 1.2341E-03
18	2.4660E+00 - 2.7253E+00	48	1.6702E-04 - 4.5400E-04
19	2.2313E+00 - 2.4660E+00	49	6.1442E-05 - 1.6702E-03
20	2.0190E+00 - 2.2313E+00	50	2.2603E-05 - 6.1442E-05
21	1.8268E+00 - 2.0190E+00	51	8.3153E-06 - 2.2603E-05
22	1.6530E+00 - 1.8268E+00	52	3.0590E-06 - 8.3153E-06
23	1.4957E+00 - 1.6530E+00	53	1.1254E-06 - 3.0590E-06
24	1.3534E+00 - 1.4957E+00	54	4.1399E-07 - 1.1254E-06
25	1.2246E+00 - 1.3534E+00	55	1.0000E-09 - 4.1399E-07
26	1.1080E+00 - 1.2246E+00		
27	1.0026E+00 - 1.1080E+00		
28	9.0718E-01 - 1.0026E+00		
29	8.2085E-01 - 9.0718E-01		
30	7.4247E-01 - 8.2085E-01		

37 - Energy Group Structure

Group No.	Energy interval (MeV)
1	1.350E+01 - 1.460E+01
2	1.250E+01 - 1.350E+01
3	1.125E+01 - 1.250E+01
4	1.000E+01 - 1.125E+01
5	8.500E+00 - 1.000E-01
6	7.000E+00 - 8.500E+00
7	6.070E+00 - 7.000E+00
8	4.720E+00 - 6.070E+00
9	3.680E+00 - 4.720E+00
10	2.870E+00 - 3.680E+00
11	1.740E+00 - 2.870E+00
12	1.150E+00 - 1.740E+00
13	8.210E-01 - 1.150E+00
14	6.390E-01 - 8.210E-01
15	3.880E-01 - 6.390E-01
16	2.350E-01 - 3.880E-01
17	1.430E-01 - 2.350E-01
18	1.110E-01 - 1.430E-01
19	8.650E-02 - 1.110E-01
20	6.740E-02 - 8.650E-02
21	4.090E-02 - 6.740E-02
22	2.480E-02 - 4.090E-02
23	1.500E-02 - 2.480E-02
24	9.120E-03 - 1.500E-02
25	4.310E-03 - 9.120E-03
26	2.040E-03 - 4.310E-03
27	9.610E-04 - 2.040E-03
28	5.830E-04 - 9.610E-04
29	2.750E-04 - 5.830E-04
30	1.660E-04 - 2.750E-04
31	7.550E-05 - 1.660E-04
32	2.770E-05 - 7.550E-05
33	1.600E-05 - 2.770E-05
34	5.000E-07 - 1.600E-05
35	1.800E-07 - 5.000E-07
36	7.000E-08 - 5.000E-07
37	1.000E-09 - 7.000E-08

ANGULAR QUADRATURE CONSTANTS

S_4

COSINE (MU)	WEIGHT
- 9.36742E-01	0.0
- 8.68890E-01	1.66667E-01
- 3.50021E-01	3.33333E-01
3.50021E-01	3.33333E-01
8.68890E-01	1.66667E-01

S_8

COSINE (MU)	WEIGHT
- 9.75900E-01	0.0
- 9.51190E-01	6.04938E-02
- 7.86796E-01	9.07407E-02
- 5.77350E-01	1.37037E-01
- 2.18218E-01	2.11728E-01
2.18218E-01	2.11728E-01
5.77350E-01	1.37037E-01
7.86790E-01	9.07407E-02
9.51190E-01	6.04938E-02